

國立交通大學

電子物理學系

博士論文

鏡摻雜之脈衝雷射

Yb-doped pulsed lasers

研究生：莊威哲

指導教授：陳永富 教授

中華民國一百零二年四月

鏡摻雜之脈衝雷射
Yb-doped pulsed lasers

研究生：莊威哲

Student : Wei-Zhe Zhuang

指導教授：陳永富

Advisor : Yung-Fu Chen

國立交通大學
電子物理學系
博士論文

A Thesis
Submitted to Department of Electrophysics
College of Science
National Chiao Tung University
in partial Fulfillment of the Requirements
for the Degree of
Doctor of Philosophy
in
Electrophysics

April 2013

Hsinchu, Taiwan, Republic of China

中華民國一百零二年四月

鏡摻雜之脈衝雷射

學生：莊威哲

指導老師：陳永富

國立交通大學電子物理學系博士班

摘要

本文旨在使用鏡摻雜增益介質為主體以研究高功率、高重覆率脈衝雷射的技術。首先我們使用 $30\ \mu\text{m}$ 芯蕊孔徑的光纖作為增益介質，我們分別使用 $\text{Cr}^{4+}:\text{YAG}$ 晶體以及半導體材料 AlGaInAs 作為飽和吸收體。在以 $\text{Cr}^{4+}:\text{YAG}$ 晶體作為飽和吸收體的實驗中可得到脈衝能量為 $0.35\ \text{mJ}$ 以及重覆率為 $38\ \text{kHz}$ 的脈衝雷射；在以半導體材料 AlGaInAs 作為飽和吸收體的實驗中，我們可得脈衝能量為 $0.45\ \text{mJ}$ 以及脈衝重覆率為 $30\ \text{kHz}$ 的雷射脈衝。此外，我們使用一個被動式 Q 開關的 $\text{Nd}:\text{YVO}_4/\text{Cr}^{4+}:\text{YAG}$ 雷射作為種子源雷射以實現光纖放大器的架構。在以相同的光纖作為增益介質下，雷射能量為 $0.192\ \text{mJ}$ 、脈衝重覆率為 $25\ \text{kHz}$ 以及脈衝寬度為 $1.6\ \text{ns}$ 的光纖放大器可被實現。

我們更進一步的在被動式 Q 開關以及光纖放大器的架構下使用芯蕊孔徑為 $70\ \mu\text{m}$ 的光子晶體光纖來提升輸出的脈衝雷射能量。在以 $\text{Cr}^{4+}:\text{YAG}$ 晶體作為飽和吸收體的實驗中，相較於 $30\ \mu\text{m}$ 芯蕊孔徑的光纖，脈衝能量為可放大 2 倍並且脈衝寬度更可縮短 2 倍。此外我們以此架構作為基礎下更進一步完成腔內光學參量振盪器，目前可得波長在 $1515\ \text{nm}$ ，輸出功率為 $0.47\ \text{W}$ 的脈衝雷射。而在以半導體材料 AlGaInAs 作為飽和吸收體的實驗中，相較於 $30\ \mu\text{m}$ 芯蕊孔徑的光纖，我們可以得到脈衝能量放大 2.5 倍並且脈衝寬度更可縮短 6 倍的雷射脈衝。此外我們以此架構作為基礎下更進一步完成腔外光學參量振盪器，目前可得波長可調範圍為 $1513\ \text{nm}$ 至 $1593\ \text{nm}$ ，輸出功率為 $0.9\ \text{W}$ 的脈衝雷射。利用此光子晶體光纖作為增益介質，我們也完成以光子晶體光纖放大器作為基頻光光源的腔外非線性波長轉換，在輸入功率為 $3.3\ \text{W}$ 的條件下，可得波長為 $532\ \text{nm}$ 的輸出功率為 $1.7\ \text{W}$ 的二倍頻波長轉換以及波長為 $355\ \text{nm}$ ，輸出功率為 $1.1\ \text{W}$ 的三倍頻

波長轉換。

微晶片之摻鏡鈮鋁石榴石雷射已在被動式 Q 開關、自鎖模、被動式鎖模等不同模式下呈現。在被動式 Q 開關的模式下，以 $\text{Cr}^{4+}:\text{YAG}$ 晶體作為飽和吸收體。我們使用鑽石散熱片來改善摻鏡鈮鋁石榴石雷射的熱效應，實驗上證實無論是在能量以及輸出功率的提升、輸出脈衝的穩定性都可以獲得很好的改善。在自鎖模的操作下，使用相同的晶體與鑽石散熱片我們可以藉由改變腔長與晶體長度之間的比值來達到不同階數的諧波鎖模雷射。此外，將自鎖模雷射架構中之輸出耦合鏡更換為一半導體飽和吸收體，我們可以達到雙波長的鎖模脈衝雷射輸出。經由兩個不同波段的光學拍頻，我們可以得到重覆率高達 5 兆赫茲的超短雷射脈衝。



Yb-doped pulsed lasers

Student: Wei-Zhe Zhuang

Advisor: Prof. Yung-Fu Chen

Institute and Department of Electrophysics
National Chiao-Tung University

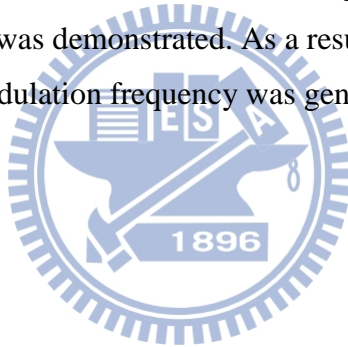
Abstract

Conventional large-mode-area (LMA), Yb³⁺-ion doped fiber with core diameter of 30 μm and inner cladding of 250 μm has been utilized in development of high power, high-repetition rate fiber lasers and amplifiers. Different saturable absorber (SA) such Cr⁴⁺:YAG crystals and AlGaInAs multi-quantum-wells were used to form a passively Q-switch (PQS) fiber lasers. The results reveal that with a Cr⁴⁺:YAG crystal as the SA, the laser could generate a pulse energy of 0.35 mJ at the pulse repetition rate of 38 kHz. By employing the AlGaInAs multi-quantum-wells (MQWs) as the SA, pulse energy up to 0.45 mJ at the repetition rate of 30 kHz can be attained. Besides, a Nd:YVO₄/ Cr⁴⁺:YAG laser was used as the seed laser in an master oscillator of power amplifier (MOPA) experiment. The amplifier could emit pulses with energy of 0.192 mJ at the repetition rate of 25 kHz and pulse width down to 1.6 ns.

Furthermore, for energy scaling, we use the photonic crystal fiber (PCF) with the core diameter up to 70 μm as the gain medium in either the PQS operation or in the MOPA scheme. The pulse energy was enhanced 1.8 times and the pulse width was 2 times shorter with the Cr⁴⁺:YAG crystal as the SA compared to the LMA fiber. An intracavity optical parametric oscillator (OPO) was demonstrated based on this scheme, output power of 0.47 W at 1515 nm was obtained. As for using the AlGaInAs MQWs as the SA, the pulse energy was enhanced 2.5 times and the pulse width was 6 times shorter in comparison with the LMA fiber. An extracavity OPO was performed

with this PQS laser as foundation. Output power of 0.9 W can be achieved and the wavelength can be tunable from 1513 nm to 1593 nm. A PCF MOPA was used to pump the extracavity nonlinear wavelength conversions module, output powers of 1.7 W of the second harmonic generation at 532 nm and 1.1 W of the third harmonic generation at 355 nm were realized at the fundamental pump power of 3.3 W.

Microchip Yb:YAG lasers were demonstrated in PQS, self-mode-locked, passively-mode-locked operations. In PQS operation, Yb:YAG laser was Q-switched with Cr⁴⁺:YAG crystal as the SA. Energy and output power scaling together with pulse stability improvement were achieved via employing a diamond window as the heat spreader. In self-mode-locked operation, high repetition rate, self-mode-locked Yb:YAG laser was attained using the same gain chip and heat spreader. Various order of harmonic mode locking was obtained by means of tuning the cavity length to match a commensurate ratio of the gain chip length. Furthermore, by replacing a semiconductor saturable absorber mirror as the output coupler, dual-wavelength mode-locked Yb:YAG laser was demonstrated. As a result of the optical beating of the dual spectral bands, THz modulation frequency was generated with an ultrashort pulse duration.



誌謝

Acknowledgement

學海無涯，在人生求知與求學の旅程上，宛如航行在浩瀚大海上的一葉扁舟，在這五年的研究所生涯，陳永富老師就如同汪洋中聳立的燈塔，總能指引我航向正確的方向，無論是在實作經驗及理論分析能力皆深厚的陳永富老師，給了我無論是在學術研究或人生態度上很大的啟發與指導。陳老師對於實驗結果的詮釋及判斷推理，常使許多難題總能豁然明朗，進而引發進一步的想法與啟發。此外，陳老師對於科學研究求知若渴的熱忱與樂觀進取的人生態度，更是我努力追尋及學習的標竿榜樣。感謝陳老師不厭其煩的指導與對我對於學習態度的啟發。另一個要感謝的是提供我實驗樣品的黃凱風老師，這些實驗材料，使得我的研究成果更加的完整與豐富。此外還要感謝時常與我討論的蘇冠暉老師，老大的細心、觀察力常能提醒我實驗中疏漏與忽略的地方。

再來要感謝的是感謝實驗室的同仁，感謝教導我做實驗的哲彥學長；感謝興弛學長、彥廷學長、依萍學姊、小江、文政、易純、郁仁、毓捷、毅帆、舜子、建至、國維、容辰、段必、小佑、政猷、及茗婷，感謝隨和的你們，讓我時時都能充滿快樂及歡笑。

最後，非常感謝我的父母，是你們無私的付出以及支持，才能讓我有繼續前進的動力與勇氣，並成就了今天的我。

Every end is a new begining. 畢業是另一個旅程的開展，我將盡力循著師長的教導及親朋的砥礪再向前行。最後，再一次感謝一切關心我的師長親朋好友。

Contents

Abstract (Chinese)	i
Abstract	iii
Acknowledgement	v
Contents	vi
List of Tables	viii
List of Figures	ix
Chapter 1 Introduction: backgrounds and motivations	1
1.1 <i>Passively Q-switched Yb-doped fiber lasers and amplifiers</i>	2
1.2 <i>Passively Q-switched Yb-doped crystal lasers</i>	15
1.3 <i>Mode-locked Yb doped crystal lasers</i>	23
Reference	27
Chapter 2 Pulsed large mode area fiber lasers and amplifier	37
2.1 <i>Passively Q-switched fiber laser with AlGaInAs MQWs</i>	44
2.2 <i>Comparative studies for Cr⁴⁺:YAG crystal and AlGaInAs MQWs in PQS fiber lasers</i>	50
2.3 <i>Hybrid Q-switched Yb-doped fiber laser</i>	59
2.4 <i>Fiber amplifier seeded by a passively Q-switched Nd:YVO₄/Cr⁴⁺:YAG laser</i>	68
2.5 <i>Conclusions</i>	83
Reference	84
Chapter 3 Pulsed photonic crystal fiber lasers and amplifier	92
3.1 <i>Passively Q-switched with Cr⁴⁺:YAG crystals and intracavity optical parametric oscillator</i>	94
3.2 <i>Passively Q-switched with AlGaInAs MQWs</i>	104
3.3 <i>Widely tunable extracavity optical parametric oscillator with the PQS PCF laser</i>	113
3.4 <i>Fiber amplifier seeded by a passively Q-switched Nd:YVO₄/Cr⁴⁺:YAG laser and extracavity third harmonic generation</i>	123

3.5 Conclusions	132
Reference	134
Chapter 4 Passively Q-switched and mode-locked Yb:YAG lasers	145
4.1 Passively Q-switched with Cr ⁴⁺ :YAG crystal.....	147
4.2 Self-mode-locked operation	156
4.3 Dual-wavelength mode-locked operation.....	163
4.4 Conclusions	172
Reference	173
Chapter 5 Summary and Future works	181
5.1 Summary.....	182
5.2 Future works	186
Reference	187
Publication List	189



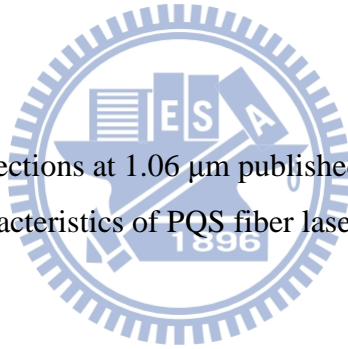
List of Tables

Chapter 1

Table 1.1: Some output characteristics of Yb-doped PQS lasers published in literatures.	18
Table 1.2: Thermal conductivities with different materials.....	22
Table 1.3: Overview of fundamentally mode-locked diode-pumped solid state lasers with pulse repetition rate higher than 1GHz.....	24

Chapter 2

Table 2.1: Cr ⁴⁺ :YAG cross sections at 1.06 μm published in literatures.....	41
Table 2.2: Some output characteristics of PQS fiber lasers published in literatures...	42



Chapter 5

Table 5.1: Summary of the performance obtained with the conventional LMA fiber.	182
Table 5.2: Summary of the performance obtained with the photonic crystal fiber. ..	183
Table 5.3: Performance summary of the OPO obtained with the photonic crystal fiber.	184

List of Figures

Chapter 1

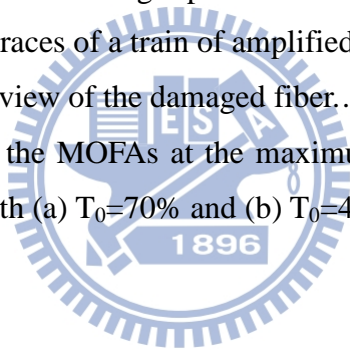
- Fig. 1.1** Double-clad fiber structure. The pump light is coupled into the inner cladding and confined between the inner and outer cladding while the signal guides in the core. 4
- Fig. 1.2** Various cladding design of the double-clad fibers. (a) center-core, (b) off-center core, (c) hexagon-shaped clad, (d) D-shaped clad, (e) rectangular-shaped clad. 5
- Fig. 1.3** Yb³⁺ energy level diagram in silica fibers. 6
- Fig. 1.4** Absorption (solid line) and emission (dotted line) cross section of Yb³⁺ ion in silica glass. 7
- Fig. 1.5** Normalized propagation constant (b defined by $b = (\beta/k)^2 - n_{\text{clad}}^2 / n_{\text{core}}^2 - n_{\text{clad}}^2$, where β is the propagation constant and k is the wave vector) for various LP (linearly polarized) modes with normalized frequency in a step-index fiber. . 9
- Fig. 1.6** Scanning electron micrograph (SEM) of (a) the first photonic crystal fiber, and (b) the first photonic crystal fiber operated at high power levels. 10
- Fig. 1.7** SEM image of the PM Yb-doped air-clad photonic crystal fiber with six index-matched stress applying parts. 11
- Fig. 1.8** SEM image of the cross-section of the large-mode-area, double cladding PCF with a zoom in the embedded micro-structured parts. 12
- Fig. 1.9** Energy level scheme of Nd and Yb ion. 17
- Fig. 1.10** 300K absorption and emission spectra of Yb:YAG crystal. 20
- Fig. 1.11** Energy level scheme of Yb ion. 20
- Fig. 1.12** Schematic of the geometries for solid state laser materials for (a) rod and (b) disk. 21
- Fig. 1.13** Deformation of a face-pumped disk with backside cooling. 21

Chapter 2

- Fig. 2.1** Nonlinear transmission of a saturable absorber versus incident fluence E_i normalized to the saturation fluence E_s of the absorber.....**39**
- Fig. 2.2** General scheme of the fiber laser with the fiber saturable absorber (FSA)..**39**
- Fig. 2.3** The energy-level diagram of Cr^{4+} :YAG with ESA. The solid lines indicate radiative optical transitions and the dashed lines indicate non-radiative transitions.....**41**
- Fig. 2.4** Transmittance spectrum at room temperature for the AR-coated AlGaInAs/InP saturable absorber. Inset, schematic diagram of a periodic AlGaInAs QW structure.**46**
- Fig. 2.5** Schematic diagram of the experimental setup. HR, high reflection; HT, high transmission.**46**
- Fig. 2.6** Average output powers at 1066 nm with respect to the incident pump power in cw and passively Q-switching operations.....**48**
- Fig. 2.7** Experimental results for the pulse repetition rate and the pulse energy versus incident pump power.**49**
- Fig. 2.8** Expanded shape of a single pulse and (b) typical oscilloscope trace of a train of output pulses.**49**
- Fig. 2.9** Saturation transmission of the AlGaInAs QWs and the Cr^{4+} :YAG crystal....**52**
- Fig. 2.10** Schematic of diode-pumped PQS Yb-doped fiber lasers. (a) with Cr^{4+} :YAG crystal (b) with AlGaInAs QWs. HR:high reflection; HT:high transmission.**53**
- Fig. 2.11** Dependence of the average output power on the launched pump power for the cw and passive Q-switching operations.**55**
- Fig. 2.12** (a) Pulse repetition rate and (b) pulse energy versus the launched pump power.....**56**
- Fig. 2.13** Pulse energy versus the resonant wavelength.**57**
- Fig. 2.14** Top: Oscilloscope traces of a typical Q-switched envelope; Bottom: Oscilloscope traces of a train of Q-switched pulses.**57**
- Fig. 2.15** Schematic diagram of the diode-pumped hybrid Q-switched Yb-doped

double-clad fiber laser. HR, high reflection; HT, high transmission; SA, saturable absorber.	61
Fig. 2.16 (a) Dependence of average output power on the launched pump power for the CW and passive Q-switching operations; (b) dependence of pulse period and timing jitter on the launched pump power; (c) the oscilloscope traces of trains of the PQS pulses at various pump powers.	63
Fig. 2.17 The oscilloscope traces of trains of (a) the PQS pulses (period = 512 μ s) and (b) the HQS pulses (period = 620 μ s) at the pump power of 3W.	63
Fig. 2.18 The oscilloscope traces of trains of the HQS fiber laser when f_{AO} was (a) higher than $0.8 \times f_{PQS}$ (b) lower than $0.7 \times f_{PQS}$	64
Fig. 2.19 (a) The pulse repetition rate of the pure PQS, the pure AQS, and the HQS lasers at the various launched pump powers; (b) the pulse energy of the three lasers at the various launched pump powers. The green and the blue regions represent the operational repetition rate of the AQS laser and the HQS laser, respectively; (c) the oscilloscope traces of trains of pure AQS laser at various repetition rates under a pump power of 24 W.	65
Fig. 2.20 (a) The pulse period and (b) the corresponding histogram of the pulse period of the PQS and the HQS lasers at the pump power of 3 W. The timing jitter is expressed in terms of standard deviation of the pulse period.	66
Fig. 2.21 The dependence of the ratio of jitter to pulse period of the HQS laser on the duty cycle of loss modulation for the pump power of 3W, 15W, and 24W. The f_{AO}^{-1} were set 620 μ s for P_p of 3W, 55.56 μ s for P_p of 15W, and 38.31 μ s for P_p of 24 W, respectively.	67
Fig. 2.22 (a) Schematic diagram of the plano-concave cavity. (b) Equivalent cavity diagram of the Nd:YVO ₄ /Cr ⁴⁺ :YAG PQS laser.	70
Fig. 2.23 Dependence of the mode-to-pump size ratio l/p_a on the pump power for different pumping spot radii.	73
Fig. 2.24 Effective mode area ratio of A/A_s as a function of the pump power in the Nd:YVO ₄ /Cr ⁴⁺ :YAG PQS laser with $L=0.9\rho_1$, $\rho_1=25$ mm, $\omega_p=100$ μ m.	74
Fig. 2.25 Schematic diagram of a diode-pumped Nd:YVO ₄ laser PQS with a Cr ⁴⁺ :YAG as a saturable absorber. HR: high reflection. HT: high transmission.	75
Fig. 2.26 (a) Dependence of the pulse repetition rate and the pulse energy on the	

initial transmission of Cr ⁴⁺ :YAG at the pump power of 5.4 W. (b) Dependence of the pulse width and the peak power on the initial transmission of Cr ⁴⁺ :YAG at the pump power of 5.4 W.	76
Fig. 2.27 Oscilloscope traces of a single pulse of (a) PQS laser with Cr ⁴⁺ :YAG of T ₀ =70%, (b) PQS laser with Cr ⁴⁺ :YAG of T ₀ =40%.....	77
Fig. 2.28 (a) Scheme of the MOFA setup. HT: high transmission HR: high reflection. (b) Cross section of the PM Yb-doped fiber.	78
Fig. 2.29 (a) Average output power and peak power of MOFA with the seed of repetition rate of 50 kHz as a function of the launched pump power. (b) Oscilloscope traces of a single pulse of the output pulse of the amplifier. (c) Oscilloscope traces of a train of amplified pulses.....	79
Fig. 2.30 (a) Average output power and peak power of MOFA with the seed of repetition rate of 25 kHz as a function of the launched pump power. (b) Oscilloscope traces of a single pulse of the output pulse of the amplifier. (c) Oscilloscope traces of a train of amplified pulses.....	80
Fig. 2.31 End view and side view of the damaged fiber.....	81
Fig. 2.32 Optical spectra of the MOFAs at the maximum output powers injected by the seed lasers with (a) T ₀ =70% and (b) T ₀ =40%.....	81

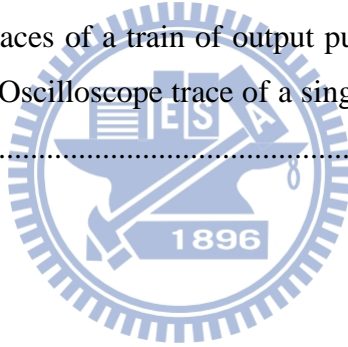


Chapter 3

Fig. 3.1 (a) Setup for the passively Q-switched PCF laser; (b) image of the cross section of PCF.	96
Fig. 3.2 Average output power with respect to launched pump power in CW and passive Q-switching operations, the inset: typical lasing spectrum. (b) Pulse repetition rate and pulse energy versus launched pump power.	98
Fig. 3.3 Typical oscilloscope traces for (a) single Q-switched pulse and (b) Q-switched pulse train.	99
Fig. 3.4 Setup for the intracavity OPO pumped by the passively Q-switched PCF laser	100
Fig. 3.5 (a) Average output power of signal wave at 1515 nm with respect to launched pump power. (b) OPO pulse repetition rate and pulse energy versus launched	

pump power.	101
Fig. 3.6 General oscilloscope traces for the fundamental (top) and OPO signal (bottom) output pulses.	102
Fig. 3.7 (a)-(c) Schematic diagrams of three periodic AlGaInAs QWs structures. (d) Low-intensity transmittance spectrum of the three QW saturable absorbers.	106
Fig. 3.8 (a) Setup for the passively Q-switched PCF laser; (b) image of the cross section of PCF.	107
Fig. 3.9 Average output power with respect to launched pump power in CW and passive Q-switching operations.	109
Fig. 3.10 Pulse repetition rates in the passive Q-switching operation versus the launched pump power.	110
Fig. 3.11 Typical oscilloscope traces for the single Q-switched pulses of the lasers with the saturable absorbers of (a) 2×30 , (b) 3×30 , and (c) 3×50 QWs, respectively.	112
Fig. 3.12 Typical oscilloscope traces for a train of output pulses of the lasers with the saturable absorbers of (a) 2×30 , (b) 3×30 , and (c) 3×50 QWs, respectively.	112
Fig. 3.13 Schematic sketch of the external-cavity optical parametric oscillator pumped by the passively Q-switched photonic crystal fiber laser.	115
Fig. 3.14 (a) image of cross section of rod-type PCF and (b) transmission spectrum and structure of AlGaInAs saturable absorber.	116
Fig. 3.15 Output power of the passively Q-switched PCF laser versus the 976-nm launched pump power. Inset – the lasing spectrum obtained with 12.5 W of pump power.	117
Fig. 3.16 Typical oscilloscope traces of output pulses of the passively Q-switched PCF laser. (a) pulse shape with 6.3 W of pump power and (b) pulse shape with 13.1 W of pump power.	118
Fig. 3.17 Schematic sketch of the OPO setup. A half-wave plate and polarization beam splitter cube were settled in front of OPO to control the input pump power.	119
Fig. 3.18 Output performance of external-cavity OPO. (a) averaged output power of signal wave versus averaged power of PCF laser and (b) temporal traces of pump and signal wave.	120

Fig. 3.19	Tuning curve of signal wavelength versus different operating temperature. Inset: the corresponding conversion efficiency with temperature.	121
Fig. 3.20	Schematic sketch of the extracavity harmonic generations pumped by a single-stage rod-like photonic crystal fiber amplifier. HR: high reflection; HT: high transmission.....	126
Fig. 3.21	Relevance of the average output power and the pulse energy with the launched pump power of the PCF amplifier. Inset: the output lasing spectrum of the PCF amplifier obtained with 10.5 W of pump power....	126
Fig. 3.22	(a) Oscilloscope traces of a train of amplified pulses. (b) Oscilloscope trace of a single pulse of the output pulse of the amplifier.....	127
Fig. 3.23	Schematic sketch of the setup of the SHG and THG. AR: anti-reflection.	128
Fig. 3.24	Dependences of the average output power at 532 nm and 355 nm on the incident pump power at 1064 nm. Inset: the spatial intensity distribution of far field of the THG output.	129
Fig. 3.25	(a) Oscilloscope traces of a train of output pulses of 532 nm (top) and 355 nm (bottom). (b) Oscilloscope trace of a single pulse of the output pulse of the THG.	131



Chapter 4

Fig. 4.1	Pulse width region for different pulsed lasers.....	146
Fig. 4.2	The schematic diagram of the PQS Yb:YAG/Cr ⁴⁺ :YAG laser experimental setup. (S1: HT at 970 nm, HR at 1030 nm; S2: HT at 1030 nm, HR at 970 nm; HT: high transmission; HR: high reflection).	149
Fig. 4.3	Dependence of the averaged output power on the absorbed pump power under the CW operation.	150
Fig. 4.4	(a) Dependence of the averaged output power on the absorbed pump power under the PQS operation, the inset: typical lasing spectrum. (b) Dependence of the pulse energy on the absorbed pump power.....	151
Fig. 4.5	Oscilloscope traces of a single pulse of the output pulse of (a) with the diamond heat spreader, (b) without the diamond heat spreader.....	153
Fig. 4.6	Oscilloscope traces of a train of output pulses of (a) with the diamond heat	

spreader, (b) without the diamond heat spreader.	154
Fig. 4.7 Schematic diagram for the experimental setup of harmonically self-mode-locked Yb:YAG lasers formed by a Fabry-Perot flat-flat cavity.	158
Fig. 4.8 Output power versus absorbed pump power for the laser schemes without and with using the diamond heat spreader at a cavity length of $L_{\text{cav}} = 5.0$ mm. Note that the output characteristics are almost the same for $L_{\text{cav}} < 9.0$ mm.	159
Fig. 4.9 Experimental traces of (a) first- and (b) second-order autocorrelations for the operation of a multiple-pulse mode locking obtained at a cavity length of 6.08 mm.	160
Fig. 4.10 (a)-(c) Experimental results of the second-order autocorrelation at the maximum output power of 4.6 W for three cases of single-pulse harmonic mode locking observed at the cavity lengths of 5.47, 6.54, and 6.91 mm, respectively. (a')-(c') FWHM widths of the central peaks of the second-order autocorrelation shown in (a)-(c), respectively.	161
Fig. 4.11 (a)-(c) Experimental results of the first-order autocorrelation traces corresponding to the results shown in figures 4(a)-(c), respectively. (a')-(c') Optical spectra corresponding to the first-order autocorrelation traces shown in (a)-(c), respectively.	162
Fig. 4.12 The schematic diagram of the mode-locked Yb:YAG laser experimental setup. (S_1 : HT at 940 nm, HR at 1030~1100 nm; S_2 : HT at 1030~1100 nm, HR at 940 nm; HT: high transmission; HR: high reflection).	165
Fig. 4.13 Transmittance spectra of the SESAM.	166
Fig. 4.14 Dependence of the average output power on the absorbed pump power in the dual-wavelength harmonically mode-locked operation.	167
Fig. 4.15 Optical lasing spectrum obtained at the maximum absorbed pump power of 5.18 W.	168
Fig. 4.16 Experimental traces of the temporal behavior of (a) first- and (b) second-order autocorrelations in a delay-time span of 50 ps. Resolution: 67 fs and 200 fs for the first- and second-order autocorrelations, respectively.	169
Fig. 4.17 Experimental traces of the temporal behavior of (a) first- and (b) second-order autocorrelations in a delay-time span of 8 ps. Resolution: 8	

fs and 20 fs for the first- and second-order autocorrelations, respectively.

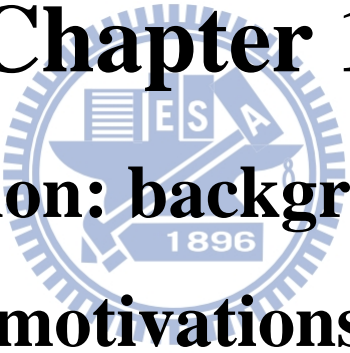
..... 170

Fig. 4.18 Experimental trace of the temporal behavior of second-order autocorrelation of the single beat pulse..... 170



Chapter 1

Introduction: backgrounds and motivations



1.1 Passively Q-switched Yb-doped fiber lasers and amplifiers

High power, pulsed lasers with few-nanosecond-long pulses at a multi-kHz pulse repetition rate (PRR) attract great interest for applications that exhibit one or more of the following characteristics: high pulse energy (e.g., range finder and scanner), high peak power (e.g., nonlinear wavelength conversion and material processing), and narrow spectral linewidth (e.g., remote sensing). In a bulk-crystal laser, heat is generated within a small volume in the center of the gain medium and dissipated in a limited surface some distance away from the center. This limits power scaling due to rod fracture by the large temperature gradient from a high heat load. Compared with conventional bulk solid-state lasers, fiber lasers have excellent thermal properties. The large surface area positioned just a few tens to a few hundreds of micrometers away from the active region allows efficient thermal dissipation and usually requires no additionally active cooling. Besides, the inherent wave-guiding property in fiber tends to reduce thermal distortion of the beam that commonly shown by bulk solid-state lasers and achieves superior beam quality.

Furthermore, due to the confinement of both the laser and pump radiation, the overlap between them is maintained over the entire fiber length that provides ultra-high gain of the fiber since the gain of the laser medium is determined by the product of pump light intensity and interaction length with the laser radiation in the gain medium. As the result, the ultra-high gain offers the option of master oscillator power amplifier (MOPA) schemes or a very efficient operation of fiber laser systems exhibiting low pump threshold values. The advantages mentioned above have paved the way for power scaling in a wide range of fiber lasers.

Rare-earth-doped fiber lasers were first proposed in early 1960s by Snitzer and co-workers [1-3] and operated with neodymium-doped fibers pumped by flashtubes. The pumping scheme was revised in the 1970s by Stone and Burrus [4] who use the laser diode end-pumped scheme to improve the laser efficiency. Another major breakthrough is the fabrication of low-loss optical fibers by means of the modified chemical vapor deposition (MCVD) technique proposed by Payne and co-workers [5-6]. Their work on neodymium-doped fibers revealed that the very low laser

threshold as low as 100 μW of absorbed power from a diode laser could be achieved in single mode operation by using the low-loss optical fiber. Consequently, even with a modest pump power of a few milliwatts provided by cheap and readily available laser diodes, levels of optical gain could be reached that were highly promising for applications such as optical telecommunication amplifiers. This begins the foundation of erbium doped fiber amplifiers (EDFAs) [7] whose operating wavelength of 1.55 μm falls in the third telecommunication window. The influence on telecommunications of this work has been profound, not only making the long-haul optical communication inexpensive and reliable but also leading to the development of Internet as we know it today. Furthermore, the excitement about telecommunication amplifiers arouse considerable interest in fiber lasers and inspired the growth of novel laser diodes and fiber components, as they offer a number of attractive features when compared to other lasers.

As well as the telecommunication, silica-based fibers are also with inherent advantages in high-power lasers owing to their high optical damage threshold and efficient thermal management mechanism. The output power scaling of conventional fiber laser was limited by the pump-coupling scheme of the laser which the pumping light from the laser diode can only coupled into the core of the fiber. In order to couple the output of the laser diode into the single-mode fiber efficiently, the use of single-mode laser diode is required. However, the output power of such pump source is limited at that time by the damage threshold of the semiconductor material to a fraction of a watt that seriously restricts the output power of the fiber laser. Moreover, the coupling efficiency from the laser diode to the core of the fiber is typically only 60% or less due to the astigmatism of the laser diode beam and only a fraction of the coupled pump power is usable.

Hence, Snitzer et al. proposed the double-clad fiber structure in 1988 to separate the signal guiding core and the pump light guiding clad as illustrated in Fig 1.1. The structure consists of a single-mode core surrounded by a first cladding of lower refractive index made by silica which itself surrounded by another cladding of even lower refractive index made by polymer. The first cladding (inner cladding), now, forms another waveguide for the pump light but capable of guiding highly multi-mode compared to the single-mode core for signal. Not only the area of the first cladding is approximately 100 times larger than the core but also the numerical aperture (N.A.) of

the first cladding becomes larger that makes it now able to inject a substantial fraction of the output power from a multi-mode, large area laser diode with very high output power into the first cladding. For silica-based fibers with a second cladding (outer cladding) made of glass, the N.A. is limited to be about 0.4. Even higher N.A. (as high as 0.6) can be attained if the second cladding is made of low-refractive-index polymer [9].

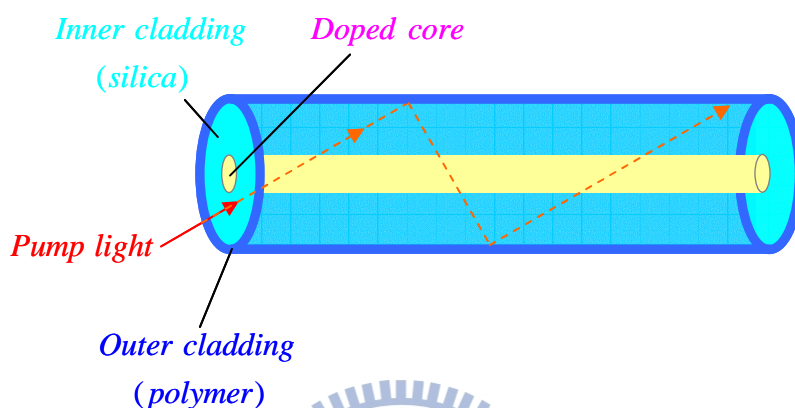


Fig 1.1 Double-clad fiber structure. The pump light is coupled into the inner cladding and confined between the inner and outer cladding while the signal guides in the core.

However, the price accompanied by the increased pump coupling efficiency is the increase of the fiber length. The spatial overlap between the pump and the doped core is small because the signal and the pump light are guided in the different waveguide now. The absorbed pump power per unit fiber length is reduced in comparison with the core-pumped fiber and either a longer fiber length or a heavily-doped core is required to achieve the same amount of population inversion. The length of the fiber is restricted by the absorption loss and the nonlinearity and the heavily-doped fiber will result in quench effect of dopants.

A large amount of research was invested in the design of the double-cladding fiber to optimize the power transfer efficiency from the pump to the dopants per unit length [10-14]. Most of the pump is launched as helical rays in whisper-gallery modes which will miss the core if the first cladding has a circular cross section as depicted in Fig. 1.2(a). Therefore the design criterion is aimed to reduce the symmetry of the first cladding to eliminate whisper-gallery modes. Figure 1.2(b) shows the off-center core method demonstrated by Snitzer et al. [15-16], the pump absorption efficiency was

increased from 5% of the center-core fiber to 28% of the off-center core fiber. The second solution is to alter the shape of the first cladding [8, 13, 17-18] as illustrated from Fig. 1.2(c) of hexagon-shaped, Fig. 1.2(d) of D-shaped, to Fig. 1.2(e) of rectangular-shaped. Helical pump rays are coupled to the meridional rays and most of the pump rays are passed through the doped-core by means of breaking the symmetry of the first cladding. Furthermore, via bending the fiber [13-14, 19-20], helical pump rays have also been reduced by mode mixing.

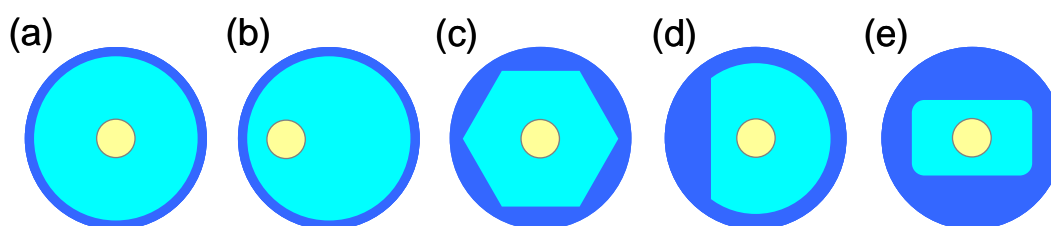


Fig 1.2 Various cladding design of the double-clad fibers. (a) center-core, (b) off-center core, (c) hexagon-shaped clad, (d) D-shaped clad, (e) rectangular-shaped clad.

In rare-earth-doped optical fibers, both the Nd and Yb dopants emit light near 1060 nm when the fibers doped with them are pumped at the suitable wavelength. However, Yb³⁺ attracted comparatively little attention than Nd³⁺ in the early years. The first Yb-doped silica fiber laser was studied by Etzel et al. [21] in 1962. The laser action at 1015nm in Yb-doped silicate glass was operated at 77K because the Yb-doped laser is a quasi-three-level system with substantial population of the lower laser level at room temperature which demands higher threshold than a four-level system. Even though Nd³⁺-doped optical fiber lasers were the first to be studied due to the four-level nature of Nd³⁺ transitions, Yb³⁺ ions have recently become the dopant of choice for high-power fiber lasers. The first reason for this is the Yb³⁺ ion's simple system with low quantum defect. The simple energy level structures in silica fibers shown in Fig. 1.3 consists of only two-manifolds: the ground manifolds (²F_{7/2}) and a well separated excited manifolds (²F_{5/2}), which include four and three Stark shifted levels. The simple energy level structure reveals that the pump wavelengths are close to the laser radiations which lead to low quantum defect. Low quantum defect equals less heat generation, which is a huge benefit for high-power lasers.

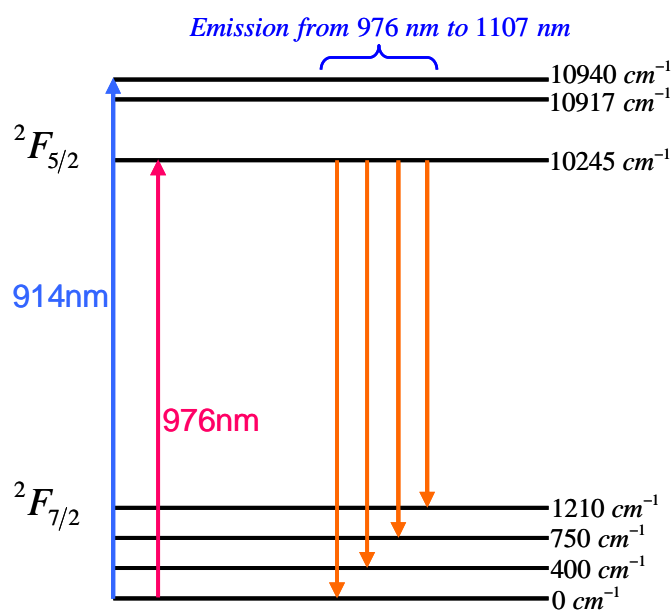


Fig 1.3 Yb^{3+} energy level diagram in silica fibers.

The simple system of ytterbium is also beneficial, because there is no need to worry too much about excited state absorption, cooperative up-conversion, and quench effects, all of which are channels for power loss. Furthermore, a glass host of the fiber also provides broader absorption and emission spectra for Yb^{3+} [22] due to strong inhomogeneous broadening, leading to less constraint on pump wavelength stability, a wider range of lasing wavelengths, and a wide gain bandwidth which allowing ultrashort pulse operation, and a wide wavelength tunability. The broad absorption band stretch from 850 nm to approximately 1050 nm as depicted in Fig. 1.2. As a result, the Yb-doped fiber can be pumped with a variety of sources such as AlGaAs (~800 nm - 850 nm), InGaAs/AlGaAs (915 nm), and InGaAs (976 nm) laser diodes together with Yb:YAG laser (1030 nm) or Nd:YLF laser (1047 nm). The upper-state fluorescence lifetime of a Yb-doped pure silicate glass lifetimes is relatively long (about 1.5 ms), which is beneficial for Q-switching. Other co-dopants such as Ge, Al, and K are used to mitigate the concentration quench that greatly decrease the pump absorption efficiency while Al, P, and B are utilized to reduce the clustering effect under high Yb-dopant concentration which cause radiative life time reduction [23].

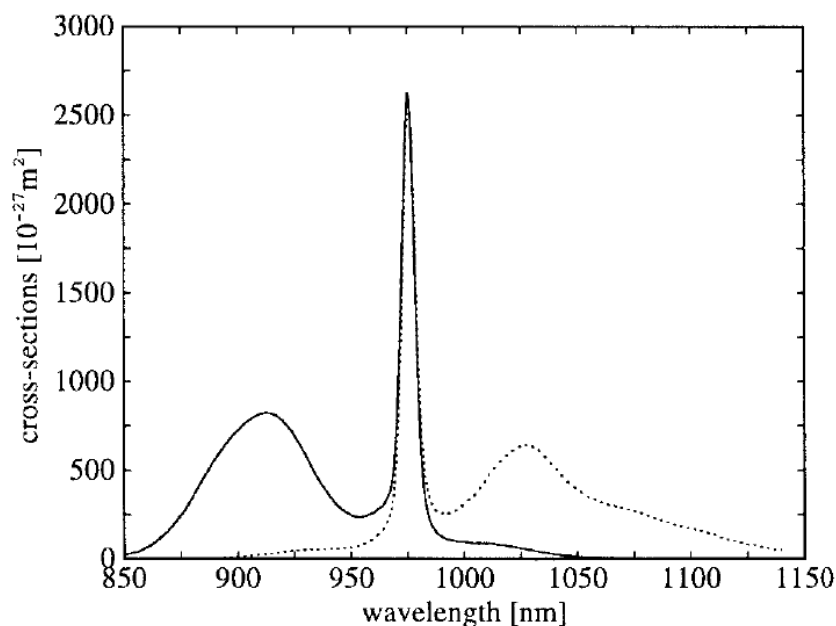


Fig 1.4 Absorption (solid line) and emission (dotted line) cross section of Yb^{3+} ion in silica glass [22].

The first Yb-doped cladding-pumped silica fiber laser was demonstrated by Gapontsev et al. [24] in 1991. Due to the low pump power of the laser diode at 875 nm, the fiber laser output at 1090 nm was limited to be only 50 mW. Nevertheless, it was still a milestone that proved efficient operation in Yb-doped fibers (5-mW of threshold, 69% of slope efficiency). The invention of double-clad fiber and the high power laser diode leads to the fast progression of high power Yb-doped fiber lasers since the mid-1990s. The output powers grow rapidly from 2 W in 1995 [25], to 110 W in 1999 [26] and 1.36 kW in 2004 [27], and even 10 kW-level in 2010 with a diffraction-limited beam quality [28]. High-power fiber lasers are penetrating the industrial and defense laser markets at a rapid rate.

Among all of the advantages provided by the fiber laser technology, in addition to the high average powers that can be achieved, is the diversity of temporal output properties that can be supported. As the result of the very large spectral bandwidths achievable from Yb-doped silica-fiber, fiber lasers can be constructed to operate from the continuous-wave (CW) regime down to pulse durations of just a few femtoseconds. Together with the development of CW lasers, short pulse width (ns-level) high power Yb-doped double-clad fiber lasers have also attracted lots of attentions due to their high pulse energy and peak power outputs. Applications such as remote sensing, industrial processing, and medical lasers that need such kind of light

sources promote the evolution comprising Q-switched fiber lasers and master oscillator of power amplifiers (MOPAs).

Even though the comparison of fiber lasers with bulk lasers is advantageous in relation to CW operation, the situation is quite different for pulsed (e.g., Q-switched) performance. In this case, the rapid buildup of amplified spontaneous emission (ASE) and ultimately the onset of lasing owing to the high gains achievable within conventional single-mode fiber that inevitably limit the energy storage to a few tens of micro-joules. The maximum energy that can be stored per unit length of the fiber at full inversion is given by:

$$E_{stored}^{max} = N_0 A_{core} h\nu_s \quad (1.1)$$

where N_0 is doping concentration limited by the ion-ion interactions that result in quenching effect, A_{core} is the area of the fiber core, and $h\nu_s$ is the photon energy of the laser. As seen in Eq. (1.1), the preferred solution to enhance the energy storage while minimizing the ASE problem is to enlarge the transverse area of the doped core [29]. This inspire the invention of large-mode-area (LMA) fibers (core diameter $> 15 \mu\text{m}$) to simultaneously enhances the extractable energy and reduces nonlinear effects such as stimulated Brillouin scattering (SBS) and stimulated Raman scattering (SRS) that limit the maximum achievable pulse energy. The LMA concepts were firstly applied to Yb-doped fibers in 2000 [30]. By using a coiled Yb-doped, double-clad fiber with a core diameter of $25 \mu\text{m}$ and a numerical aperture of ~ 0.1 ($V \approx 7.4$) as an amplifier, the output beam quality was measured to be $M^2 = 1.09$. Furthermore, decreasing the N.A. to about 0.06 (relative to standard telecommunication values of ~ 0.15) allows the core size to be increased while maintaining single transverse mode operation. In addition, the lower N.A. reduces the fraction of spontaneous emission captured by the fiber, thereby increasing energy storage. High energy Q-switched pulses of 7.7 mJ at the pulse repetition rate of 500 Hz and pulse width of 250 ns was attained using a fiber with a $60 \mu\text{m}$ core (N.A. ≈ 0.05) in the laser oscillator [31]. Single mode pulsed operation was later achieved by bend-loss-induced mode filtering of the gain fiber with pulse energy of 255 μJ , peak power of 300 kW and a pulse duration of 0.8 ns in a fiber amplifier [32].

As mentioned above, increasing the effective mode area within the core of the fiber provides the most effective way of enhancing the pulse energy and minimizing

Ch1 Introduction: backgrounds and motivations

the nonlinearity—reducing both the peak intensities and the fiber length due to improved pump absorption (for fixed inner-cladding dimension). However, there is a compromise between the mode area and the order of the transverse mode guided by the fiber governed by the V-number (normalized frequency) of the fiber:

$$V = \frac{2\pi a_{\text{core}}}{\lambda} (N.A.) = \frac{2\pi a_{\text{core}}}{\lambda} (\sqrt{n_{\text{core}}^2 - n_{\text{clad}}^2}) \quad (1.2)$$

in which a_{core} is the radius of the fiber core, λ is the free space wavelength, and n_{core} together with n_{clad} is the effective refractive index of the core and the cladding, respectively. As can be seen from Fig. 1.5 that a fiber becomes single transverse mode for $V < 2.405$, thus, one approach for increasing the core diameter while maintain a certain value of V is to decrease the numerical aperture. However, the lowest refractive index contrast between the core and the cladding of a doped core that can be reliably fabricated with conventional fiber preform manufacturing techniques corresponds to a N.A. of about 0.06. The requirement of single transverse mode confinement translates this as a maximum core diameter of about 15 μm for a conventional step-index fiber in the 1- μm wavelength region. A larger core would normally lead to the propagation of higher-order transverse modes.

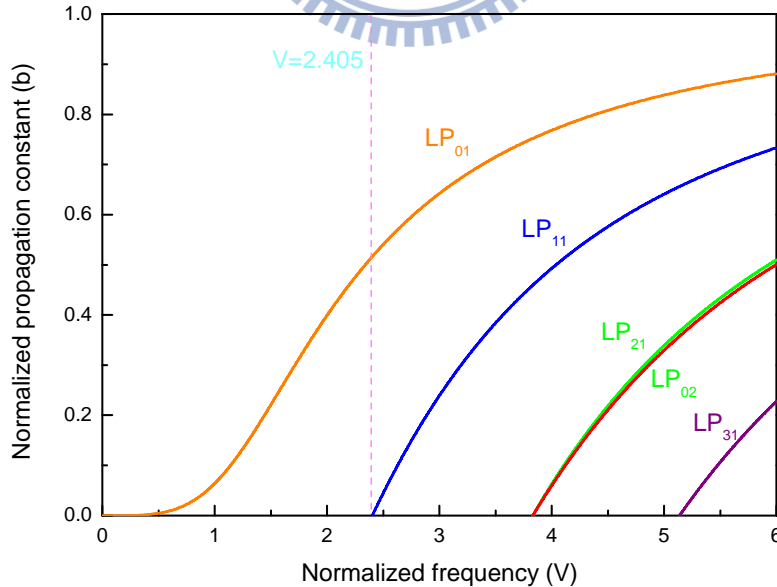


Fig 1.5 Normalized propagation constant (b defined by $b = (\beta/k)^2 - n_{\text{clad}}^2 / n_{\text{core}}^2 - n_{\text{clad}}^2$, where β is the propagation constant and k is the wave vector) for various LP (linearly polarized) modes with normalized frequency in a step-index fiber.

Photonic crystal fibers (PCFs) as depicted as Fig. 1.6(a) were first demonstrated in the late 1990s [33-35]. Its potential for achieving high-power single-mode operation with large cores was realized by the air-cladding structure of the PCF as shown in Fig. 1.6(b) that consists of a hexagonal array of air holes [36]. Due to design freedom in the PCF cladding an additional functionality such as polarizing or polarization maintaining (PM) properties can be added [37], as shown in Fig. 1.7. The refractive index of the doped core is averaged by the nano-structuring and the inner cladding index is precisely adjusted by adapting the air hole size and the hole-to-hole distance. Therefore, the diameter of the fiber core up to 100 μm can be obtained with low N.A. that only guides the fundamental mode [38].

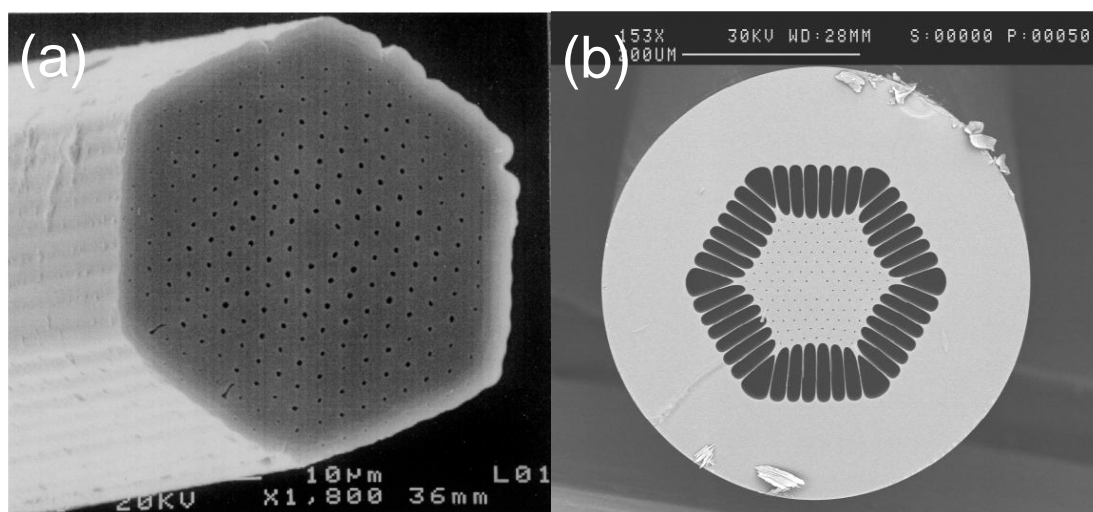


Fig 1.6 Scanning electron micrograph (SEM) of (a) the first photonic crystal fiber [34], and (b) the first photonic crystal fiber operated at high power levels [36].

The other advantage of the PCF is the possibility of forming the double-cladding fiber with an air-cladding [39-41]. The double cladding PCF can be achieved by surrounding the inner cladding with a web of silica bridges as depicted in Fig. 1.8, which are substantially narrower than the wavelength of the guided radiation. The result is a significantly greater index difference between the inner and surrounding region, and therefore a higher numerical aperture to about 0.8, than can be achieved in conventional double-clad fibers with the low-refractive index polymer cladding. Furthermore, removal of the polymer from the also improves the long-term reliability of the fiber, especially for high power operation. Besides, higher numerical aperture allows for reducing the diameter of the inner cladding that permits the shorter fiber

Ch1 Introduction: backgrounds and motivations

absorption length owing to the increased overlap ratio of the core to the inner cladding.

Due to the low N.A. of the fiber core, the confinement of the fundamental mode is very weak and sensitive to perturbations, especially bending losses. Large outer cladding up to 1.5 mm is primarily introduced to keep the fiber straight and is referred to as fiber rod or rod-type fiber [42-43], hence preventing bend-induced losses or distortions of the weakly guided fundamental mode. Thus, in such a straight structure the large mode area is accessible over the whole fiber length, which is not the case for conventional bent large mode area fibers. Besides, the outer cladding makes the fiber mechanically robust on its own, so that no coating material is applied allowing for straightforward high power extraction.

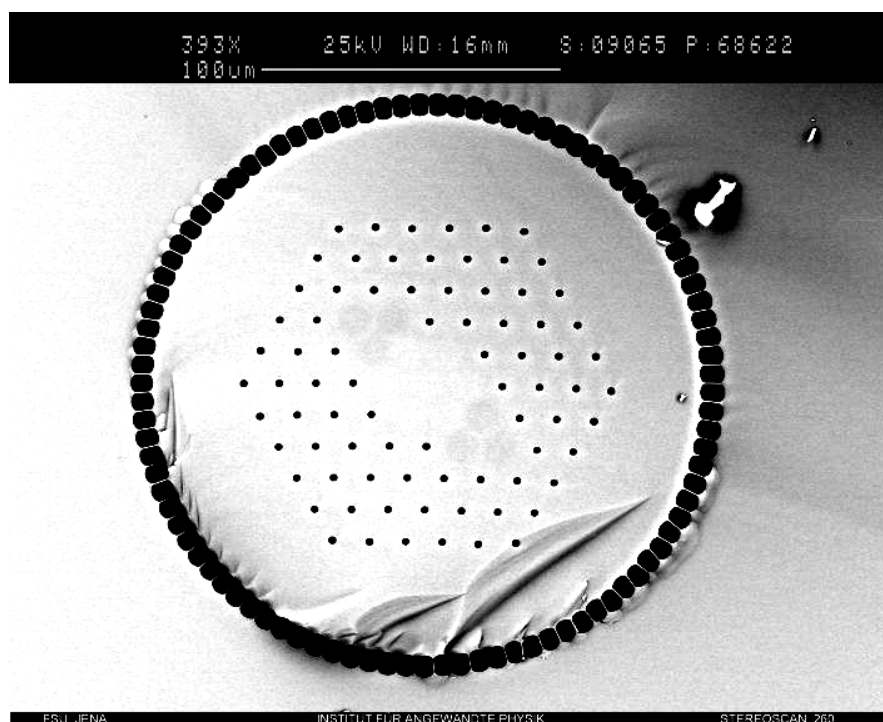


Fig 1.7 SEM image of the PM Yb-doped air-clad photonic crystal fiber with six index-matched stress applying parts [37].

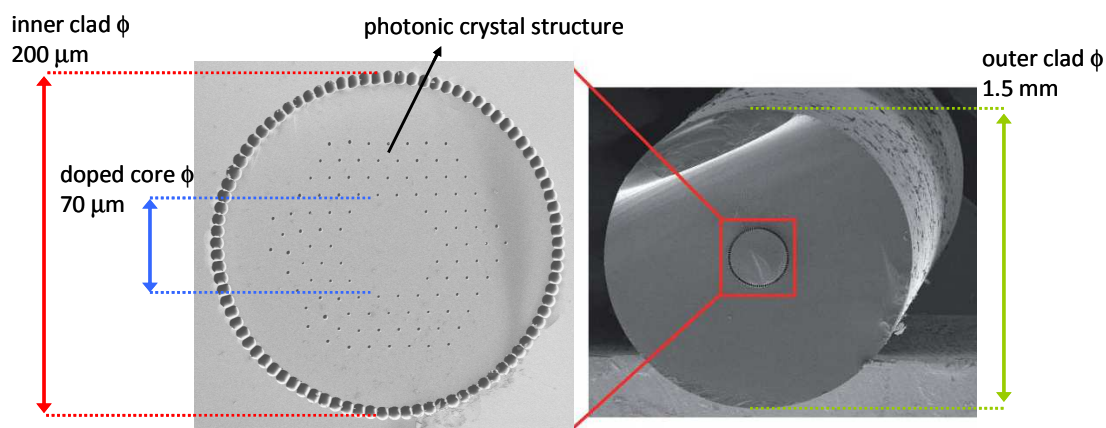


Fig 1.8 SEM image of the cross-section of the large-mode-area, double cladding PCF with a zoom in the embedded micro-structured parts [41].

The combination of sub-mJ to multi-mJ of pulse energies, multi-nanosecond of pulse width, tens of kW to hundreds of kW of peak power, and a compact cavity arrangement without the need of active cooling make fiber lasers and amplifiers attractive alternatives to comparable solid state lasers for pulsed laser applications, such as micro-machining, nonlinear wavelength conversion, range finding, and remote sensing. There are two methods of generating the desired light sources, one by the Q-switched fiber laser oscillator and the other by the master oscillator of power amplifier. Both of these solutions utilize the technique of Q-switching in either the fiber laser oscillator or the seed laser cavity to generate nanosecond pulses. This requires the incorporation of some element within the laser cavity to switches the optical loss of the cavity from high to low during a suitably short time scale. Controlling the Q-value of the cavity could allow the oscillator to store ultra-high gain than CW regime and can emit higher energy within a short duration. Both actively Q-switching (AQS) and passively Q-switching (PQS) can be employed to modulate the cavity Q-value to produce pulses with high energy. Below are the researches in this thesis.

(A). Passively Q-switched fiber lasers

In comparison with AQS, for PQS lasers, the losses are automatically modulated with a saturable absorber (SA). The advantages of the PQS include simplicity and cost-effectiveness due to the lack of high power driving devices, and suitability for

very high pulse repetition rates. Various approaches to PQS fiber lasers have been demonstrated in the literature based on a number of different material approaches which include the use of crystals such as $\text{Co}^{2+}:\text{ZnS}$ [44], $\text{Co}^{2+}:\text{ZnSe}$ [45], $\text{Cr}^{4+}:\text{YAG}$ [46], semiconductor saturable absorbers [47], and graphene [58]. However, the performance of the developed system mentioned above were restricted within low average output power (less than 10 W) and low pulse energy (lower than 0.1 mJ) by not only the fiber core size but also the mechanical stability such as thermal management and damage threshold of SAs.

In this section, I utilize a $\text{Cr}^{4+}:\text{YAG}$ crystal with the initial transmission of 28% as the SA to Q-switch a conventional Yb-doped LMA fiber (fiber core diameter of 30 μm). Moreover, I also demonstrate the PQS fiber laser with the same LMA fiber by using the semiconductor saturable absorber (SESA) as the Q-switch element. The AlGaInAs quaternary alloy with a larger conduction band offset can provide a better electron confinement covering the 0.84–1.65 μm spectral region [49-50] and lattice-matching to their substrate of InP in comparison with the traditional InGaAsP materials. Here, I use the AlGaInAs/InP periodic multi-quantum-wells (MQWs) saturable absorber with the same initial transmission as in the $\text{Cr}^{4+}:\text{YAG}$ experiment for comparison. Besides, by means of using the PCF with the core diameter up to 70 μm , I also perform the energy scaling with either the $\text{Cr}^{4+}:\text{YAG}$ or the AlGaInAs/InP MQWs as the SAs.

(B). Master oscillator of fiber amplifiers

Although the PQS fiber laser offers the benefits of compactness and simplicity, it does not provide the feasibility of controlling the output temporal pulse shape limited by the cavity length (generally the fiber length) in the order of sub-meters to multi-meters. In master oscillator of power amplifier (MOPA) sources, a low-power laser acts as the seeder for a single or multistage amplifier. As such, MOPAs enable function separation and independent optimization of the spectral and temporal aspects of the pulse formation and the generation of high power. The great majority of nanosecond pulsed fiber-based MOPAs have featured a Q-switched bulk solid-state laser as the master oscillator [38, 51-53]. Such bulk DPSS sources exhibit an extremely compact form factor that is very amenable to integration in a fiber-based system, as well as a short cavity that naturally yields pulses of ~ 1 ns or shorter at

Ch1 Introduction: backgrounds and motivations

multikilohertz repetition rates, with pulse energies $\sim 10 \mu\text{J}$, while providing support for single longitudinal mode operation.

Here, I use both the AQS and the PQS diode-pumped solid state lasers (DPSSL) as the seed laser for amplification. Nd:GdVO₄ AQS laser by a Raman-Nath type of acoustic-optics modulator is employed as the seed to amplify the conventional LMA fiber. Besides, I also apply the PQS Nd:YVO₄/Cr⁴⁺:YAG laser as the master oscillator to demonstrate the high-pulse-energy amplification with either the conventional LMA fiber or the PCF. Furthermore, due to the high peak power of the amplified pulses from the MOPA, I utilize the PCF MOPA as the fundamental light source to perform an extracavity second and third harmonic generation (SHG and THG).



1.2 Passively Q-switched Yb-doped crystal lasers

High power, pulsed lasers with high pulse energy (hundreds of microjoule) at a multi-kHz pulse repetition rate (PRR) attract lots of attention owing to widely applications such as material processing (e.g. drilling, cutting, laser marking), nonlinear optics, supercontinuum generation, time-resolved fluorescence measurements, and laser range finding. Continuously diode-pumped Q-switched solid state lasers produce such light source with compactness and high efficiency. There are two methods of generating energetic pulses: actively Q-switching (AQS) and passively Q-switching (PQS). Compared with the AQS scheme that requires high voltage, fast electro-optic driver, or RF generator, PQS offers the advantage of remarkable simple design which leads to compact, robust, and low cost systems.

The rare earth (RE) ions are promising candidates to furnish as active ions in solid state laser gain media because they possess a wealth of sharp fluorescent transitions within nearly every region of the visible and near-infrared (NIR) portions of the electromagnetic spectrum. Generally-known efficient RE ions of diode-pumped solid state lasers in the NIR region have been realized with Nd^{3+} (wavelengths $\lambda \sim 0.9$, 1.06 , and $1.3 \mu\text{m}$), Yb^{3+} ($\lambda \sim 1 \mu\text{m}$), Er^{3+} ($\lambda \sim 1.5$, $3 \mu\text{m}$), Ho^{3+} ($\lambda \sim 2 \mu\text{m}$), and Tm^{3+} ($\lambda \sim 2 \mu\text{m}$). Among these RE ions, the most intensively studied class of solid state lasers is based on the Nd^{3+} -doped laser materials. The Nd^{3+} -ion offers different groups of laser lines in the NIR spectral range that from the ${}^4\text{F}_{3/2}$ upper laser level into the ${}^4\text{I}_{13/2}$ ($\lambda \sim 1.32 \mu\text{m}$), ${}^4\text{I}_{11/2}$ ($\lambda \sim 1.06 \mu\text{m}$), and ${}^4\text{I}_{9/2}$ ($\lambda \sim 0.95 \mu\text{m}$) manifolds. The strongest and most commonly used laser transition for the Nd^{3+} -ion is between ${}^4\text{F}_{3/2}$ and ${}^4\text{I}_{11/2}$ which corresponds to the wavelength at around $1 \mu\text{m}$. On the other hand, the most promising active ion that can be used in a non-Nd laser in the same range of emission wavelength ($\lambda \sim 1 \mu\text{m}$) is Yb^{3+} . Both of the Nd^{3+} and Yb^{3+} laser materials can be efficiently pumped, respectively, at 808nm with InGaAsP/GaAs or AlGaAs/GaAs laser diodes for Nd^{3+} , and between 900 and 980 with InGaAs/GaAs diodes for Yb^{3+} (as depicted in Fig. 1.9).

At the beginning of the high power solid state laser development, the Nd^{3+} -ion

doped materials were preferred to the Yb^{3+} -ion doped ones mainly due to the four level property and their many absorption lines such as 808 nm ($^4\text{I}_{9/2} \rightarrow ^4\text{F}_{5/2}$), 880 nm ($^4\text{I}_{9/2} \rightarrow ^4\text{F}_{3/2}$), 914 nm ($^4\text{I}_{9/2} \rightarrow ^4\text{F}_{3/2}$), and 938 nm ($^4\text{I}_{9/2} \rightarrow ^4\text{F}_{3/2}$), which are more convenient as far as flash lamp pumping is concerned. However, as for efficient and high average power laser diode pumping, Yb^{3+} -ion doped materials are more suited because of their very simple electronic level structure which consists on two manifolds as shown in in Fig. 1.9. The ground state $^2\text{F}_{7/2}$ and the excited state $^2\text{F}_{5/2}$ manifolds, which are separated by an energy of about 10000 cm^{-1} (as depicted in Fig. 1.10). This simple energy level structure allows avoiding most of the parasitic effects such as cross relaxation, up-conversion, and excited-state-absorption (ESA) which are present in Nd^{3+} -ion doped materials because of the existence of higher excited-state energy levels ($^4\text{G}_{9/2}$ manifolds for laser emission at $1 \mu\text{m}$). Besides, due to the small Stokes shift between pump and laser transitions and the related small quantum defects (typically 500 cm^{-1}). In fact, when pumped at 980 nm the quantum defect for Yb^{3+} -ion is around 5% compared to 30% for Nd^{3+} -ion (in YAG host). The heat generation in the laser radiation process of Yb^{3+} -ion is small and makes it suitable for high average power lasers.

For high-pulse-energy Q-switched lasers, the energy storage capability of a material is of principal interest. Obviously, high radiative lifetime of the upper laser level allows a material to store more energy for a given pump rate, which is unambiguously helpful for Q-switched operation. The long radiative lifetime of the $^2\text{F}_{5/2}$ excited manifold of Yb:YAG crystal was found to be about 1 ms which is almost 4 times longer than the 0.23 ms lifetime of the $^4\text{F}_{3/2}$ upper manifold of Nd:YAG. Besides, the small emission cross section (σ) of Yb:YAG ($2.1 \times 10^{-20} \text{ cm}^{-2}$) supports larger pulse energies compared to Nd:YAG ($\sigma = 28 \times 10^{-20} \text{ cm}^{-2}$) in the same wavelength regime, as the pulse energy of a PQS laser is proportional to the saturation energy of the gain medium which is inversely proportional to the emission cross section. For large emission cross section, amplified spontaneous emission (ASE) can prematurely depopulate the upper laser level, clamping the obtainable inversion density and limiting the output pulse energy.

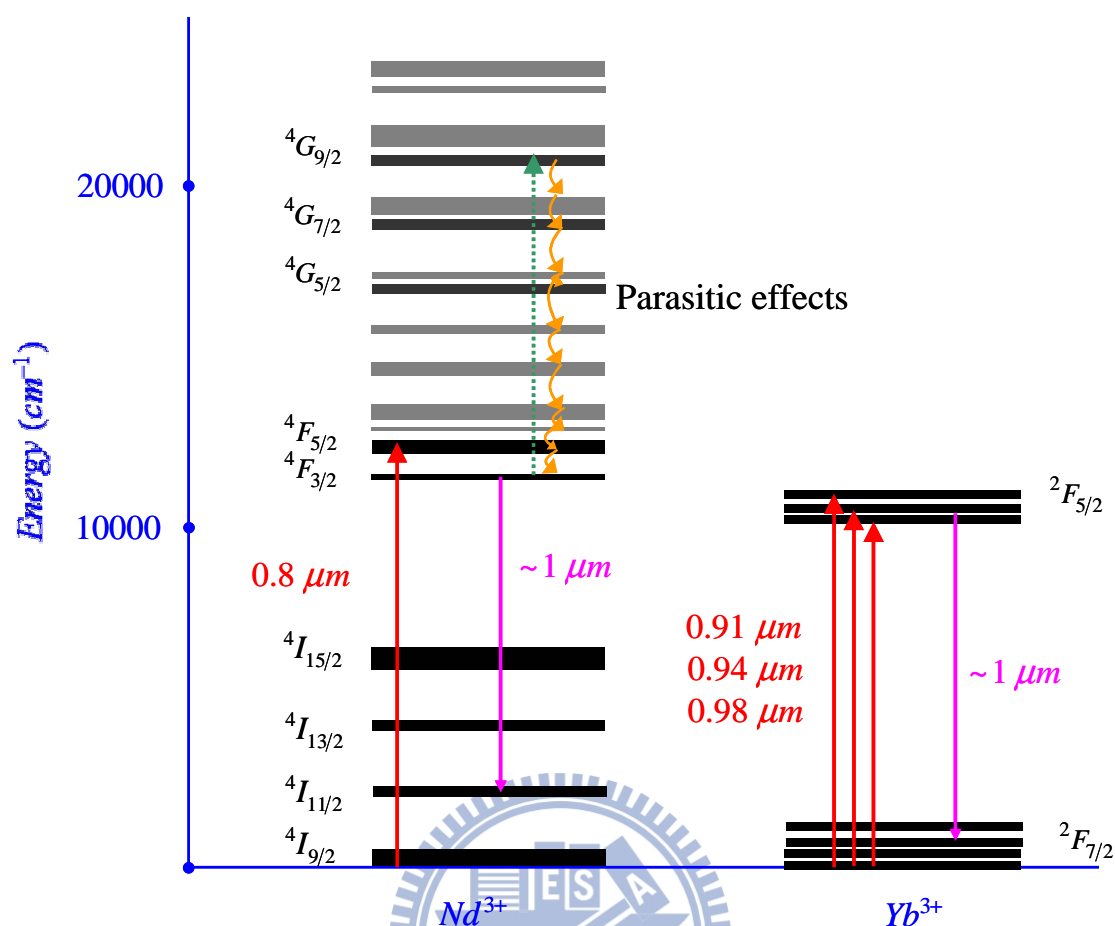


Fig 1.9 Energy level scheme of Nd and Yb ion.

PQS laser of various Yb-doped laser crystals (Yb:YAG crystal [54-55], Yb:Y₂O₃ ceramics [56], Yb:NLM [57], Yb:LYSO [58], Yb:LuAG [59], Yb:NaGdW [60], Yb:GAB [61], Yb:YAG ceramics [62], Yb:YSAG [63], Yb:CYB [64], and so on) with different saturable absorber (SA) such as InGaAs/GaAs quantum wells [54], Cr⁴⁺:YAG [55, 57, 59-63], GaAs [56], and V:YAG [64] have been demonstrated. Some output characteristics of Yb-doped PQS lasers with different SAs in various experimental setups are listed in in Table 1.1. Yttrium aluminum garnet, Y₃Al₅O₁₂ (YAG) is stable, hard, optically isotropic, and have good thermal conductivities, which permits laser operation at high average power levels and can be fabricated in a manner that yields rods of high optical quality. At the present time, it is the best commercially available and most widely investigated crystalline laser host for Yb³⁺-ion. Comparing with Nd:YAG crystals, Yb:YAG crystals have longer fluorescence lifetimes [65], smaller emission cross sections [66], low quantum defects, and broad absorption bandwidths [66]. Therefore, the Yb:YAG microchips have been employed to construct high pulse- energy light sources with stability, compactness,

and reliability

Ref.	Gain medium	SA	P_{in}	P_{out}	Energy	Pulse width	Repetition rate
54	Yb:YAG crystal	InGaAs/GaAs	0.48W	0.01W	1.1 μ J	0.53 ns	12 kHz
55	Yb:YAG crystal	Cr ⁴⁺ :YAG	1.2W	0.12W	13 μ J	0.48 ns	9.2 kHz
56	Yb:Y ₂ O ₃ ceramics	GaAs	17.7W	0.51W	7.7 μ J	50 ns	52.6 kHz
57	Yb:NLM	Cr ⁴⁺ :YAG	0.18W	0.07W	2.8 μ J	60 ns	25 kHz
58	Yb:LYSO	Cr ⁴⁺ :YAG	3W	0.17W	6.4 μ J	5.6 μ s	27 kHz
59	Yb:LuAG	Cr ⁴⁺ :YAG	0.77W	0.24W	19 μ J	0.61 ns	12.8 kHz
60	Yb:NaGdW	Cr ⁴⁺ :YAG	7.7W	2.05W	154 μ J	33 ns	13.3 kHz
61	Yb:GAB	Cr ⁴⁺ :YAG	1.9W	0.74W	165 μ J	30 ns	4.5 kHz
62	Yb:YAG ceramics	Cr ⁴⁺ :YAG	2.55W	0.48W	125 μ J	1.2 ns	3.8 kHz
63	Yb:YSAG	Cr ⁴⁺ :YAG	3.78W	0.39W	31 μ J	2.5 ns	12.7 kHz
64	Yb:CYB	V:YAG	6.6W	0.15W	14 μ J	46 ns	11 kHz

Table 1.1: Some output characteristics of Yb-doped PQS lasers published in literatures.

In 2001, Spühler et al. [54] reported the first PQS Yb:YAG laser using a 20-at %-doped Yb:YAG plate with 200- μ m of thickness and a semiconductor saturable absorber mirrors (SESAMs). Because of its extremely short cavity length, this microchip laser was able to emit 530-ps-long pulses with 1.1 μ J of pulse energy at 12

Ch1 Introduction: backgrounds and motivations

kHz pulse repetition rate. Also in 2001, Dong et al. [67] were the first to use Cr^{4+} :YAG to passively Q-switch a Yb:YAG laser. They used a Ti:sapphire-pumped Yb:YAG PQS laser with Cr^{4+} :YAG crystal as the SA to generate pulses with pulse duration of 350 ns and 3.2 μJ of pulse energy at 17 kHz of repetition rate. Later in 2006, Ostby and co-workers [68] operated their microchip laser using Yb:YAG ceramic as the gain medium and claimed that their ceramic material was competitive with crystalline Yb:YAG in terms of output performance. In order to attain operation with single linear polarization, they employed a small Brewster window inside the laser cavity. The ceramic Yb:YAG laser operated in multi-longitudinal mode producing pulses with pulse duration of 1.9 ns and 63 μJ of pulse energy at 11.4 kHz of repetition rate. Dong et al. [69] built an all-ceramic microchip laser with 9.8-at%-doped ceramic Yb:YAG gain section with thickness of 1 mm and 0.2 mm-thick ceramic Cr^{4+} :YAG which produced 380-ps-long pulses with about 30 μJ of pulse energy. The laser operated in single longitudinal mode at pulse repetition rate up to 4 kHz. Later in 2007, the same group demonstrated a composite Yb:YAG/ Cr^{4+} :YAG ceramics laser [70] that emitted pulses with peak power of 0.72 MW. The pulse energy was 172 μJ at the repetition rate of 3.5 kHz. The laser oscillated at stable single- and multi- longitudinal-modes due to the combined etalon effects in the Yb:YAG and Cr^{4+} :YAG parts of its binary structure.

However, as a disadvantage connected with the small Stokes shift between pump and laser transitions, Yb-doped lasers operate in a quasi-three-level scheme. The room temperature absorption and emission spectra of Yb:YAG crystal is shown in Fig. 1.10. The main emission transition at 1030 nm is between the lowest Stark level of the $^2\text{F}_{5/2}$ manifold at 10327 cm^{-1} and the Stark level of the ground $^2\text{F}_{7/2}$ manifold at 612 cm^{-1} (as depicted in Fig. 1.11). The thermal energy at room temperature is 200 cm^{-1} ; therefore the terminal laser level is thermally populated that makes Yb:YAG a quasi-three-level system. At room temperature, the thermal population of the terminal laser level is about 5.5%. Thus, at least 5.5% of all Yb ions must be pumped into the initial laser Stark level to achieve gain material transparency. This implies two deleterious effects when temperature increases: (1) a reduction of the the laser inversion population which strongly relates to the laser optical efficiency, (2) an increase of the reabsorption at the laser wavelength. Therefore, a special care concerning the thermal load and thermal management will be then necessary to develop efficient lasers based on Yb-doped materials.

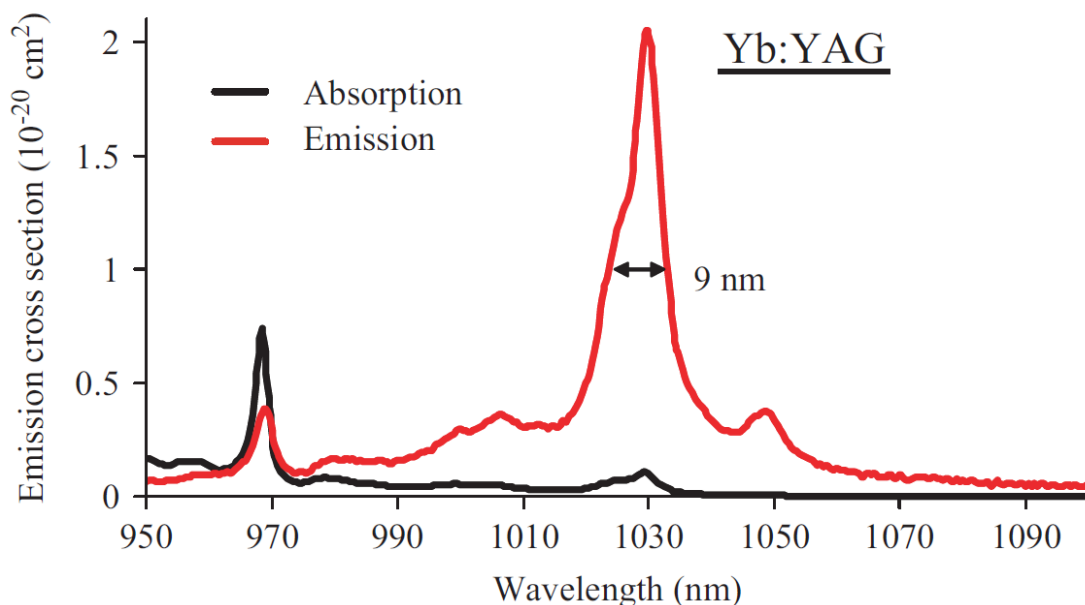


Fig. 1.10 300K absorption and emission spectra of Yb:YAG crystal [71].

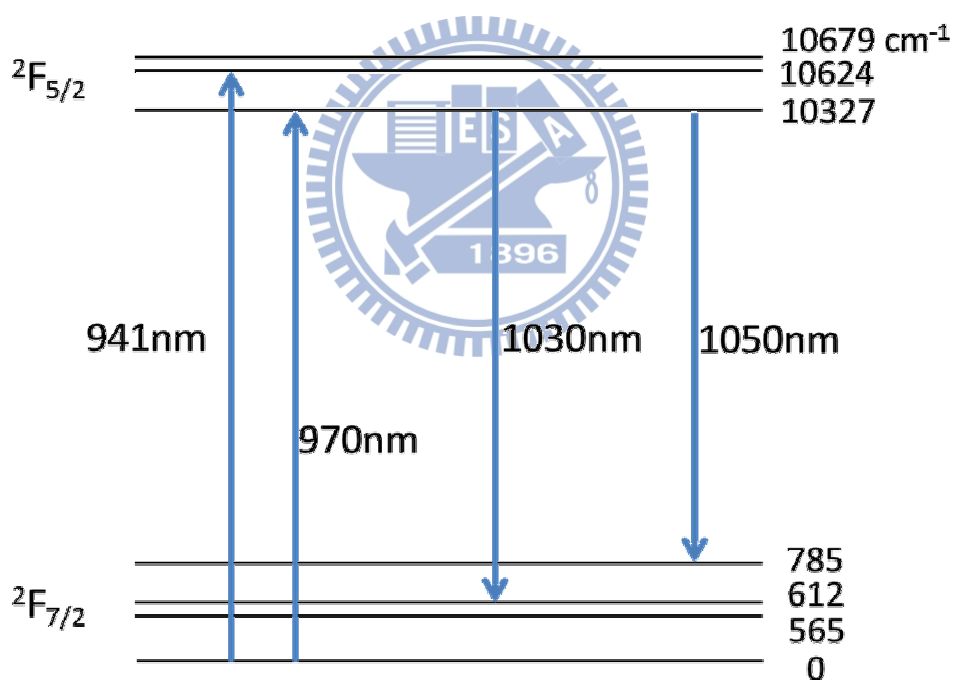


Fig. 1.11 Energy level scheme of Yb ion.

A proper geometry of the gain medium can improve the thermal management for solid state laser gain materials with a specific pump and laser wavelength constellation. A large ratio between the cooled surface and the pumped volume as well as a short distance between them is essential for a good heat removal. The rod type of solid state laser gain medium in geometry is most widely used nowadays. However,

the beam quality is limited as the heat flow via the edgeways area of the rod which give rise to a radial heat gradient as shown in Fig. 1.12(a). This radial heat gradient results in strong thermal lensing and, further, the resulting tensions between the colder surface areas and the hot pump volume can easily cause cracking of the rod.

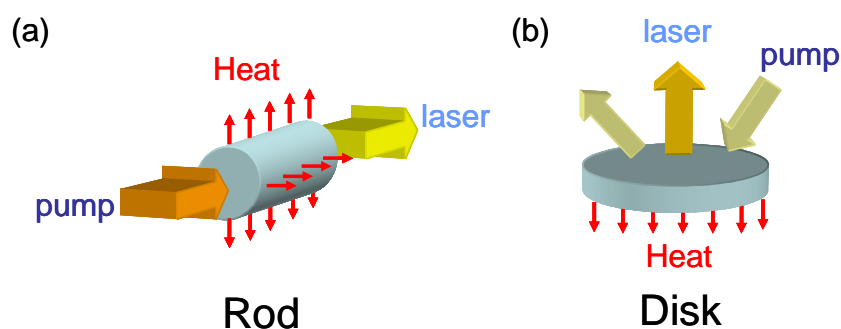


Fig. 1.12 Schematic of the geometries for solid state laser materials for (a) rod and (b) disk.

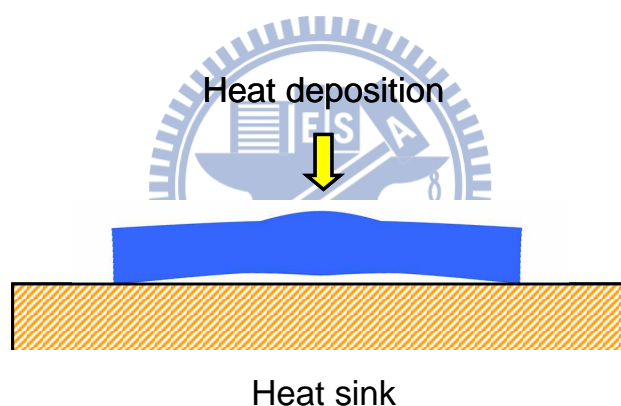
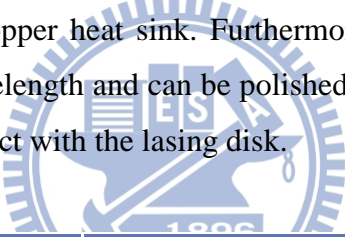


Fig. 1.13 Deformation of a face-pumped disk with backside cooling.

As depicted in Fig. 1.12(b), the active medium of a few hundred micrometers to nearly one millimeter thick has a shape of a disk. The back side of the disk is coated with highly reflection for the pump and the laser wavelengths and attached onto a water-cooled heat sink so that an efficient heat removal through the whole backside of the disk is realized. Since the heat is extracted from the backside of the disk, the thermal gradients approach a longitudinal cooling geometry that is along the pump direction. Thus, the thermal distortions are minimized and the beam quality is improved than in the rod geometry. Nevertheless, there is still some beam distortion arising from the bending and bulging of the disk as shown in Fig. 1.13. The bend comes from a larger thermal expansion on the pumped side of the disk compared to

the cooling side bounded onto the heat sink. The bulging is the result of the finite pump beam diameter causing a concentration of heat deposition at the center of the crystal. These effects inevitably increase the scattering loss and reduce the heat removal efficiency owing to the limited contact surface between the disk and the heat sink. Therefore, more suitable and efficient thermal management method is derivable for Yb:YAG microchip laser that use a disk form of gain chip.

Recently, the exceptional optical and mechanical properties together with high thermal conductivity of the synthetic diamond have attracted increasing interest for thermal management in optically pumped solid-state lasers-in in semiconductor disk lasers [72] and Nd-doped vanadate lasers [73-75]. Used with doped crystal lasers, diamond can help to ameliorate thermal lensing and stress; with semiconductors, it helps to reduce the temperature rises that limit the output power. As list in Table 1.2, the diamond has higher thermal conductivity than sapphire that used to minimized the physical distortion mentioned above by clamping down the gain disk between the sapphire window and the copper heat sink. Furthermore, the diamond windows are transparent at the pump wavelength and can be polished to optical quality so that they can be brought in close contact with the lasing disk.



Material	Thermal Conductivity (W·m⁻¹·K⁻¹)
Diamond	1900-2200 (at 300K) 1500-1600 (at 425K)
Sapphire	18.7-20.2 (at 310K)
Copper	401 (at 300K)
Nd:YAG	10.5-14 (at 293-373K)
Nd:YVO4	5.1-5.2 (at 300K)
Yb:YAG	14 (at 293K)

Table 1.2: Thermal conductivities with different materials.

In this section, I utilize the diamond as the heat spreader that directly attach onto the pump side of the pump side of the Yb:YAG gain chip to eliminate the beam distortion arising from the bending and bulging of the disk. A Cr⁴⁺:YAG crystal with the initial transmission of 84% as the SA to form a PQS Yb:YAG microchip laser.

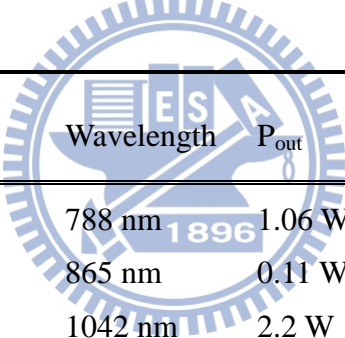
1.3 Mode-locked Yb doped crystal lasers

Pulsed lasers with repetition rates of multi-gigahertz attract noticeable interest due to its wide applications. Mode-locked laser pulses with pulse duration that ranges from picosecond to femtosecond at such repetition rates are required for various applications such as wireless communication [76], telecommunications [77], quantum communication [78], optical clocking [79], high-speed optical sampling [80], high signal-to-noise ratio measurements [81], nonlinear bio-photonic application [82], photonic switching [83], and large-mode-spacing supercontinuum generation [84]. Various schemes are intensively being investigated to generate mode-locked pulses for achieving such high repetition rate. Actively and passively, harmonically mode-locked fiber lasers are one of the general approaches to reach such high repetition rate [85-86]. Pulse repetition rate up to 200 GHz can be attained but at the cost of a high complexity due to harmonic mode locking and relatively low output powers of at most a few tens of milliwatts. Quantum-well Fabry–Perot lasers [87] and quantum-dash-based Fabry–Perot mode-locked laser [88] are also candidates. Pulse duration of 10 ps and 0.9 ps at the repetition rate of 100 GHz and 134 GHz was obtained with the Quantum-well laser and the quantum-dash-based laser, respectively. However, the average output powers were limited to a few tens of milliwatts. Optically pumped mode-locked vertical-external cavity surface-emitting semiconductor lasers (VECSELs) that are passively mode-locked with a semiconductor saturable absorber (SESAM) [89-90] at fundamental repetition rate can generate in sub-picosecond pulses of good quality with higher average power up to 220 mW. By harmonically mode-locking, the VECSELs can also generate mode-locked pulses with repetition rate up to 92 GHz [91-92]. Nevertheless, the average output powers were still relatively small.

Rare earth ion-doped solid-state lasers are promising for their potential to generate mode-locked pulse trains with high average powers in diffraction-limited beams [93-95]. They feature efficient, robust, compact, and reliable operation. Repetition rate up to 160 GHz can be achieved with a Nd:YVO₄ laser [93] with average output power of 50 mW and pulse duration of 2.7 ps. However, the laser

Ch1 Introduction: backgrounds and motivations

should use Ti-sapphire lasers with high brightness as the pump source. With diode-pumped scheme, the pulse repetition rate was limited to be 40 GHz for the Nd:YVO₄ laser [94] and 100 GHz for the Er:Yb:glass laser [95] at the spectral range of 1.06 μm and at 1.5 μm , respectively. These lasers were all operated at the fundamental repetition rate that corresponds inversely to the cavity round trip times. Nevertheless, due to their relatively low laser cross sections, they exhibit a strong tendency toward Q-switched modelocking (QML) when they are operated with short cavities to achieve high repetition rate operation. The mode-locked pulse train is further modulated in amplitude with a long Q-switched envelope [96]. For this reason, the repetition rates of passively mode-locked ion-doped solid-state lasers were limited. Therefore, there were only a few demonstrations of diode-pumped solid state lasers that combines gigahertz pulse repetition rates and femtosecond pulse durations. An overview of fundamentally mode-locked diode-pumped solid state lasers with pulse repetition rate higher than 1GHz is given in Table 1.3.



Ref.	Gain medium	Wavelength	P_{out}	Pulse width	Repetition rate
97	Ti-sapphire	788 nm	1.06 W	42 fs	10 GHz
98	Cr:LiSAF	865 nm	0.11 W	55 fs	1 GHz
99	Yb:KGW	1042 nm	2.2 W	290 fs	1 GHz
100	Yb:KGW	1043 nm	1.9 W	396 fs	4.8 GHz
101	Yb:KYW	1045 nm	0.68 W	162 fs	2.8 GHz
102	Yb:KYW	1047 nm	0.05 W	168 fs	1.2 GHz
94	Nd:YVO ₄	1064 nm	0.29 W	6.5 ps	40 GHz
95	Er:Yb:glass	1550 nm	0.04 W	1.1 ps	100 GHz

Table 1.3: Overview of fundamentally mode-locked diode-pumped solid state lasers with pulse repetition rate higher than 1GHz.

Harmonic modelocking (with multiple pulses circulating in the laser cavity) give another solution for generating high repetition rate of a solid-state laser [103]. An advantage of this approach is that the QML tendency, which depends on the cavity length, is then weaker compared to the case of a short fundamentally mode-locked laser with the same repetition rate. Spontaneous subpicosecond pulses with pulse repetition rate of 80 GHz at the tenth-order harmonic mode-locked operation. Pulse

Ch1 Introduction: backgrounds and motivations

duration of 616 fs was attained under the average output power of 0.45 W which, for the first time, demonstrated the mode-locked operation with subpicosecond pulses at pulse repetition rate higher than 10 GHz in the 1 μm spectral regime. The etalon effect formed by the separation between the laser crystal and the input mirror plays an important role in modulating the optical spectrum of the mode-locked laser [104]. The intracavity etalon results in the coupled cavity effect within the original cavity. Coupled cavity effect was used to obtain higher pulse repetition rate in passively mode-locked lasers [105-108].

Consider a linear cavity with optical length l . The pulse repetition rate R is equal to $c/2l$, where c is the speed of light. When coupled cavity is introduced, the original cavity was divided into two subcavities which named main cavity with cavity length of l_m and external cavity with cavity length of l_e , where $l_m + l_e = l$. When $l_m/l_e = N/M$ is a ration number (N and M are positive integers with no common denominators), for each split of pulse at the interface of the two subcavities, the reflected pulse lags either $M/[(M+N)R]$ or $N/[(M+N)R]$ in time behind the transmitted pulse. With this effect, the time interval between any split intracavity pulse and the initial pulse can be expressed as $K/[(M+N)R]$, where K is an integer ranged from 0 to $M+N-1$. When the system is mode-locked, there will be N pulses circulating in the main cavity and M pulses circulating in the external cavity. The final number of intracavity pulses is therefore $M+N$, and the pulse repetition rate is multiplied to $(M+N)R$. This means that, for a given laser cavity length, one can multiply the pulse repetition rate by choosing an appropriate ratio of the subcavity lengths.

Yb:YAG laser medium has low quantum defects and high quantum efficiencies. Moreover, the host YAG has a high thermal conductivity and high tensile strengths. Thus, Yb:YAG lasers are considered as a candidate for efficient high-power femtosecond-pulse laser sources. Efficient, femtosecond-pulse mode-locked operations have been demonstrated in passively mode-locked scheme [109-111] and Kerr-lens mode-locked (KLM) scheme [112-114]. For both SESAM based and Kerr-lens modelocking experiments, although pulses as short as 35 fs were generated from the Kerr-lens mode-locked operation [114], pulse repetition rate from the Yb:YAG laser oscillators remained below 1GHz.

In this section, I demonstrate a high-power high-repetition-rate self-mode-locked lasers with a Yb:YAG microchip in a linear Fabry-Perot cavity. The front surface of

Ch1 Introduction: backgrounds and motivations

the gain medium is coated to form a cavity mirror and is bonded with a diamond heat spreader to reduce the thermal effects. The rear surface of the Yb:YAG plate is coated not only to lead to a second pass of the pump light but also to play an etalon for achieving harmonic mode locking. Furthermore, a semiconductor saturable absorber mirror (SESAM) is incorporated into the cavity for dual wavelength operation. With the specially fabricated SESAM, I successfully develop a high-power dual-wavelength harmonically mode-locked Yb:YAG laser.



Reference

- [1]. E. Snitzer, "Proposed fiber cavities for optical lasers," *J. Appl. Phys.* **32**, 36–39 (1961).
- [2]. E. Snitzer, "Optical maser action of Nd^{3+} in a barium crown glass," *Phys. Rev. Lett.* **7**, 444–446 (1961).
- [3]. C. J. Koester and E. Snitzer, "Amplification in a fiber laser," *Appl. Opt.* **3**, 1182–1186 (1964).
- [4]. J. Stone and C. A. Burrus, "Neodymium-doped silica lasers in end-pumped fiber geometry," *Appl. Phys. Lett.* **23**, 388–389 (1973).
- [5]. S. B. Poole, D. N. Payne, and M. E. Fermann, "Fabrication of low loss optical fibres containing rare-earth ions," *Electron. Lett.* **21**, 737–738 (1985).
- [6]. R. J. Mears, L. Reekie, S. B. Poole, and D. N. Payne, "Neodymium-doped silica single-mode fibre laser," *Electron. Lett.* **21**, 738–740 (1985).
- [7]. R. J. Mears, L. Reekie, I. M. Jauncey, and D. N. Payne, "Low-noise erbium-doped fibre amplifier operating at 1.54 μm ," *Electron. Lett.* **23**, 1026–1028 (1987).
- [8]. E. Snitzer, H. Po, F. Hakimi, R. Tumminelli, and B.C. McCollum, "Double-clad, offset core Nd fiber laser," *Optical Fiber Sensors Conference*, New Orleans, 1988, PD5.
- [9]. D. J. DiGiovanni and M. H. Muendel, "High-power fiber lasers and amplifiers," *Opt. Photon. News* **10**, 26–30 (1999).
- [10]. L. Zenteno, "High-power double-clad fiber lasers," *IEEE J. Lightwave Technol.* **11**, 1435–1446 (1993).
- [11]. A. Bertoni and G. C. Reali, "A model for the optimization of double-clad fiber laser operation," *Appl. Phys. B* **66**, 547–554 (1998).
- [12]. E. M. Dianov, A. V. Belov, I. A. Bufetov, V. N. Protopopov, A. N. Gur'yanov, D. D. Gusovski, and S. V. Kobis', "High-power single-mode neodymium fibre laser," *Quantum Electron.* **27**, 1-2 (1997).
- [13]. A. Liu and K. Ueda, "The absorption characteristics of circular, offset, and

- rectangular double-clad fibers,” *Optics Commun.* **132**, 511-518 (1996).
- [14]. H. Zellmer, A. Tünnermann, H. Welling, and V. Reichel, “Double-clad fiber laser with 30 W output power,” in: *Optical Amplifier and their Applications* (Optical Society of America, Washington D.C.), paper WC7-1, 251 (1997).
- [15]. E. Snitzer, H. Po, F. Hakimi, R. Tumminelli, and B.C. McCollum, “Double-clad offset core Nd fiber laser,” in *Proc. Of Optical Fiber Sensors '88*, Optical Fiber Sensors Conference, New Orleans, PD5 (1988).
- [16]. H. Po, E. Snitzer, R. Tumminelli, L. Zenteno, F. Hakimi, N.M. Cho, and T. Haw, “Double-clad high brightness Nd fiber laser pumped by GaAlAs phased array,” in *Optical Fiber Communication Conference* (Optical Society of America, Washington, D.C.), Pp. PD7 (1989).
- [17]. M. Muendel, “Optimal inner cladding shapes for double-clad fiber lasers,” in *Conference on Lasers and Electro-Optics, Technical Digest*, (Optical Society of America, Washington DC), pp. 209 (1996).
- [18]. V. Reichel, S. Unger, H.-R. Müller, and H. Zellmer, “High-power single-mode Nd-doped fiber-laser,” *Solid State Lasers VII. Proc. SPIE 3265*, 192–199 (1998).
- [19]. H. Zellmer, U. Willamowski, A. Tünnermann, H. Welling, S. Unger, V. Reichel, H.-R. Müller, J. Kirchhof, and P. Albers, “High-Power cw Neodymium-Doped Fiber Laser Operating at 9.2 W with High Beam Quality,” *Opt. Lett.* **20**, 578–580 (1995).
- [20]. A. Liu and K. Ueda, “The absorption characteristics of rare earth doped circular double-clad fibers,” *Opt. Rev.* **3**, 276-281 (1996).
- [21]. H. W. Etzel, H. W. Gandy. and R. J. Ginther, “Stimulated emission of infrared radiation from ytterbium-activated silicate glass,” *Appl. Opt.* **1**, 534-536 (1962).
- [22]. R. Paschotta, J. Nilsson, A. C. Tropper, and D. C. Hanna, “Ytterbium-doped fiber amplifiers,” *IEEE J. Quantum Electron.* **33**, 1049-1056 (1997).
- [23]. K. Lu and N. K. Dutta, “Spectroscopic properties of Yb-doped silica glass,” *J. Appl. Phys.* **91**, 576-581 (2002).
- [24]. V. P. Gapontsev, I. E. Samartsev, A. A. Zayats. and R. R. Loryan, “Laser diode pumped Yb-doped single-mode tunable fiber laser,” *Conference of advanced solid-state lasers*, Hilton Head, NC, Tech. Dig., paper WCI-I. 214-216 (1991).
- [25]. H. M. Pask, R. J. Carman, D. C. Hanna, A. C. Tropper, C. J. Mackechnie, P. R. Barber, and J. M. Dawes, “Ytterbium-doped silica fiber lasers: versatile sources for the 1-1.2 μ m region,” *IEEE J. Sel. Top. Quantum Electron.* **1**, 2-13 (1995).

- [26]. V. Dominic, S. MacCormack, R. Waarts, S. Sanders, S. Bicknese, R. Dohle, E. Wolak, P. S. Yeh, and E. Zucker, "110 W fibre laser," *Electron. Lett.* **35**, 1158-1160 (1999).
- [27]. Y. Jeong, J. Sahu, D. Payne, and J. Nilsson, "Ytterbium-doped large-core fiber laser with 1.36 kW continuous-wave output power," *Opt. Express* **12**, 6088-6092 (2004).
- [28]. V. Fomin, M. Abramov, A. Ferin, A. Abramov, D. Mochalov, N. Platonov, and V. Gapontsev, "10kW single mode fiber laser," SyTu-1.3, Symposium on High-Power Fiber Lasers, 14th International Conference, Laser Optics 2010, St. Petersburg, Fla. (2010).
- [29]. J. Nilsson and B. Jaskorzynska, "Modeling and optimization of low-repetition-rate high-energy pulse amplification in cw-pumped erbium-doped fiber amplifiers," *Opt. Lett.* **18**, 2099–2101 (1993).
- [30]. J. P. Koplow, D. A. V. Kliner, and L. Goldberg, "Single-mode operation of a coiled multimode fiber amplifier," *Opt. Lett.* **25**, 442-444 (2000).
- [31]. C. C. Renaud, J. A. Alvarez-Chavez, J. K. Sahu, J. Nilsson, D. J. Richardson, and W. A. Clarkson, "7.7 mJ pulses from a large core Yb-doped cladding pumped Q-switched fibre laser," CLEO 2001 Baltimore 6-11 May 2001 CTuQ5 (2001).
- [32]. F. D. Teodoro, J. P. Koplow, S. W. Moore, and D. A. V. Kliner, "Diffraction-limited, 300-kW peak-power pulses from a coiled multimode fiber amplifier," *Opt. Lett.* **27**, 518-520 (2002).
- [33]. J. C. Knight, T. A. Birks, P. S. J. Russell, and D. M. Atkin, "All-silica single-mode optical fiber with photonic crystal cladding," *Opt. Lett.* **21**, 1547-1549 (1996).
- [34]. T. A. Birks, J. C. Knight, and P.S. J. Russell, "Endlessly single-mode photonic crystal fiber," *Opt. Lett.* **22**, 961-963 (1997).
- [35]. J. C. Knight, T. A. Birks, R. F. Cregan, P. S. Russell, and J. P. D. Sandro, "Large mode area photonic crystal fibre," *Electron. Lett.* **34**, 1347–1348 (1998).
- [36]. J. Limpert, T. Schreiber, S. Nolte, H. Zellmer, A. Tünnermann, R. Iliew, F. Lederer, J. Broeng, G. Vienne, A. Petersson, and C. Jakobsen, "High-power air-clad large-mode-area photonic crystal fiber laser," *Opt. Express* **11**, 818-823 (2003).
- [37]. T. Schreiber, F. Röser, O. Schmidt, J. Limpert, R. Iliew, F. Lederer, A. Petersson, C. Jacobsen, K. Hansen, J. Broeng, and A. Tünnermann, "Stress-induced

- single-polarization single-transverse mode photonic crystal fiber with low nonlinearity," *Opt. Express* **13**, 7621-7630 (2005).
- [38]. C. D. Brooks and F. Di Teodoro, "Multimegawatt peak-power, single-transverse-mode operation of a 100 μm core diameter, Yb-doped rodlike photonic crystal fiber amplifier," *Appl. Phys. Lett.* **89**, 111119 (2006).
- [39]. A. Tünnermann, S. Ermeneux, P. Yvernault, and F. Salin, "Extended single-mode photonic crystal fiber lasers," *Opt. Express* **14**, 2715–2720 (2006).
- [40]. W. J. Wadsworth, R. M. Percival, G. Bouwmans, J. C. Knight, and P. S. J. Russell, "High power air-clad photonic crystal fibre laser," *Opt. Express* **11**, 48–53 (2003).
- [41]. O. Schmidt, J. Rothhardt, F. Röser, S. Linke, T. Schreiber, K. Rademaker, J. Limpert, S. Ermeneux, P. Yvernault, F. Salin, and A. Tünnermann, "Millijoule pulse energy Q-switched short-length fiber laser," *Opt. Lett.* **32**, 1551–1553 (2007).
- [42]. J. Limpert, N. Deguil-Robin, I. Manek-Hönninger, F. Salin, F. Röser, A. Liem, T. Schreiber, S. Nolte, H. Zellmer, A. Tünnermann, J. Broeng, A. Petersson, and C. Jakobsen, "High-power rod-type photonic crystal fiber laser," *Opt. Express* **13**, 1055-1058 (2005).
- [43]. T. T. Alkeskjold, M. Laurila, L. Scolari, and J. Broeng, "Single-mode ytterbium-doped large-mode-area photonic bandgap rod fiber amplifier," *Opt. Express* **19**, 7398–7409 (2011).
- [44]. M. Laroche, A. M. Chardon, J. Nilsson, D. P. Shepherd, W. A. Clarkson, S. Girard and R. Moncorgé, "Compact diode-pumped passively Q-switched tunable Er-Yb double-clad fiber laser," *Opt. Lett.* **27**, 1980-1982 (2002).
- [45]. V. N. Philippov, A. V. Kiryanov and S. Unger, "Advanced configuration of erbium fiber passively Qswitched laser with $\text{Co}^{2+}:\text{ZnSe}$ crystal as saturable absorber," *IEEE Photonics Technol. Lett.* **16**, 57-59 (2004).
- [46]. J. Y. Huang, H. C. Liang, K. W. Su, and Y. F. Chen, "High power passively Q-switched ytterbium fiber laser with $\text{Cr}^{4+}:\text{YAG}$ as a saturable absorber," *Opt. Express* **15**, 473-479 (2007).
- [47]. R. Paschotta, R. Häring, E. Gini, H. Melchior, U. Keller, H. L. Offerhaus and D. J. Richardson, "Passively Q-switched 0.1-mJ fiber laser system at 1.53 μm ," *Opt. Lett.* **24**, 388-390 (1999).
- [48]. J. Liu, S. Wu, Q. H. Yang, and P. Wang, "Stable nanosecond pulse generation

- from a graphene-based passively Q-switched Yb-doped fiber laser,” *Opt. Lett.* **36**, 4008-4010 (2011).
- [49]. W. T. Tsang and N. A. Olsson, “New current injection 1.5- μm wavelength $\text{Ga}_x\text{Al}_y\text{In}_{1-x-y}\text{As}/\text{InP}$ double-heterostructure laser grown by molecular beam epitaxy,” *Appl. Phys. Lett.* **42**, 922-924 (1983).
- [50]. N. Nishiyama, C. Caneau, B. Hall, G. Guryanov, M. H. Hu, X. S. Liu, M.-J. Li, R. Bhat, and C. E. Zah, “Long-wavelength vertical-cavity surface-emitting lasers on InP with lattice matched AlGaInAs–InP DBR grown by MOCVD,” *IEEE J. Sel. Top. Quantum Electron.* **11**, 990-998 (2005).
- [51]. A. V. Kir'yanov, S. M. Klimentov, I. V. Mel'nikov, and A. V. Shestakov, “Specialty Yb fiber amplifier for microchip Nd laser: Towards $\sim 1\text{-mJ}/1\text{-ns}$ output at kHz-range repetition rate,” *Opt. Commun.* **282**, 4759-4764 (2009).
- [52]. P. E. Schrader, R. L. Farrow, D. A. V. Kliner, J.-P. Fève and N. Landru, “High-power fiber amplifier with tunable repetition rate, fixed pulse duration, and multiple output wavelengths,” *Opt. Express* **14**, 11528-11538 (2006).
- [53]. C. Ye, M. Gong, P. Yan, Q. Liu, and G. Chen, “Linearly-polarized single-transverse-mode high-energy multi-ten nanosecond fiber amplifier with 50W average power” *Opt. Express* **14**, 7604–7609 (2006).
- [54]. G. J. Spühler, R. Paschotta, M. P. Kullberg, M. Graf, M. Moser, E. Mix, G. Huber, C. Harder, and U. Keller, “A passively Q-switched Yb:YAG microchip laser,” *Appl. Phys. B* **72**, 285-287 (2001).
- [55]. J. Dong, A. Shirakawa and K. Ueda, “Sub-nanosecond passively Q-switched Yb:YAG/ Cr^{4+} :YAG sandwiched microchip laser,” *Appl. Phys. B: Lasers Opt.* **85**, 513-518 (2006).
- [56]. J. Kong, D. Tang, J. Lu, K. Ueda, H. Yagi, and T. Yanagitani, “Passively Q-switched Yb:Y₂O₃ ceramic laser with a GaAs output coupler,” *Opt. Express* **12**, 3560-3566 (2004).
- [57]. A. V. Mandrik, A. E. Troshin, V. E. Kisel, A. S. Yasukevich, G. N. Klavsut, N. V. Kuleshov, and A. A. Pavlyuk, “CW and Q-switched diode-pumped laser operation of Yb³⁺:NaLa(MoO₄)₂,” *Appl. Phys. B* **81**, 1119-1121 (2005).
- [58]. L. Su, D. Zhang, H. Li, J. Du, Y. Xu, X. Liang, G. Zhao, and J. Xu, “Passively Q-switched Yb³⁺ laser with Yb³⁺-doped CaF₂ crystal as saturable absorber,” *Opt. Express* **15**, 2375-2379 (2007).

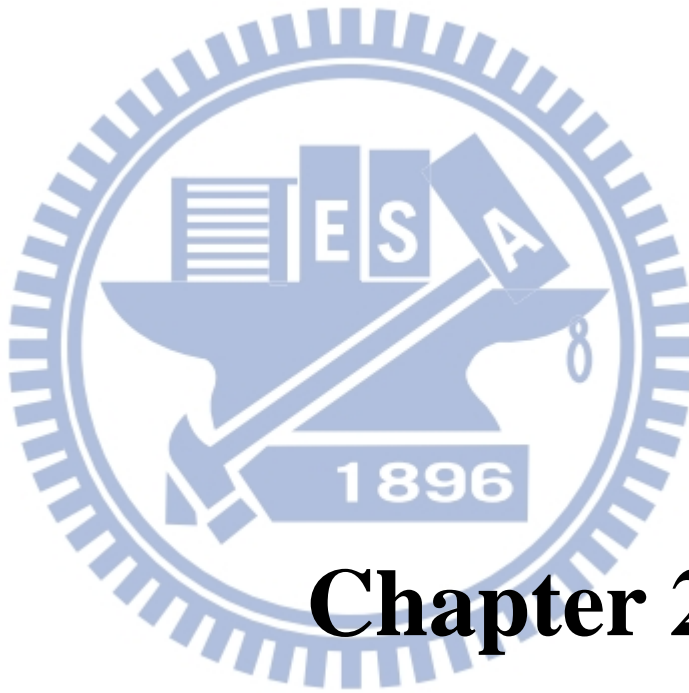
- [59]. J. Dong, K. Ueda, and A. A. Kaminskii, "Efficient passively Q-switched Yb:LuAG microchip laser," *Opt. Lett.* **32**, 3266-3268 (2007).
- [60]. J. Liu, V. Petrov, H. Zhang, J. Wang, and M. Jiang, "Efficient passively Q-switched laser operation of Yb in the disordered NaGd(WO₄)₂ crystal host," *Opt. Lett.* **32**, 1728-1730 (2007).
- [61]. A. Brenier, C. Tu, Z. Zhu, and J. Li, "Diode pumped passive Q switching of Yb³⁺-doped GdAl₃(BO₃)₄ nonlinear laser crystal," *Appl. Phys. Lett.* **90**, 071103 (2007).
- [62]. J. Dong, A. Shirakawa, K. Ueda, H. Yagi, T. Yanagitani and A. A. Kaminskii, "Ytterbium and chromium doped composite Y₃Al₅O₁₂ ceramics self-Q-switched laser," *Appl. Phys. Lett.* **90**, 191106 (2007).
- [63]. J. Dong, K. Ueda, and A. A. Kaminskii, "Continuous-wave and Q-switched microchip laser performance of Yb:Y₃Sc₂Al₃O₁₂ crystals," *Opt. Express* **16**, 5241-5251 (2008).
- [64]. J. L. Xu, J. L. He, H. T. Huang, J. F. Yang, B. T. Zhang, C.-Y. Tu, "Performance of diode pumped Yb:Y₂Ca₃B₄O₁₂ laser with V³⁺:YAG as saturable absorber for passively Q-switched mode-locking operation," *Laser Phys. Lett.* **7**, 198-202 (2010).
- [65]. D. S. Sumida and T. Y. Fan, "Effect of radiation trapping on fluorescence lifetime and emission cross section measurements in solid-state laser media," *Opt. Lett.* **19**, 1343-1345 (1994).
- [66]. H. W. Bruesselbach, D. S. Sumida, R. A. Reeder, and R. W. Byren, "Low-heat high-power scaling using InGaAs-diode-pumped Yb:YAG lasers," *IEEE J. Sel. Top. Quantum Electron.* **3**, 105-116 (1997).
- [67]. J. Dong, P. Deng, Y. Liu, Y. Zhang, J. Xu, W. Chen, and X. Xie, "Passively Q-switched Yb:YAG laser with Cr⁴⁺:YAG as the saturable absorber," *Appl. Opt.* **40**, 4303-4307 (2001).
- [68]. E. P. Ostby, R. A. Ackerman, J. C. Huie, and R. L. Gentilman, "Ceramic Yb:YAG microchip laser," in *Solid State Lasers XV: Technology and Devices*, Proc. SPIE **6100**, 610004 (2006).
- [69]. J. Dong, A. Shirakawa, K. Takaichi, K. Ueda, H. Yagi, T. Yanagitani, and A. A. Kaminskii, "All-ceramic passively Q-switched Yb:YAG/Cr⁴⁺:YAG microchip laser," *Electronics Letters* **42**, 1154-1155 (2006).
- [70]. J. Dong, K. Ueda, A. Shirakawa, H. Yagi, T. Yanagitani, and A. A. Kaminskii,

- “Composite Yb:YAG/Cr⁴⁺:YAG ceramics picosecond microchip lasers,” *Opt. Express* **15**, 14516-14523 (2007).
- [71]. S. Chénais, F. Druon, S. Forget, F. Balembois, and P. Georges, “On thermal effects in solid state laser: the case of Ytterbium-doped materials,” *Prog. Quantum Electron.* **30**, 89-153 (2006).
- [72]. J. M. Hopkins, S. A. Smith, C. W. Jeon, H. D. Sun, D. Burns, S. Calvez, M. D. Dawson, T. Jouhti, and M. Pessa, “0.6 W CW GaInNAs vertical external-cavity surface emitting laser operating at 1.32 μm ,” *Electron. Lett.* **40**, 30-31 (2004).
- [73]. Y. Tzuk, A. Tal, S. Goldring, Y. Glick, E. Lebiush, G. Kaufman, and R. Lavi, “Diamond cooling of high-power diode-pumped solid-state lasers,” *IEEE J. Quantum Electron.* **40**, 262-269 (2004).
- [74]. P. Millar, A. J. Kemp, and D. Burns, “Power scaling of Nd:YVO₄ and Nd:GdVO₄ disk lasers using synthetic diamond as a heat spreader,” *Opt. Lett.* **34**, 782-784 (2009).
- [75]. P. Millar, R. B. Birch, A. J. Kemp, and D. Burns, “Synthetic diamond for intracavity thermal management in compact solid-state lasers,” *IEEE J. Quantum Electron.* **44**, 709-717 (2008).
- [76]. J. Federici and L. Moeller, “Review of terahertz and subterahertz wireless communications,” *J. Appl. Phys.* **107**, 111101 (2010).
- [77]. T. Tomaru and H. Petek, “Femtosecond Cr⁴⁺:YAG laser with an L-fold cavity operating at a 1.2-GHz repetition rate,” *Opt. Lett.* **25**, 584-586 (2000).
- [78]. Ch. Silberhorn, P.K. Lam, O. Weiß, F. König, N. Korolkova, and G. Leuchs, “Generation of continuous variable Einstein-Podolsky-Rosen entanglement via the Kerr nonlinearity in an optical fiber,” *Phys. Rev. Lett.* **86**, 4267-4270 (2001).
- [79]. D. A. B. Miller, “Optical Interconnects to Silicon,” *IEEE J. Sel. Topics Quantum Electron.* **6**, 1312-1317 (2000).
- [80]. K. J. Weingarten, M. J.W. Rodwell, and D. M. Bloom, “Picosecond optical sampling of GaAs integrated circuits,” *IEEE J. Quantum Electron.* **24**, 198-220 (1988).
- [81]. A. Bartels, T. Dekorsy, H. Kurz, “Femtosecond Ti:sapphire ring laser with a 2-GHz repetition rate and its application in time-resolved spectroscopy,” *Opt. Lett.* **24**, 996-998 (1999).
- [82]. R. Aviles-Espinosa, G. Filippidis, C. Hamilton, G. Malcolm, K. J. Weingarten, T. Südmeyer, Y. Barbarin, U. Keller, S. I. C. O. Santos, D. Artigas, and P.

- Loza-Alvarez, "Compact ultrafast semiconductor disk laser: targeting GFP based nonlinear applications in living organisms," *Biomed. Opt. Express* **2**, 739-747 (2011).
- [83]. D. A. B. Miller, "Optics for low-energy communication inside digital processors: quantum detectors, sources, and modulators as efficient impedance converters," *Opt. Lett.* **14**, 146-148 (1989).
- [84]. A. Bartels, D. Heinecke, and S. A. Diddams, "10-GHz self-referenced optical frequency comb," *Science* **326**, 681 (2009).
- [85]. E. Yoshida and M. Nakazawa, "80~200 GHz erbium doped fibre laser using a rational harmonic mode-locking technique," *Electron. Lett.* **32**, 1370-1372 (1996).
- [86]. J. Schröder, S. Coen, F. Vanholsbeek, and T. Sylvestre, "Passively mode-locked Raman fiber laser with 100 GHz repetition rate," *Opt. Lett.* **31**, 3489-3491 (2006).
- [87]. K. Sato, "Optical pulse generation using fabry-Pe´rot lasers under continuous-wave operation," *IEEE J. Sel. Top. Quantum Electron.* **9**, 1288-1293 (2003).
- [88]. C. Gosset, K. Merghem, A. Martinez, G. Moreau, G. Patriarche, G. Aubin, A. Ramdane, J. Landreau, and F. Lelarge, "Subpicosecond pulse generation at 134 GHz using a quantum-dash-based Fabry-Perot laser emitting at 1.56 μm ," *Appl. Phys. Lett.* **88**, 241105-241105-3 (2006).
- [89]. S. Hoogland, S. Dhanjal, A. C. Tropper, S. J. Roberts, R. Häring, R. Paschotta, and U. Keller, "Passively mode-locked diode-pumped surface-emitting semiconductor laser," *IEEE Photon. Technol. Lett.* **12**, 1135-1138 (2000).
- [90]. R. Häring, R. Paschotta, E. Gini, F. Morier-Genoud, H. Melchior, D. Martin, and U. Keller, "Picosecond surface-emitting semiconductor laser with >200 mW average power," *Electron. Lett.* **37**, 766-767 (2001).
- [91]. A. H. Quarterman, K. G. Wilcox, V. Apostolopoulos, Z. Mihoubi, S. P. Elsmere, I. Farrer, D. A. Ritchie, and A. C. Tropper, "A passively mode-locked external-cavity semiconductor laser emitting 60-fs pulses," *Nature Photonics* **3**, 729 - 731 (2009).
- [92]. P. Klopp, U. Griebner, M. Zorn, and M. Weyers, "Pulse repetition rate up to 92 GHz or pulse duration shorter than 110 fs from a mode-locked semiconductor disk laser," *Appl. Phys. Lett.* **98**, 071103-071103-3 (2011).
- [93]. L. Krainer, R. Paschotta, S. Lecomte, M. Moser, K. J. Weingarten, and U. Keller, "Compact Nd:YVO₄ lasers with pulse repetition rates up to 160 GHz," *IEEE J.*

- Quantum Electron. **38**, 1331-1338 (2002).
- [94]. S. Lecomte, M. Kalisch, L. Krainer, G.J. Spühler, R. Paschotta, M. Golling, D. Ebling, T. Ohgoh, T. Hayakawa, S. Pawlik, B. Schmidt, U. Keller, “Diode-pumped passively mode-locked Nd:YVO₄ lasers with 40-GHz repetition rate,” IEEE J. Quantum Electron. **41**, 45-52 (2005).
- [95]. A. E. H. Oehler, T. Südmeyer, K. J. Weingarten, and U. Keller, “100 GHz passively mode-locked Er:Yb:glass laser at 1.5 μm with 1.6-ps pulses,” Opt. Express **16**, 21930-21935 (2008).
- [96]. C. Hönninger, R. Paschotta, F. Morier-Genoud, M. Moser, and U. Keller, “Q-switching stability limits of continuous-wave passive mode locking,” J. Opt. Soc. Amer. B **16**, 46-56 (1999).
- [97]. D. C. Heinecke, A. Bartels, and S. A. Diddams, “Offset frequency dynamics and phase noise properties of a self-referenced 10 GHz Ti:sapphire frequency comb,” Opt. Express **19**, 18440-18451 (2011).
- [98]. D. Li, U. Demirbas, J. R. Birge, G. S. Petrich, L. A. Kolodziejski, A. Sennaroglu, F. X. Kärtner, and J. G. Fujimoto, “Diode-pumped passively mode-locked GHz femtosecond Cr:LiSAF laser with kW peak power,” Opt. Lett. **35**, 1446-1448 (2010).
- [99]. S. Pekarek, T. Südmeyer, S. Lecomte, S. Kundermann, J. M. Dudley, and U. Keller, “Self-referenceable frequency comb from a gigahertz diode-pumped solid-state laser,” Opt. Express **19**, 16491-16497 (2011).
- [100]. S. Pekarek, A. Klenner, T. Südmeyer, C. Fiebig, K. Paschke, G. Erbert, and U. Keller, “Femtosecond diodepumped solid-state laser with a repetition rate of 4.8 GHz,” Opt. Express **20**, 4248-4253 (2012).
- [101]. S. Yamazoe, M. Katou, T. Adachi, and T. Kasamatsu, “Palm-top-size, 1.5 kW peak-power, and femtosecond (160 fs) diode-pumped mode-locked Yb³⁺:KY(WO₄)₂ solid-state laser with a semiconductor saturable absorber mirror,” Opt. Lett. **35**, 748-750 (2010).
- [102]. H. W. Yang, C. Kim, S. Y. Choi, G. H. Kim, Y. Kobayashi, F. Rotermund, and J. Kim, “1.2-GHz repetition rate, diode-pumped femtosecond Yb:KYW laser mode-locked by a carbon nanotube saturable absorber mirror” Opt. Express **20**, 29518-29523 (2012).
- [103]. Y. F. Chen, H. C. Liang, J. C. Tung, K. W. Su, Y. Y. Zhang, H. J. Zhang, H. H. Yu, and J. Y. Wang, “Spontaneous subpicosecond pulse formation with pulse

- repetition rate of 80 GHz in a diode-pumped Nd:SrGdGa₃O₇ disordered crystal laser,” *Opt. Lett.* **37**, 461-463 (2012).
- [104]. M. F. Becker, D. J. Kuizenga, and A. E. Siegman, “Harmonic Mode Locking of the Nd:YAG laser,” *IEEE J. Quantum Electron.* **8**, 687-693 (1972).
- [105]. M. N. Kong, J. K. Chee, and J. M. Liu, “Passive mode locking with a nonlinear external coupled cavity at high pulse repetition rates,” *Opt. Lett.* **16**, 73-75 (1991).
- [106]. P. Glas, M. Naumann, I. Reng, A. Schirmacher, L. Dong, and J. Caplen, “High repetition rate fiber laser coupled to a linear cavity generating picosecond pulses,” *Fiber Integr. Opt.* **17**, 207-212 (1998).
- [107]. T. M. Liu, F. X. Kärtner, J. G. Fujimoto, C. K. Sun, “Multiplying the repetition rate of passive mode-locked femtosecond lasers by an intracavity flat surface with low reflectivity,” *Opt. Lett.* **30**, 439-441 (2005).
- [108]. G. Q. Xie, L. J. Qian, H. Y. Zhu, and H. Yang, “Repetition rate multiplication in a diode-pumped femtosecond Nd:Glass laser by using a coupled cavity,” *J. Korean Phys. Soc.* **49**, 1438-1443 (2006).
- [109]. J. Aus der Au, S. F. Schaer, R. Paschotta, C. Hönninger, U. Keller, and M. Moser, “High-power diode-pumped passively mode-locked Yb:YAG lasers,” *Opt. Lett.* **24**, 1281-1283 (1999).
- [110]. H. Yoshioka, S. Nakamura, T. Okawa, and S. Wada, “Diode-pumped mode-locked Yb:YAG ceramic laser,” *Opt. Express* **17**, 8919-8925 (2009).
- [111]. J. Aus der Au, G. J. Spühler, T. Südmeyer, R. Paschotta, R. Hövel, M. Moser, S. Erhard, M. Karszewski, A. Giesen, and U. Keller, “16.2-W average power from a diode-pumped femtosecond Yb:YAG thin disk laser” *Opt. Lett.* **25**, 859-861 (2000).
- [112]. S. Uemura and K. Torizuka, “Kerr-lens mode-locked diode-pumped Yb:YAG laser with the transverse mode passively stabilized,” *Jpn. J. Appl. Express* **1**, 012007-1 - 012007-3 (2008).
- [113]. O. Pronin, J. Brons, C. Grasse, V. Pervak, G. Boehm, M. C. Amann, V. L. Kalashnikov, A. Apolonski, and F. Krausz, “High-power 200 fs Kerr-lens mode-locked Yb:YAG thin-disk oscillator,” *Opt. Lett.* **36**, 4746-4748 (2011).
- [114]. S. Uemura and K. Torizuka, “Sub-40-fs pulses from a diode-pumped Kerr-lens mode-locked Yb-doped yttrium aluminum garnet laser,” *Jpn. J. Appl. Phys.* **50**, 010201(2011).



Chapter 2

Pulsed large mode area fiber lasers and amplifier

The way for achieving PQS operation is to insert a saturable absorber (SA) into the laser cavity. The SAs can absorb light of their optical transition wavelength and has a transmission characteristic as depicted in Fig. 2.1. The material becomes more transparent as the incident fluence increases, and at higher incident energy fluence levels the material saturates or bleaches, leading to a high transmission. The PQS operation is achieved by the behavior of the absorption of the SA which initially provides a high loss in the resonator to prevent laser oscillation and to store the population inversion in the gain medium. As the SA is pumped continuously by the fluence of the gain medium and finally the gain exceeds the round-trip losses, the intracavity power density increases dramatically causing the SA to bleach and a Q-switched pulse builds up.

One type among Q-switched SAs is to add additional doped fibers doped with Cr^{4+} [1], Sm [2-3], Bi [4], and Tm^{3+} - Yb^{3+} co-doped [5] in the 1.0-1.1 μm regime. The cavity scheme with the fiber saturable absorber is depicted in Fig. 2.2 and is usually in the all-fiber form. The advantages of all-fiber laser systems like compact set-up, low adjustment requirements and low sensitivity to thermal effects and mechanical perturbations which can not fully be exploited in laser systems with free-space cavity part. With 273 mW of pump power, the fiber laser presented in Ref. [1] can emit pulses at the repetition rate of 84 kHz with pulse width of 3 μs and pulse energy of 15 nJ. But the stability of the output pulse train was very poor and the laser efficiency was rather low because cavity parameters were not optimized. Operated with the Sm-doped fiber as described in Ref. [2-3], at the pump power of 6 W, the output pulses generation occurs in stable manner with the repetition rate of 130 kHz, pulse width of 650 ns, and pulse energy of 20 μJ . The pulse energy can be increased by optimizing the length of the Sm-doped fiber.

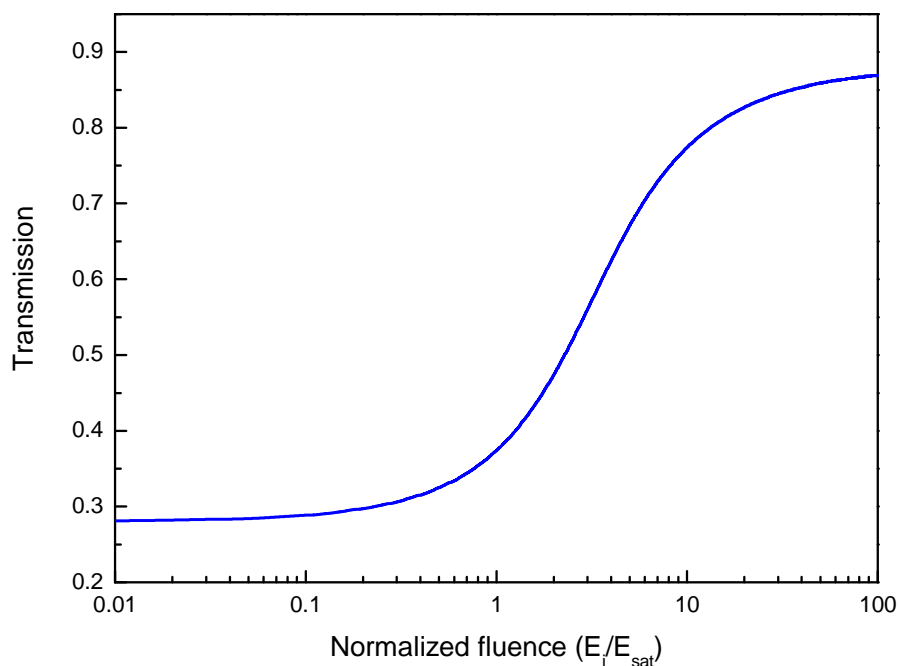


Fig. 2.1 Nonlinear transmission of a saturable absorber versus incident fluence E_i normalized to the saturation fluence E_s of the absorber.

In contrast to Cr^{4+} and Sm -doped fibers, Bi active centers have the long lifetime to be about 1 ms which has the advantage for higher pulse energy. The pulse energy of 0.1 mJ can be achieved at the emission wavelength of 1066 nm. Maximum average power of 3.5 W was attained under the pump power of 8 W at this wavelength. Minimum pulse width was of 1 μs while the pulse repetition rate ranges from 10 kHz to 100 kHz.

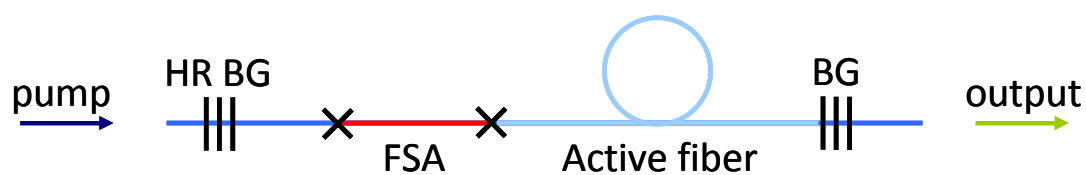


Fig. 2.2 General scheme of the fiber laser with the fiber saturable absorber (FSA).
BG: Bragg grating, HR BG: high reflective Bragg grating.

The laser system with Tm^{3+} - Yb^{3+} co-doped fiber as the self-Q-switched element showed up to 2.4 W output power at the pump power of 10.8 W, up to 140 kHz repetition rate, a maximum pulse energy of 17.2 μJ and a minimum pulse duration of 1.5 μs . Besides, using a grating pair in Littrow-Littman configuration the emission

wavelength was tunable between 1055 nm and 1090 nm. Nevertheless, the pulse energy was limited to below 0.1 mJ for all PQS fiber lasers using various fiber saturable absorbers because of the restricted modulation depth that forms the obstacle to deliver high-pulse-energy laser.

In terms of the bulk-type SAs, especially doped crystals, Cr⁴⁺:YAG crystals are the most widely used SA at the spectral range of 0.9 μm to 1.2 μm owing to its good chemical and photochemical stability, high thermal conductivity, and high damage threshold. Besides, as the result of its large absorption cross section, low saturation intensity, and long excited-state lifetime required for optical absorption, Cr⁴⁺:YAG crystal has been the most recognized SA with Yb-doped PQS fiber lasers have been intensively studied in varied experimental setup schemes and output characteristics [6-10].

The optical energy diagram of the Cr⁴⁺:YAG crystal is depicted in Fig. 2.3. The energy levels of the Cr⁴⁺:YAG passive Q-switch can be modeled as a four level system. The solid line and the dash line indicate radiative and non-radiative transitions, respectively. The E₁ to E₃ transition is the targeted saturable transition in the absorption band of 1.0~1.1 μm with the ground state absorption cross-section σ₁₃. When a photon at the laser wavelength is absorbed by the ground state, energy level 3 immediately relaxes to the fluorescing state level 2. This level has a long lifetime (4.1 μs), allowing the 1-3 transition to become saturated as the population of level 1 is depleted. The transition from level 2 to level 4 corresponds to the excited-state absorption (ESA). The ESA not only results in a residual loss in the resonator when the ground state absorption has been saturated but also leads to a degradation of final transmission of the SA. The transition from level 2 to level 4 does not saturate because of the fast relaxation of the level 4 (~0.5 ns).

The criterion for a useful SA in Q-switching is that σ₁₃ > σ₂₄, where σ₂₄ is the absorption cross-section for ESA. The values of the absorption cross-section for both the ground-state and the excited-state still can not be determined exactly so far and can vary greatly in magnitude because the measured cross-section depends on the property of the probe light source such as the pulse repetition rate together with the pulse width, the doping concentration and homogeneity of Cr⁴⁺:YAG crystals, and diverse fitting procedures to determine the values. Several published values [11-15] for absorption cross-section for ground-state (σ_{gs}) and the excited-state (σ_{es}) have

been shown in Table 2.1.

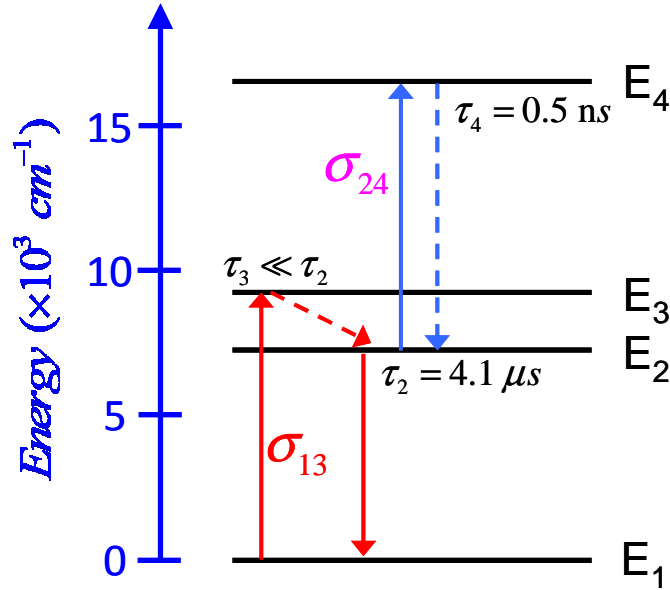


Fig. 2.3 The energy-level diagram of Cr⁴⁺:YAG with ESA. The solid lines indicate radiative optical transitions and the dashed lines indicate non-radiative transitions.

Reference	σ_{gs}	σ_{es}	σ_{es}/σ_{gs}
11	$(7.0\pm 0.8)\times 10^{-18} \text{ cm}^2$	$(2.0\pm 0.3)\times 10^{-18} \text{ cm}^2$	0.29
12	$(1.9\pm 0.5)\times 10^{-18} \text{ cm}^2$	$(5.0\pm 1.0)\times 10^{-19} \text{ cm}^2$	0.26
13	$(5.7\pm 0.2)\times 10^{-18} \text{ cm}^2$	$(8.0\pm 2.0)\times 10^{-19} \text{ cm}^2$	0.14
14	$(8.7\pm 0.8)\times 10^{-19} \text{ cm}^2$	$(2.2\pm 0.2)\times 10^{-19} \text{ cm}^2$	0.25
15	$(3.3\pm 0.2)\times 10^{-18} \text{ cm}^2$	$(6.3\pm 0.5)\times 10^{-19} \text{ cm}^2$	0.19

Table 2.1: Cr⁴⁺:YAG cross sections at 1.06 μm published in literatures

The final transmission of the Cr⁴⁺:YAG crystal could not approach to 100% because it is the SA with ESA effects that the final transmission is governed by the following equation:

$$T_f = T_i^\beta \tag{2.1}$$

where T_f together with T_i is the final and initial transmission of the SA, and β is the ratio of the absorption cross-section of the excited-state and the ground-state, i.e. $\beta = \sigma_{es}/\sigma_{gs}$ as calculated in the last column in Table 2.1. The ratios of σ_{es}/σ_{gs} are less duplicitous than the absolute values of σ_{gs} or σ_{es} and were reported to range from 0.14

to 0.29 [16]. Hence the lossy phenomenon was attributed mainly to the ESA.

Some output characteristics of PQS fiber lasers with the Cr⁴⁺:YAG crystal in various experimental setups are listed in in Table 2.2.

Ref.	Core diameter/ length	P _{in}	P _{out}	Energy	Pulse width
6	7 μm/ 2 m	1.7 W	0.3 W	25 μJ	2.7 ns
7	6 μm/ 3 m	9.8 W	4.7 W	18.5 μJ	143 ns
8	10 μm/ 2.8 m	13.8 W	7.8 W	65 μJ	116 ns
9	25 μm/ 3 m	17.5 W	6.2 W	130 μJ	6.5 ns
10	25 μm/ 1 m	4.1 W	0.637 W	245 μJ	0.49 ns

Table 2.2: Some output characteristics of PQS fiber lasers published in literatures

From Table 2.2, we can see that the output pulse energy were all below 100 μJ for fiber lasers with small core diameter (core diameter < 10 μm). By using the LMA fiber, the PQS fiber laser demonstrated in Ref. 9 can emit pulse energy up to 130 μJ at the pulse repetition rate of 47.7 kHz with the Cr⁴⁺:YAG of initial transmission of 40%. The pulse width could be reduced to approximately 0.49 ns in Ref. 10 by incorporating the pulse formation procedure with the stimulated Brillouin scattering (SBS) effect. However, the output power was limited to 0.637 W because not only the spectral but also the temporal stability of the PQS fiber became severely unstable when the pump power increased to beyond 4.1 W. The timing jitter of the pulse train was deteriorated to 24% in root mean square at the pulse repetition rate of about 22 kHz.

In addition to transition-metal-doped crystals such as Cr⁴⁺:YAG SAs, semiconductor saturable absorbers [17], and graphene [18] have also been applied as SAs in Yb-doped fiber lasers. InGaAs/GaAs quantum wells (QWs) with 70% modulation depth were employed as SA with core-pumped 15-cm Yb-doped fiber in Ref. 17. Pulse width as short as 8 ns was obtained in this scheme. However, the output pulse energy with InGaAs QWs in passively Q-switched lasers is limited to 0.1 μJ by the lattice mismatch with the substrate GaAs for the spectral region of above 1.0 μm. As for the graphene based SA described in Ref. 18, the average output power of 12 mW with the pulse energy of 45 nJ and pulse width of 71 ns at the repetition rate of 257 kHz was attained under the pump power of 360 mW. As the result of the lower damage threshold of the graphene membrane, the pulse energy was much lower than

Ch2 Pulsed large mode area fiber lasers and amplifier

other bulk-type SAs mentioned above.



2.1 Passively Q-switched fiber laser with AlGaInAs MQWs

Fiber lasers have been confirmed to possess the merits of high efficiency, excellent beam quality, and good heat dissipation. High-pulse-energy Q-switched fiber lasers are practically useful in numerous applications, such as range finding, remote sensing, industrial processing, and coherent lidar systems [19-22]. Passively Q-switched lasers with saturable absorbers have attracted significant attention because of their compactness and simplicity in operation. Several saturable absorbers have been developed to replace the dyes used in solid-state lasers, such as Cr⁴⁺-doped crystals [23-27] and semiconductor saturable absorber mirrors (SESAMs) [28-29]. Currently, Cr⁴⁺:YAG crystals are the most recognized saturable absorbers in the spectral region of 0.9–1.2 μm. Passively Q-switched fiber lasers with Cr⁴⁺:YAG saturable absorbers have been recently demonstrated [6-7, 9], among which the maximum pulse energy achieved with a large-mode-area Yb-doped fiber was 120 μJ.

Alternatively, InGaAs/GaAs quantum wells (QWs) have been used to develop the SESAMs for Nd-doped or Yb-doped lasers. The obtainable absorption change between low and high intensities, however, is hindered by the lattice mismatch for the spectral region of above 1.0 μm. As a consequence, the output pulse energies and the conversion efficiencies with InGaAs SESAMs in passively Q-switched lasers are significantly lower than those with Cr⁴⁺:YAG crystals. Recently, an AlGaInAs with a periodic QW/barrier structure has been exploited to be an efficient saturable absorber for a passively Q-switched Nd:YVO₄ laser [30]. Compared with InGaAsP materials, the AlGaInAs quaternary alloy with a larger conduction band offset is confirmed to offer a superior electron confinement in the 0.84–1.65 μm spectral region [31-33]. Nevertheless, AlGaInAs/InP QWs have not been employed to passively Q switch Yb-doped fiber lasers.

I demonstrate a high-pulse-energy passively Q-switched Yb-doped fiber laser with an AlGaInAs/InP QWs saturable absorber. With an incident pump power of 7.6 W, an average output power of 3.8 W with a Q-switched pulse width of 30 ns at a pulse repetition rate of 12.5 kHz was obtained; consequently, the maximum pulse energy was up to 300 μJ. More importantly, the overall Q-switching efficiency could

exceed 90% because of a low nonsaturable loss.

The structure of the semiconductor saturable absorber was essentially similar to that reported in [30]. The previous saturable absorber consisted of 30 groups of two QWs, spaced at half-wavelength intervals by InAlAs barrier layers with a bandgap wavelength around 805 nm. Here we fabricated a saturable absorber with 50 groups of three QWs to increase the modulation strength. The luminescence wavelength of the saturable absorber was designed to be near 1066 nm. An InP window layer was deposited on the QW/barrier structure to avoid surface recombination and oxidation. The backside of the substrate was mechanically polished after growth. Each side of the semiconductor saturable absorber was antireflection coated to reduce back reflections and the couplecavity effects. Figure 2.4 shows the measured result for the low-intensity transmittance spectrum of the QW saturable absorber. The initial transmission of the absorber at the wavelength of 1066 nm was found to be approximately 26%. The operation bandwidth of the absorber is approximately 8 nm. With the z-scan method, the absorption change between low and high intensities was observed to be approximately 70% in a single pass, and the total nonsaturable losses were lower than 5%. Furthermore, the saturation fluence of the saturable absorber was estimated to be in the range of 1 mJ/cm^2 , and its relaxation time was on the order of 100 ns.

Figure 2.5 depicts the schematic of the experimental setup for the passively Q-switched fiber laser, which is composed of a 1.5 m Yb-doped fiber and an external feedback cavity. The external cavity comprises a reimaging lens, a saturable absorber, a highly reflective mirror at $1.06 \mu\text{m}$ for feedback, and a Fabry–Perot thin film filter (FP filter) for controlling the lasing wavelength. The peak of the FP filter is at 1100 nm with a FWHM bandwidth of 5 nm at normal incidence. The end facets of the fiber were cut to be normal incident. The fiber has a peak cladding absorption coefficient of 10.8 dB/m at 976 nm and a double-clad structure with a diameter of $350 \mu\text{m}$ octagonal outer cladding, a diameter of $250 \mu\text{m}$ octagonal inner cladding with an N.A. of 0.46, and a $25 \mu\text{m}$ circular core with an N.A. of 0.07. Note that the robust single-mode output was achieved with a unique low N.A. feature of the core.

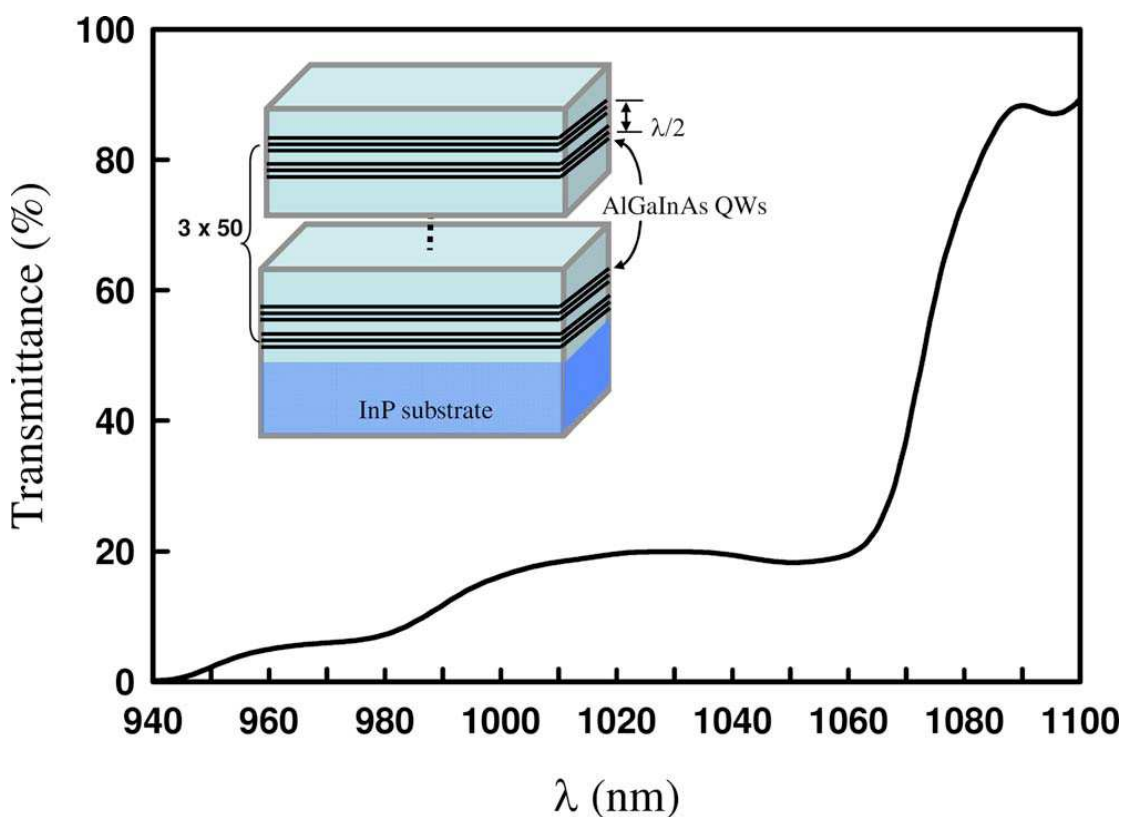


Fig. 2.4 Transmittance spectrum at room temperature for the AR-coated AlGaInAs/InP saturable absorber. Inset, schematic diagram of a periodic AlGaInAs QW structure.

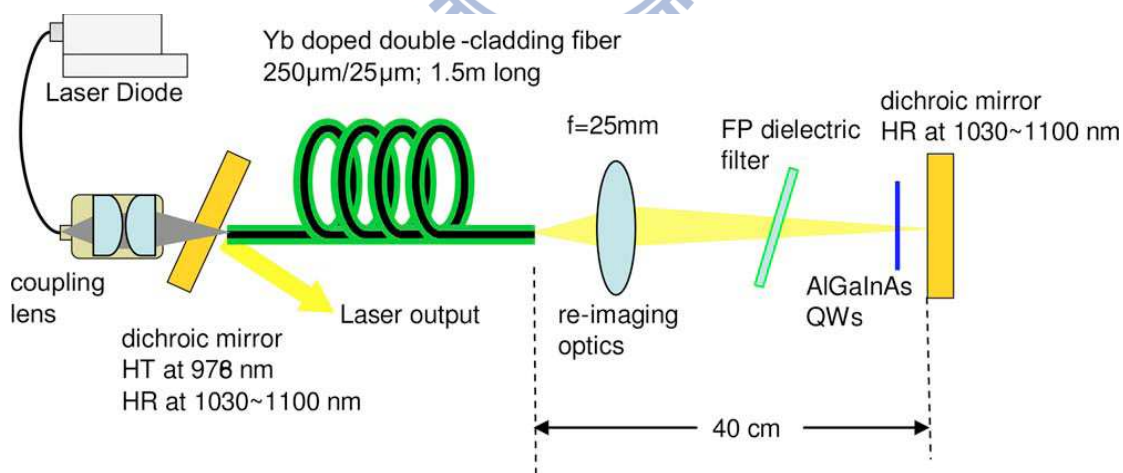


Fig. 2.5 Schematic diagram of the experimental setup. HR, high reflection; HT, high transmission.

The pump source was a 10 W 976 nm fiber-coupled laser diode with a core diameter of 400 μm and an N.A. of 0.22. A focusing lens with 25 mm focal length and 90% coupling efficiency was used to re-image the pump beam into the fiber through a dichroic mirror with high transmission ($> 90\%$) at 976 nm and high reflectivity ($> 98.8\%$) at 1066 nm. The pump spot radius was approximately 200 μm . With launching into an undoped fiber, the pump coupling efficiency was measured to be approximately 80%. The pulse temporal behavior was recorded with a digital oscilloscope (LeCroy Wavepro 7100; 10G samples/s; 1 GHz bandwidth) and a fast InGaAs photodiode. The laser spectrum was measured by an optical spectrum analyzer with 0.1 nm resolution (Advantest Q8381A).

Figure 2.6 shows the average output powers with respect to the incident pump power in cw and passive Q-switching operations. The cw operation was performed to make an evaluation for the passively Q-switched efficiency. Without the saturable absorber in the cavity, the laser had an output power of 4 W at an incident pump power of 7.6 W in a cw operation, and the corresponding slope efficiency was 66%. In the passive Q-switching operation, an average output power of 3.8 W was obtained at an incident pump power of 7.6 W. The Q-switching efficiency, which is defined as ratio of the Q-switched output power to the cw power, at the same pump power, can be found to exceed 90%. This Q-switching efficiency is considerably better than the results obtained with the Cr^{4+} :YAG saturable absorber [9]. The superior Q-switching efficiency confirms that the AlGaInAs QW material can be exploited to be an efficient absorber with a large modulation change and a quite low nonsaturable loss. The lasing linewidth was narrower than 1.0 nm with the help of a dielectric bandpass filter, as shown in the inset of Fig. 2.6. The M^2 factor was also measured to be less than 1.5 over the complete output power range, owing to the low-N.A. feature of the fiber. Furthermore, I also detuned the resonant wavelength (by tilting the FP filter) to investigate the bandwidth of comparable Q-switching performance. It is found that the output pulse energy of $> 280 \mu\text{J}$ with the identical Q-switching efficiency could be obtained within $1066 \pm 4 \text{ nm}$.

Figure 2.7 shows the pulse repetition rate and the pulse energy versus the incident pump power. It can be seen that the pulse repetition rate increases monotonically with the pump power up to 12.5 kHz and that the pulse energy is approximately 300 μJ for all pump power range. The pulse duration, as shown in Fig. 2.8(a), was found to be almost constant at 30 ns for all pump powers. As a

consequence, the maximum peak power reaches approximately 10 kW. A typical oscilloscope trace of a train of output pulses is shown in Fig. 2.8(b). Under the optimum alignment condition, the pulse-to-pulse amplitude fluctuation was found to be within 10%. In passively Q-switched Yb-doped fiber lasers, on the whole, the performances with AlGaInAs QWs saturable absorbers are superior to the results obtained with Cr⁴⁺:YAG crystals [6-7, 9].

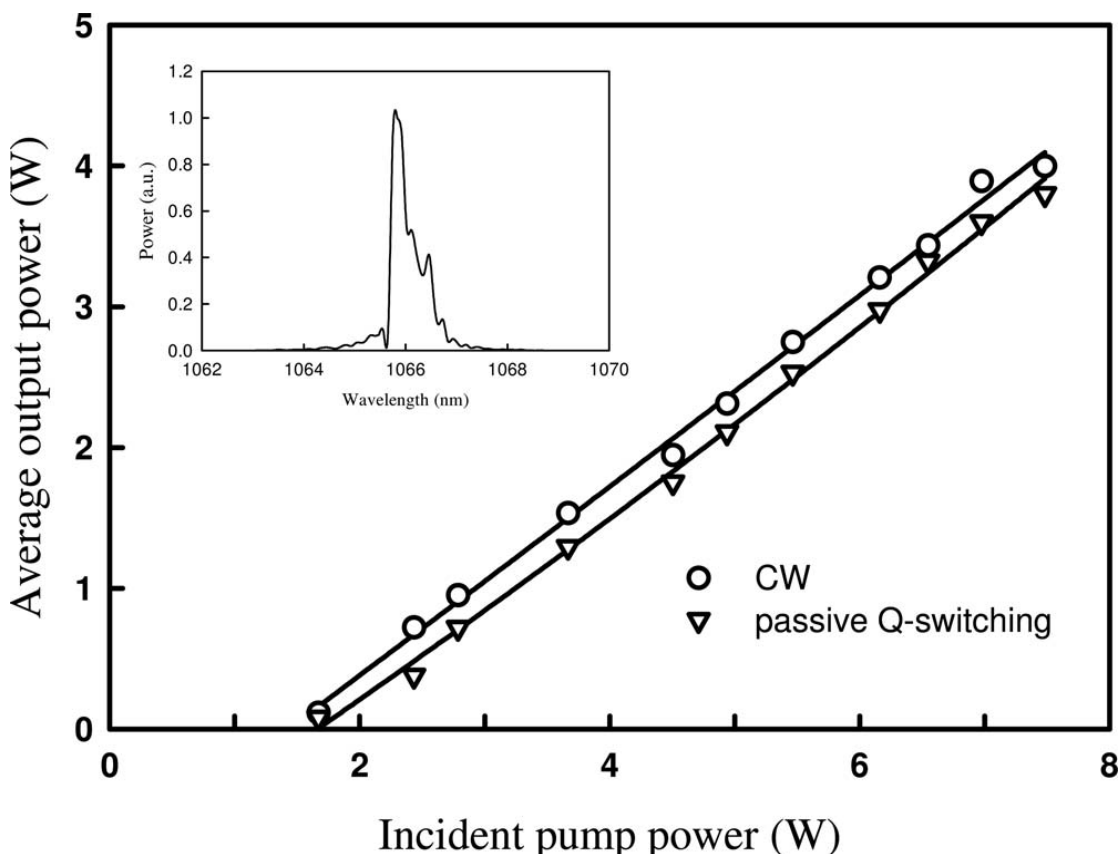


Fig. 2.6 Average output powers at 1066 nm with respect to the incident pump power in cw and passively Q-switching operations.

In summary, a high-pulse-energy passively Q-switched Yb-doped fiber laser was developed with an AlGaInAs/InP QW saturable absorber. Stable Q-switched pulses of 30 ns duration with an average output power of 3.8 W and a repetition rate of 12.5 kHz were obtained at an incident pump power of 7.6 W. The overall Q-switching efficiency was found to exceed 90%. Excellent results confirm that the AlGaInAs QW material can be exploited to be an efficient absorber with a large modulation change and a quite-low nonsaturable loss.

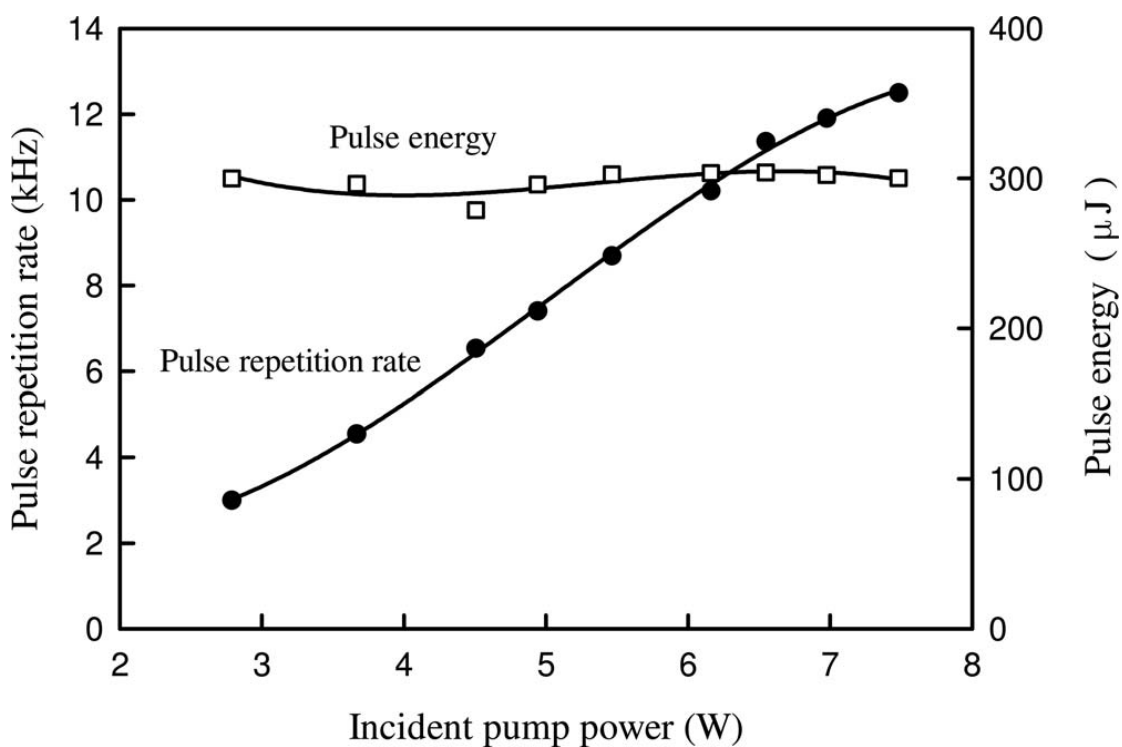


Fig. 2.7 Experimental results for the pulse repetition rate and the pulse energy versus incident pump power.

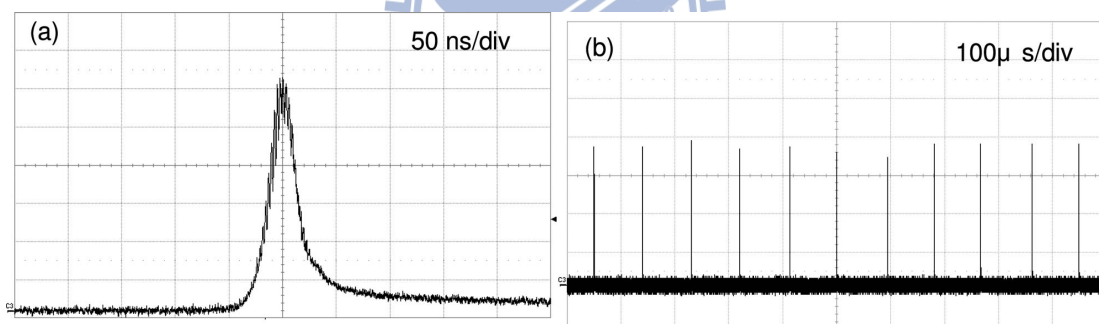


Fig. 2.8 Expanded shape of a single pulse and (b) typical oscilloscope trace of a train of output pulses.

2.2 Comparative studies for Cr⁴⁺:YAG crystal and AlGaInAs MQWs in PQS fiber lasers

The rapid development of double-clad rare-earth doped fibers and high-power laser diodes spurs the generation of high-power and high-brightness light sources [34-36]. Pulsed fiber lasers have attracted a great deal of attentions in applications owing to their higher peak power than in CW operation. Passive Q-switching (PQS) is a sophisticated and an efficient technique to create high-pulse-energy and high-peak-power pulses. Besides, PQS lasers are more compact and lower cost than the active Q-switching cause of that they utilize saturable absorbers (SAs) in replace of acoustic-optic or electro-optic modulators as the Q-switch.

Fiber-type SA [1-2, 37] offers the in-line configuration, nevertheless they are restricted by modulation depth to deliver high-pulse-energy laser. Crystal-based and semiconductor-based SAs are other choices of passive Q-switch. Their high mechanical robustness and well-developed fabrication process make them more common in Q-switched fiber lasers [6, 17, 38-40]. In the spectral region of 1.0~1.1 μm , Cr⁴⁺:YAG crystals [6] and InGaAs/GaAs quantum wells (QWs) [17] have been adopted to Q-switch fiber lasers. However, the output pulse energies with InGaAs SESAMs in passively Q-switched lasers are limited by the lattice mismatch with the substrate GaAs for the spectral region of above 1.0 μm . Alternatively, AlGaInAs material has the advantages of lattice match with the substrate InP and better electron confinement in the 0.84-1.65 μm spectral region than AlGaInP materials [31-32]. We have recently utilized AlGaInAs periodic QWs to Q-switch a Nd:YVO₄ laser [41] and an Yb fiber laser [42], they could emit pulse energy up to 40 and 300 μJ , respectively. Furthermore both of them delivered pulse peak power ≥ 10 kW. Consequently, AlGaInAs semiconductor QWs is comparable with Cr⁴⁺:YAG crystal in the region of 1.0~1.1 μm .

Here, I demonstrate comparative studies for Cr⁴⁺:YAG crystal and AlGaInAs semiconductor used as a SA in Q-switched Yb-doped fiber lasers. The two SAs were designed to be possessed of nearly identical small-signal transmission of ~28%.

Experimental results reveal that the maximum transmissions are 85% and 96% for the Cr⁴⁺:YAG crystal and the AlGaInAs QWs, respectively. Under a pump power of 24 W, the average output powers were up to 14.4 W and 13.8 W obtained with the AlGaInAs QWs and with the Cr⁴⁺:YAG crystal, respectively. The maximum pulse energies obtained with the AlGaInAs QWs and with the Cr⁴⁺:YAG crystal were found to be 0.45 mJ and 0.35 mJ, respectively.

(A) Characteristics of saturable absorbers

The Cr⁴⁺:YAG crystal has thickness of 3 mm and was highly doped with a small signal transmission of 28%. Both sides of the Cr⁴⁺:YAG crystal were coated for antireflection at 1030 ~1080 nm (R<0.2%). The AlGaInAs absorber was designed with 50 groups of three QWs as described in Ref [42]. Both sides of the semiconductor SA were coated for anti-reflecting to reduce back reflections and the couple-cavity effects. Figure 2.9 shows the saturation transmission of the SAs, where the pump source was a nanosecond Nd:YAG Q-switched laser. The saturation energy density of AlGaInAs QWs and Cr⁴⁺:YAG crystal are estimated to about 1 mJ/cm² and 300 mJ/cm², respectively. The deduced absorption crosssection of the Cr⁴⁺:YAG crystal is in the order of 10⁻¹⁹ cm² and agrees approximately with Ref. [26, 43-44]. Besides, the cross-section for the AlGaInAs QWs was obtained in the order of 10⁻¹⁵ cm². The 95% final transmission of AlGaInAs reveals the low nonsaturable loss induced by the facet reflection and absorption by the substrate. On the other hand, the final transmission of the Cr⁴⁺:YAG was only 85%, the lossy phenomenon was attributed mainly to the excited-state absorption (ESA) [11]. The final transmission influenced by the ESA effect could be express approximately as $T_f = T_i^\beta$, where T_f and T_i are the final and the initial transmission, respectively and the parameter β is the ratio of the absorption cross-section of the excited-state and the ground-state, i.e. $\beta = \sigma_{es}/\sigma_{gs}$. The values of β derived from Ref [26, 43-44] ranges from 0.1~0.28 and is 0.128 in our experiment. The modulation depth could be found to be 68% for AlGaInAs QWs and 57% for the Cr⁴⁺:YAG crystal. Furthermore, the relaxation time of the AlGaInAs QWs the Cr⁴⁺:YAG crystal were estimated to be on the order of 100 ns and 3 μ s respectively.

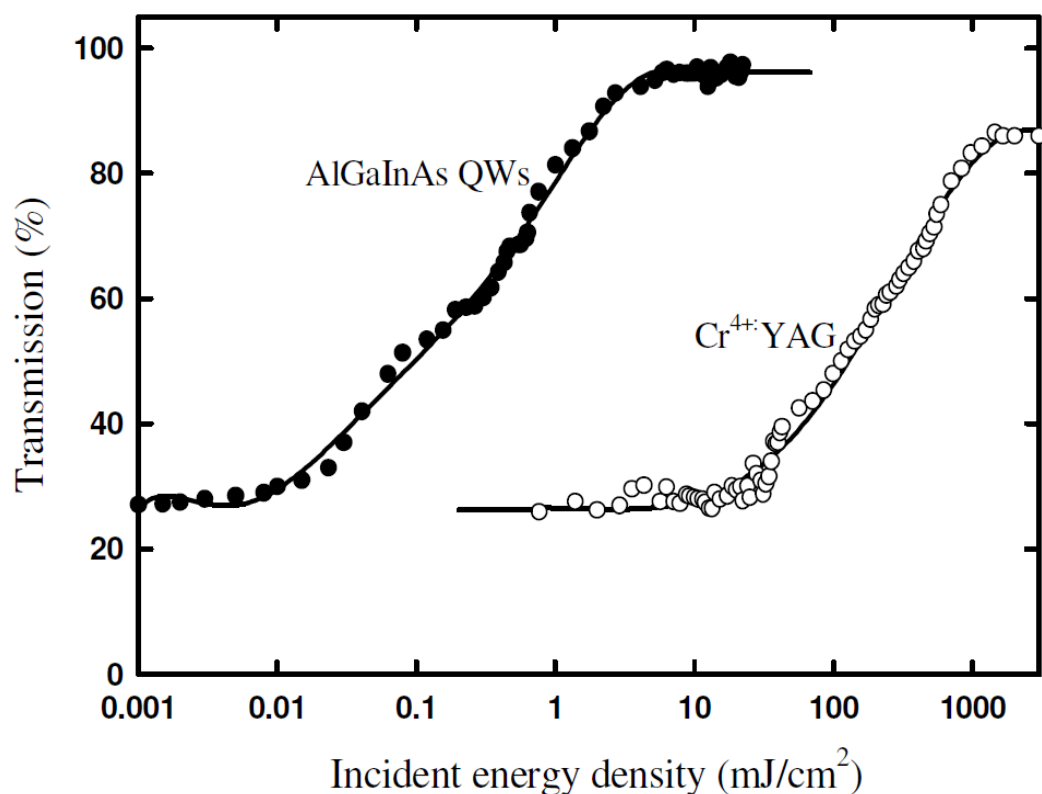


Fig. 2.9 Saturation transmission of the AlGaInAs QWs and the Cr⁴⁺:YAG crystal.

(B) Experimental setup

The cavity consists of a 3-m Yb-doped fiber and an external feedback cavity with a SA. Figures 2.10 (a) and (b) show the setups for PQS fiber lasers by use of a Cr⁴⁺:YAG crystal and a AlGaInAs semiconductor, respectively. The fiber has an absorption coefficient of 10.8 dB/m at 976 nm and a double-clad structure with a 350 μm octagonal outer cladding, a 250 μm inner cladding with a numerical aperture (N.A.) of 0.46, and 30 μm circular core with a N.A. of 0.07. The use of the large-mode-area fiber with low N.A. is beneficial for storing higher pulse energies and sustaining excellent beam quality simultaneously. The external cavity in Fig. 2.10 (a) consists of a focusing lens of 25-mm focal length to focus the fiber output into the Cr⁴⁺:YAG crystal, a re-imaging lens to re-image the beam on a highly reflective mirror for feedback, and a thin film filter for controlling the resonant wavelength. The SA was wrapped with indium foil and mounted in a copper block without active cooling. Here I used a tight focusing configuration to enhance the energy inside the Cr⁴⁺:YAG crystal. The beam waist was about 20 μm and a translation stage was used to adjust the longitudinal position of the Cr⁴⁺:YAG saturable absorber for minimizing

the beam volume inside the crystal and achieving the lowest Q-switching threshold. On the other hand, the low saturation energy density of the AlGaInAs QWs could allow a simple external cavity, as shown in Fig. 2.10 (b), where the beam spot diameter was approximately 300 μm . And the peak optical intensity allowed on the AlGaInAs QWs is estimated to be 300 MW/cm^2 without damage. The SA was tilted slightly to avoid facet reflection back to the gain fiber, which usually incurs parasitic fluctuation in pulse stability in high gain fiber lasers.

The pump source was a 35-W 976-nm fiber-coupled laser diode with a core diameter of 400 μm and a N.A. of 0.22. Focusing lens with 25 mm focal length and 92% coupling efficiency was used to re-image the pump beam into the fiber through a dichroic mirror with high transmission (>90%) at 976 nm and high reflectivity (>99.8%) within 1030~1100 nm. The pump spot radius was approximately 200 μm . With launching into an undoped fiber, the pump coupling efficiency was measured to be approximately 80%.

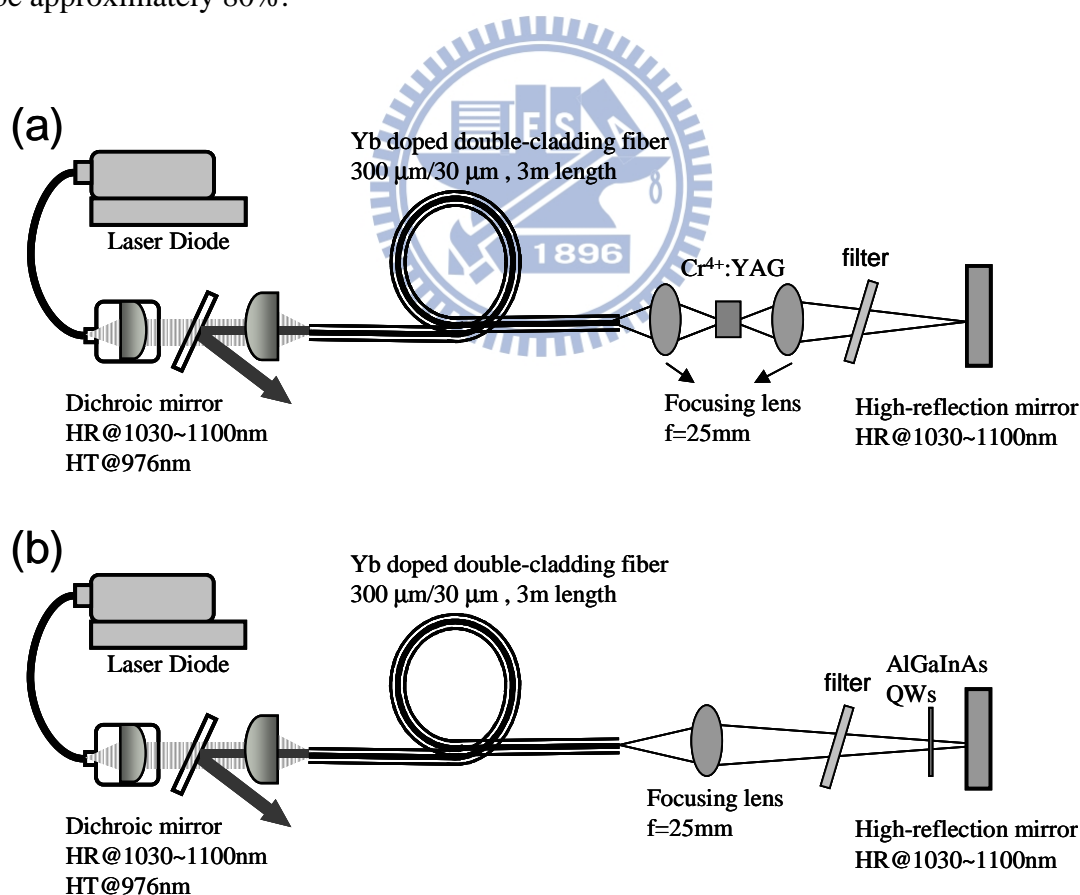


Fig. 2.10 Schematic of diode-pumped PQS Yb-doped fiber lasers. (a) with Cr⁴⁺:YAG crystal (b) with AlGaInAs QWs. HR: high reflection; HT: high transmission.

(C) Results and discussions

Figure 2.11 shows the average output powers with respect to the launched pump power in cw and PQS operations. The cw operation was performed with an external cavity only comprising a re-imaging lens and a reflective mirror. In the cw regime, the laser had a slope efficiency of 74% and the output power reached 15.8 W at a launched pump power of 24 W. In the PQS regime, the maximum average output powers at a launched pump power of 24 W were up to 14.4 W and 13.8 W with the AlGaInAs QWs and with the Cr⁴⁺:YAG crystal, respectively. The Q-switching efficiencies were 91% and 87% for the lasers with with the AlGaInAs QWs and with the Cr⁴⁺:YAG crystal, respectively.

The pulse temporal behavior was recorded by a Leroy digital oscilloscope (Wavepro 7100; 10G samples/sec; 4 GHz bandwidth) with a fast InGaAs photodiode. Figure 3.9 shows the pulse characteristics including the pulse repetition rate and the pulse energy. Figure 2.12 (a) shows the pulse repetition rate versus the launched pump power. The repetition rates of both lasers increased monotonically with the pump power. At a launched pump power of 24 W, the repetition rates were 38 kHz and 30 kHz for using the Cr⁴⁺:YAG crystal and the AlGaInAs QWs, respectively. Figure 2.12 (b) shows the pulse energy versus the launched pump power. The pulse energy with the Cr⁴⁺:YAG crystal was almost constant at 0.3 mJ for the pump power less than 20 W and slightly increased up to 0.35 mJ at a pump power of 24 W. On the other hand, the pulse energy with the AlGaInAs QWs increases gradually, from 0.25 mJ at the threshold to 0.45 mJ at a pump power of 24 W.

Another interesting characteristic of saturable absorbers is the wavelength-dependent absorption. In this investigation the thin film filter was tilted for controlling the lasing wavelength from 1055 nm to 1083 nm. Figure 2.13 shows the pulse energy versus the lasing wavelength at a pump power of 24 W. Since the absorption bandwidth of the AlGaInAs QWs was rather narrower, the variation of the pulse energy with the AlGaInAs QWs was more significant than that with the Cr⁴⁺:YAG crystal. Therefore, the Cr⁴⁺:YAG crystal is more suitable than the AlGaInAs QWs for using in tunable operation.

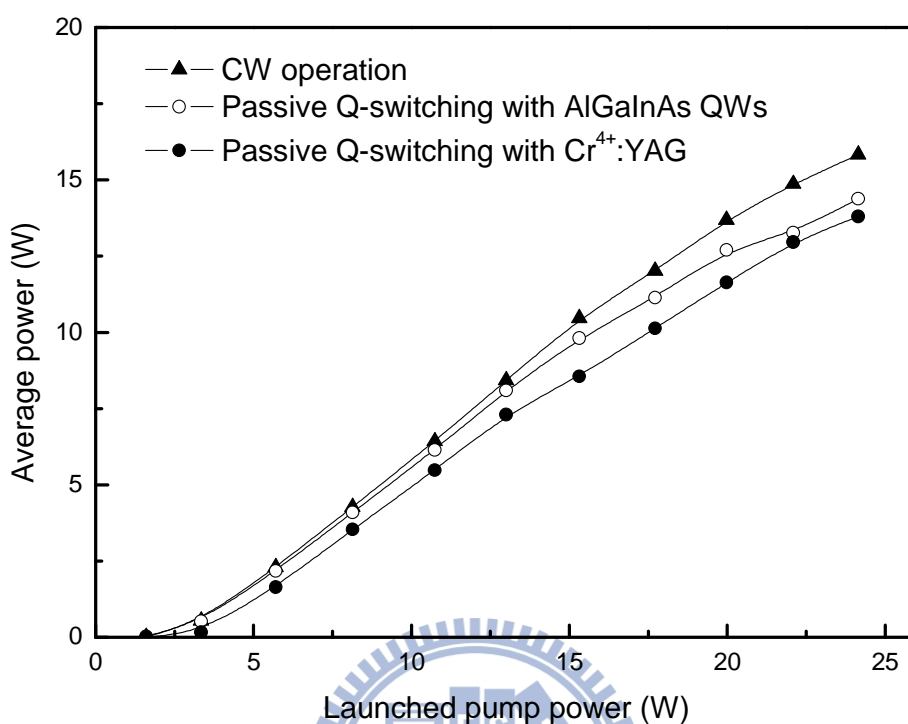


Fig. 2.11 Dependence of the average output power on the launched pump power for the cw and passive Q-switching operations.

The temporal shapes of the Q-switched pulses for the maximum pulse energy were depicted in Fig. 2.14. The top of Fig. 2.14 shows the single Q-switched envelopes. The pulse durations were 70 ns and 60 ns for using the Cr⁴⁺:YAG crystal and the AlGaInAs QWs, respectively. The bottom of Fig. 2.14 show the typical oscilloscope traces of Q-switched pulse train with the optimum alignment. The pulse-to-pulse stability was found to be noticeably better with the AlGaInAs QWs than with the Cr⁴⁺:YAG crystal under 30 °C because of the proper cooling ability by the copper sink. Without any cooling mechanism, the pulse-to-pulse stability and the laser output energy will be reduced.

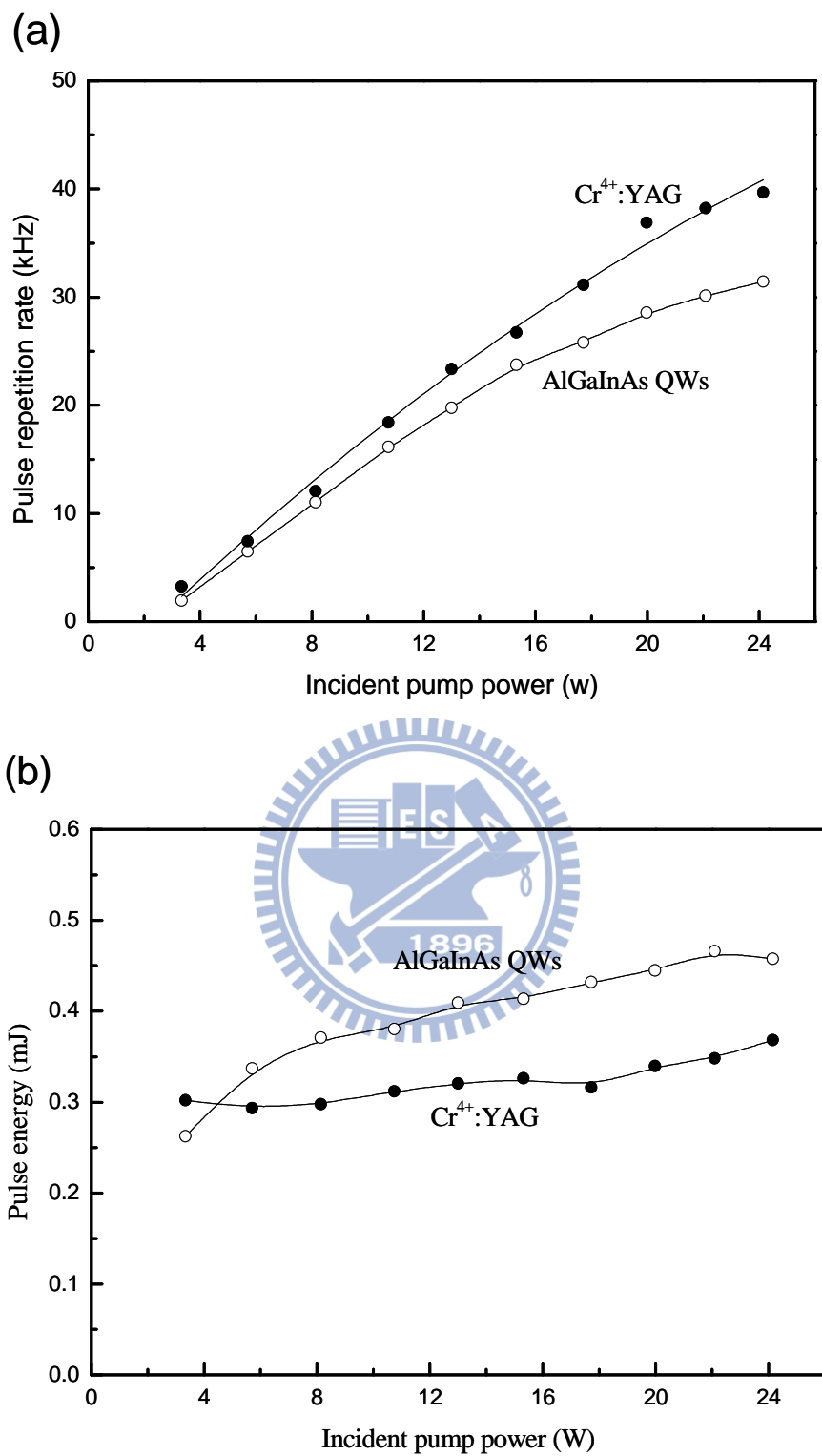


Fig. 2.12 (a) Pulse repetition rate and (b) pulse energy versus the launched pump power.

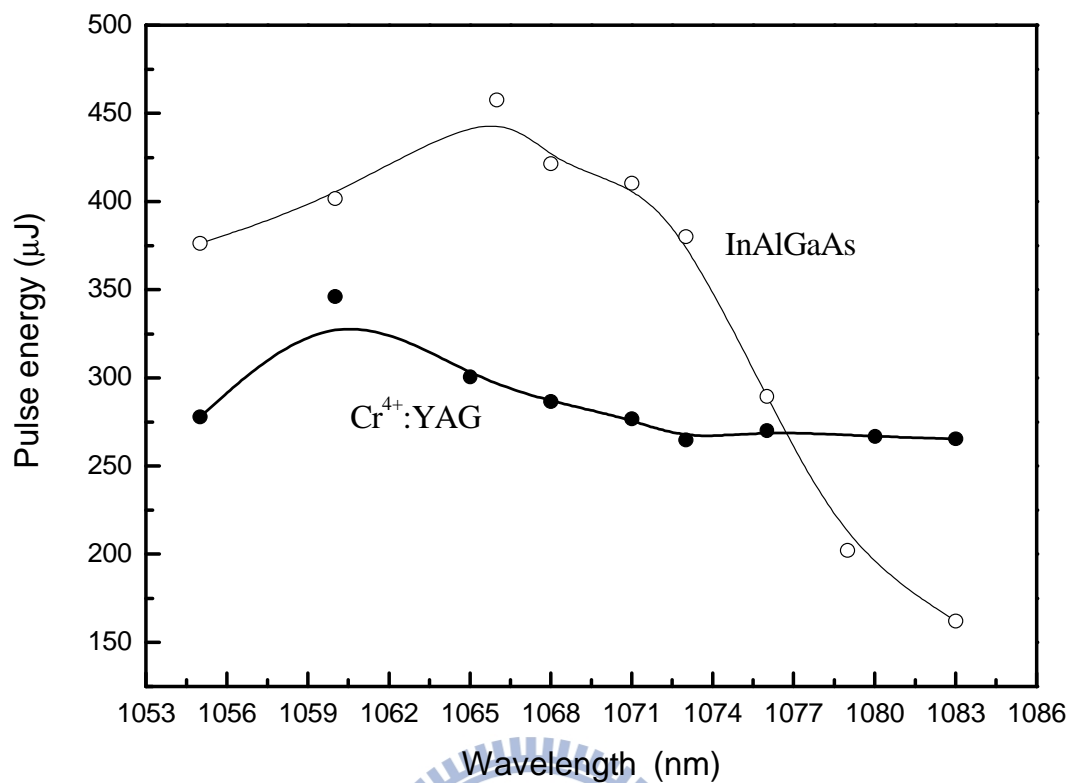


Fig. 2.13 Pulse energy versus the resonant wavelength.

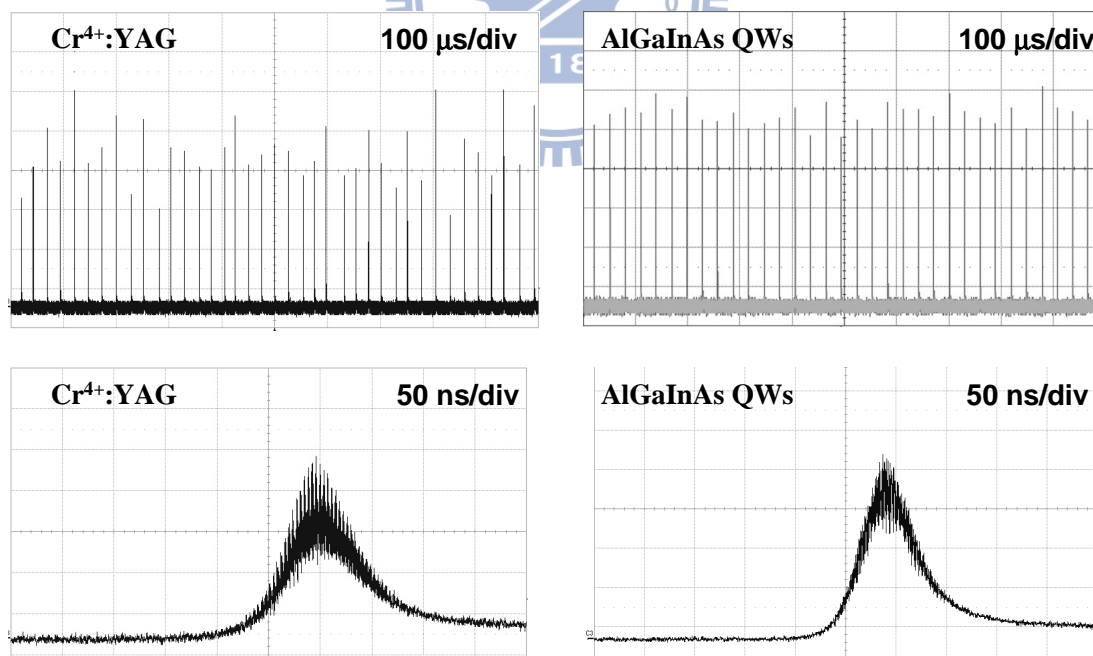
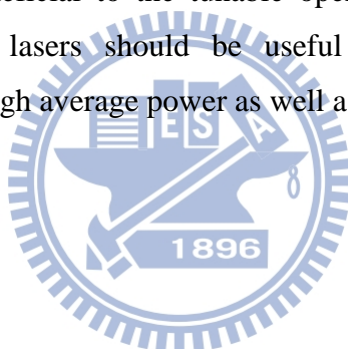


Fig. 2.14 Top: Oscilloscope traces of a typical Q-switched envelope; Bottom: Oscilloscope traces of a train of Q-switched pulses.

(D) Conclusion

In conclusion, I have demonstrated comparative studies for the Cr⁴⁺:YAG crystal and the AlGaInAs QWs used as a SA in efficient high-pulse-energy PQS Yb-doped fiber lasers. The two SAs were designed to exhibit nearly identical small-signal transmission of ~28%. Under a pump power of 24 W, the average output powers were up to 14.4 W and 13.8 W obtained with the AlGaInAs QWs and with the Cr⁴⁺:YAG crystal, respectively. The maximum pulse energies obtained with the AlGaInAs QWs and with the Cr⁴⁺:YAG crystal were 0.45 mJ and 0.35 mJ, respectively. The pulse-to-pulse stability was found to be noticeably better with the AlGaInAs QWs than with the Cr⁴⁺:YAG crystal. Nevertheless, the Cr⁴⁺:YAG crystal has a broader absorption band that is beneficial to the tunable operation. It is believed that the efficient Q-switched fiber lasers should be useful light sources for technical applications because of its high average power as well as high pulse energy.



2.3 Hybrid Q-switched Yb-doped fiber laser

Double-clad ytterbium (Yb) doped large-mode-area fiber lasers have been confirmed to possess the advantages of good heat dissipation, high efficiency, and high gain. Compared to CW fiber lasers, high-power and high-pulse-energy Q-switched fiber lasers have proved to be practically useful in various applications such as range finding, remote-sensing, and coherent lidar systems [19-20, 22]. The Q-switched pulse energy is mainly determined by the mode field area, the lifetime of active ions, and the modulation depth of Q-switch. To achieve high-pulse-energy Yb-doped LMA Q-switched fiber lasers, a Q-switch with large modulation loss is requested. Acousto-optic modulators (AOMs) with high diffraction loss [19-20, 22] and saturable absorbers with high modulation depth [45-46] have been recently employed as Q-switchers to obtain high-power and high-pulse-energy Yb-doped fiber lasers, respectively. The advantages of active Q-switching (AQS) are tunable repetition rate and stable pulse generation. However AOMs, or acousto-optic (AO) Q-switches demand high driving RF-power to realize high modulation losses for high power lasers. Hence the RF-power drivers and the cooling systems would be complicated. On the other hand, passive Q-switching (PQS) by saturable absorbers can operate without external driving electronics. The timing jitter, however, of PQS fiber lasers is inevitable and it would limit the availability for applications. Timing jitter is mainly attributed to the fact that lasers originate from photons of the spontaneous emission which would be affected by fluctuations of temperature in gain medium and wavelength of pump sources [47,48]. There are many works done to reduce the timing jitter for PQS lasers such as composite pump scheme [47] and optical triggering saturable absorbers by electrically controlled light sources [49-51]. The former method is limited to operate only near the lasing threshold while the latter would decrease the pulse energy owing to the pre-bleaching to saturable absorbers.

Compared to AQS and PQS, an alternative method is to use a large-modulation-depth saturable absorber and a low-RF-power driven AO Q-switch simultaneously. In the hybrid Q-switched (HQS) operation, the saturable absorber is used for generating high modulation loss while the AO Q-switch is used for reducing

the timing jitter. The HQS method has been employed in CO₂ laser [52], solid-state microchip laser [53,54], and high average power solid-state laser [55]. Nevertheless, to our best knowledge hybrid Q-switched fiber lasers have not yet been investigated so far.

In this section I investigate the performance of a HQS fiber laser that is constructed with a low RF-power driven AO Q-switch and an AlGaInAs semiconductor saturable absorber. Compared to a PQS fiber laser, the ratio of timing jitter to pulse period can be significantly reduced from 2% to 0.3% in the regime of far above threshold. On the other hand, the prelasing effect in a pure AO Q-switched fiber laser can be considerably improved. More importantly, the maximum pulse energy of the HQS fiber laser can be increased approximately 25% in comparison with the result of the PQS fiber laser. At a pump power of 24 W, the highest pulse energy is up to 0.56 mJ with the pulse duration of 50 ns at a repetition rate of 23 kHz.

(A) Experimental setup

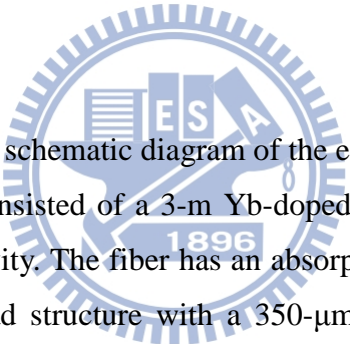


Figure 2.15 presents the schematic diagram of the experimental setup of the HQS Yb-doped fiber laser that consisted of a 3-m Yb-doped fiber (nLIGHT Corporation) and an external feedback cavity. The fiber has an absorption coefficient of 10.8 dB/m at 976 nm and a double-clad structure with a 350- μ m octagonal outer cladding, a 250- μ m inner cladding with a numerical aperture (N.A.) of 0.46, and a 30- μ m circular core with a N.A. of 0.07. The fiber end facet near the external cavity was angle-cleaved to prevent Fresnel reflection and parasitic lasing and the other end facet was normal-cleaved as an output coupler with reflectivity of 4%. The external feedback cavity comprised an aspheric lens with the focal length of 25 mm, the saturable absorber, a highly reflective mirror for 1030nm~1100nm, a Fabry-Pérot thin film filter (FP filter), and an AO Q-switch. The peak of the FP filter is at 1100 nm with a full-width-at-half-maximum bandwidth of 5 nm at normal incidence. The FP filter was used here for shortening and selecting the resonant wavelength, which was chosen as 1066 nm to match the resonant wavelength of the absorber. The AlGaInAs absorber was designed with 50 groups of three quantum wells (QWs) as described in Ref [30, 45]. Both sides of the semiconductor absorber were coated for anti-reflecting to reduce back reflections and the couple-cavity effects. The saturation energy density, the initial transmission, and the final transmission of AlGaInAs QWs are 1 mJ/cm²,

6 dB/m. The value of absorption coefficient was lower than the specification and might be due to different spectral profile and beam quality of the pump source. The performances of the PQS fiber laser are shown in Fig. 2.16. Figure 2.16 (a) describes the dependence of average power on the pump power for continuous-wave (CW) and PQS operations. The threshold pump powers were both nearly 2 W for CW and PQS operation and the maximum average powers were 16 W and 14 W, respectively. The corresponding optical slope efficiencies were 74% and 67% for CW and PQS regimes, respectively. The roll-over at the highest pump power was attributed to the spectral shifting and broadening of the pump source. The Q-switching efficiency (the ratio of the maximum PQS power to the maximum CW power) was about 88%. The shortest pulse width was 60 ns obtained at a pump power of 24 W. Figure 2.16 (b) shows the dependences of pulse period and the ratio of timing jitter to pulse period on the launched pump power. As I increased launched pump power from 3 W to 24 W, the pulse period decreased from 512 μ s to 31 μ s and the ratio of timing jitter to pulse period was also found diminished from 12% to 2%. The oscilloscope traces of trains of the PQS laser at various pump power are shown in Fig. 2.16 (c).

In order to improve the jitter, the AO Q-switch was inserted inside the external cavity. The diffraction efficiency of the AO Q-switch was measured to be about 30% by using the aforementioned CW fiber laser. The duty cycle of loss modulation of the AO Q-switch was set 90%, i.e. the ON-time of the RF-power was 90% of the pulse period. In the HQS operation, the pulse repetition rate of the HQS laser (f_{HQS}) could be operated stably between approximately 0.7 and 0.8 times the pulse repetition rate of the PQS laser (f_{PQS}) for all pump powers. In a conventional PQS laser, the pulse repetition rate is proportional to the cavity gain-to-loss ratio. Since AO Q-switch introduced additional losses in the cavity, the stable range of the f_{HQS} was less than the value of f_{PQS} . Figure 2.17 shows the oscilloscope traces of (a) the PQS pulses (period = 512 μ s) and (b) the HQS pulses (period = 620 μ s) at the pump power of 3W, respectively.

When the operational frequency in HQS configuration was out or range of stable region, the output pulse was found to be irregular. Figure 2.18 (a) shows the oscilloscope traces of trains of the HQS laser when f_{AO} was higher than $0.8 \times f_{\text{PQS}}$, where the output pulse train was extremely unstable. As the repetition rate of the AO Q-switch (f_{AO}) was decreased to lower than $0.7 \times f_{\text{PQS}}$, a prelasing effect occurred, as shown in Fig. 2.18 (b). The prelasing was attributed to the lasing by residual feedback

Ch2 Pulsed large mode area fiber lasers and amplifier

within the low-Q time interval rather than amplified spontaneous emission (ASE). Furthermore, I measured the lasing optical spectrum and confirmed no obvious ASE effect in HQS configuration.

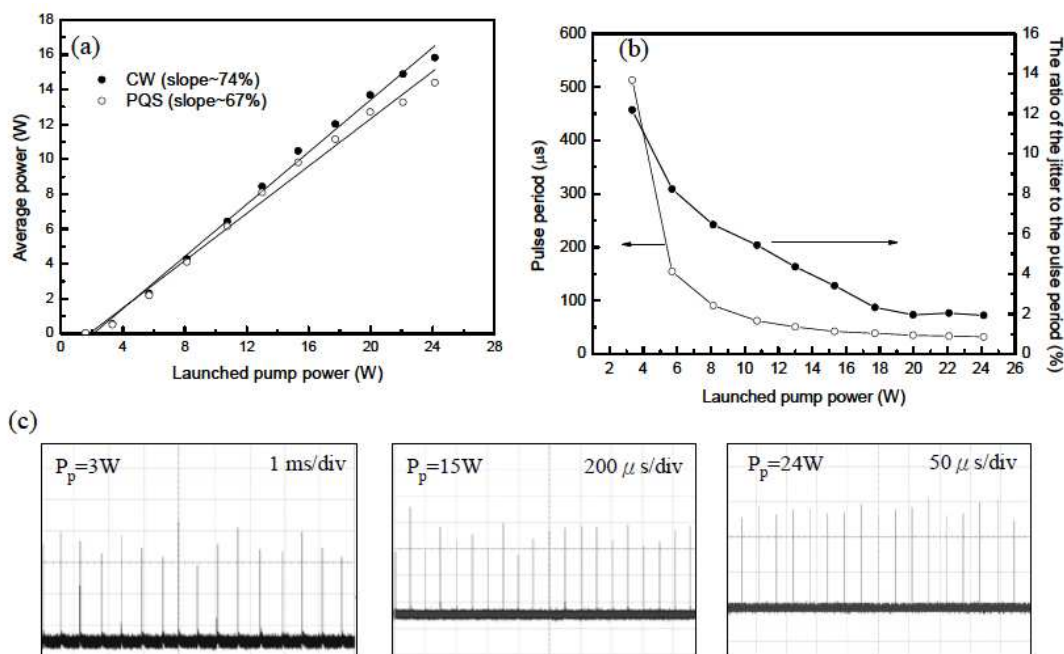


Fig. 2.16 (a) Dependence of average output power on the launched pump power for the CW and passive Q-switching operations; (b) dependence of pulse period and timing jitter on the launched pump power; (c) the oscilloscope traces of trains of the PQS pulses at various pump powers.

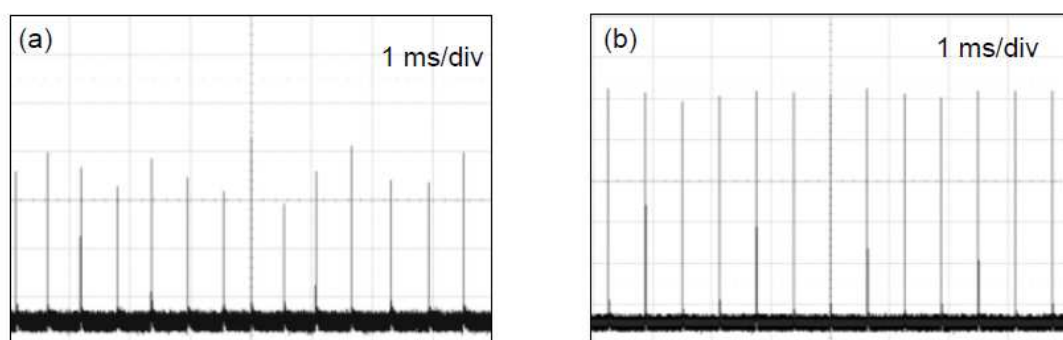


Fig. 2.17 The oscilloscope traces of trains of (a) the PQS pulses (period = 512 μs) and (b) the HQS pulses (period = 620 μs) at the pump power of 3W.

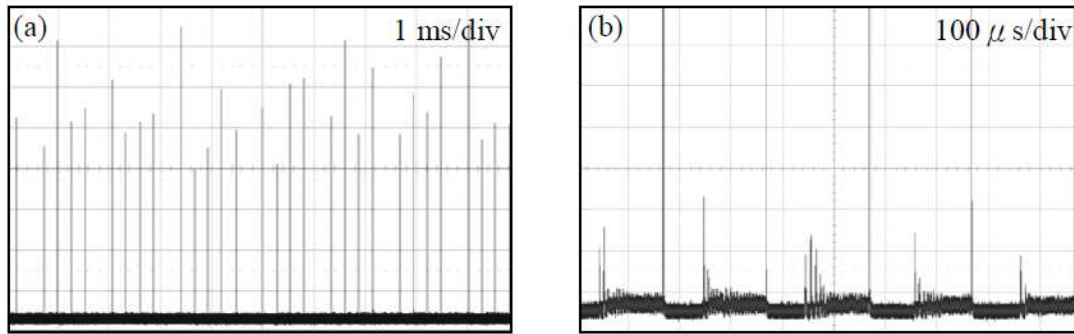


Fig. 2.18 The oscilloscope traces of trains of the HQS fiber laser when f_{AO} was (a) higher than $0.8 \times f_{PQS}$ (b) lower than $0.7 \times f_{PQS}$.

To investigate the performances of the HQS laser, a pure AQS laser with the identical AO Q-switch was also demonstrated for comparison. Figure 2.19 (a) and (b) presents the comparison of the pulse repetition rate and the pulse energy of the PQS laser, the HQS laser, and the AQS laser, respectively. The green and the blue regions represent the operational repetition rate and the pulse energy of the AQS laser and the HQS laser, respectively. As shown in Fig. 2.19 (a), at the pump power of 24 W the highest and the lowest pulse repetition rate of the pure AQS laser were 200 kHz and 54 kHz, respectively. Figure 2.19 (c) shows the oscilloscope of traces of trains of the pure AQS laser at various repetition rates under a pump power of 24W.

The upper and the lower pulse repetition rates of the pure AQS laser were limited by low intracavity circulating photon density and the prelasing effect, respectively. On the other hand the pulse repetition rate of the HQS laser at the pump power of 24 W could be operated from 23.6 kHz to 28.6 kHz. In Fig. 2.19 (b), the maximum pulse energy of the HQS laser was 0.56 mJ, which was virtually twice higher than the pulse energy of the AQS laser and 25% higher than that of the PQS laser. The shortest pulse widths in the three regimes were 150 ns, 60 ns, and 50 ns for the AQS, the PQS, and the HQS lasers at the pump power of 24 W, respectively. Note that although the gain fiber could guide 15 modes (V number ~ 6), the M^2 beam-quality factors of the three regimes were measured to be < 1.5 by coiling the fiber with a diameter of 10 cm.

For studying the jitter reduction, I measured the pulse period and the jitter of both the PQS and the HQS lasers at a pump power of 3 W where the PQS laser experienced the largest jitter. Figure 2.20 shows both the pulse period and the corresponding histogram for about 1000 pulses of the PQS and the HQS lasers, respectively. The average periods of the HQS and the PQS operations were $620 \pm$

Ch2 Pulsed large mode area fiber lasers and amplifier

0.074 μs and $512 \pm 31 \mu\text{s}$, respectively. The jitter is expressed in terms of the standard deviation of the pulse period. The jitter was reduced significantly from 62 μs to 140 ns which is almost the same as the jitter (~ 120 ns) obtained in the AQS fiber laser at the same pump power.

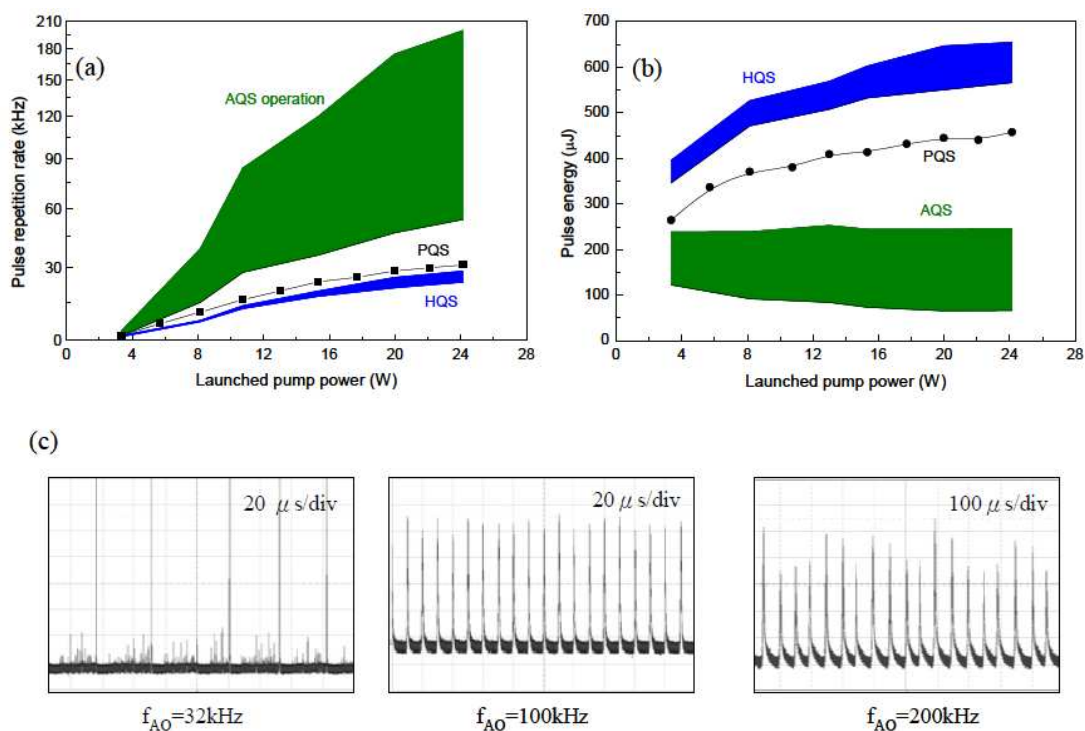


Fig. 2.19 (a) The pulse repetition rate of the pure PQS, the pure AQS, and the HQS lasers at the various launched pump powers; (b) the pulse energy of the three lasers at the various launched pump powers. The green and the blue regions represent the operational repetition rate of the AQS laser and the HQS laser, respectively; (c) the oscilloscope traces of trains of pure AQS laser at various repetition rates under a pump power of 24 W.

This result could be also observed in the previous experiments [53,54]. In Ref [53], the minimal jitter ~ 400 ns is slightly larger than the jitter of 200 ns obtained in their AQS laser. The larger jitter was attributed to the fact that the Cr^{4+} : YAG crystal absorber was not bleached fast enough when the AO Q-switch was opened (RF-power OFF). In contrast, the semiconductor absorber requires a shorter bleaching time due to the smaller saturation fluence of semiconductor absorbers compared to the Cr^{4+} :YAG crystal [45].

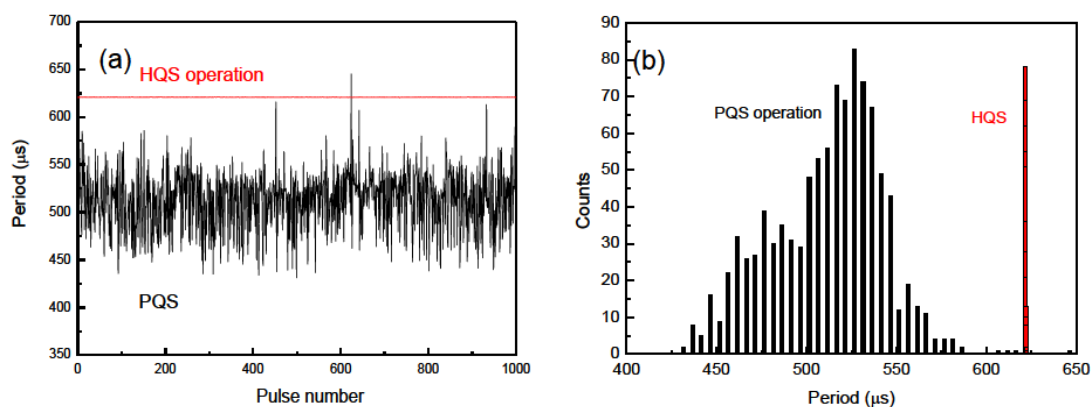


Fig. 2.20 (a) The pulse period and (b) the corresponding histogram of the pulse period of the PQS and the HQS lasers at the pump power of 3 W. The timing jitter is expressed in terms of standard deviation of the pulse period.

Moreover, to study the dependence of the jitter on the duty cycle of loss modulation, I varied the duty cycle from 0% (i.e. PQS operation) to 90% for three different pump powers of 3 W, 15 W, and 24 W. The f_{AO}^{-1} were set $620 \mu\text{s}$ for P_p of 3W, $55.56 \mu\text{s}$ for P_p of 15W, and $38.31 \mu\text{s}$ for P_p of 24 W, respectively. Figure 2.21 depicts the dependence of the ratio of jitter to pulse period of the HQS laser on the duty cycle of loss modulation for the three pump powers. At the duty cycle = 0%, the jitters for the three pump powers were $62 \mu\text{s}$ (pump power, $P_p = 3 \text{ W}$; period = $512 \mu\text{s}$), $1.4 \mu\text{s}$ ($P_p = 15 \text{ W}$; period = $54 \mu\text{s}$), and $0.6 \mu\text{s}$ ($P_p = 24 \text{ W}$; period = $38 \mu\text{s}$). The ratios were reduced substantially at the duty cycle = 40%. At the pump power of 3W, the ratio was reduced greatly from 12% (jitter = $62 \mu\text{s}$) to 0.05% (jitter = $0.3 \mu\text{s}$). Besides, the ratios for the higher two pump powers decreased from 3.4% (jitter = $1.43 \mu\text{s}$) to 0.35% (jitter = $0.2 \mu\text{s}$) for $P_p = 15 \text{ W}$ and 1.9% (jitter = $0.61 \mu\text{s}$) to 0.3% (jitter = $0.1 \mu\text{s}$) for $P_p = 24 \text{ W}$. Increasing continuously the duty cycle to 90%, the ratios decreased to 0.02% (140 ns) for $P_p = 3\text{W}$, 0.19% (100 ns) for $P_p = 15 \text{ W}$, and 0.2% (80 ns) for $P_p = 24 \text{ W}$. The minimal jitters were nearly the same results obtained in the AQS laser, implying that the restriction is mainly due to the jitter of the pump scheme and the driving electronics of the AO Q-switch. The experimental result reveals that a further jitter-reduction would be achieved by using a more stable pump source and driving electronics.

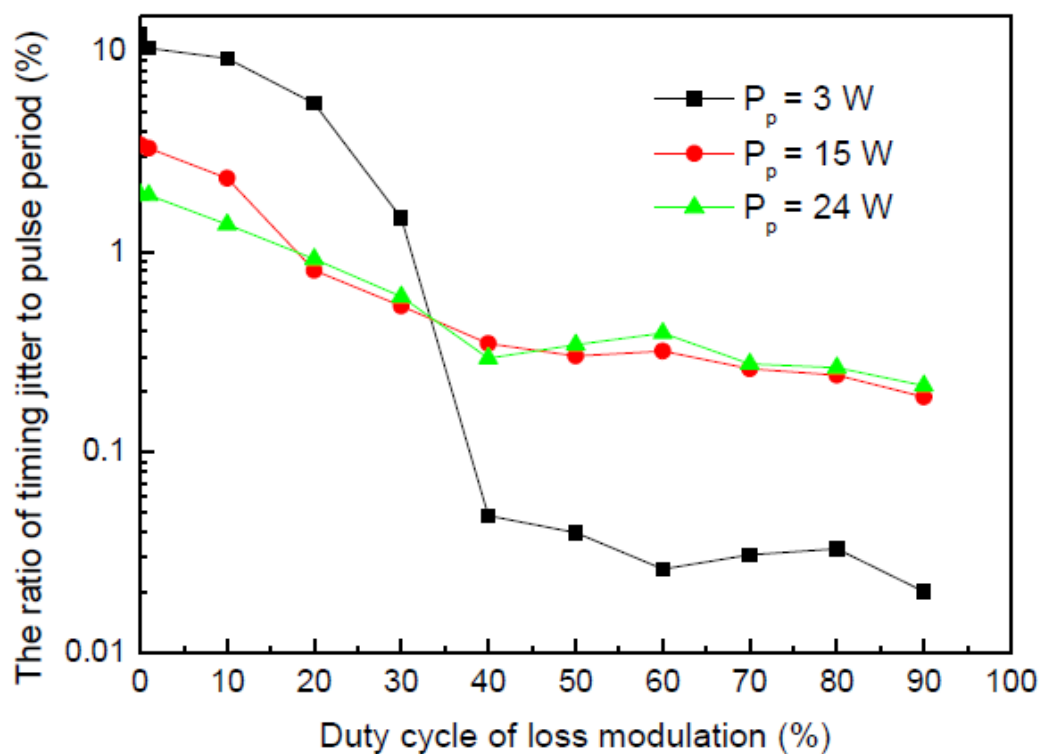


Fig. 2.21 The dependence of the ratio of jitter to pulse period of the HQS laser on the duty cycle of loss modulation for the pump power of 3W, 15W, and 24W. The f_{AO}^{-1} were set $620\ \mu\text{s}$ for P_p of 3W, $55.56\ \mu\text{s}$ for P_p of 15W, and $38.31\ \mu\text{s}$ for P_p of 24 W, respectively.

(C) Conclusion

In conclusion, I have investigated the performance of a HQS fiber laser that was constructed with a low RF-power driven AO Q-switch and an AlGaInAs semiconductor saturable absorber. The HQS method combines the advantages of the passive Q-switching and the active Q-switching. Compared to a pure PQS fiber laser, the ratio of timing jitter to pulse period can be significantly reduced from 2% to 0.3% in the regime of far above threshold. On the other hand, the pre-lasing effect in a pure actively Q-switched fiber laser can be considerably improved. The maximum pulse energy of the HQS fiber laser can be increased approximately 100% and 25% in comparison with the results of the AQS and the PQS fiber laser, respectively. At a pump power of 24 W, the highest pulse energy is up to 0.56 mJ with the pulse duration of 50 ns at a repetition rate of 23 kHz.

2.4 Fiber amplifier seeded by a passively Q-switched Nd:YVO₄/Cr⁴⁺:YAG laser

High-peak-power, linearly-polarized lasers with pulse repetition rates up to several tens of kHz have a wide variety of applications in range finding, nonlinear wavelength conversion, and material processing [56-58]. The thermally induced distortion is the main hindrance for power scale-up in solid-state crystal lasers [59]. The master-oscillator fiber power-amplifier (MOFA) that collects the advantages of good beam quality, high efficiency, compactness, and superior heat dissipation has been identified as a promising light source [60-64]. To achieve the high-peak-power pulses with single-stage amplification, diode-pumped actively Q-switched (AQS) [65,66] or passively Q-switched (PQS) Nd-doped lasers [67-69] are often used as the seed lasers of the Yb-doped MOFAs.

Compared to the active Q-switching, the PQS laser with a saturable absorber offers the advantages of compactness, robustness, and low cost. Since Cr⁴⁺:YAG crystals possess the advantages of high absorption cross section near the infrared region, high damage threshold, and low temperature-sensitive properties [70-76], they have been proved to be reliable saturable absorbers for Nd³⁺-doped lasers. Nevertheless, the Cr⁴⁺:YAG crystal is usually not convenient for the Nd-doped vanadate crystal lasers due to the mismatch between the stimulated emission cross section of the gain medium and the absorption cross section of the absorber. Several methods, including the three-element resonator with the intra-cavity focusing [70, 75, 77] or the employment of a *c*-cut crystal as the gain medium [78-80], have been proposed to overcome this mismatch. The three-element resonators, however, not only increase the complexity of the cavities but also lead to relatively long pulse durations owing to the long cavity lengths. On the other hand, the employment of a *c*-cut crystal inevitably raises the pumping threshold and loses the characteristic of linear polarization. Therefore, it is highly useful for the seed laser of MOFA to develop high-peak-power PQS lasers with *a*-cut vanadate crystals in a simple compact cavity.

In this work, I systematically consider the second threshold criterion and the

thermal lensing effect to develop compact and high-peak-power Nd:YVO₄/Cr⁴⁺:YAG PQS lasers with nearly hemispherical cavities. I further exploit several Cr⁴⁺:YAG crystals with different initial transmissions (T_0) to realize the designed PQS laser. Experimental results reveal that at a pump power of 5.4 W the output pulse energy increases from 22 μ J to 36 μ J and the pulse repetition rate decreases from 50 kHz to 25 kHz for the initial transmission of the Cr⁴⁺:YAG crystal decreasing from 70% to 40%. Injecting the seed laser obtained with $T_0=70\%$ into a polarization maintained Yb-doped fiber, the pulse energy and peak power at a pump power of 16 W are enhanced up to 178 μ J and 37 kW, respectively. Excellent amplification confirms the PQS performance. Employing the seed laser obtained with $T_0=40\%$, I find that the surface damage of the fiber limits the maximum pulse energy and peak power to be 192 μ J and 120 kW, respectively. The polarization extinction ratio is approximately 100:1 for both MOFAs in the whole pump power. To the best of our knowledge, this is the first time to realize high-peak-power, single-stage, linearly-polarized MOFAs with the compact Nd:YVO₄/Cr⁴⁺:YAG PQS lasers as seed oscillators.

(A) Analysis and optimization of the PQS laser

To achieve good passive Q-switching, absorption saturation in the absorber must occur before gain saturation in the laser crystal [65]. From the analysis of the coupled rate equation, the good passively Q-switching criterion which is also called second threshold condition is given by:

$$\frac{\ln(1/T_0^2)}{\ln(1/T_0^2) + \ln(1/R) + L} \frac{\sigma_{gsa}}{\sigma} \frac{A}{A_s} > \frac{\gamma}{1 - \beta}, \quad (2.1)$$

where R is the reflectivity of the output coupler, σ is the stimulated emission cross-section of the gain medium, σ_{gsa} is the ground-state absorption cross-section of the saturable absorber with the initial transmission T_0 , L is the nonsaturable intracavity round-trip dissipative optical loss, A/A_s is the ratio of the effective area in the gain medium to that in the saturable absorber, γ is the inversion reduction factor with a value between 0 and 2 [81], and β is the ratio of the excited-state absorption cross-section to that of the ground-state absorption in the saturable absorber. The challenge of obtaining a compact and stable Nd:YVO₄/Cr⁴⁺:YAG PQS laser results from which the emission cross-section of Nd:YVO₄ crystals ($\sim 2.5 \times 10^{-18} \text{ cm}^2$) [70] is

comparable with the ground-state absorption cross-section of Cr^{4+} :YAG crystals ($\sim(2 \pm 0.5) \times 10^{-18} \text{cm}^2$) [12]. It was found that unstable pulse trains with satellite pulses would occur when the good Q-switching criterion is not achieved [82, 83]. To fulfill the good passive Q-switching criterion in $\text{Nd}:\text{YVO}_4/\text{Cr}^{4+}$:YAG PQS lasers, the ratio A/A_s generally needs to be greater than 10 [83].

Even though the three-element resonator can be used to achieve the requirement of the ratio $A/A_s \geq 10$, the long cavity usually leads to a wide pulse duration. Here I utilize the nearly hemispherical resonator to develop compact high-peak-power $\text{Nd}:\text{YVO}_4/\text{Cr}^{4+}$:YAG PQS lasers to be seed oscillators. In terms of the g-parameters, the beam radii ω_1 and ω_2 on the rear and front mirrors are given by [84]:

$$g_i = 1 - \frac{L}{\rho_i}, \quad (2.2)$$

$$\omega_i = \sqrt{\frac{\lambda L}{\pi}} \sqrt{\frac{g_j}{g_i(1-g_1g_2)}}; \quad i, j = 1, 2; i \neq j, \quad (2.3)$$

where L is the cavity length, λ is the wavelength of laser mode, and ρ_1 and ρ_2 are the radii of curvature of the rear and front mirrors, respectively. For a simple plano-concave resonator, as depicted in Fig. 2.22(a), $g_1 = 1 - (L/\rho_1)$ and $g_2 = 1$.

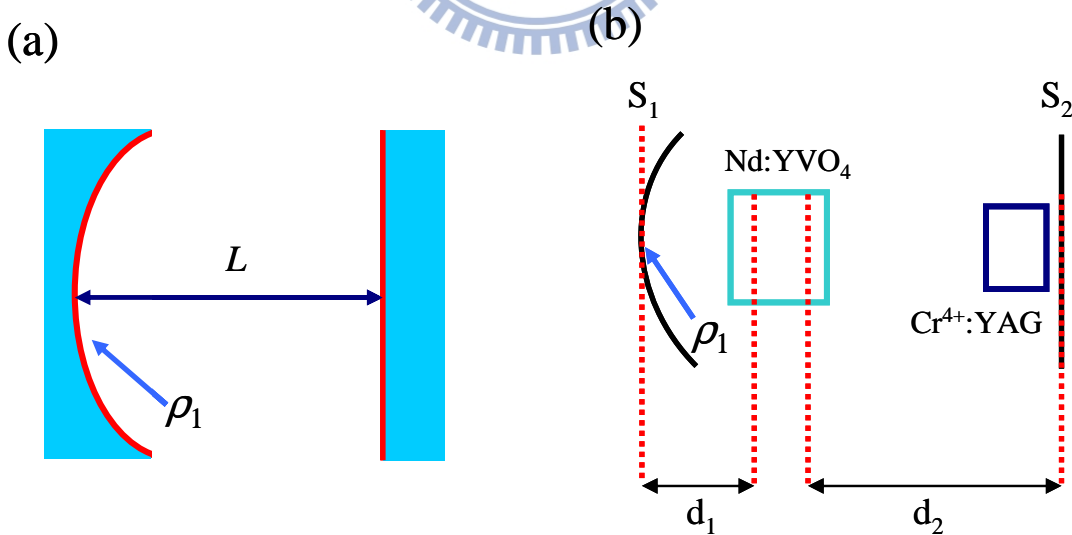


Fig. 2.22 (a) Schematic diagram of the plano-concave cavity. (b) Equivalent cavity diagram of the $\text{Nd}:\text{YVO}_4/\text{Cr}^{4+}$:YAG PQS laser.

Given that the gain medium and the saturable absorber are as close as possible to the rear mirror and the flat output coupler, the ratio of the effective area in the gain medium to that in the saturable absorber A/A_s can be found to be

$$\frac{A}{A_s} = \frac{\omega_1^2}{\omega_2^2} = \frac{\rho_1}{\rho_1 - L} \quad (2.4)$$

Equation (2.4) reveals that the ratio A/A_s can be up to 10 under the circumstance of a nearly hemispherical cavity with $L=0.9 \rho_1$. A smaller ρ_1 consequently corresponds to a shorter cavity length that is beneficial for the generation of Q-switched pulses with narrower pulse duration. Nevertheless, the geometrical sizes of the gain medium, the saturable absorber, and the heat sinks limit the minimum cavity length. Therefore, $\rho_1=25$ mm is chosen for further optimizing the compact high-peak-power Nd:YVO₄/Cr⁴⁺:YAG PQS laser.

The next design parameter is the pump size that needs to be optimized to reach the good mode matching for the fundamental transverse mode. Since the thermal lensing effect in the gain medium always affects the cavity mode size, it is practically important to consider the thermal lensing effect for determining the optimum pump size. For an end-pumped crystal laser, the thermal lens is given by [85]:

$$\frac{1}{f_{th}} = \frac{\xi P_{in}}{\pi K_c} \int_0^l \frac{\alpha e^{-\alpha z}}{1 - e^{-\alpha l}} \frac{1}{\omega_p^2(z)} \left[\frac{1}{2} \frac{dn}{dT} + (n-1)\alpha_T \frac{\omega_p(z)}{l} \right] dz \quad (2.5)$$

where

$$\omega_p(z) = \omega_{p0} \sqrt{1 + \left[\frac{\lambda_p M_p^2 (z - z_0)}{n \pi \omega_{p0}^2} \right]^2} \quad (2.6)$$

z_0 is the focal plane of the pump beam in the laser crystal, M_p^2 is the pump beam quality factor, ω_{p0} is the pump beam radius, n is the refractive index of along the c -axis of the laser crystal, λ_p is the wavelength of the pump laser diode, ξ is the fractional thermal loading, K_c is the thermal conductivity, P_{in} is the incident pump power, α is the absorption coefficient of the gain medium, l is the crystal length, dn/dT is the thermal-optic coefficient of n , and α_T is the thermal expansion coefficient along the a -axis.

Figure 2.22(b) depicts the configuration of a nearly hemispherical resonator for a Nd:YVO₄/Cr⁴⁺:YAG PQS laser. Considering the thermal lens effect and taking S_1 as the reference plane, the ray transfer matrix from S_1 to S_2 of the cavity configuration

can be presented as [86]:

$$M_D = \begin{pmatrix} g_1^* & L^* \\ \frac{g_1^* g_2^* - 1}{L^*} & g_2^* \end{pmatrix} \quad (2.7)$$

$$g_i^* = g_i - \frac{d_j}{f_{th}} \left(1 - \frac{d_i}{\rho_i}\right) \quad (2.8)$$

$$g_i = 1 - \frac{d_1 + d_2}{\rho_i} ; i, j = 1, 2 ; i \neq j, \quad (2.9)$$

$$L^* = d_1 + d_2 - \frac{d_1 d_2}{f_{th}} \quad (2.10)$$

Here d_1 and d_2 are the optical path length between the cavity mirrors and the principal planes of the laser crystal, and f_{th} is the effective focal length of the thermal lens. With the following parameters: $\xi=0.24$, $K_c=5.23$ W/K-m, $d_1=2$ mm, $d_2=0.9\rho_1-d_1$, $\rho_2=\infty$, $n=2.165$, $l=12$ mm, $dn/dT=3.0 \times 10^{-6}$ K⁻¹, $M_p^2=80$, $\alpha=6$ mm⁻¹, $\alpha_T=4.43 \times 10^{-6}$ K⁻¹, and $\lambda_p=808$ nm, the effective focal length of the thermal lens effect and g^* -parameters of the resonator can be calculated as functions of the incident pump power. In terms of the g^* -parameters for the thermal lensing effect, the beam radii ω_1 and ω_2 on the rear and front mirrors can be expressed as [86]:

$$\omega_i = \sqrt{\frac{\lambda L^*}{\pi}} \sqrt{\frac{g_j^*}{g_i^* (1 - g_1^* g_2^*)}} ; i, j = 1, 2 ; i \neq j \quad (2.11)$$

Figure 2.23 shows the mode-to-pump size ratio ω_1 / ω_{pa} of different pumping spot radii as a function of the pump power with the radius of curvature of the rear mirror of 25 mm, where the averaged pump size along the gain medium is given by [87]:

$$\omega_{pa} = \int_0^l \omega_p(z) e^{-\alpha z} dz / \int_0^l e^{-\alpha z} dz \quad (2.12)$$

According to the optimal mode matching condition [87], the ratio of ω_1 / ω_{pa} should be in the range of 0.8 to 1.2 for $P_{in} < 10$ W. In our design, the maximum pump power is approximately 5.5 W. As can be seen from the Fig. 2.23, the optimum pump radius is in the region of 100 μ m.

With $\omega_{p0}=100$ μ m and $\rho_1=25$ mm, I consider the thermal lensing effect to calculate the effective mode area ratio of A/A_s as a function of the pump power. Figure 2.24 shows the calculated result for the dependence of the effective mode area ratio of A/A_s on the pump power. It can be seen that the effective mode area ratio of

A/A_s is generally greater than 10 for the pump power less than 5.5 W. To be brief, I choose a nearly hemispherical cavity with the radius of curvature of the rear mirror of 25 mm and the pumping spot radius of 100 μm to simultaneously satisfy the optimal mode matching condition and the good Q-switching criterion.

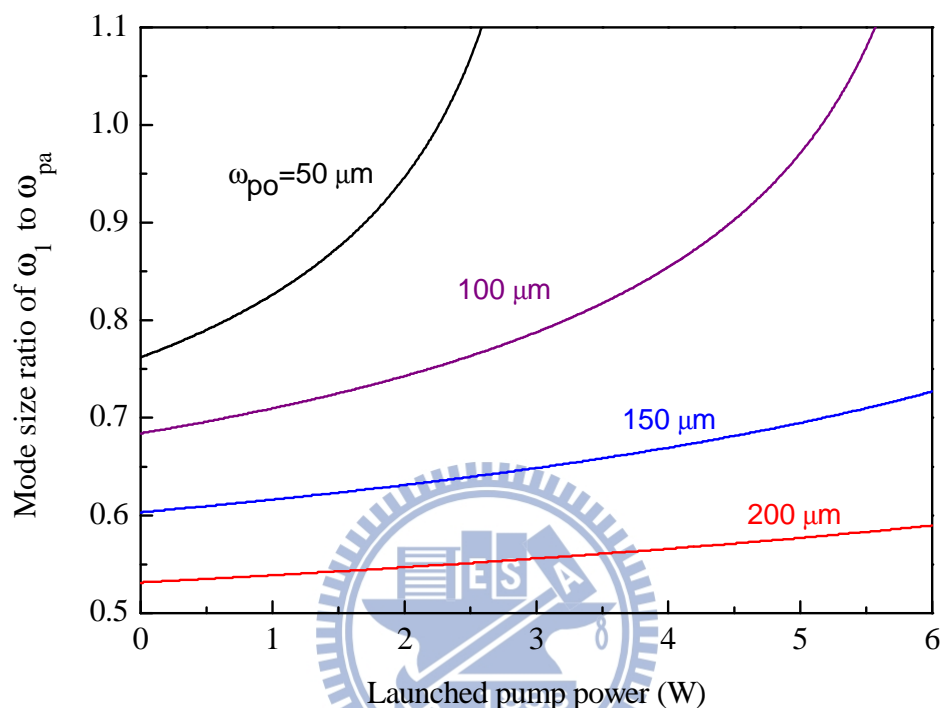


Fig. 2.23 Dependence of the mode-to-pump size ratio ω_1/ω_{pa} on the pump power for different pumping spot radii.

(B) Experimental results for the PQS laser

I followed the theoretical analysis to construct a nearly hemispherical cavity for realizing the compact high-peak-power Nd:YVO₄/Cr⁴⁺:YAG PQS laser, as shown in Fig. 2.25 for the experimental setup. The rear mirror was a concave mirror with a radius-of-curvature of 25 mm with high-transmission coating at 808 nm ($T \sim 95\%$) and high-reflection at 1064 nm ($R > 99.8\%$). The output coupler was a flat mirror with partially reflection at 1064 nm ($R = 60\%$). The pumping source was a 7-W 808-nm fiber-coupled laser diode with a core diameter of 200 μm and a numerical aperture of 0.22. The focusing lens with 25 mm focal length and 80% coupling efficiency was used to re-image the pump beam into the laser crystal. The gain medium was an *a*-cut

Ch2 Pulsed large mode area fiber lasers and amplifier

12-mm-long Nd:YVO₄ crystal with 0.3 at.% Nd³⁺ concentration. Several Cr⁴⁺:YAG absorbers with T₀ of 70 %, 60 %, 50 %, and 40 % were used to investigate the performance. The Cr⁴⁺:YAG crystals were all 2 mm in thickness. Both sides of the Nd:YVO₄ and the Cr⁴⁺:YAG crystals were coated for antireflection at 1064 nm. All the laser crystal were wrapped within indium foils and mounted in the water cooled heat sinks that keep at 19°C. The Nd:YVO₄ crystal and Cr⁴⁺:YAG crystals were placed as close as possible to the rear mirror and the output coupler respectively. The effective cavity length was set to be 22.5 mm based on the design rule of $L=0.9\rho_1$.

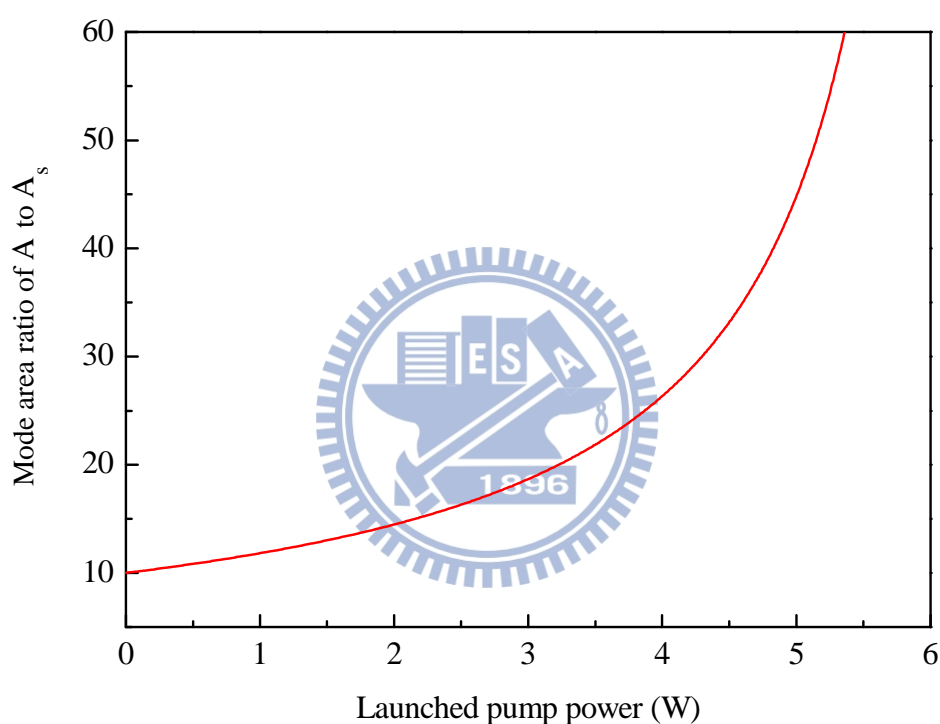


Fig. 2.24 Effective mode area ratio of A/A_s as a function of the pump power in the Nd:YVO₄/Cr⁴⁺:YAG PQS laser with $L=0.9\rho_1$, $\rho_1=25$ mm, $\omega_p=100$ μ m.

The pulse temporal behavior was recorded by Leroy digital oscilloscope (Wavepro 7100; 10G samples/sec; 4 GHz bandwidth) with a fast InGaAs photodiode. Figure 2.26(a) shows the output pulse energies and pulse repetition rates for Cr⁴⁺:YAG saturable absorbers with different initial transmissions T₀ at the pump power of 5.4 W. It can be seen that for the initial transmission T₀ decreasing from 70% to 40% the output pulse energy increases from 22 μ J to 36 μ J; at the same time, the pulse repetition rate decreases from 50 kHz to 25 kHz. Figure 2.26(b) depicts the

Ch2 Pulsed large mode area fiber lasers and amplifier

pulse widths and peak powers for saturable absorbers with different initial transmissions T_0 at the pump power of 5.4 W. For the initial transmission T_0 decreasing from 70% to 40% the pulse width can be seen to decrease from 4.8 ns to 1.6 ns; consequently, the peak power was enhanced from 4.5 kW to 22.5 kW. Figure 2.27(a) and 2.27(b) show typical oscilloscope traces for a single pulse at the maximum output powers of the seeds with $T_0=70\%$ and 40%, respectively. Experimental results reveal that the characteristics of the output pulse in the present PQS laser display a simple pulse train without the satellite pulses phenomenon. It is worth mentioning that the satellite pulses phenomena such as two pulses oscillate simultaneously or one giant pulse followed by a weak pulse are often observed when the laser cavity does not properly comply with the second threshold criterion in Eq. (2.1). The spectral spectrum was measured by an optical spectrum analyzer with 0.1-nm resolution (Advantest Q8381A). The spectral linewidths for all the present PQS lasers were nearly the same to be 0.5 nm. In the next section, I will employ these high-peak-power PQS lasers to realize a single stage, linear-polarized fiber amplifier.

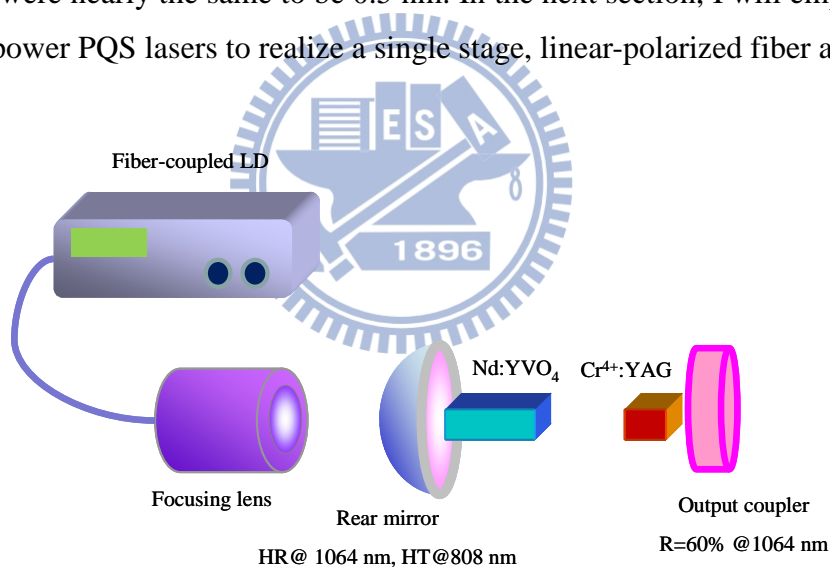


Fig. 2.25 Schematic diagram of a diode-pumped Nd:YVO₄ laser PQS with a Cr⁴⁺:YAG as a saturable absorber. HR: high reflection. HT: high transmission.

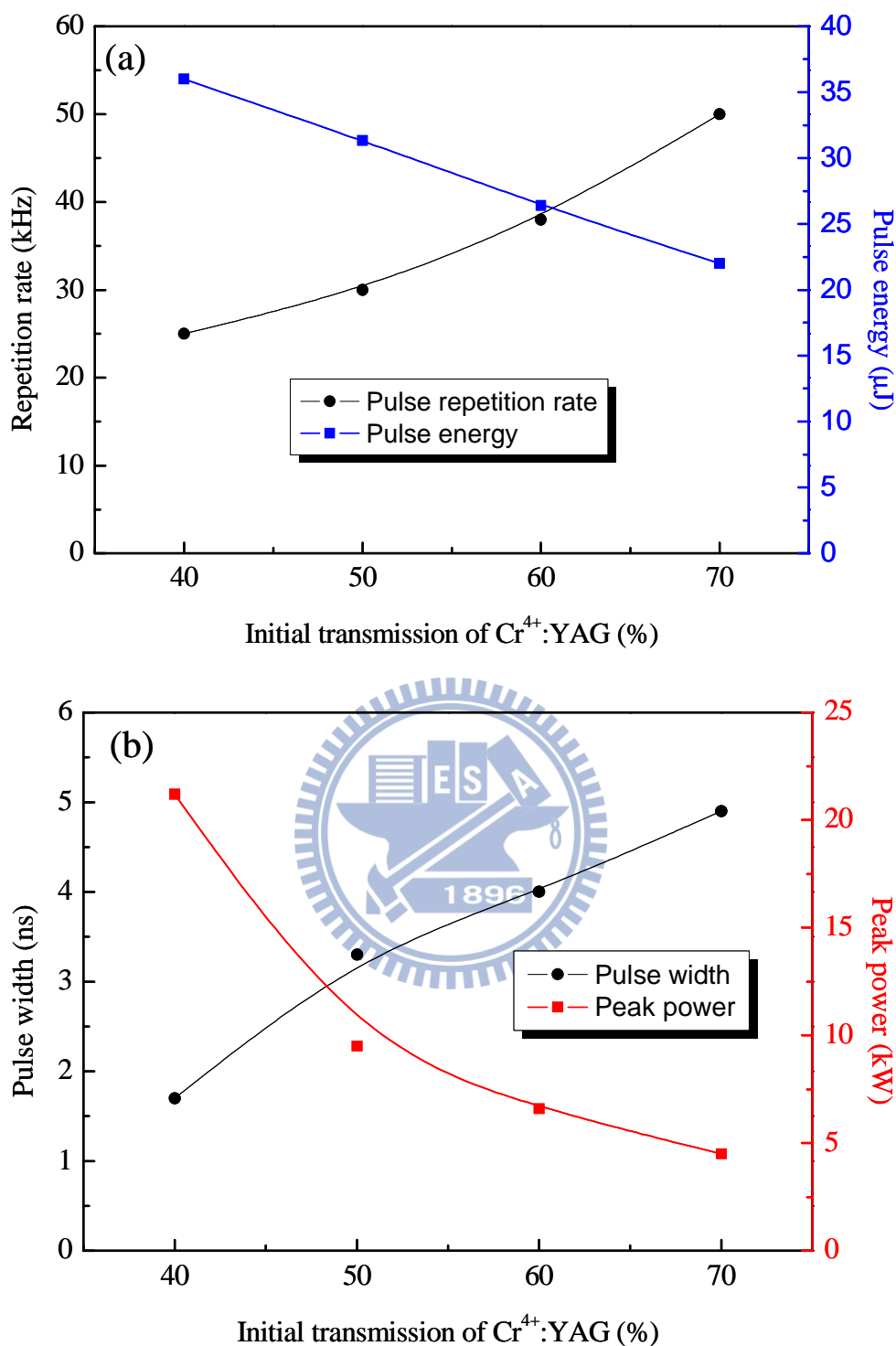


Fig. 2.26 (a) Dependence of the pulse repetition rate and the pulse energy on the initial transmission of Cr⁴⁺:YAG at the pump power of 5.4 W. (b) Dependence of the pulse width and the peak power on the initial transmission of Cr⁴⁺:YAG at the pump power of 5.4 W.

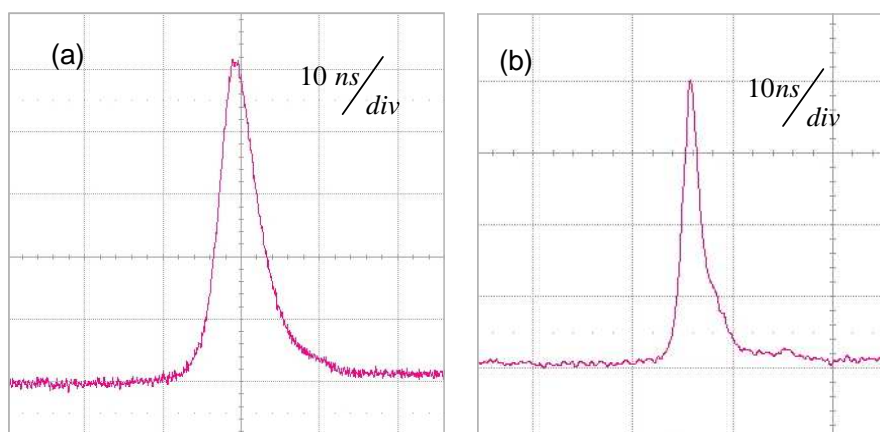


Fig. 2.27 Oscilloscope traces of a single pulse of (a) PQS laser with Cr^{4+} :YAG of $T_0=70\%$, (b) PQS laser with Cr^{4+} :YAG of $T_0=40\%$.

(C) Experimental results for the MOFA system

The experimental architecture for the MOFA system is shown in Fig. 2.28(a). The gain fiber was a 3-m-long Yb-doped Panda-style PM double clad fiber (Nufern) with a core diameter of $30\ \mu\text{m}$ (N.A.=0.06) and an inner clad diameter of $250\ \mu\text{m}$ (N.A.=0.46) with pump absorption of $6.6\ \text{dB/m}$ at $975\ \text{nm}$. The Panda-style stress applying parts around the core generate a birefringence of 1.5×10^{-4} . A microscope image of the fiber cross-section is depicted in Fig. 2.28(b). Both ends of the fiber were polished at an angle of 8° to eliminate the end facet reflection. The pump source was a 20-W 976-nm fiber-coupled laser diode with a core diameter of $200\ \mu\text{m}$ and a numerical aperture of 0.2. A focusing lens with 25-mm focal length was used to re-image the pump beam into the fiber through a dichroic mirror with high transmission (HT, $T > 90\%$) at $976\ \text{nm}$ and high reflectivity (HR, $R > 99.8\%$) within $1030\text{--}1100\ \text{nm}$. The pump spot radius was approximately $100\ \mu\text{m}$, and the pump coupling efficiency was estimated to be nearly 80%. The seed laser was coupled through a focusing lens into the core of the fiber. A half-wave plate was used to control the polarization direction of the seed laser to match the fast-axis of the PM fiber.

Figure 2.29(a) shows the average output power of the MOFA injected by the seed laser with $T_0=70\%$ as a function of launched pump power at a repetition rate of 50 kHz. Under the launched pump power of 16 W, the output power of the amplifier was 8.9 W, corresponding to the pulse energy of $178\ \mu\text{J}$. The slope efficiency was

approximately 54 %. Figure 2.29(b) shows the typical oscilloscope trace for a single pulse at the maximum output power of amplifier. The pulse duration was 4.8 ns and the corresponding peak power was 37 kW. The oscilloscope trace of a train of output pulses of the amplifier is shown in Fig. 2.29(c). The pulse-to-pulse amplitude fluctuation was generally less than 1.5% in root mean square (rms).

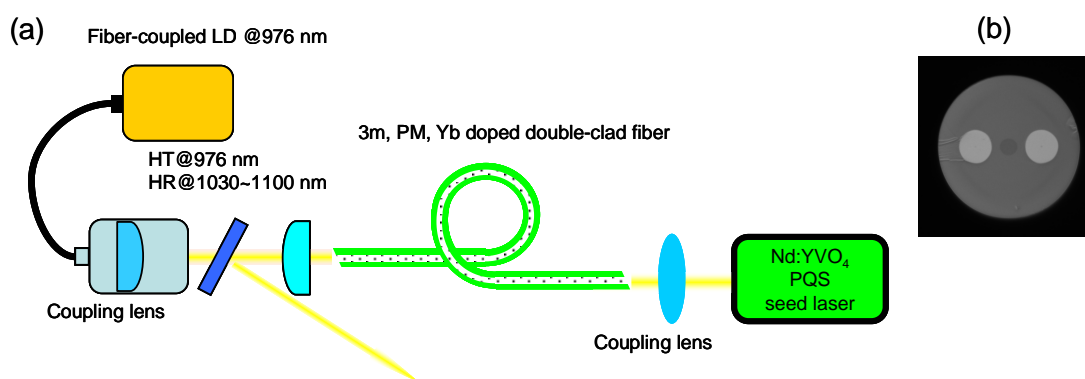


Fig. 2.28 (a) Scheme of the MOFA setup. HT: high transmission HR: high reflection.
(b) Cross section of the PM Yb-doped fiber.

Figure 2.30(a) shows the average output power of the MOFA injected by the seed laser with $T_0=40\%$ as a function of launched pump power at a repetition rate of 25 kHz. It was found that the end facet damage of the fiber limited the maximum average output power to be approximately 4.8 W under the pump power of 10 W. As a result, the maximum pulse energy was restricted to 192 μJ . Figure 2.31 depicts the microscope image of the damaged end view and the side view of the fiber. Figure 2.30(b) shows the typical oscilloscope trace for a single pulse at the maximum output powers of amplifier. The pulse duration was 1.6 ns and the corresponding peak power was 120 kW. The calculated optical intensity on the end facet of the fiber was 27.2 J/cm^2 which agrees with the surface damage threshold of fused silica at 1064 nm [88]. The oscilloscope trace of a train of output pulses of the amplifier is shown in Fig. 2.30(c). The pulse-to-pulse amplitude fluctuation was generally less than 4.0% in rms.

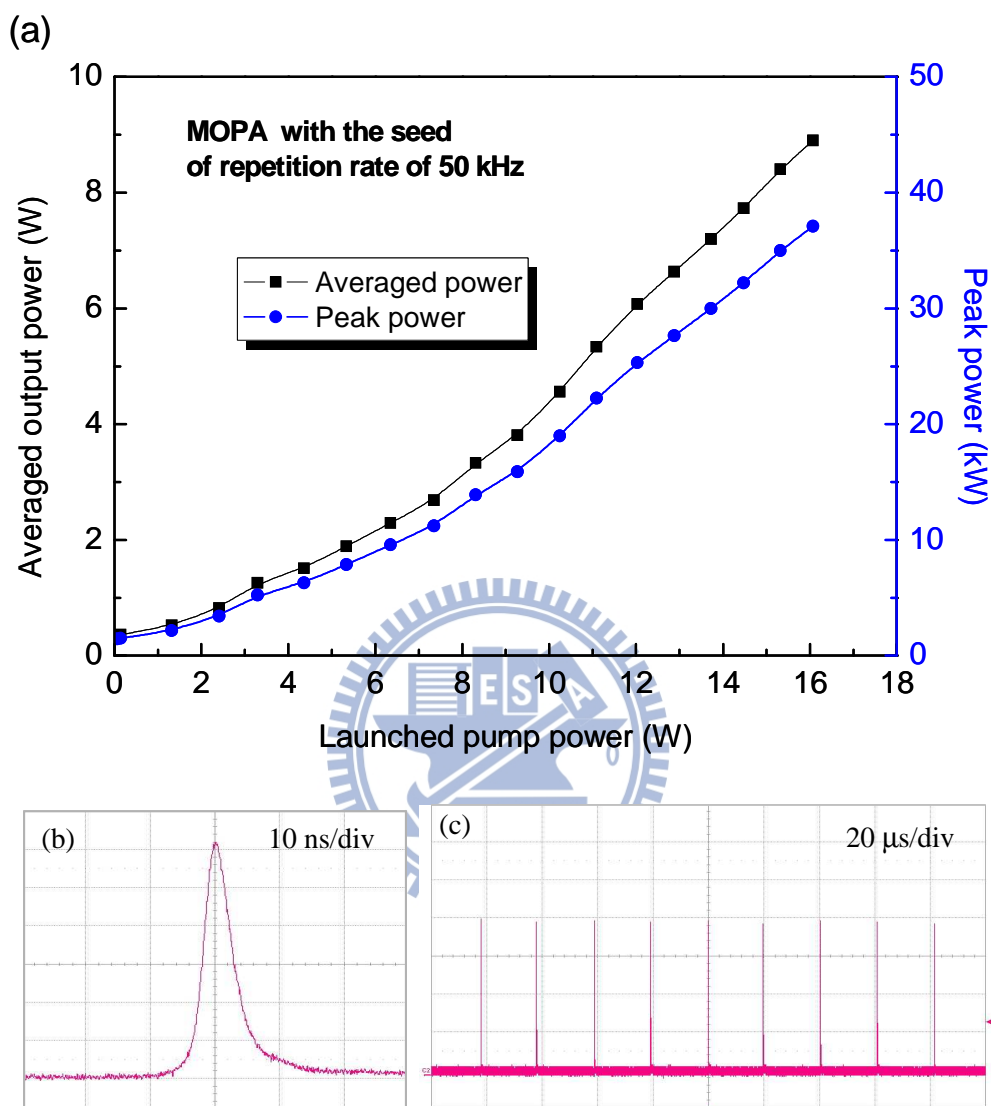


Fig. 2.29 (a) Average output power and peak power of MOFA with the seed of repetition rate of 50 kHz as a function of the launched pump power. (b) Oscilloscope traces of a single pulse of the output pulse of the amplifier. (c) Oscilloscope traces of a train of amplified pulses.

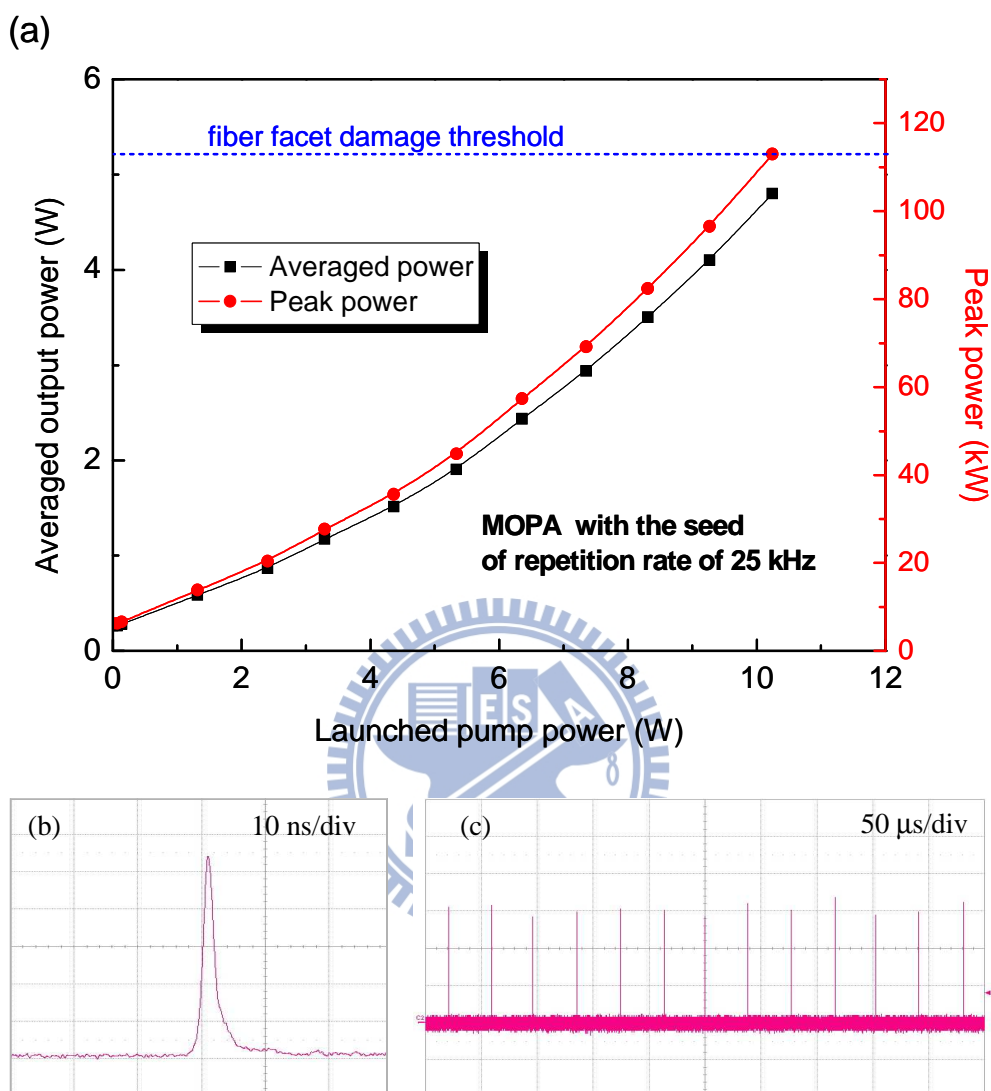


Fig. 2.30 (a) Average output power and peak power of MOFA with the seed of repetition rate of 25 kHz as a function of the launched pump power. (b) Oscilloscope traces of a single pulse of the output pulse of the amplifier. (c) Oscilloscope traces of a train of amplified pulses.

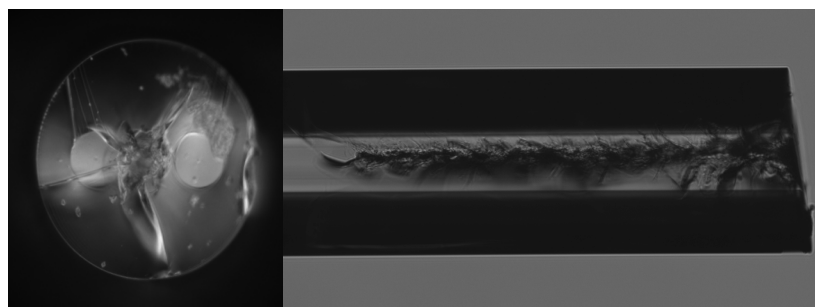


Fig. 2.31 End view and side view of the damaged fiber.

The timing jitters for both the amplifiers shown in Figs. 2.29 and 2.30 were generally less than 2 % in rms. The M^2 factors were found to be smaller than 1.3 over the entire output power range. Furthermore, the polarization extinction ratios for both the amplifiers were measured to be about 100:1. Figures 2.32(a) and 2.32(b) show the optical spectra of the MOFAs at the maximum output powers injected by the seed lasers with $T_0=70\%$ and $T_0=40\%$, respectively. It can be seen that the peak levels of the amplified spontaneous emission (ASE) around 1040 nm shown in Figs. 2.32(a) and 2.32(b) were approximately 30 dB and 40 dB below the signal peak intensity, respectively. The power levels of the whole ASE intensities at the maximum output powers shown in Figs. 2.32(a) and 2.32(a) were measured to be less than 2% and 0.5%, respectively.

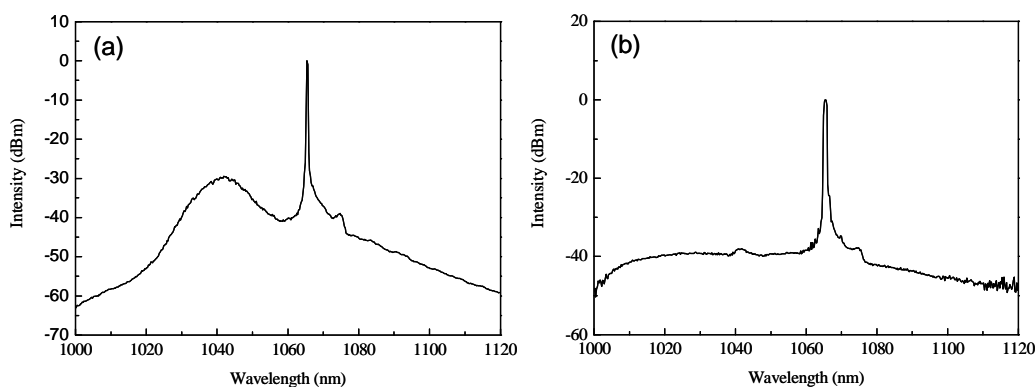


Fig. 2.32 Optical spectra of the MOFAs at the maximum output powers injected by the seed lasers with (a) $T_0=70\%$ and (b) $T_0=40\%$.

(D) Conclusions

In conclusion, I have developed compact Nd:YVO₄/Cr⁴⁺:YAG PQS lasers as seed oscillators for high-peak-power, single-stage, linear-polarized MOFAs. Compact and high-peak-power Nd:YVO₄/Cr⁴⁺:YAG PQS lasers were theoretically optimized by considering the second threshold criterion and the thermal lensing effect in a nearly hemispherical cavity. Several Cr⁴⁺:YAG crystals with different initial transmissions (T_0) have been used to confirm the performance of the designed PQS laser. It was experimentally found that at a pump power of 5.4 W the output pulse energy increases from 22 μ J to 36 μ J and the pulse repetition rate decreases from 50 kHz to 25 kHz for the initial transmission of the Cr⁴⁺:YAG crystal decreasing from 70% to 40%. Injecting the seed laser obtained with $T_0=70\%$ into a polarization maintained Yb-doped fiber, the pulse energy and peak power at a pump power of 16 W were found to be 178 μ J and 37 kW, respectively. Employing the seed laser obtained with $T_0=40\%$, it was found that the surface damage of the fiber limited the maximum pulse energy and peak power to be 192 μ J and 120 kW, respectively. The polarization extinction ratio was approximately 100:1 for both MOFAs in the whole pump power. It is believed that the high peak-power and high polarization-extinction-ratio suggest further applications such as industrial material processing and nonlinear optics researches.

2.5 Conclusions

In this chapter, I demonstrate efficient, high peak power fiber amplifier and PQS fiber lasers with either Cr^{4+} :YAG crystal or AlGaInAs MQWs as the SA. For timing jitter reduction, I also utilize the “hybrid Q-switch” technique by combining AQS and PQS into a single laser resonator. The pulse energy can be further enhanced and the pulse duration was also reduced. For applications that need short durations, I also demonstrate fiber amplifiers that seeded by Nd:YVO₄/Cr⁴⁺:YAG PQS lasers with different pulse repetition rate. However, the pulse peak power was limited by the fiber end facet damage that suggests the enlargement of the fiber core size. Nevertheless, the pulse energies were still superior to those of others due to the use of a LMA fiber with core diameter of 30 μm and SAs with large modulation depth and low non-saturable loss.



Reference

- [1]. T. Tordella, H. Djellout, B. Dussardier, A. Saissy, and G. Monnom, “High repetition rate passively Q-switched Nd³⁺:Cr⁴⁺ all-fibre laser,” *Electron. Lett.* **39**, 1307-1308 (2003).
- [2]. A. Fotiadi, A. Kurkov, and I. Razdobreev, “All-fiber passively Q-switched ytterbium laser,” in *CLEO/Europe-EQEC 2005, IEEE Technical Digest, CJ 2-3* (2005).
- [3]. A. Fotiadi, I. Razdobreev, B. Segard, and A. Kurkov, “Stable self-pulse behavior of two-core Yb/Sm fiber laser,” in *CLEO/Europe-EQEC 2009, IEEE Technical Digest, CJ 3–5* (2009).
- [4]. V. V. Dvoyrin, V. M. Mashinsky, and E. M. Dianov, “Yb-Bi pulsed fiber lasers,” *Opt. Lett.* **32**, 451–453 (2007).
- [5]. P. Adel, M. Auerbach, C. Fallnich, S. Unger, H.-R. Müller, and J. Kirchhof, “Passive Q-switching by Tm³⁺ co-doping of a Yb³⁺-fiber laser,” *Opt. Express* **11**, 2730–2735 (2003).
- [6]. M. Laroche, H. Gilles, S. Girard, N. Passilly, and K. Aït-Ameur, “Nanosecond pulse generation in a passively Q-switched Yb-doped fiber laser by Cr⁴⁺: YAG saturable absorber,” *IEEE Photon. Technol. Lett.* **18**, 764-766 (2006).
- [7]. L. Pan, I. Utkin, and R. Fedosejevs, “Passively Q-switched ytterbium-doped double-clad fiber laser with a Cr⁴⁺:YAG saturable absorber,” *IEEE Photon. Technol. Lett.* **19**, 1979-1981 (2007).
- [8]. L. Pan, I. Utkin, and R. Fedosejevs, “Experiment and numerical modeling of high-power passively Q-switched ytterbium-doped double-clad fiber lasers,” *IEEE J. Quantum Electron.* **46**, 68-75 (2010).
- [9]. J. Y. Huang, H. C. Liang, K. W. Su, and Y. F. Chen, “High power passively Q-switched ytterbium fiber laser with Cr⁴⁺:YAG as a saturable absorber,” *Opt. Express* **15**, 473-479 (2007).
- [10]. L. Pan, I. Utkin, R. J. Lan, Y. Godwal, and R. Fedosejevs, “High-peak-power subnanosecond passively Q-switched ytterbium-doped fiber laser,” *Opt. Lett.* **35**, 895-897 (2010).

- [11]. Z. Burshtein, P. Blau, Y. Kalisky, Y. Shimony, and M. R. Kokta, "Excited-state absorption studies of Cr^{4+} ions in several garnet host crystals," *IEEE J. Quantum Electron.* **34**, 292–299 (1998).
- [12]. G. Xiao, J. H. Lim, S. Yang, E. V. Stryland, M. Bass, and L. Weichman, "Z-scan measurement of the ground and excited state absorption cross section of Cr^{4+} in yttrium aluminum garnet," *IEEE J. Quantum Electron.* **35**, 1086-1091 (1999).
- [13]. H. Eilers, K. R. Hoffman, W. M. Dennis, S. M Jacobsen, and W. M. Yen, "Saturation of 1.064 μm absorption in $\text{Cr,Ca:Y}_3\text{Al}_5\text{O}_{12}$ crystals," *Appl. Phys. Lett.* **61**, 2958-2960 (1992).
- [14]. Y. Shimony, Z. Burshtein, and Y. Kalisky, " Cr^{4+} :YAG as passive Q-Switch and Brewster plate in a pulsed Nd:YAG laser," *IEEE J. Quantum Electron.* **31**, 1738–1741 (1995).
- [15]. B. Lipavsky, Y. Kalisky, Z. Burshtein, Y. Shimony, and S. Rotman, "Some optical properties of Cr^{4+} - doped crystals," *Opt. Mater.* **13**, 117–127 (1999).
- [16]. S. H. Yim, D. R. Lee, B. K. Rhee, and D. Kim, "Nonlinear absorption of Cr^{4+} :YAG studied with lasers of different pulsewidth," *Apl. Phys. Lett.* **73**, 3193–3195 (1998).
- [17]. T. Hakulinen, and O. G. Okhotnikov, "8 ns fiber laser Q switched by the resonant saturable absorber mirror," *Opt. Lett.* **32**, 2677–2679 (2007).
- [18]. J. Liu, S. Wu, Q. H. Yang, and P. Wang, "Stable nanosecond pulse generation from a graphene-based passively Q-switched Yb-doped fiber laser," *Opt. Lett.* **36**, 4008-4010 (2011).
- [19]. Z. J. Chen, A. B. Grudinin, J. Porta, and J. D. Minelly, "Enhanced Q switching in double-clad fiber lasers," *Opt. Lett.* **23**, 454-456 (1998).
- [20]. Y. X. Fan, F. Y. Lu, S. L. Hu, K. C. Lu, H. J. Wang, X. Y. Dong, J. L. He, and H. T. Wang, "Tunable high-peak-power, high-energy hybrid Q-switched double-clad fiber laser," *Opt. Lett.* **29**, 724-726 (2004).
- [21]. O. Schmidt, J. Rothhardt, F. Röser, S. Linke, T. Schreiber, K. Rademaker, J. Limpert, S. Ermeneux, P. Yvernault, F. Salin, and A. Tünnermann, "Millijoule pulse energy Q-switched short-length fiber laser," *Opt. Lett.* **32**, 1551-1553 (2007).
- [22]. J. A. Alvarez-Chavez, H. L. Offerhaus, J. Nilsson, P. W. Turner, W. A. Clarkson, and D. J. Richardson, "High-energy, high-power ytterbium-doped Q-switched fiber laser," *Opt. Lett.* **25**, 37-39 (2000).
- [23]. J. J. Zayhowski and C. Dill III, "Diode-pumped passively Q-switched

- picosecond microchip lasers,” *Opt. Lett.* **19**, 1427-1429 (1994).
- [24]. X. Zhang, S. Zhao, Q. Wang, Q. Zhang, L. Sun, and S. Zhang, “Optimization of Cr^{4+} -doped saturable-absorber Q-switched lasers,” *IEEE J. Quantum Electron.* **33**, 2286-2294 (1997).
- [25]. A. Agnesi and S. Dell’acqua, “High-peak-power diode-pumped passively Q-switched Nd:YVO₄ laser,” *Appl. Phys. B* **76**, 351-354 (2003).
- [26]. Y. Kalisky, “ Cr^{4+} -doped crystals: their use as lasers and passive Q-switches,” *Prog. Quantum Electron.* **28**, 249-303 (2004).
- [27]. A. Sennaroglu, U. Demirbas, S. Ozharar, and F. Yaman, “Accurate determination of saturation parameters for Cr^{4+} -doped solid-state saturable absorbers,” *J. Opt. Soc. Am. B* **23**, 241-249 (2006).
- [28] G. J. Spühler, R. Paschotta, R. Fluck, B. Braun, M. Moser, G. Zhang, E. Gini, and U. Keller, “Experimentally confirmed design guidelines for passively Q-switched microchip lasers using semiconductor saturable absorbers,” *J. Opt. Soc. Am. B* **16**, 376-388 (1999).
- [29] R. Häring, R. Paschotta, R. Fluck, E. Gini, H. Melchior, and U. Keller, “Passively Q-switched microchip laser at 1.5 μm ,” *J. Opt. Soc. Am. B* **18**, 1805-1812 (2001).
- [30] S. C. Huang, S. C. Liu, A. Li, K. W. Su, Y. F. Chen, and K. F. Huang, “AlGaInAs quantum-well as a saturable absorber in a diode-pumped passively Q-switched solid-state laser,” *Opt. Lett.* **32**, 1480-1482 (2007).
- [31]. K. Alavi, H. Temkin, W. R. Wagner, and A. Y. Cho, “Optically pumped 1.55- μm double heterostructure $\text{Ga}_x\text{Al}_y\text{In}_{1-x-y}\text{As}/\text{Al}_u\text{In}_{1-u}\text{As}$ lasers grown by molecular beam epitaxy,” *Appl. Phys. Lett.* **42**, 254-256 (1983).
- [32]. W. T. Tsang and N. A. Olsson, “New current injection 1.5- μm wavelength $\text{Ga}_x\text{Al}_y\text{In}_{1-x-y}\text{As}/\text{InP}$ double-heterostructure laser grown by molecular beam epitaxy,” *Appl. Phys. Lett.* **42**, 922-924 (1983).
- [33]. N. Nishiyama, C. Caneau, B. Hall, G. Guryanov, M. H. Hu, X. S. Liu, M.-J. Li, R. Bhat, and C. E. Zah, “Long-wavelength vertical-cavity surface-emitting lasers on InP with lattice matched AlGaInAs–InP DBR grown by MOCVD,” *IEEE J. Sel. Top. Quantum Electron.* **11**, 990-998 (2005).
- [34] Y. Jeong, J. K. Sahu, R. B. Williams, D. J. Richardson, K. Furusawa, and J. Nilsson, “Ytterbium-doped largecore fibre laser with 272 W output power,” *Electron. Lett.* **39**, 977-978 (2003).

- [35] Y. Jeong, J. K. Sahu, D. N. Payne, and J. Nilsson, "Ytterbium-doped large-core fibre laser with 1 kW of continuous-wave output power," *Electron. Lett.* **40**, 470-471 (2004).
- [36] A. Liem, J. Limpert, H. Zellmer, A. Tünnermann, V. Reichel, K. Mörl, S. Jetschke, S. Unger, H.-R. Müller, J. Kirchhof, T. Sandrock, and A. Harschak, "1.3 kW Yb-doped fiber laser with excellent beam quality," in *Proc. Conference on Lasers and Electro-Optics 2004*, San Francisco, USA, May 16-21, 2004, postdeadline paper CPDD2.
- [37] P. Adel, M. Auerbach, C. Fallnich, S. Unger, H.-R. Müller, and J. Kirchhof, "Passive Q-switching by Tm^{3+} codoping of a Yb^{3+} -fiber laser," *Opt. Express* **11**, 2730-2735 (2003).
- [38] M. Laroche, A. M. Chardon, J. Nilsson, D. P. Shepherd, W. A. Clarkson, S. Girard, and R. Moncorgé, "Compact diode-pumped passively Q-switched tunable Er-Yb double-clad fiber laser," *Opt. Lett.* **27**, 1980-1982 (2002).
- [39] F. Z. Qamar and T. A. King, "Passive Q-switching of the Tm-silica fiber laser near 2 μ m by Cr^{2+} :ZnSe saturable absorber crystal," *Opt. Commun.* **248**, 501-505 (2005).
- [40] S. Kivistö, R. Koskinen, J. Paajaste, S. D. Jackson, M. Guina, and O. G. Okhotnikov, "Passively Q-switched Tm^{3+} , Ho^{3+} -doped silica fiber laser using a highly nonlinear saturable absorber and dynamic gain pulse compression," *Opt. Express* **16**, 22058-22063 (2008).
- [41] S. C. Huang, S. C. Liu, A. Li, K. W. Su, Y. F. Chen, and K. F. Huang, "AlGaInAs quantum-well as a saturable absorber in a diode-pumped passively Q-switched solid-state laser," *Opt. Lett.* **32**, 1480-1482 (2007).
- [42] J. Y. Huang, W. C. Huang, W. Z. Zhuang, K. W. Su, Y. F. Chen, and K. F. Huang, "High-pulse-energy, passively Q-switched Yb-doped fiber laser with AlGaInAs quantum wells as a saturable absorber," *Opt. Lett.* **34**, 2360-2362 (2009).
- [43] H. Ridderbusch, and T. Graf, "Saturation of 1047- and 1064nm absorption in Cr^{4+} :YAG crystals," *IEEE J. Quantum Electron.* **43**, 168-173 (2007).
- [44] V. G. Shcherbitsky, S. Girard, M. Fromager, R. Moncorgé, N. V. Kuleshov, V. I. Levchenko, V. N. Yakimovich, and B. Ferrand, "Accurate method for the measurement of absorption cross sections of solid-state saturable absorbers," *Appl. Phys. B* **74**, 367-374 (2002).
- [45] J. Y. Huang, W. Z. Zhuang, W. C. Huang, K. W. Su, C. Hu, K. F. Huang, and Y. F.

- Chen, "Comparative studies for Cr⁴⁺:YAG crystal and AlGaInAs semiconductor used as a saturable absorber in Q-switched Yb-doped fiber lasers," *Opt. Express* **17**, 20800-20805 (2009).
- [46] W. Z. Zhuang, W. C. Huang, P. Y. Chiang, K. W. Su, K. F. Huang, and Y. F. Chen, "Millijoule-level Yb-doped photonic crystal fiber laser passively Q-switched with AlGaInAs quantum wells," *Opt. Express* **18**, 27910-27915 (2010).
- [47] J. B. Khurgin, F. Jin, G. Solyar, C. C. Wang, and S. Trivedi, "Cost-effective low timing jitter passively Q-switched diode-pumped solid-state laser with composite pumping pulses," *Appl. Opt.* **41**, 1095-1097 (2002).
- [48] S. L. Huang, T. Y. Tsui, C. H. Wang, and F. J. Kao, "Timing jitter reduction of a passively Q-switched laser," *Jpn. J. Appl. Phys.* **38**(Part 2, No. 3A), L239-L241 (1999).
- [49] T. Hakulinen, R. Koskinen, and O. G. Okhotnikov, "Low jitter Q-switched fiber laser using optically driven surface-normal saturable absorber modulator," *Opt. Express* **16**, 8720-8726 (2008).
- [50] B. Cole, L. Goldberg, C. W. Trussell, A. Hays, B. W. Schilling, and C. McIntosh, "Reduction of timing jitter in a Q-Switched Nd:YAG laser by direct bleaching of a Cr⁴⁺:YAG saturable absorber," *Opt. Express* **17**, 1766-1771 (2009).
- [51] D. Nodop, J. Rothhardt, S. Hädrich, J. Limpert, and A. Tünnermann, "Wavelength-independent all-optical synchronization of a Q-switched 100-ps microchip laser to a femtosecond laser reference source," *Appl. Phys. B* **74**, 367-374 (2002).
- [52] O. M. Stafsudd, O. Ersoy, and S. Pizzica, "CO₂ LASER with simultaneous active and passive Q-switching," *Appl. Opt.* **10**, 141-143 (1971).
- [53] X. Wang, and Z. Xu, "Single-longitudinal-mode operation of a 1 Watt combined actively and passively Q-switched Cr,Nd:YAG laser," *Opt. Express* **13**, 6693-6698 (2005).
- [54] M. Arvidsson, B. Hansson, M. Holmgren, and C. Lindstrom, "A combined actively and passively Q-switched microchip laser," in *Solid State Lasers VII*, R. Scheps, ed., *Proc. SPIE* **3265**, 106-113 (1998).
- [55] T. Dascalu, C. Dascalu, and N. Pavel, "Nd:YAG laser continuous wave pumped, Q-switched by hybrid "passive-active" methods," *ROMOPTO 2000: Sixth Conference on Optics*, Ed. V.I. Vlad, Bucharest, Romania, September 2000, *Proc. SPIE* **4430**, 52-61 (2001).

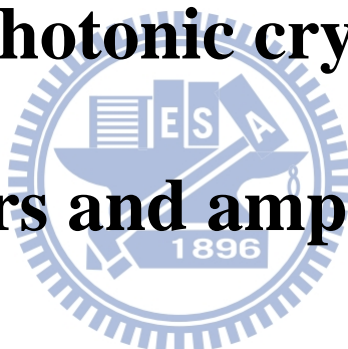
- [56]. E. Molva, "Microchip lasers and their applications in optical microsystems," *Opt. Mater.* **11**, 289-299 (1999).
- [57]. Q. Liu, and X. P. Yan, "High power all-solid-state fourth harmonic generation of 266 nm at the pulse repetition rate of 100 kHz," *Laser Phys. Lett.* **6**, 203-206 (2009).
- [58]. S. V. Garnov, V. I. Konov, T. Kononenko, V. P. Pashinin, and M. N. Sinyavsky, "Microsecond laser material processing at 1.06 μm ," *Laser Phys.* **14**, 910-915 (2004).
- [59] L. Sun, L. Zhang, H. J. Yu, L. Guo, J. L. Ma, J. Zhang, W. Hou, X. C. Lin, and J. M. Li, "880 nm LD pumped passive mode-locked TEM₀₀ Nd:YVO₄ laser based on SESAM," *Laser Phys. Lett.* **7**, 711 (2010).
- [60] X. S. Cheng, B. A. Hamida, A. W. Najji, H. Ahmad, and S. W. Harun, "67 cm long bismuth-based erbium doped fiber amplifier with wideband operation," *Laser Phys. Lett.* **8**, 814-817 (2011).
- [61] A. S. Kurkov, V. A. Kamynin, E. M. Sholokhov, and A. V. Marakulin, "Mid-IR supercontinuum generation in Ho-doped fiber amplifier," *Laser Phys. Lett.* **8**, 754-757 (2011).
- [62] X. Wushouer, P. Yan, H. Yu, Q. Liu, X. Fu, X. Yan, and M. Gong, "High peak power picosecond hybrid fiber and solid-state amplifier system," *Laser Phys. Lett.* **7**, 644-649 (2010).
- [63] H. J. Liu, and X. F. Li, "High power tunable picosecond green laser pulse generation by frequency doubling of an Yb-doped fiber power amplifier seeded by a gain switch laser diode," *Laser Phys.* **21**, 2118-2121 (2011).
- [64] Z. Y. Dong, S. Z. Zou, H. J. Yu, Z. H. Han, Y. G. Liu, L. Sun, W. Hou, X. C. Lin, and J. M. Li, "High peak power green light generation using ytterbium fiber amplifier and lithium triborate crystal," *Laser Phys.* **21**, 1804-1807 (2011).
- [65] Z. Y. Dong, S. Z. Zou, Z. H. Han, H. J. Yu, L. Sun, W. Hou, X. C. Lin, and J. M. Li, "High power, high energy nanosecond pulsed fiber amplifier with a 20 μm core fiber," *Laser Phys.* **21**, 536-539 (2011).
- [66] C. Ye, P. Yan, L. Huang, Q. Liu, and M. Gong, "Stimulated Brillouin scattering phenomena in a nanosecond linearly polarized Yb-doped double-clad fiber amplifier," *Laser Phys. Lett.* **4**, 376-381 (2007).
- [67] A. V. Kir'yanov, S. M. Klimentov, I. V. Mel'nikov, and A. V. Shestakov, "Specialty Yb fiber amplifier for microchip Nd laser: Towards ~1-mJ/1-ns output

- at kHz-range repetition rate,” *Opt. Commun.* **282**, 4759-4764 (2009).
- [68] P. E. Schrader, R. L. Farrow, D. A. V. Kliner, J.-P. Fève and N. Landru, “High-Power fiber amplifier with widely tunable repetition rate, fixed pulse duration, and multiple output wavelengths,” *Opt. Express* **14**, 11528-11538 (2006).
- [69] C. D. Brooks and F. Di Teodoro, “Multimegawatt peak-power, single-transverse-mode operation of a 100 μm core diameter, Yb-doped rodlike photonic crystal fiber amplifier,” *Appl. Phys. Lett* **89**, 111119 (2006).
- [70] C. Li, J. Song, D. Shen, N. S. Kim, J. Lu, and K. Ueda, “Diode-pumped passively Q-switched Nd:GdVO₄ lasers operating at 1.06 μm wavelength,” *Appl. Phys. B* **70**, 471 (2000).
- [71] Z.-Y. Li, H.-T. Huang, J.-L. He, B.-T. Zhang, and J.-L. Xu, “High peak power eye safe intracavity optical parametric oscillator pumped by a diode pumped passively Q-switched Nd:GGG laser,” *Laser Phys.* **20**, 1302-1306 (2010).
- [72] J.-L. Li, D. Lin, L.-X. Zhong, K. Ueda, A. Shirakawa, M. Musha, and W.-B. Chen, “Passively Q-switched Nd:YAG ceramic microchip laser with azimuthally polarized output,” *Laser Phys. Lett.* **6**, 711-714 (2009).
- [73] R. J. Lan, M. D. Liao, H. H. Yu, Z. P. Wang, X. Y. Hou, X. G. Xu, H. J. Zhang, D. W. Hu, and J. Y. Wang, “3.3 ns Nd:LuVO₄ micro-type laser,” *Laser Phys. Lett.* **6**, 268-271 (2009).
- [74] S. Y. Zhang, H. T. Huang, M. J. Wang, L. Xu, W. B. Chen, J. Q. Xu, J. L. He, and B. Zhao, “Diode-pumped continuous wave and passively Q-switched operation of Nd:Gd_{0.33}Lu_{0.33}Y_{0.33}VO₄ crystal,” *Laser Phys. Lett.* **8**, 189-192 (2011).
- [75] Y. Bai, N. Wu, J. Zhang, J. Li, S. Li, J. Xu, and P. Deng, “Passively Q-switched Nd:YVO₄ laser with a Cr⁴⁺:YAG crystal saturable absorber,” *Appl. Opt.* **36**, 2468-2472 (1997).
- [76] M. Liu, J. Liu, S. Liu, L. Li, F. Chen, and W. Wang, “Experimental study on passively Q-switched mode-locking diode-pumped Nd:KGW laser with Cr⁴⁺:YAG,” *Laser Phys.* **19**, 923-926 (2009).
- [77] Y. F. Chen, S. W. Tsai, and S. C. Wang, “High-power diode-pumped Q-switched and mode-locked Nd:YVO₄ laser with a Cr⁴⁺:YAG saturable absorber,” *Opt. Lett.* **25**, 1442-1444 (2000).
- [78] F. Q. Liu, J. L. He, J. L. Xu, B. T. Zhang, J. F. Yang, J. Q. Xu, C. Y. Gao, and H. J. Zhang, “Passively Q-switched mode-locking in a diode-pumped c-cut

- Nd:LuVO₄ laser with Cr⁴⁺:YAG,” *Laser Phys. Lett.* **6**, 567-570 (2009).
- [79] H. Yu, H. Zhang, Z. Wang, J. Wang, Z. Shao, and M. Jiang, “CW and Q-switched laser output of LD-end-pumped 1.06 μm c-cut Nd:LuVO₄ laser,” *Opt. Express* **15**, 3206-3211 (2007).
- [80] H. Yu, H. Zhang, Z. Wang, J. Wang, Y. Yu, M. Jiang, and X. Zhang, “Passively Q-switched laser performance of c-cut Nd:Gd_{0.63}Y_{0.37}VO₄ crystal,” *Opt. Commun.* **281**, 5199-5201 (2008).
- [81] H.-J. Qi, X.-D. Liu, X.-Y. Hou, Y.-F. Li, and Y.-M. Sun, “A c-cut Nd:GdVO₄ solid-state laser passively Q-switched with Co²⁺:LaMgAl₁₁O₁₉ lasing at 1.34 μm,” *Laser Phys. Lett.* **4**, 576-579 (2007).
- [82] A. Agnesi and S. Dell’acqua, “High-peak-power diode-pumped passively Q-switched Nd:YVO₄ laser,” *Appl. Phys. B* **76**, 351-354 (2003).
- [83] Y.F. Chen, Y.C. Chen, S.W. Chen, and Y.P. Lan, “High-power efficient diode-pumped passively Q-switched Nd:YVO₄/KTP/Cr⁴⁺:YAG eye-safe laser,” *Opt. Commun.* **234**, 337-342 (2004).
- [84] N. Hodgson, and H. Weber, *Laser Resonators and Beam Propagation*, 2nd edn. (Springer, Berlin, 2005), Ch. 5.
- [85] W. Koechner, *Solid-State Laser Engineering*, 6th edn. (Springer, Berlin, 2005), Ch. 7.
- [86] N. Hodgson, and H. Weber, *Laser Resonators and Beam Propagation*, 2nd edn. (Springer, Berlin, 2005), Ch. 8.
- [87] Y. F. Chen, T. M. Huang, C. F. Kao, C. L. Wang, and S. C. Wang, “Optimization in scaling fiber-coupled laser-diode end-pumped lasers to higher power: influence of thermal effect,” *IEEE J. Quantum Electron.* **33**, 1424-1429 (1997).
- [88] J. H. Campbell, and F. Rainer, “Optical glasses for high-peak-power laser applications,” *Proc. of SPIE* **1761**, 246-255 (1992).

Chapter 3

Pulsed photonic crystal fiber lasers and amplifier



Photonic crystal fibers (PCFs) were first invented in the late 1990s [1-2]. It is promising for achieving single-mode operation with large cores compared to the conventional large mode area fibers was realized very early on [3]. A PCF is drawn from a hexagonal stack of capillaries, with typically one to seven capillaries replaced by doped rods in the center. Pressurization of the airholes is typically used to keep the holes from collapsing from surface tension during drawing. The center doped rods form the core of the PCFs. The composite cladding material composed of glass and air holes makes it easy to achieve a very low refractive index contrast between the core and the composite cladding, consequently providing much better control at achieving fibers with very low NAs [4]. PCFs, however, are very sensitive in bending due to its weak guiding property, especially at large core diameters. Thus, they need to be kept straight beyond core diameters of 40 μm in practical use. Fibers with these large core diameters are made into rods with outer diameters ranging from 1 to 2 mm and are referred to as fiber rods [5-6]. Ultra-large-core PCF with core diameters as large as 100 μm and an effective mode area of about 4500 μm^2 have been demonstrated [7]. The first Q-switched PCF fiber laser was demonstrated with a PCF rod of core diameter of 35 μm by using an E-O Q-switch composed of a Pockels cell and a thin film polarizer [8]. Pulse trains with pulse duration of 10 ns and pulse energy of 0.5 mJ was attained with pulse repetition rate of 100 kHz.

Here, I proposed a scheme that use PQS elements such as Cr^{4+} :YAG crystal and AlGaInAs semiconductor multi-quantum-wells to form a compact and efficient system without high energy consuming AQS elements. Furthermore, by using a compact and high peak power Nd:YVO₄/ Cr^{4+} :YAG PQS laser as the seed, we demonstrate a high peak power PCF fiber amplifier system. Employing this efficient pulsed system as the fundamental light source, extracavity second harmonic generation and third harmonic generation were demonstrated.

3.1 Passively Q-switched with Cr⁴⁺:YAG crystals and intracavity optical parametric oscillator

In recent years, double-cladding rare-earth doped fiber lasers have attracted a lot of attention due to their good beam confinement, excellent heat dissipation, spatial beam quality, and high efficiency [9-15]. Q-switched lasers have many applications on industrial processing, measurements of positions, and medical treatments owing to their high peak power than in CW operation [16-18]. By enlarging the active volume of the gain medium, corresponding to the doped core size of the fiber, one can achieve the merit of the high pulse energy [19-20]. However, the conventional large core fibers suffer from mode-quality degradation and their long lengths usually lead to long pulse widths and low peak powers.

Recently, a novel technology [5] has been developed to provide photonic crystal fibers (PCFs) with large single mode core and high absorption efficiency. The PCF laser was lately employed to perform an actively Q-switched operation in which the pulse energy was up to 2 mJ with a pulse width shorter than 10 ns at a repetition rate of 10 kHz. Compared to the active Q-switching, passive Q-switching lasers are more compact and lower cost because they use saturable absorbers in replace of acoustic-optic or electro-optic modulators as the Q-switch.

Crystal-based [21-24] saturable absorbers have been well developed to replace the dye-cells used in solid-state lasers. Cr⁴⁺:YAG crystals have been exploited as saturable absorbers in large-mode-area Yb-doped fibers [25-28], among which the maximum pulse energy was 350 μJ. Nevertheless, the passive Q-switching in a PCF laser has not been investigated so far.

In this paper, we report, for the first time to our knowledge, on the performance of a single-polarization passively Q-switched Yb-doped PCF laser and its application to intracavity optical parametric oscillator (OPO). With a Cr⁴⁺:YAG crystal as a saturable absorber and under a pump power of 14.2 W, the PCF laser generates an average output power of 3.4 W at 1030 nm at the repetition rate of 5.6 kHz, corresponding to the pulse energy up to 630 μJ. The pulse width and the peak power

Ch3 Pulsed photonic crystal fiber lasers and amplifier

are 36 ns and 17.4 kW, respectively. Experimental results revealed that since the Yb-doped PCF provokes a narrow linewidth and a high polarization extinction ratio, the pulse-to-pulse amplitude fluctuation and the temporal jitter were well below 5% for the pump power greater than 8 W. The overall quality of the output pulses is noticeably superior to that obtained in conventional passively Q-switched fiber lasers. With the passively Q-switched PCF laser to pump an intracavity OPO, the output pulse energy of 140 μ J can be generated for the signal wave at 1515 nm at a repetition rate of 3.3 kHz. Owing to the efficient cavity-dumping effect, the signal pulse width is found to be as short as 1.0 ns; consequently, the peak power can reach 140 kW.

(A) Performance of passively Q-switched PCF laser

Figure 3.1(a) shows the setup for the passively Q-switched PCF laser. The cavity consists of a 55 cm polarization maintaining (PM) Yb-doped PCF and an external feedback cavity with a saturable absorber. The external cavity incorporates with a focusing lens of 50-mm focal length to focus the fiber output into the Cr⁴⁺:YAG crystal and a high reflective mirror behind the saturable absorber for feedback. The rod-type PCF has a mode field diameter of 55 μ m and a low numerical aperture of 0.02 to sustain the excellent beam quality. The pump cladding of the PCF has a diameter of 200 μ m and an air-cladding to maintain a high numerical aperture of 0.6, as depicted in Fig. 3.1(b) for the image of the cross section of the PCF. The small ratio between the inner pump cladding and core diameters brings about the pump absorption coefficient to be approximately 30dB/m at 976nm. The PCF was surrounded with a 1.7-mm thick outer cladding and was sealed with end-caps for protection. The boron doped stress-applying parts were adopted to induce birefringence that produces diverse spectral losses to form a linearly polarization state for the fundamental mode. The Cr⁴⁺:YAG saturable absorber had a thickness of 3 mm and was highly doped with a small signal transmission of 28%. Both sides of the saturable absorber were coated for antireflection at 1030 nm ($R < 0.2\%$) and the mode diameter on the saturable absorber was approximately 400 μ m. The pump source was an 18-W 976-nm fiber-coupled laser diode with a core diameter of 100 μ m and a numerical aperture of 0.2. Focusing lens with 25-mm focal length and 90% coupling efficiency was used to re-image the pump beam into the fiber through the dichroic

Ch3 Pulsed photonic crystal fiber lasers and amplifier

mirror with high transmission (HT, $T > 90\%$) at 976 nm and high reflectivity (HR, $R > 99.8\%$) within 1030~1100 nm. The pump spot radius was approximately 50 μm , and the pump coupling efficiency was estimated to be around 80%. The pulse temporal behavior was recorded by Leroy digital oscilloscope (Wavepro 7100; 10G samples/sec; 4 GHz bandwidth) with a fast InGaAs photodiode.

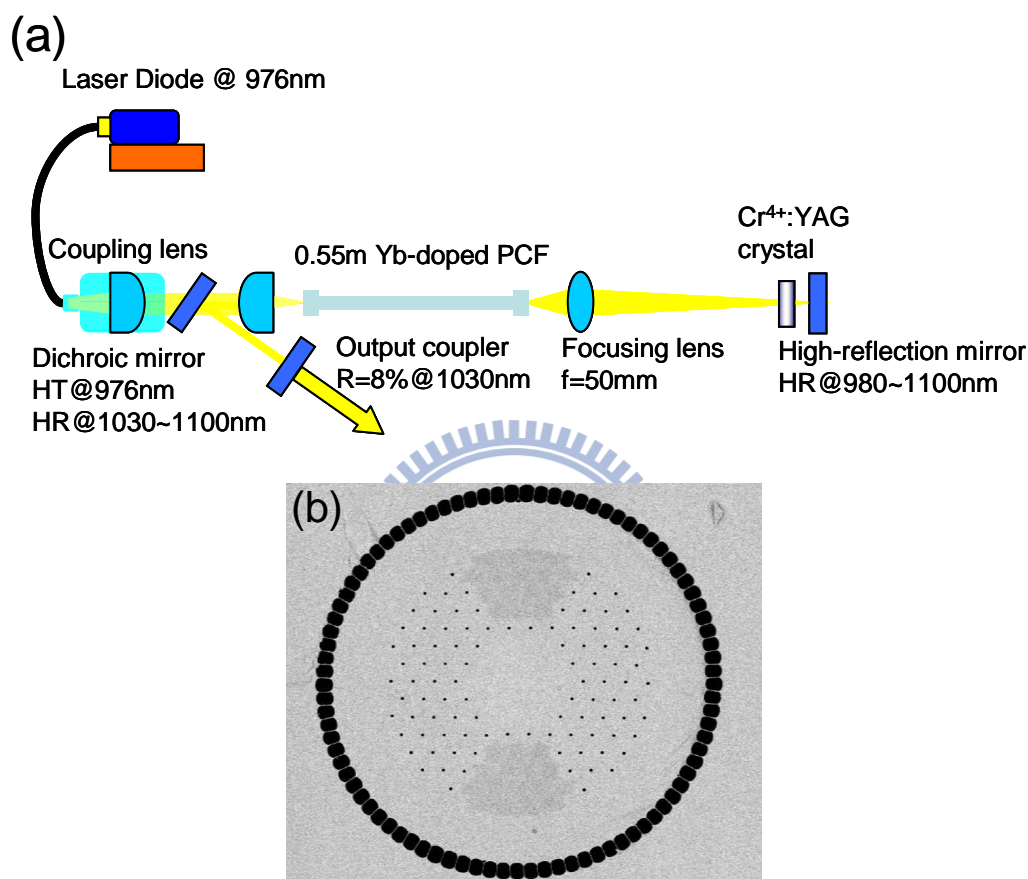


Fig. 3.1 (a) Setup for the passively Q-switched PCF laser; (b) image of the cross section of PCF.

Figure 3.2(a) shows the average output power with respect to the launched pump power in the CW and passive Q-switching operations. The external cavity in the CW operation only included a re-imaging lens and a reflective mirror. At a launched pump power of 14.2 W, the average output power in the CW and passive Q-switching operations were 5.4 W and 3.4 W, respectively. The slope efficiency seemed to decrease slightly above 12.5 W of pump power which was due to temperature lifting induced wavelength shift of the pumping laser diode. The lasing spectra for both operations were quite similar with the peaks near 1030 nm and bandwidths to be

Ch3 Pulsed photonic crystal fiber lasers and amplifier

approximately 0.4 nm, as shown in the inset of Fig. 3.2(a). The M^2 factor was also measured to be less than 1.3 over the complete output power range, owing to the low-NA feature of the fiber. The laser output was found to be linearly polarized with an extinction ratio of approximately 100:1, evidencing the function of the polarization maintaining in PCF. The pulse repetition rate and the pulse energy versus the launched pump power are shown in Fig. 3.2(b). The pulse repetition rate increased monotonically with the pump power up to 5.6 kHz at a pump power of 14.2 W. The pulse energy was maintained to be nearly constant at 630 μJ for all the pump power range. Figures 3.3(a) and 3.3(b) show typical oscilloscope traces for a single Q-switched pulse and a Q-switched pulse train, respectively. The temporal shape of the single pulse reveals a self-mode-locking (SML) phenomenon that has been observed in conventional fiber lasers and the possible mechanisms for its origin have been discussed in Refs [26,29,30]. During the early research on mode-locking, the SML phenomenon was observed on different types of lasers including He-Ne [31], ruby [32], Nd:glass [33], and argon ion [34] laser systems. Based on the statistical analysis, it has been shown that the mode-locked behavior will always be observed in a multimode laser except when a systematic phase fluctuation over 2π is introduced [35,36]. Although systematic phase fluctuation is usually caused by dispersion effects, theoretical studies on the SML mechanism have confirmed that the combination tones of the third order nonlinear polarization terms can help in compensating the dispersion-induced phase shift [37-39]. Consequently, the SML typically occurs in a multimode laser without employing an extra nonlinearity except the gain medium. Recently, fairly stable SML pulses have been observed in the experiments of Nd-doped double clad fiber lasers [39] and Nd-doped vanadate crystal lasers [40]. On the other hand, Laroche et al. [26] found that the SML phenomenon can be eliminated by setting the Cr^{4+} :YAG crystal exactly at the focal point of the lens. However, I did not attempt to eliminate the SML phenomenon because this phenomenon did not deteriorate the pulse stability in the present PCF laser. Moreover, putting the Cr^{4+} :YAG crystal at the focal position may cause damage due to the high pulse energy and peak power. Experimental results revealed that both the pulse-to-pulse amplitude fluctuation and the temporal jitter were well below 5% for the pump power greater than 8 W because of the narrow linewidth and the high polarization extinction ratio of the PCF. More importantly, the pulse width of the Q-switched pulse envelope was as short as 36 ns. In short, the overall quality of the

output pulses is significantly superior to that obtained in conventional passively Q-switched fiber lasers [41].

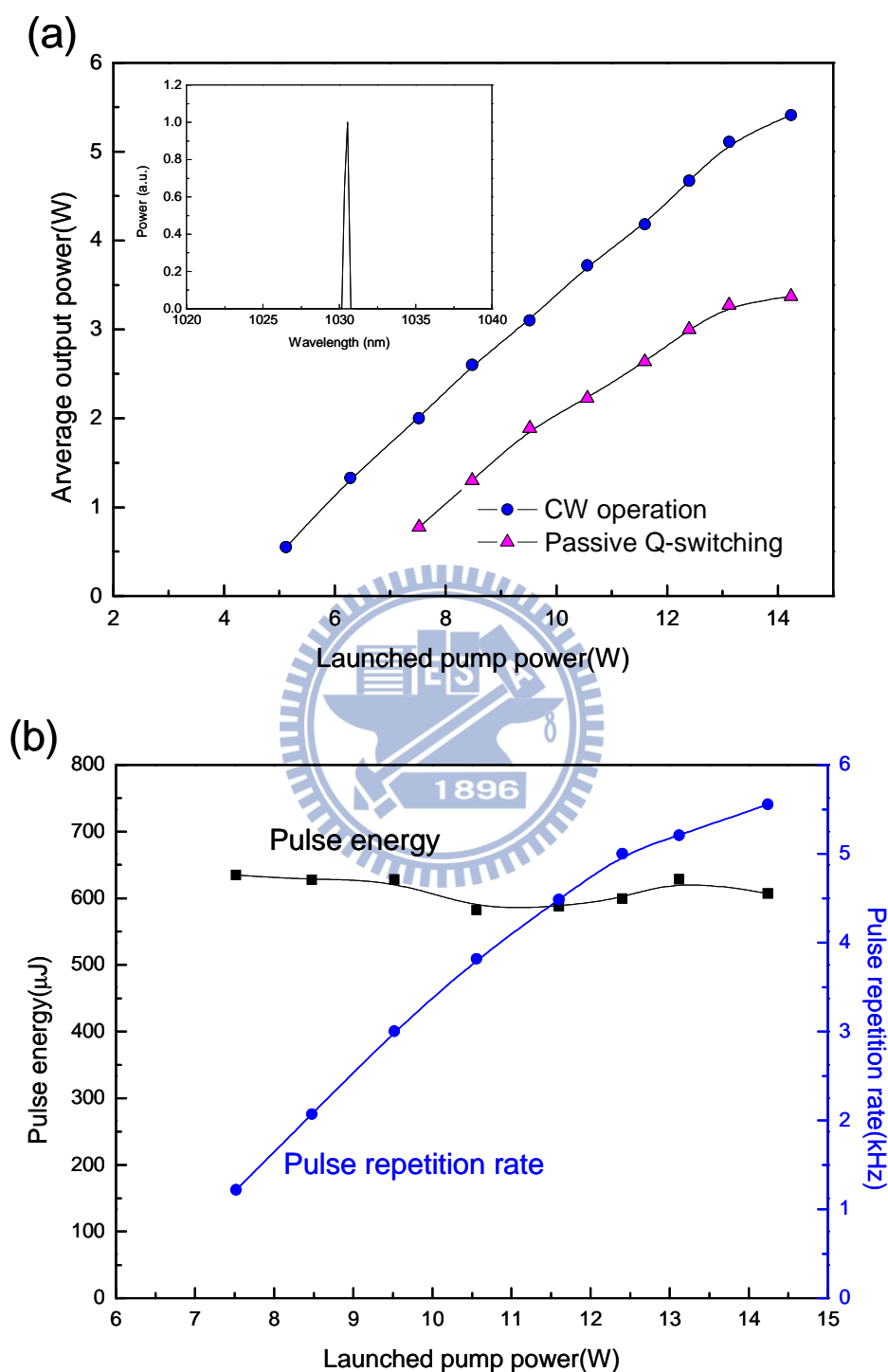


Fig. 3.2 Average output power with respect to launched pump power in CW and passive Q-switching operations, the inset: typical lasing spectrum. (b) Pulse repetition rate and pulse energy versus launched pump power.

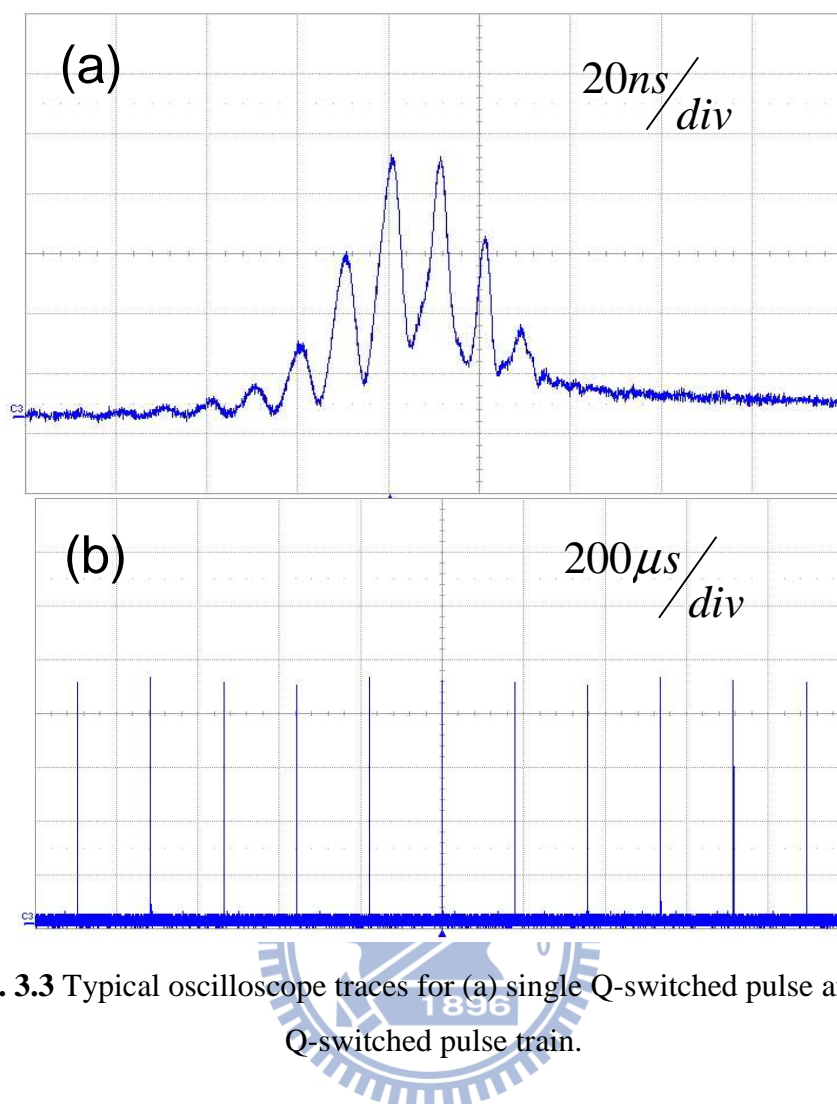


Fig. 3.3 Typical oscilloscope traces for (a) single Q-switched pulse and (b) Q-switched pulse train.

(B) Performance of intracavity OPO

To construct an intracavity OPO, the output coupler in the passively Q-switched PCF laser was replaced with a high-reflection mirror at 1030 nm and inserting a singly resonant OPO cavity behind the Cr⁴⁺:YAG crystal. Figure 3.4 shows the experimental setup for the intracavity OPO pumped by the passively Q-switched PCF laser. The OPO cavity is composed of a dichroic front mirror (HT at 1030 nm and HR at 1515 nm), a KTP nonlinear crystal, and an output coupler with partial transmission (PR) of $R = 38\%$ at 1515 nm and high reflectivity at 1030 nm. The nonlinear crystal KTP was x-cut with the dimension of $4 \times 4 \times 20 \text{ mm}^3$ and both sides of the KTP crystal were coated for antireflection at 1030 nm and 1515 nm ($R < 0.5\%$). The KTP crystal was mounted on a water-cooled copper heat sink with an indium thermal contact. The length of the OPO cavity was approximately 3 cm. The Cr⁴⁺:YAG crystal

Ch3 Pulsed photonic crystal fiber lasers and amplifier

was placed very close (~ 1.0 mm) to the front mirror of the OPO cavity to control the mode diameter on the Cr^{4+} :YAG crystal in the range of $400 \mu\text{m}$.

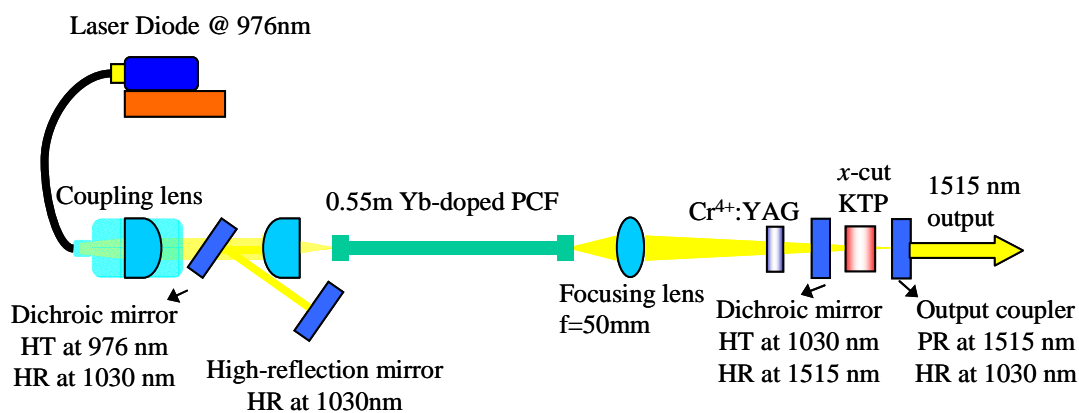


Fig. 3.4 Setup for the intracavity OPO pumped by the passively Q-switched PCF laser.

The average output power of the signal wave at 1515 nm with respect to the launched pump power is shown in Fig. 3.5(a). Under a pump power of 14.2 W, the average output power of the signal wave was found to be approximately 470 mW. No idler signal was detected because of the high absorption of the idler radiation in the KTP crystal and the BK7 substrate of the output coupler, so the OPO is resonant on the signal frequency only. Note that no saturation of average output power was seen at the highest pump power, which implied that larger OPO signal output power can be expected with higher pump power. The OPO pulse repetition rate and the pulse energy versus the launched pump power are shown in Fig. 3.5(b). The pulse repetition rate increased monotonically with the pump power up to 3.3 kHz at a pump power of 14.2 W. The pulse energy was nearly $140 \mu\text{J}$ for all the pump power range. The signal output pulse energy obtained with a Q-switched PCF laser was 3-6 times higher than the results obtained with solid-state Nd-doped crystal lasers at the same level of diode pumped power [42-44]. In other words, the Yb-doped gain medium has a superior energystoring ability than conventional Nd-doped laser crystals, such as Nd:YAG and Nd:YVO₄.

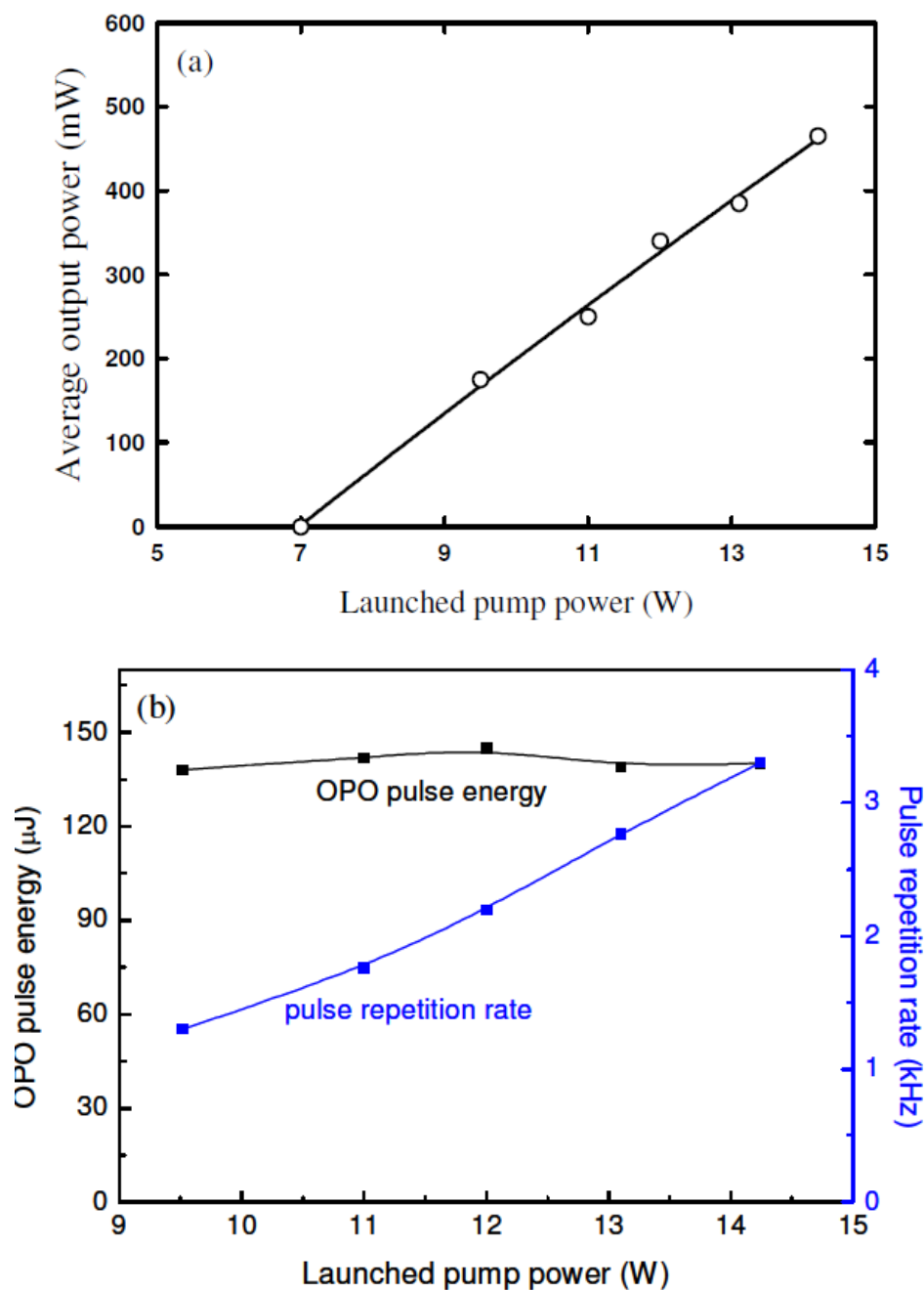


Fig. 3.5 (a) Average output power of signal wave at 1515 nm with respect to launched pump power. (b) OPO pulse repetition rate and pulse energy versus launched pump power.

Figure 3.6 shows general oscilloscope traces for the fundamental and OPO signal output pulses. The top half of Fig. 3.6 depicts the temporal trace of the fundamental wavelength and the bottom half shows the pulse profile of the OPO signal wavelength. The pulse width of the OPO signal can be seen to be as short as 1.0 ns due to the efficient cavity-dumping effect. As a result, the maximum peak power of the signal

Ch3 Pulsed photonic crystal fiber lasers and amplifier

wave can be up to 140 kW. The optical to optical conversion efficiency of OPO output power to laser diode launched pump power was about 3.3%, and the pulse energy conversion efficiency of OPO wavelength to 1030 nm wavelength was about 22.3%. The large pre- and post- pedestals in Fig. 3.6 arise from the SML effect. Note that the pulse shapes at 1030 nm were quite different for the cavity with and without the intracavity OPO. The number of the mode-locked pulses at 1030 nm shown in Fig. 3.6 was considerably less than that obtained with pure passive Q-switching shown in Fig. 3.3(a) because the effective output coupling in the intracavity OPO was a nonlinear cavitydumping process. Since water absorption in eye tissue and the intraocular fluid prevents light in the spectral range of 1.4-1.8 μm from reaching the retina, there is a considerable interest in laser sources with wavelengths in this eye-safe regime [45-47]. A number of efficient eyesafe intracavity OPOs pumped by passively [42-44] Q-switched Nd-doped crystal lasers have been demonstrated to produce pulse energies of tens of μJ with pulse peak powers of 1-50 kW. Here the PCF laser was recently employed to realize an intracavity OPO with pulse energies greater than 100 μJ with peak powers greater than 100 kW. Although the conversion efficiency for the average power is inferior to that obtained with Nd-doped crystal lasers, this situation might be improved with a shorter cavity to match the OPO cavity. However, the challenge is to manufacture a shorter PCF with sufficient absorption efficiency.

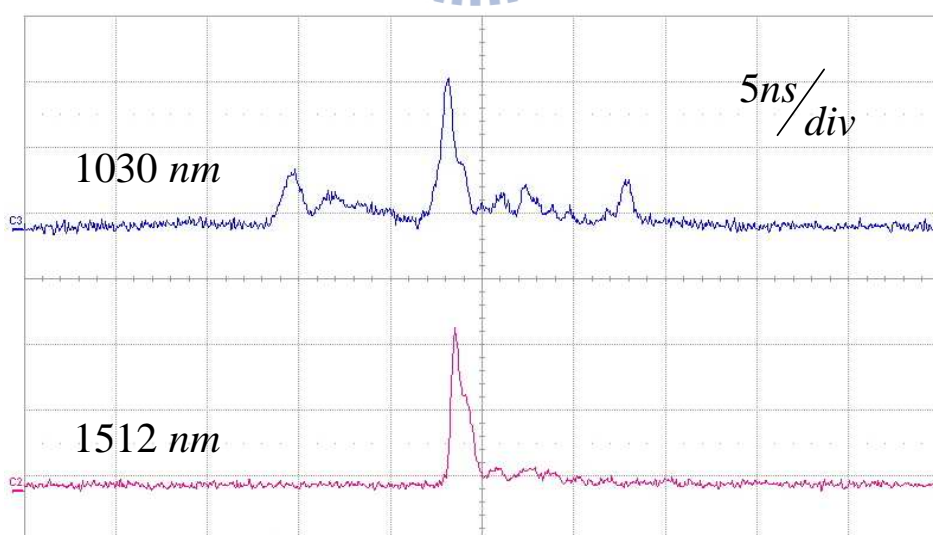


Fig. 3.6 General oscilloscope traces for the fundamental (top) and OPO signal (bottom) output pulses.

(C) Conclusion

In conclusion, I have, for the first time to our knowledge, demonstrated a high-pulse-energy passively Q-switched Yb-doped PCF laser by utilizing Cr⁴⁺:YAG crystal as saturable absorber. Stable pulses with an average output power of 3.4 W and a repetition rate of 5.6 kHz were obtained at a launched pump power of 14.2 W. The maximum pulse energy reached 630 μJ which was superior to the results obtained in conventional Yb-doped fiber lasers. Furthermore, the passively Q-switched PCF laser has been employed to pump an intracavity OPO to generate a pulse energy of 140 μJ at a pulse repetition rate of 3.3 kHz with a 14.2 W diode pump power. Owing to the efficient cavity-dumping effect, the pulse duration of the signal wave was approximately 1.0 ns, leading to a peak power up to 140 kW. This high-peakpower intracavity OPO could be a potential light source for many technical applications.



3.2 Passively Q-switched with AlGaInAs MQWs

High-power diode-pumped double-clad rare-earth doped fiber lasers have been proved to be efficient and compact with excellent beam quality, high efficiency, and good thermal management [13-14, 48]. Q-switched fiber lasers are practically useful in a variety of applications in virtue of their high pulse energy, such as remote sensing, industrial processing, and medical needs [16, 49-50]. Compared with active Q-switching techniques, passive Q-switching methods that employ saturable absorbers can considerably enhance the compactness and simplify the operation [27-28, 51-52]. By enlarging the active volume of the gain medium, corresponding to the doped core size of the fiber, one can achieve the merit of the high pulse energy. However, the conventional large-core fibers suffer from mode-quality degradation and their long lengths usually lead to long pulse widths and low peak powers. For improving these deficiencies, photonic crystal fibers (PCFs) have been developed to provide large single-mode cores and high absorption efficiencies. The PCF was recently employed to demonstrate a passively Q-switched laser with a Cr⁴⁺:YAG crystal as a saturable absorber in which under a pump power of 14.2 W, an average output power of 3.4 W with a repetition rate of 5.6 kHz was generated, corresponding to a pulse energy of 630 μJ [53]. However, the scale-up of the pulse energy is hindered by the nonsaturable loss of the Cr⁴⁺:YAG crystal [28].

In recent years, an AlGaInAs semiconductor material with a periodic quantum-well (QW) structure grown on a Fe-doped InP structure has been successfully used as a saturable absorber in an Yb-doped fiber laser to produce pulse energy up to 450 μJ [28]. It was found that the saturation fluence of the AlGaInAs QW absorber was two orders of magnitude smaller than that of Cr⁴⁺:YAG crystal. This property enables the AlGaInAs QW devices to be appropriate saturable absorbers for high-gain lasers. More importantly, experimental results also revealed that the AlGaInAs QW absorber has a lower nonsaturable loss than the Cr⁴⁺:YAG crystal with the same initial transmission. This result indicates that AlGaInAs QW absorbers have a potential to generate much higher pulse energies. So far, AlGaInAs QWs have not been employed to passively Q-switch Yb-doped PCF lasers.

Here I demonstrate, for the first time to our knowledge, on a millijoule-level passive Q-switched Yb-doped photonic crystal fiber laser with AlGaInAs QWs as a saturable absorber. We fabricate three types of AlGaInAs devices with different QW numbers to investigate the performance of passively Q-switched PCF lasers. With 50 groups of three AlGaInAs QWs as a saturable absorber and under a pump power of 16 W, the PCF laser generates an average power of 7.1 W at the pulse repetition rate of 6.5 kHz, corresponding to a pulse energy of approximately 1.1mJ. The overall pulse-to-pulse amplitude fluctuation and the temporal jitter are found to be well below 10% in root mean square (rms). We also calculated the peak power by integrating the photodiode traces and found its maximum value to reach 110 kW.

(A) AlGaInAs QWs absorber and experimental setup

Similar to the previous structure [28] the saturable absorbers that offered by TrueLight Corporation were AlGaInAs QW/barrier structures grown on a Fe-doped InP substrate by metalorganic chemical-vapor deposition. The saturable absorbers were designed to consist of many groups of several QWs, spaced at half-wavelength intervals by InAlAs barrier layers with the band-gap wavelength around 806 nm and with the luminescence wavelength near 1064 nm. The thickness of the saturable absorbers was approximately 400 μm . Compared with other similar QWs devices, AlGaInAs material has the advantages of lattice match with the substrate InP over InGaAs/GaAs that output pulse energy of the passive Q-switch and the conversion efficiency are limited as a result of the lattice mismatch. AlGaInAs materials is also superior to InGaAsP material which can be grown on InP substrate because of its better electron confinement covering the wavelength range in 0.84-1.65 μm provided by the larger conduction band offset [54-55]. In this work we fabricated three types of AlGaInAs QWs that posses 50 groups of three QWs (3×50 QWs), 30 groups of three QWs (3×30 QWs), and 30 groups of two QWs (2×30 QWs). Figures 3.7(a)-3.7(c) depict the schematic diagrams of three periodic AlGaInAs QWs structures. Figure 3.7(d) shows the measured results for the low-intensity transmittance spectrum of the three QW saturable absorbers. The initial transmissions of the absorbers near the wavelength of 1030 nm can be seen to be 18%, 36%, and 48% for the devices of 3×50 QWs, 3×30 QWs, and 2×30 QWs, respectively. With the z-scan method [28], we found that the modulation depths between low and high intensities were approximately 77%, 59%, and 47% for the absorbers of 3×50 QWs, 3×30 QWs, and 2×30 QWs, respectively.

We also found that the nonsaturable losses for three devices were less than 5%. The low nonsaturable losses indicate the quality of the QW devices to be rather high. Furthermore, the saturation fluence of the QW absorbers was measured to be in the range of 1 mJ/cm^2 and the relaxation time to be on the order of 100 ns [56]. The damage threshold for the AlGaInAs QWs was found to be approximately 300 MW/cm^2 . Both sides of the semiconductor absorber have a simple single layer coating to reduce back reflections and the couple-cavity effects.

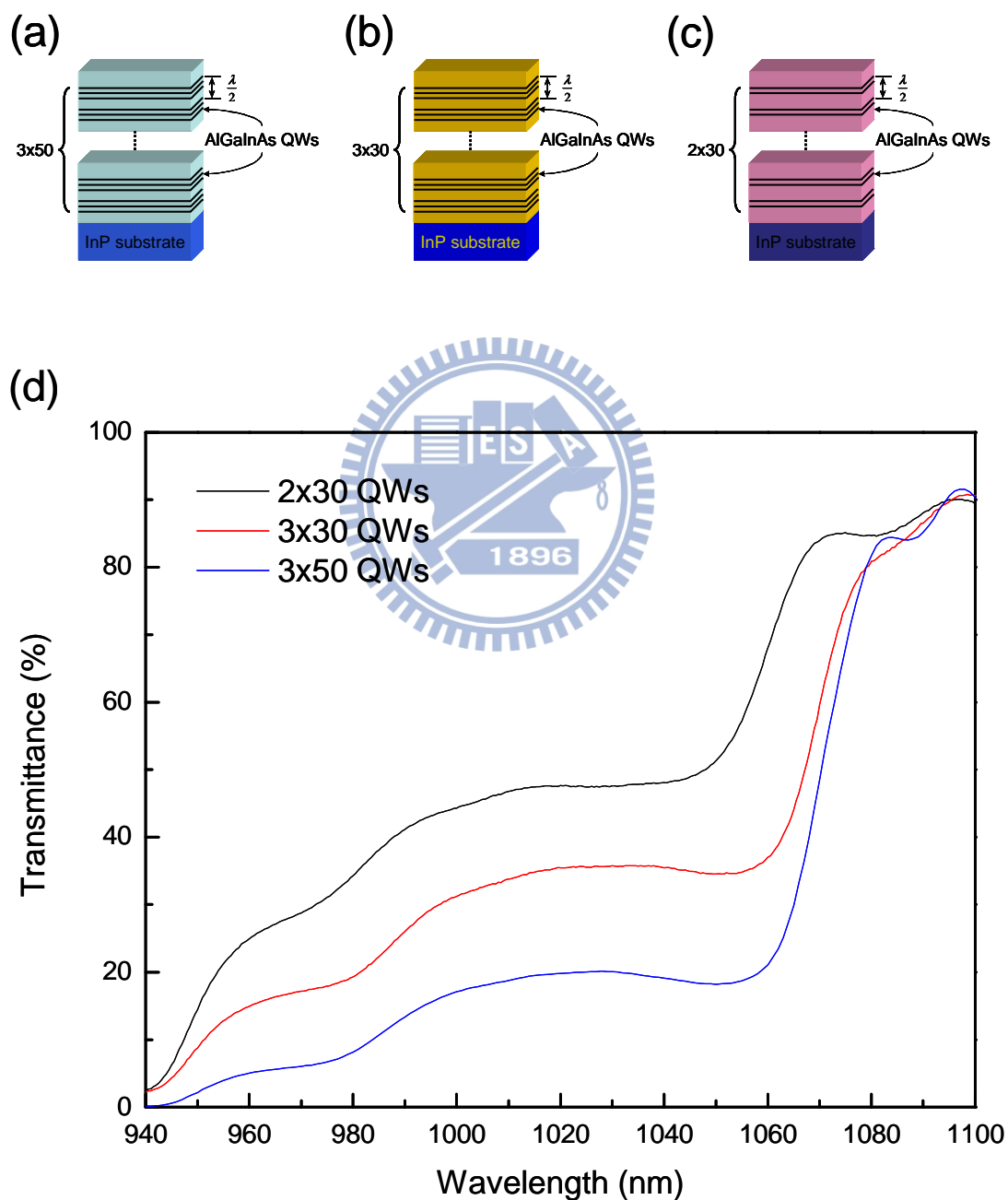


Fig. 3.7 (a)-(c) Schematic diagrams of three periodic AlGaInAs QWs structures. (d) Low-intensity transmittance spectrum of the three QW saturable absorbers.

Ch3 Pulsed photonic crystal fiber lasers and amplifier

The scheme of the experimental setup is shown in Fig. 3.8(a). The cavity is composed of a 0.55 m polarization maintaining Yb-doped PCF (NKT photonics) that is the same one described in Ref. 53 and an external feedback cavity with a saturable absorber. Figure 3.8(b) depicts the image of the cross section of the PCF pumped by a 532 nm light source. Since the absorption coefficient of the PCF was approximately 30 dB/m at 976 nm, the overall absorption efficiency could reach 95%. The rod-type PCF has a mode field diameter of 55 μm and a low numerical aperture (N.A.) of 0.02 to sustain the excellent beam quality. The pump cladding of the PCF has a diameter of 200 μm and an air-cladding to maintain a high N.A. of 0.6. The PCF was surrounded with a 1.7-mm thick outer cladding and was sealed with end-caps for protection. The boron doped stress-applying parts near the core were adopted to induce birefringence that produces diverse spectral losses to form a linearly polarization state for the fundamental mode.

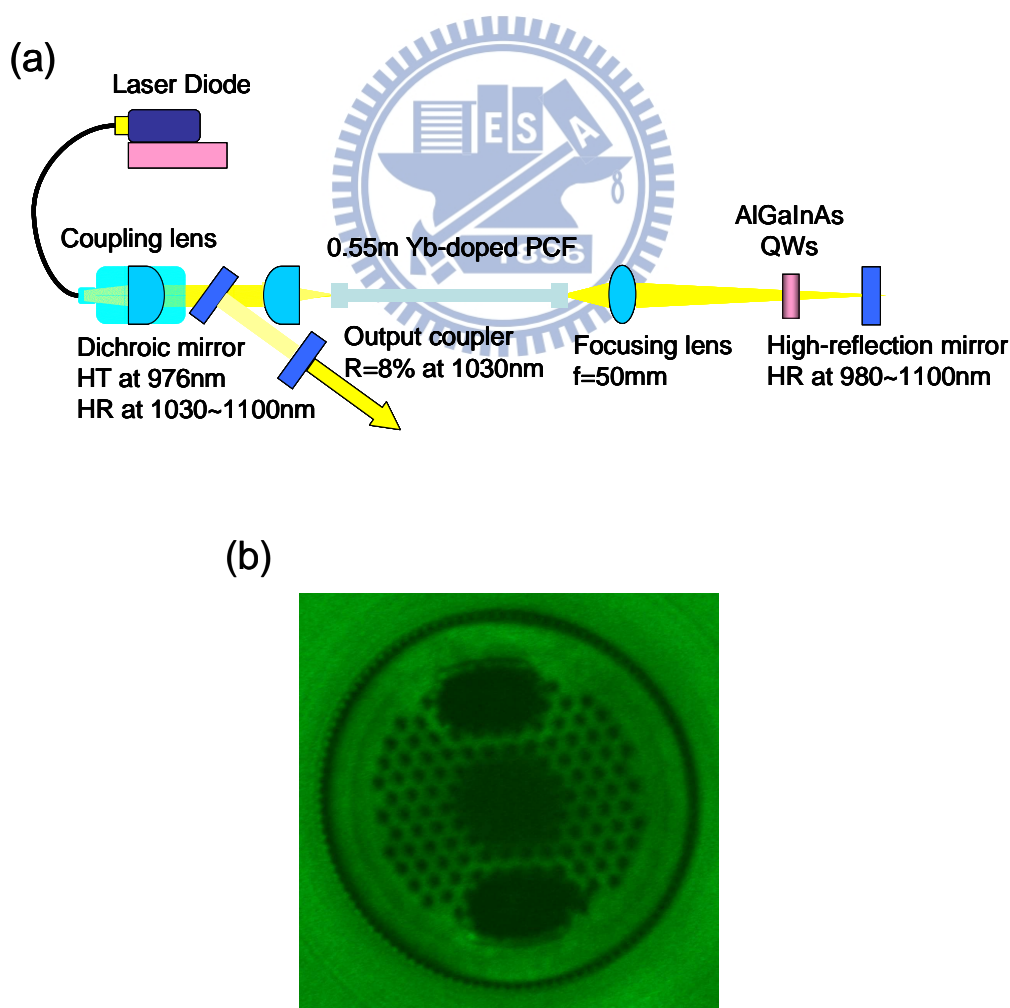


Fig. 3.8 (a) Setup for the passively Q-switched PCF laser; (b) image of the cross section of PCF.

The external cavity incorporates with a focusing lens of 50-mm focal length to focus the fiber output into the AlGaInAs QW absorber and a high reflective mirror behind the absorber for feedback. The AlGaInAs QW absorber was mounted in a copper block as a heat sink and with water cooling. The mode diameter on the saturable absorber was approximately 200 μm . The pump source was a 20-W 976-nm fiber-coupled laser diode with a core diameter of 200 μm and a numerical aperture of 0.2. Focusing lens with 25-mm focal length as one of the lens pairs depicted in Fig. 3.8(a) and 90% coupling efficiency was used to re-image the pump beam into the fiber through the dichroic mirror with high transmission (HT, $T > 90\%$) at 976 nm and high reflectivity (HR, $R > 99.8\%$) within 1030~1100 nm. The pump spot radius was approximately 100 μm , and the pump coupling efficiency was estimated to be around 80%. The laser spectrum was measured by an optical spectrum analyzer with 0.1 nm resolution (Advantest Q8381A). The pulse temporal behavior was recorded by Leroy digital oscilloscope (Wavepro 7100; 10G samples/sec; 4 GHz bandwidth) with a fast InGaAs photodiode.

(B) Experimental results and discussions

Figure 3.9 depicts the average output power versus the launched pump power in CW and passive Q-switching operation. The external cavity in the CW operation contained only a re-imaging lens and a reflective mirror without the saturable absorber. At a launched pump power of 16 W, the CW PCF laser was found to generate an output power of 8.7 W, corresponding to a slope efficiency of 78%. In the passive Q-switching operation, the average output powers at a launched pump power of 16 W were 7.1 W, 7.7 W, and 8.0 W for the lasers with the saturable absorbers of 3×50 , 3×30 , and 2×30 QWs, respectively. The signal intensity of the amplified spontaneous emission (ASE) is 40 dB below the lasing signal of 1030 nm measured by the optical spectrum analyzer, so the fraction of the ASE output power can be neglected. As a result, the Q-switching efficiency (the ratio of the average power of Q-switched operation to that of CW one) were approximately 82%, 89%, and 92% for the lasers with the saturable absorbers of 3×50 , 3×30 , and 2×30 QWs, respectively. The overall Q-switching efficiency was significantly superior to the results obtained with Cr^{4+} :YAG crystals as saturable absorbers [53]. The lasing spectra for CW and passive Q-switching operations were quite similar with the peaks near 1030 nm and

bandwidths to be approximately 0.4 nm. The laser output was found to be linearly polarized with an extinction ratio of approximately 100:1, evidencing the function of the polarization maintaining in PCF. The M^2 factor was found to be generally smaller than 1.3 over the entire output power range, owing to the low- N.A. feature of the PCF.

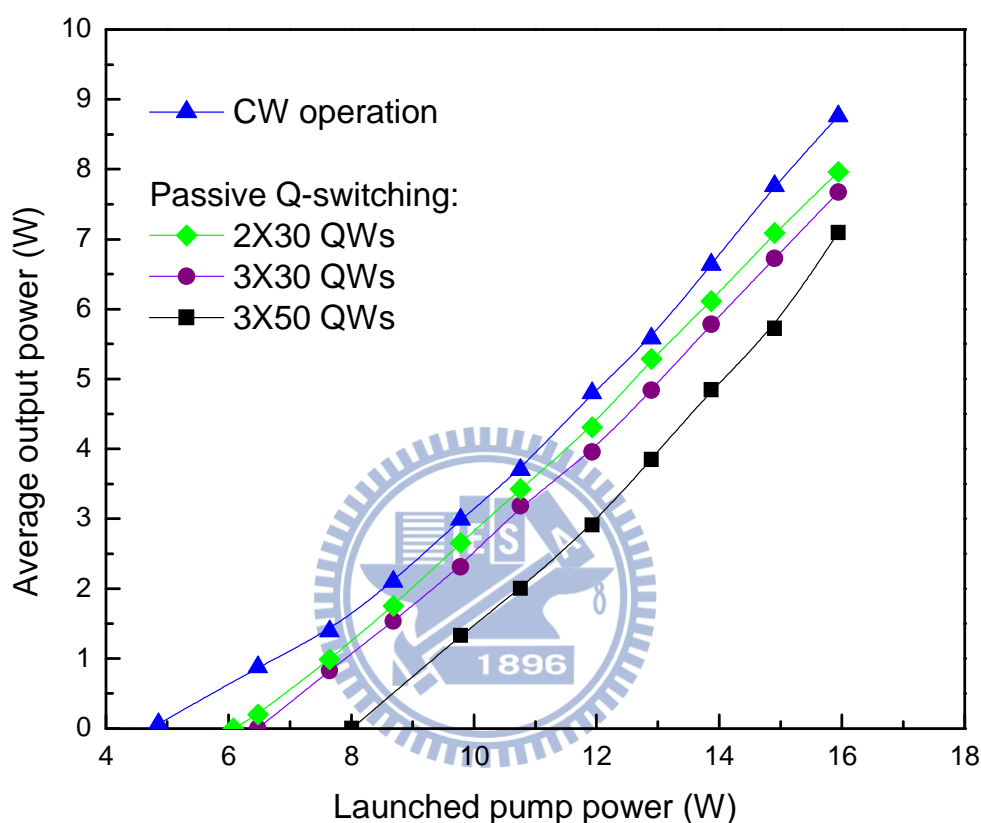


Fig. 3.9 Average output power with respect to launched pump power in CW and passive Q-switching operations.

Figure 3.10 shows the pulse repetition rates in the passive Q-switching operation versus the launched pump power. Experimental results reveal that the pulse repetition rates for all cases increase monotonically with the pump power. At a launched pump power of 16 W, the pulse repetition rates were found to be 6.5 kHz, 16 kHz, and 23 kHz for the lasers with the saturable absorbers of 3×50 , 3×30 , and 2×30 QWs, respectively. With the experimental results of the average output power and the pulse repetition rate, we calculated the pulse energies versus the launched pump power. It was found that the pulse energies were nearly independent of the pump power and their average values were 1.1 mJ, 0.49 mJ, and 0.35 mJ for the lasers with the

saturable absorbers of 3×50 , 3×30 , and 2×30 QWs, respectively. Fiber laser systems with energy of millijoule-class had been demonstrated with either actively Q-switched oscillator [17, 57-58] or the master oscillator power fiber amplifier scheme [59-61]. To the best of our knowledge, this is the first time that the millijoule-level energy output was achieved with the passive Q-switching scheme in a PCF laser.

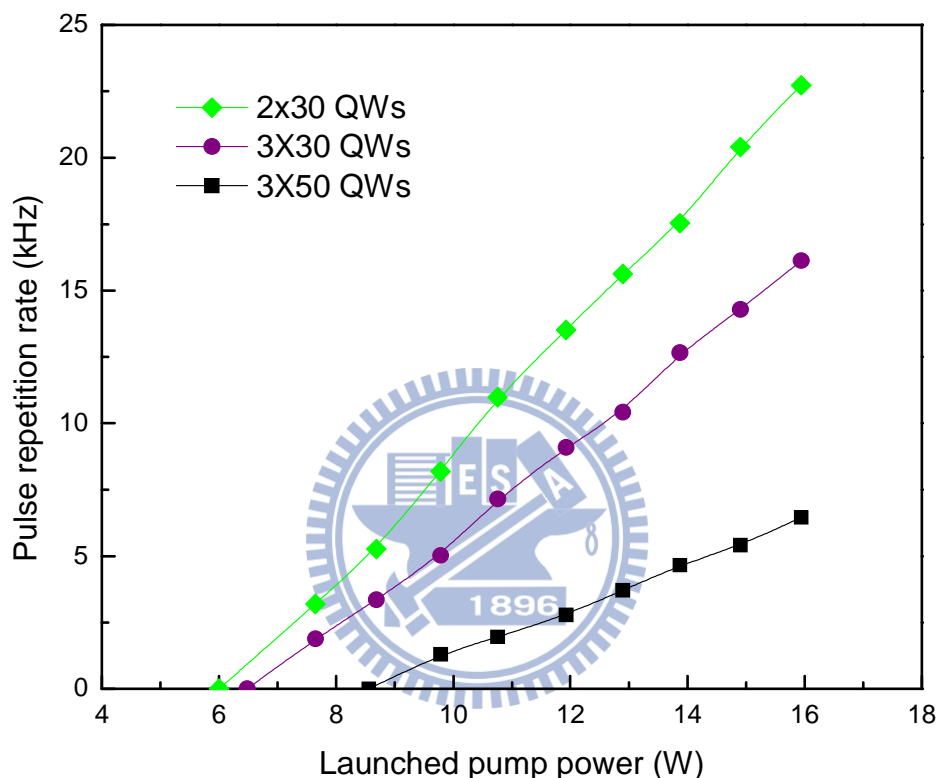


Fig. 3.10 Pulse repetition rates in the passive Q-switching operation versus the launched pump power.

Figures 3.11(a)-3.11(c) depict typical oscilloscope traces for the single Q-switched pulses of the lasers with the saturable absorbers of 2×30 , 3×30 , and 3×50 QWs, respectively. It can be seen that the temporal shape of the single Q-switched pulse obtained with the absorber of 2×30 QWs is a simple pulse, whereas the temporal shape obtained with the absorber of 3×50 QWs reveal conspicuous modulation whose period is nearly equal to the round trip time. The self-modulation phenomenon inside the Q-switched envelope has been frequently observed in pulsed fiber lasers. This phenomenon is generally considered to arise from the stimulated Brillouin scattering (SBS) which can provide strong feedback to the cavity together

with pulse compression. The SBS-related pulses have been demonstrated in different fiber laser designs, such as self-Q switched [62-64], actively Q-switched [16, 29], and passively Q-switched [26,65] fiber lasers. Note that another self-modulation phenomenon was found in passively Q-switched Nd-doped crystal lasers with Cr^{4+} :YAG crystals as saturable absorbers [66-69]; however, the origin is attributed to the excited-state absorption of the absorber and the fluctuation mechanism [70-71]. Our results reveal that the pulse energy obtained with the absorber of 3×30 QWs is just above the SBS threshold. As seen in Fig. 3.11(b), the rear end of the pulse exhibits a fast transient dynamics. On the other hand, the intense SBS effect leads to the pulse to be strongly modulated, as seen in Fig. 3.11(c). With the numerical integration, we found the maximum peak powers were 7.4 kW, 12.8 kW, and 110 kW for the lasers with the saturable absorbers of 2×30 , 3×30 , and 3×50 QWs, respectively. The corresponding optical intensity on the 3×50 QWs was 350 MW/cm^2 which is quite close to the damage threshold of the saturable absorber, but no optical damage was observed. Figures 3.12(a)-3.12(c) show typical oscilloscope traces of a train of output pulses obtained with the saturable absorbers of 2×30 , 3×30 , and 3×50 QWs, respectively. It can be seen that for the laser with the absorber of 2×30 QWs the pulse-to-pulse amplitude fluctuation was generally less than 4% in rms. Even for the case of 3×30 QWs, just above the SBS threshold, the pulse-to-pulse amplitude fluctuation was also smaller than 4% in rms. Although the strong SBS effect might deteriorate the pulse stability to some extent, the pulse-to-pulse amplitude fluctuation could still be maintained to be 8.5% in rms for the laser with the saturable absorber of 3×50 QWs, as shown in Fig. 3.12(c). Compared with the previous results, the pulse stability was superior to that obtained in Ref. 28 and slightly diminished with respect to Ref. 53 as a result of the high pulse energy induced SBS effect. The overall pulse energy scaling was 2.4 times as high as the one in Ref. 28 and 1.8 times as that in Ref. 53.

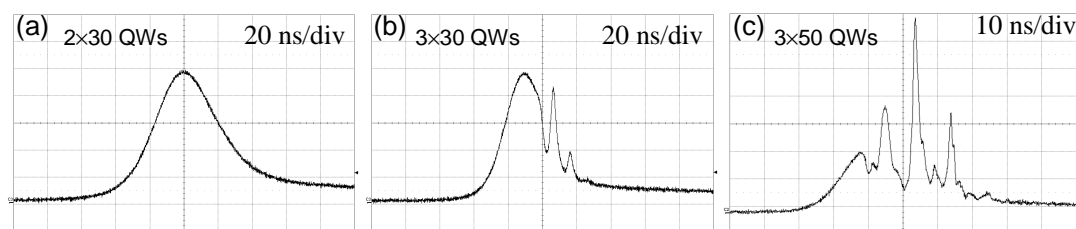


Fig. 3.11 Typical oscilloscope traces for the single Q-switched pulses of the lasers with the saturable absorbers of (a) 2×30 , (b) 3×30 , and (c) 3×50 QWs, respectively.

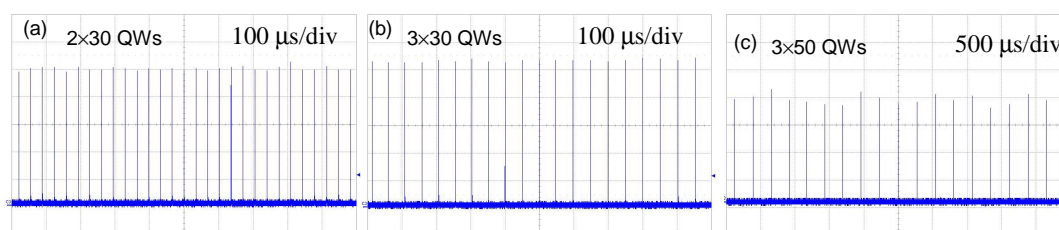


Fig. 3.12 Typical oscilloscope traces for a train of output pulses of the lasers with the saturable absorbers of (a) 2×30 , (b) 3×30 , and (c) 3×50 QWs, respectively.

(C) Conclusion

In conclusions, I have, for the first time to our knowledge, demonstrated a millijoule-level passively Q-switched Yb-doped photonic crystal fiber laser with AlGaInAs QWs as a saturable absorber. At a launched pump power of 16 W, the average output powers were 7.1 W, 7.7 W, and 8.0 W for the lasers with the saturable absorbers of 3×50 , 3×30 , and 2×30 QWs, respectively. The pulse energies were found to be 1.1 mJ, 0.49 mJ, and 0.35 mJ for the lasers with the saturable absorbers of 3×50 , 3×30 , and 2×30 QWs, respectively. The maximum peak power could be up to 110 kW. The overall pulse-to-pulse amplitude fluctuation and the temporal jitter could be maintained to be well below 10% in rms. These high-pulse-energy high-peak-power passively Q-switched PCF lasers are potentially useful light sources for many technical applications.

3.3 Widely tunable extracavity optical parametric oscillator with the PQS PCF laser

High-peak-power tunable laser sources have been in demand for the applications in the eye-safe wavelength regime near 1.55- μm such as free-space communication, gas sensing, spectroscopy, and medical treatment [72-75]. In recent years, double-cladding rare-earth doped fiber lasers are of great interest due to their good beam confinement, excellent heat dissipation, spatial beam quality, and high efficiency [10-15, 76-79]. Because of the broad bandwidth resulted from the amorphous nature of the glass host, directly utilizing erbium doped fiber (EDF) lasers or erbiumytterbium-codoped double-clad fiber lasers (EYDFL) possess the potential of wavelength tunability [80-84]. However, traditionally a wavelength-selective element such as grating or etalon is desired in the cavity and thus increases the complexity of laser cavity [85-88]. An alternative method for flexibility in tuning wavelength is an optical parametric oscillator (OPO) pumped by a laser source with shorter wavelength [89-93]. Based on the phase matching condition, the signal output wavelength could be controlled by adjusting the temperature of nonlinear crystal, pump incident direction, or pump wavelength.

For pulsed OPO operation, the passively Q-switch gives the advantage of simplification and compactness in experimental setup. In addition to the mostly used transition metal-doped crystals, semiconductor material with a periodic quantum-well (QW) structure has been demonstrated as a saturable absorber in the EYDFL to achieve a 105- μJ passively Q-switched 1.54- μm laser [94] and in the ytterbium doped photonic crystal fiber (PCF) laser to achieve an 1.1-mJ passively Q-switched 1.03- μm laser [63]. In 2010, the performance of eye-safe laser with a passively Q-switched PCF laser in an intracavity OPO was firstly reported [53]. In the published work, the fundamental wavelength is fixed at the maximum gain peak and a temperature-insensitive x-cut KTiOPO (KTP) was used in the OPO, this makes it inflexible to realize a broadly tunable laser. Periodically poled lithium niobate (PPLN)

Ch3 Pulsed photonic crystal fiber lasers and amplifier

is a powerful quasi-phase-matching (QPM) nonlinear crystal in OPOs for generating near-infrared (NIR) to midinfrared (MIR) radiation because of its advantages of high nonlinear coefficient (~ 15 pm/V) and broad transmission spectrum (up to $4.5 \mu\text{m}$) [93, 95-97]. In addition, the high refractive-index-temperature coefficient makes a signal wavelength shift up to $0.5 \text{ nm}/^\circ\text{C}$ at a pump source of 1030 nm for a grating period of $28\text{-}30 \mu\text{m}$. Therefore, it is well worthy of investigation to utilize the QPM nonlinear crystal in an OPO pumped by a passively Q-switched ytterbium-doped PCF laser to generate broadly tunable eye-safe wavelength radiation.

Here I demonstrate, for the first time to my knowledge, on a widely tunable eye-safe laser based on a PCF. An optical parametric oscillator was pumped by a passively Q-switched PCF laser with AlGaInAs QWs as a saturable absorber. First, the 1029-nm PCF laser with pulse energy of $750 \mu\text{J}$ at a pulse repetition rate of 6.5 kHz was established under a pump power of 13.1 W at 976 nm . The PCF laser was used to pump an OPO to generate eye-safe signal wave. By tuning the temperature of PPLN in the OPO cavity from 20 to 140°C , the tuning range of signal wavelength was over 80 nm from 1513 to 1593 nm . A maximum peak power of 19 kW and pulse energy of $138 \mu\text{J}$ was obtained under the pump energy of $390 \mu\text{J}$.

(A) Diode pumped PCF laser with AlGaInAs semiconductor absorber

The schematic of external-cavity OPO pumped by a passively Q-switched PCF laser is depicted as Fig. 3.13. The experimental setup could be separated into two major parts, one is a diode pumped passively Q-switched PCF laser and the other one is a singly resonating OPO. The PCF laser cavity consists of a 55-cm polarization maintaining (PM) Yb-doped PCF and an external feedback cavity with a saturable absorber. The external cavity incorporates with a focusing lens of 50-mm focal length to focus the fiber output into the saturable absorber and a high reflective mirror behind the saturable absorber for feedback. The rod-type PCF has a large mode field diameter of $55 \mu\text{m}$ to push the nonlinear threshold up to higher level than conventional single mode fiber. And a low numerical aperture value of 0.02 permits to sustain the operation in single transverse mode and excellent beam quality. The pump cladding of the PCF has a diameter of $200 \mu\text{m}$ and an air-cladding to maintain a high numerical aperture of 0.6 . The image of the cross section of the PCF is depicted as Fig. 3.14(a). The small ratio between the inner pump cladding and $70\text{-}\mu\text{m}$ core diameters

brings about the pump absorption coefficient to be 30 dB/m at 976 nm.

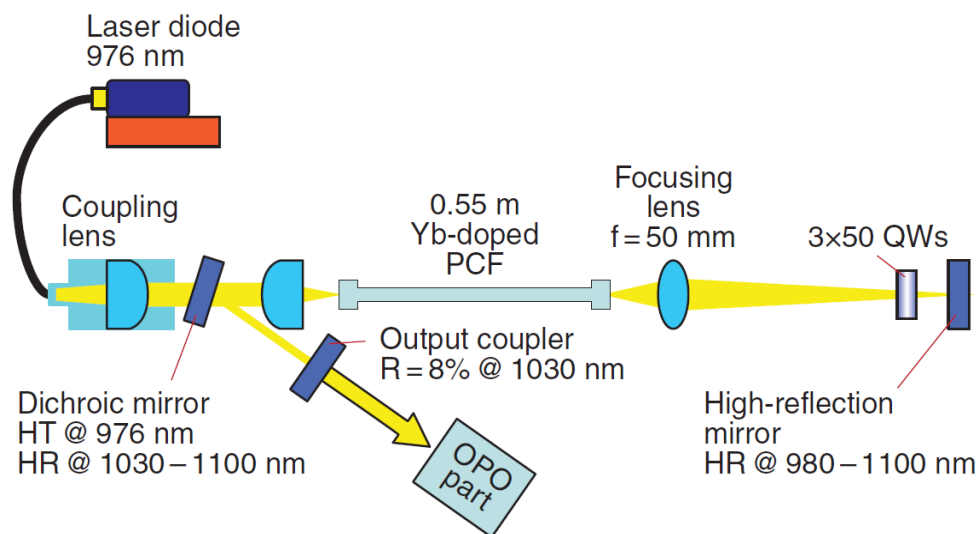


Fig. 3.13 Schematic sketch of the external-cavity optical parametric oscillator pumped by the passively Q-switched photonic crystal fiber laser.

The PCF was surrounded with a 1.7-mm thick outer cladding and was sealed with end-caps for protection. The boron doped stress-applying parts were adopted to induce birefringence that produces diverse spectral losses to form a linearly polarization state for the fundamental mode. The saturable absorber is a structure of AlGaInAs QW/barrier grown on a Fe-doped InP substrate by metalorganic chemical-vapor deposition, as depicted in Fig. 3.14(b) The structure consists of 50 groups of AlGaInAs QW/barrier. Each group contains three 8-nm-thick QWs and 10-nm-thick barriers. In order to increase the damage threshold, each group of quantum wells is designed to be located at the nodes of the pumping mode, or to have intervals of half-wavelength separated by barriers. A window layer of InP was deposited on the gain structure to prevent surface recombination and oxidation. Both surfaces of the saturable absorber were coated to have anti-reflection coating at 1030 nm ($R < 0.2\%$). The initial transmission of the saturable absorber was measured to be 19%. The mode diameter on the saturable absorber was estimated to be approximately 400 μm . The pump source was a 20-W 976-nm fiber-coupled laser diode with a core diameter of 200 μm and a numerical aperture of 0.2. Focusing lens with 25-mm focal length and 90% coupling efficiency was used to re-image the pump beam into the fiber through the dichroic mirror with high transmission (HT, $T > 90\%$) at 976 nm and high reflectivity (HR, $R > 99.8\%$) within 1030-1100 nm. The pump spot radius was

Ch3 Pulsed photonic crystal fiber lasers and amplifier

approximately 100 μm , and the pump coupling efficiency was estimated to be around 80%. The pulse temporal behavior was recorded by Leroy digital oscilloscope (Wavepro 7100, 10 G samples/sec, 4 GHz bandwidth) with a fast InGaAs photodiode.

(a)

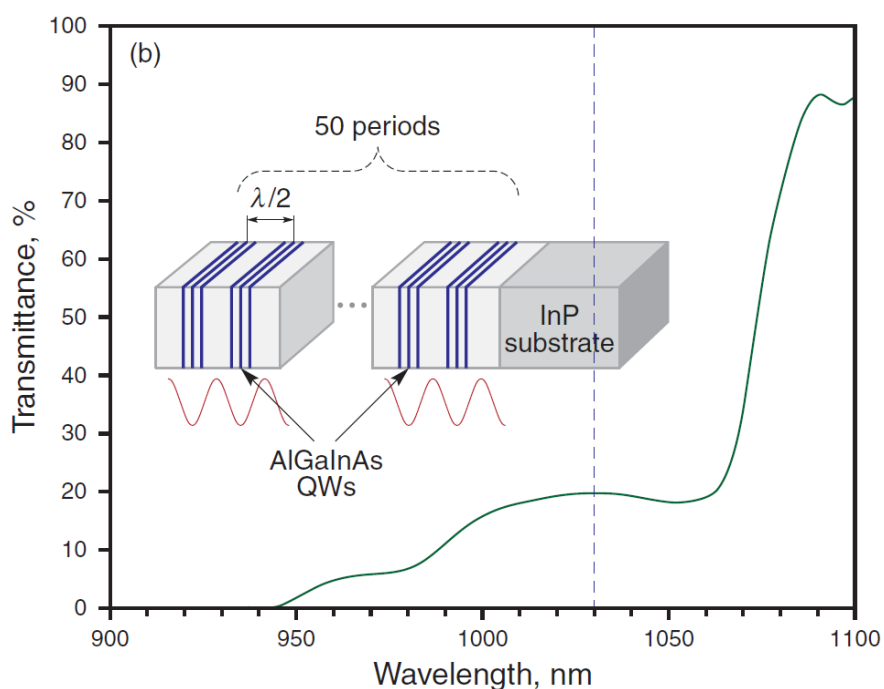


Fig. 3.14 (a) image of cross section of rod-type PCF and (b) transmission spectrum and structure of AlGaInAs saturable absorber.

The output power, pulse energy and output spectrum are shown in Fig. 3.15. The maximum output power was obtained to be 4.9 W under the 13.1 W of pump power and it turns out conversion efficiency over 37%. The central peak of wavelength is dependent on the pump power and distributes from 1031 to 1029 nm with increasing

the pump power. The inset of Fig. 3.15 shows the output spectrum of PCF laser with the 13.1 W of pump power. The full width at half maximum FWHM of bandwidth is around 0.5 nm and the M^2 factor was measured to be less than 1.3 over the complete output power range, owing to the low-N.A. feature of the fiber. The laser output was measured to be linearly polarized with an extinction ratio of approximately 100:1.

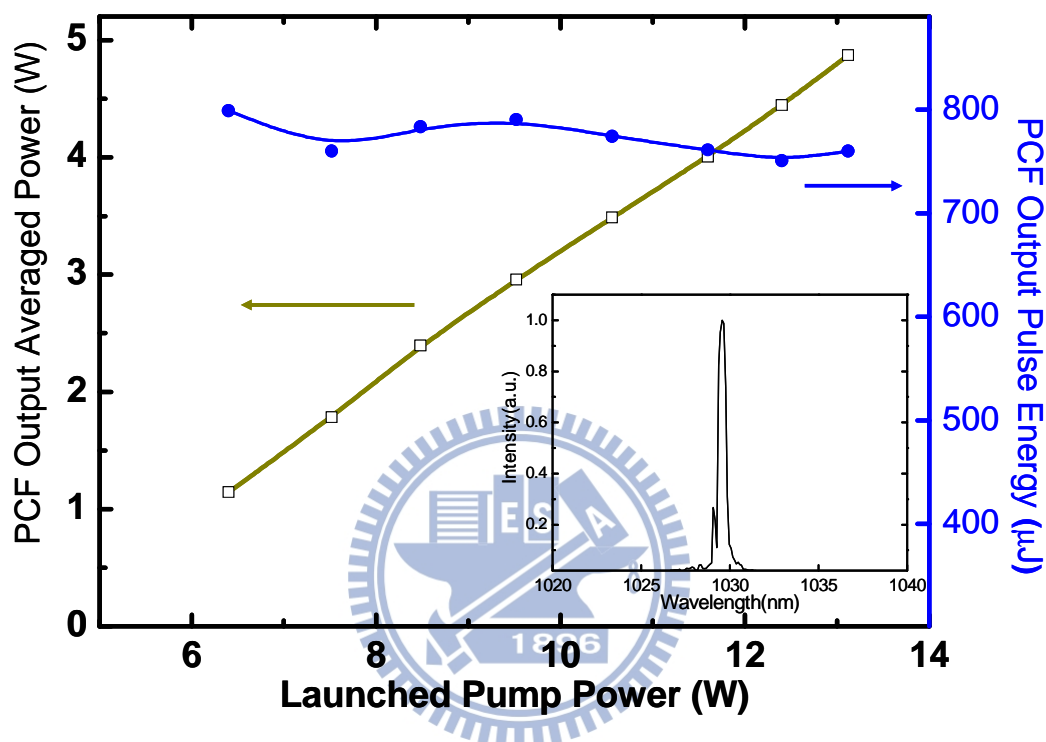


Fig. 3.15 Output power of the passively Q-switched PCF laser versus the 976-nm launched pump power. Inset – the lasing spectrum obtained with 12.5 W of pump power.

Fig. 3.16(a) and Fig. 3.16(b) show the traces of output pulses under a lower and higher pump power level, 6.3 and 13.1 W, respectively. A self-modulation phenomenon inside the Q-switched envelope was obviously observed in pulsed fiber lasers for high pump power. This phenomenon is generally considered to arise from the stimulated Brillouin scattering (SBS) which can provide strong feedback to the cavity together with pulse compression [16, 62-64]. The SBS related pulses have been demonstrated in different fiber laser designs, such as self-Q switched [62-64], actively Q-switched [16,98], and passively Q-switched [65, 99] fiber lasers. Although the strong SBS effect might deteriorate the pulse stability to some extent, the

pulse-to-pulse amplitude fluctuation could still be maintained to be less than 8.0% in rms at the maximum pump power of 13.1 W. The output repetition rate ranges from 1.5 to 6.5 kHz and is related to pump power. The pulses with maximum peak power of 170 kW and pulse energy up to 750 μJ were obtained.

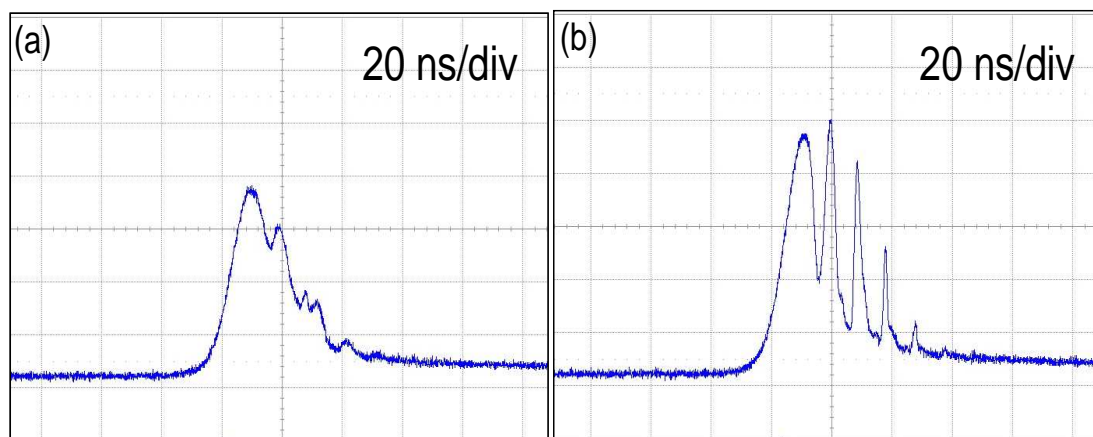


Fig. 3.16 Typical oscilloscope traces of output pulses of the passively Q-switched PCF laser. (a) pulse shape with 6.3 W of pump power and (b) pulse shape with 13.1 W of pump power.

(B) Tunable eye-safe laser with an external-cavity OPO

The 750 μJ passively Q-switched PCF laser at a repetition rate of 6.5 kHz was used as a pump source in the external-cavity OPO, as depicted in Fig. 3.17. The nonlinear crystal in is a 0.76-mm thick and 2-cm long congruent PPLN with a poling period of 29.6 μm . The singly-resonant OPO cavity consists of two BK7 plane mirrors, the front mirror and output coupler. The front mirror is coated with high transmission at pump wavelength ($T > 90\%$) and high reflectivity from 1500 to 1600 nm ($R > 99\%$). The output coupler is coated with high transmission at pump wavelength ($T > 90\%$) and partial reflectivity from 20 to 90% corresponding to the wavelength from 1510 to 1590 nm. A focusing lens with 75-mm focal length was used to focus the pump source into the PPLN crystal. The pump spot size inside PPLN was measured to be around 300 μm . Between the PCF laser and external-cavity OPO, a half-wave plate and a polarization cube were bundled together to control the pump incident power. The maximum average pump incident power was limited to 2.6 W, or the pulse energy limited to 390 μJ for the consideration of photorefractive effect and damage threshold

of PPLN. The PPLN was temperature controlled from 20 to 140°C by an oven to adjust the phase matching wavelength.

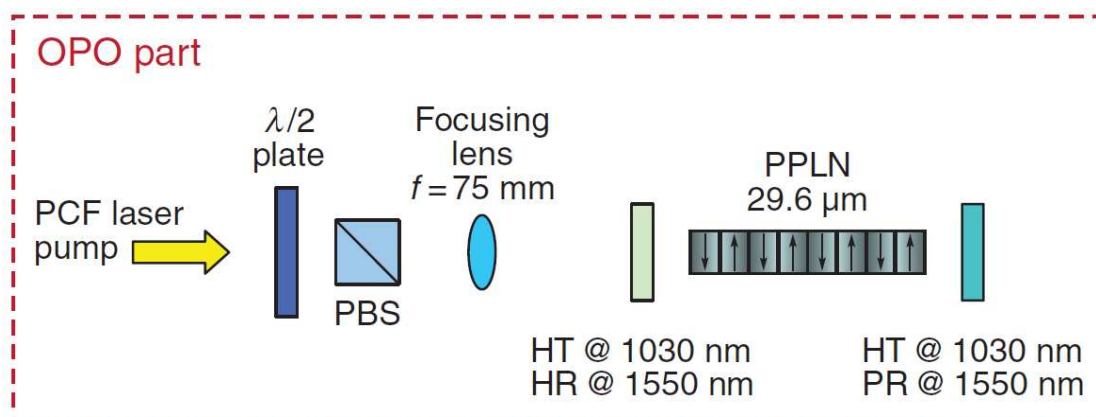


Fig. 3.17 Schematic sketch of the OPO setup. A half-wave plate and polarization beam splitter cube were settled in front of OPO to control the input pump power.

The performance of output power of external-cavity OPO pumped by passively Q-switched PCF laser is shown in Fig. 3.18(a). The temperature of PPLN was controlled at 100°C. Under the pump power of 2.6 W, the output average power of 0.9 W at signal wave was obtained and corresponds to pulse energy of 138 μJ . The conversion is about 35% and the slope efficiency is up to 37.5%. From the temporal pulse traces of pump and signal wave shown in Fig. 3.18(b), the signal pulse shape possesses several spikes which were resulted from SBS effect in pump source as mentioned above. Such an effect can be reduced for lower operating power of PCF laser as depicted in Fig. 3.45(a). The maximum output peak power of signal wave was estimated to be 19 kW with an effective pulse width of 7.3 ns.

The temperature of PPLN was tuned from 20 to 140°C in an interval of 20°C. The output wavelength of signal wave shifts from 1513 to 1593 nm and total 80-nm tuning range was obtained. Fig. 3.48 shows the wavelength of output signal in different operating temperature. The experimental data with empty circles is in good agreement with theoretical data calculated from Selmier's equations [100-101]. Higher temperature and larger wavelength is possible. However, the reflectivity of output coupler used is not uniform within the tuning range. Besides, with increasing the temperature higher than 140°C, the idler phase-matching wavelength gradually approaches 2.8 μm , which locates at the peak absorption of lithium niobate [102].

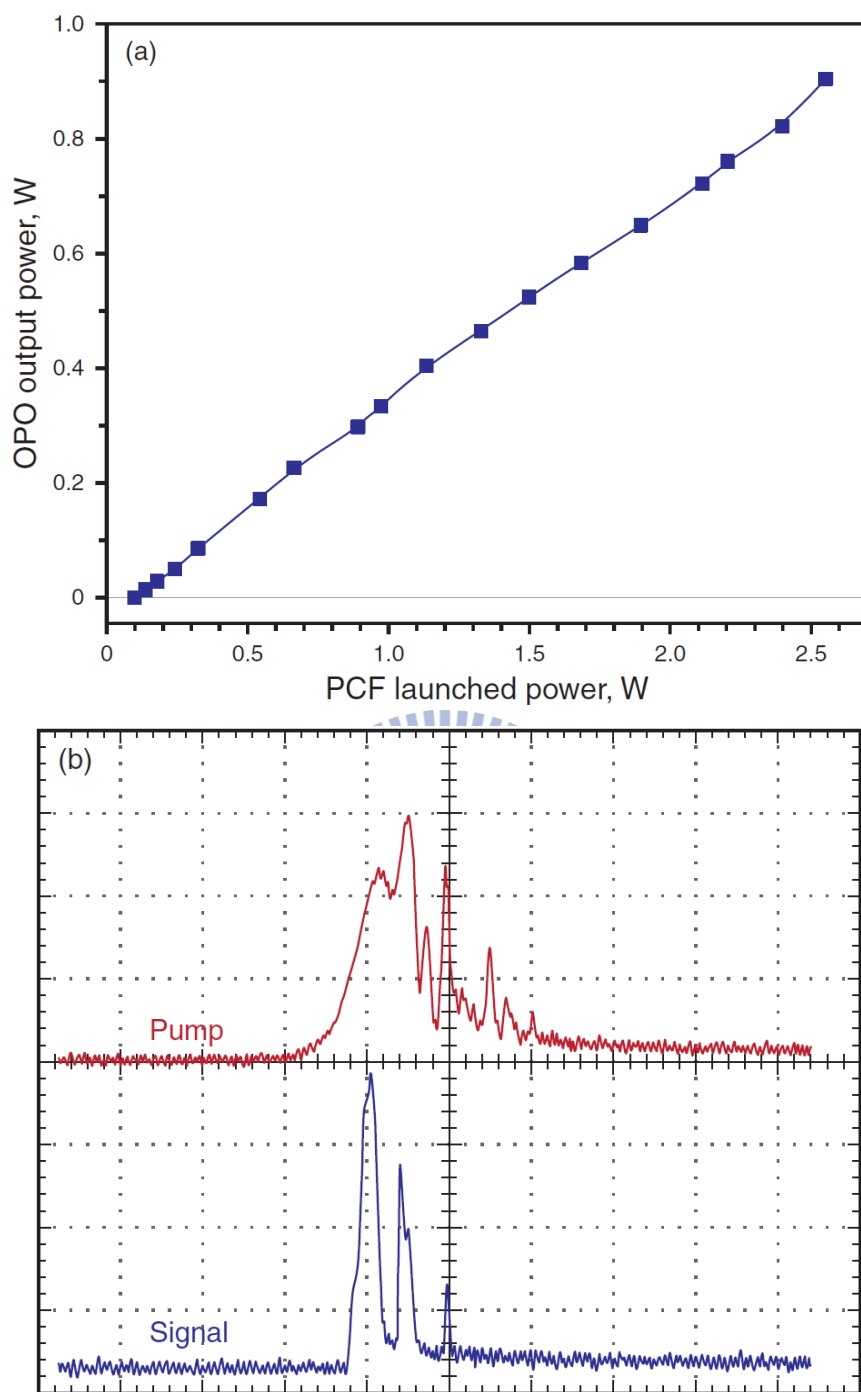


Fig. 3.18 Output performance of external-cavity OPO. (a) averaged output power of signal wave versus averaged power of PCF laser and (b) temporal traces of pump and signal wave.

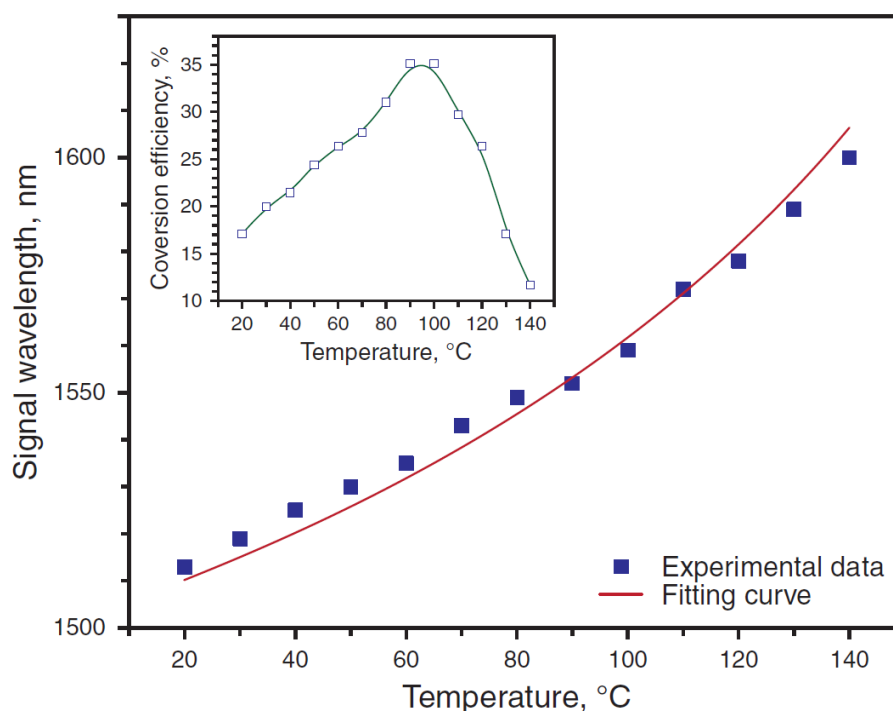


Fig. 3.19 Tuning curve of signal wavelength versus different operating temperature.

Inset: the corresponding conversion efficiency with temperature.

As a result, higher loss will be induced in the cavity for operating temperature higher than 140°C. On the other hand, for lower operating temperature, the photorefractive effect of congruent PPLN will get stronger and limit the output performance. Therefore, there is an optimum efficiency for a specific temperature, as depicted in the inset of Fig. 3.48. In this experiment, the conversion efficiency varies from 11 to 35% and the optimum temperature is found to be around 100°C. At the optimum point, the phase-matching signal wavelength is 1559 nm with a corresponding output reflectivity of 65%.

(C) Summary

I achieved a widely tunable passively Q-switched photonic crystal fiber laser by means of an external-cavity optical parametric oscillator. With an AlGaInAs Qs/barrier structure as a saturable absorber in the 1029-nm PCF laser, the fundamental pulse with energy up to 750 μJ was obtained and was incident into the OPO cavity. Under the pump energy of 390 μJ , the maximum output energy and peak power of signal wave was found to be 138 μJ and 19 kW, respectively. By tuning the temperature of nonlinear crystal, PPLN, over 80-nm tuning range of the signal output

Ch3 Pulsed photonic crystal fiber lasers and amplifier

wavelength from 1513 to 1593 nm was obtained.



3.4 Fiber amplifier seeded by a passively Q-switched Nd:YVO₄/Cr⁴⁺:YAG laser and extracavity third harmonic generation

High efficiency and short pulse duration pulsed light sources of ultraviolet (UV) radiation are attractive for a variety of applications in industry, scientific, and medical needs such as micro-precision processing, laser lithography, and optical data storage [103-104]. Shorter pulse duration is advantageous for laser processing that has lower material removal thresholds. In company with low material removal thresholds, laser machining with shorter pulses at low fluences also leads to cleaner and narrower scribes and reduced the potential damage to the electrical performance of the device [105-106]. Linearly polarized, good beam quality, and high peak power lasers with nanosecond-duration and multi-kilohertz repetition rate pulses are promising candidates for optical nonlinear wavelength conversions. Fiber lasers and amplifiers in the near-infrared (NIR) region, owing to the splendid heat dissipation and the wave-guiding property, have been extensively proved to be favorable light sources for the generation of UV radiation [107-111]. Fiber laser in actively Q-switched scheme [109] was employed for third harmonic generation (THG) and the wavelength conversion efficiency (from IR to THG) of 25% was attained. However, the pulse duration was relatively long (11 ns) due to the lengthy fiber oscillator configuration. The THG pumped by single-stage fiber amplifiers that seeded with passively Q-switched (PQS) Nd:YAG lasers were used to demonstrate UV radiation with shorter pulse width (approximately 1 ns). Nevertheless, the conversion efficiency was relatively lower with 12% [110] and 18% [56], respectively. With the higher conversion efficiency of 26%, the two-stage fiber amplifier [111] was used to produce 1 ns pulse with the average power of 1.5 W. However, the multi-stage architecture led to a complicated and power consuming system. Therefore, it is with much practical significance to design a compact, efficient THG with short pulse duration pumped by a single-stage fiber amplifier.

Large-mode-area (LMA) fibers were used to attain high peak powers and alleviate detrimental nonlinear effects such as stimulated Brillouin scattering (SBS), stimulated Raman scattering (SRS), and self-phase modulation which not only degrade the monochromaticity but also cause optical damages. Nevertheless, conventional LMA fibers suffer from mode-quality degradation with the increasing core size diameter. Recently, photonic crystal fiber (PCF) lasers and amplifiers [61, 112-113] are proved to be reliable light sources with high peak power and good beam quality thanks to the ultra-large mode area core, the high absorption efficiency, and the air holes assisted wave-guiding property. Consequently, a PCF amplifier is much advantageous for nonlinear wavelength conversions rather than the conventional LMA fiber amplifier. However, up to now, the extracavity THG pumped by a single-stage PCF amplifier has not been reported.

In this work, I use a single-stage rod-like PCF amplifier to demonstrate compact harmonic generations with high efficiency and short pulse width. We obtain pulses with average power of 3.3 W at the pulse repetition rate (PRR) of 14.9 kHz and pulse width of 2.2 ns in the IR wavelength by seeding an efficient PQS Nd:YVO₄/Cr⁴⁺:YAG laser into a LMA rod-like PCF amplifier. In addition, we utilize the extracavity nonlinear wavelength conversion architecture to attain the second harmonic generation (SHG) wave at 532 nm and the THG wave at 355 nm. Average powers for SHG and THG were 1.7 W and 1.1 W at the IR input power of 3.3 W which correspond to the conversion efficiency of 52% and 33%, respectively. The pulse width for the UV radiation was 2.1 ns with the pulse amplitude fluctuation of 7.4% in standard deviation.

(A) Single-stage rod-like fiber amplifier

The scheme of the extracavity THG pumped by a single-stage rod-like PCF amplifier is depicted in Fig. 3.20 The experimental setup could be separated into two major parts, one is a PQS Nd:YVO₄/Cr⁴⁺:YAG laser seeded PCF amplifier and the other one is a single-pass harmonic generation. We have demonstrated that the Nd:YVO₄/Cr⁴⁺:YAG PQS laser was a compact and efficient laser source with high peak power and can be applied to THG generation [114] and seed laser [115]. The nearly hemispherical cavity based Nd:YVO₄/Cr⁴⁺:YAG PQS laser was used to simultaneously satisfy the optimal mode matching condition and the good

Ch3 Pulsed photonic crystal fiber lasers and amplifier

Q-switching criterion. The seed laser is a home-made, nearly hemispherical cavity Nd:YVO₄/Cr⁴⁺:YAG PQS laser that emitted pulses with pulse energy of 38 μJ and pulse width of 2.2 ns at the PRR of 14.9 kHz. The seed laser was coupled through a focusing lens into the core of the fiber. A half-wave plate was used to control the polarization direction of the seed laser to match the fast-axis of the polarization maintaining (PM) fiber. The 36-cm in length, PM Yb-doped rod-type PCF has a signal core diameter of 70 μm and a low numerical aperture (N.A.) of 0.02 to sustain the excellent beam quality. The pump cladding of the PCF has a diameter of 200 μm and an air-cladding to maintain a high N.A. of 0.6. The PCF was surrounded with a 1.7-mm thick outer cladding and was sealed with end-caps for protection. The boron doped stress-applying parts near the core were adopted to induce birefringence that produces diverse spectral losses to form a linearly polarization state for the fundamental mode. The pump source was a 15-W 976-nm fiber-coupled laser diode with a core diameter of 200 μm and a numerical aperture of 0.2. Focusing lens with 25-mm focal length was used to re-image the pump beam into the fiber through the dichroic mirror with high transmission (HT, T>90%) at 976 nm and high reflectivity (HR, R>99.8%) within 1030~1100 nm. The pump spot radius was approximately 100 μm, and the pump coupling efficiency was estimated to be around 80%. The laser spectrum was measured by an optical spectrum analyzer with 0.1 nm resolution (Advantest Q8381A). The pulse temporal behavior was recorded by Leroy digital oscilloscope (Wavepro 7100; 10G samples/sec; 1 GHz bandwidth) with a fast InGaAs photodiode.

The average output power and pulse energy versus the launched pump power of the fiber amplifier were shown in Fig. 3.21. Under a launched pump power of 10.5 W, 3.3 W of output power was acquired which corresponds to the pulse energy of 221 μJ. The inset of Fig. 3.50 shows the output spectrum of the PCF amplifier with the output power of 3.3 W. The signal peak wavelength was at 1064.6 nm and its full width at half maximum (FWHM) is around 0.6 nm. The M² factor was measured to be less than 1.3 over the complete output power range owing to the low-N.A. feature of the fiber. The output of the amplifier was linear polarized and the polarization extinction ratio was measured to be higher than 100:1 for all the pump power range that evidences the function of the PM structure in the fiber.

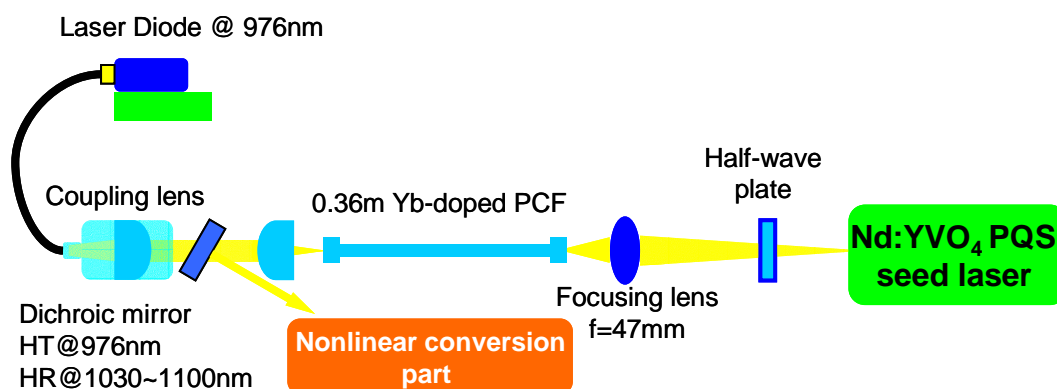


Fig. 3.20 Schematic sketch of the extracavity harmonic generations pumped by a single-stage rod-like photonic crystal fiber amplifier. HR: high reflection; HT: high transmission.

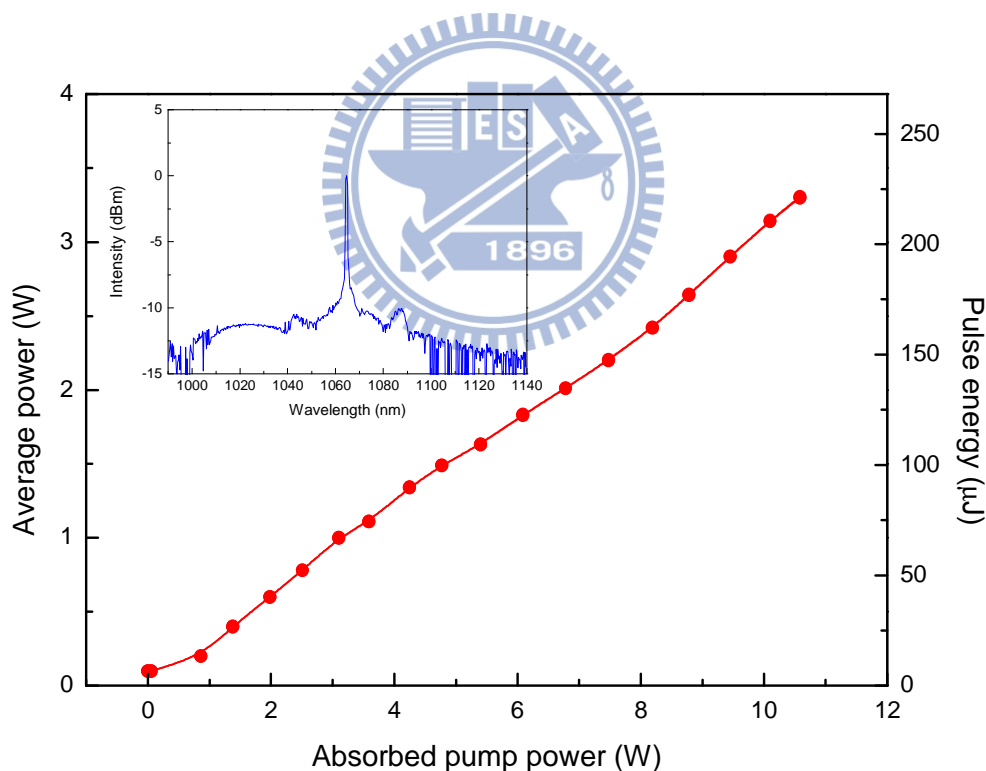


Fig. 3.21 Relevance of the average output power and the pulse energy with the launched pump power of the PCF amplifier. Inset: the output lasing spectrum of the PCF amplifier obtained with 10.5 W of pump power.

Ch3 Pulsed photonic crystal fiber lasers and amplifier

The oscilloscope trace of a train of output pulses of the amplifier is shown in Fig. 3.22(a). The pulse-to-pulse amplitude fluctuation was generally less than 8% in root mean square (rms). Figure 3.22(b) shows the typical oscilloscope trace for a single pulse at the maximum output power of the amplifier. The pulse duration was 2.2 ns and the corresponding peak power was 100 kW.

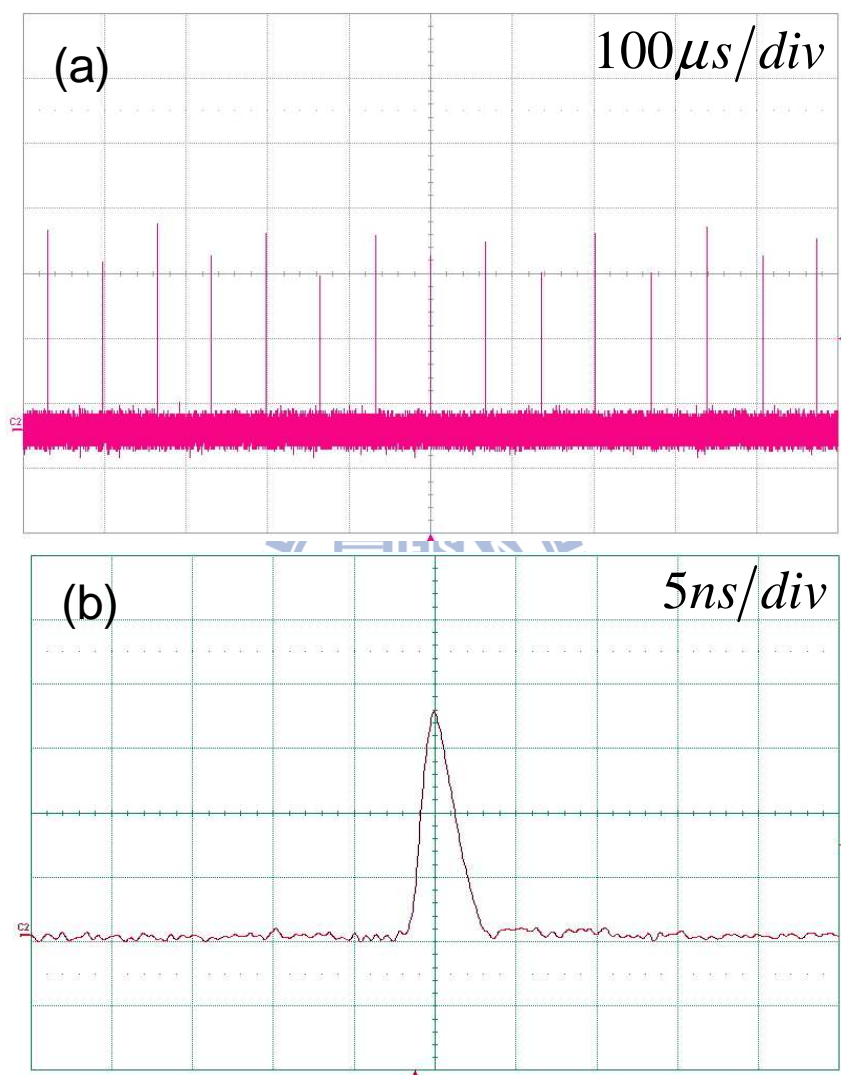


Fig. 3.22 (a) Oscilloscope traces of a train of amplified pulses. (b) Oscilloscope trace of a single pulse of the output pulse of the amplifier.

(B) Single-stage rod-like fiber amplifier

The scheme of the extracavity harmonic generations was depicted in Fig. 3.23. The IR source from the amplifier was focused by a lens with a focal length of 75 mm which was with anti-reflection (AR) coating at 1064 nm. The SHG was demonstrated

Ch3 Pulsed photonic crystal fiber lasers and amplifier

by delivering the focused IR beam into a $3 \times 3 \times 15 \text{ mm}^3$ -in-dimension, type I phase-matched lithium triborate (LBO) crystal which was cut at $\theta=90^\circ$ and $\phi=10.4^\circ$ and operated at 46.6°C . Both end facets of the LBO crystal were coated with AR coating at 1064 nm and 532 nm. The residual IR laser and the generated 532 nm beam were then focused by a lens which had the focal length of 19 mm and was coated with AR coating at 1064 nm and 532 nm. The type II, $3 \times 3 \times 10 \text{ mm}^3$ -in-dimension LBO crystal cut at $\theta=44^\circ$ and $\phi=90^\circ$ was used for sum-frequency-mixing operated at 48°C . The entrance together with the exit end facets of the LBO crystal were coated with AR coating at 1064 nm and 532 nm. The temperature of the SHG and THG nonlinear crystals were temperature-controlled by thermoelectric coolers with the precision of 0.1°C .

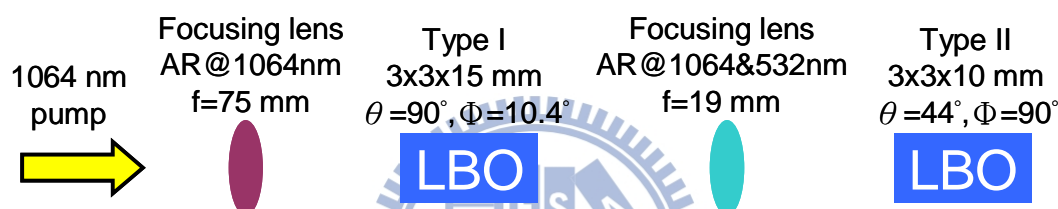


Fig. 3.23 Schematic sketch of the setup of the SHG and THG. AR: anti-reflection.

Figure 3.24 shows the average power obtained with the SHG (532nm) and the THG (355nm), respectively. Under a pump power of 3.3 W of the IR wavelength, an average output power of SHG was 1.7 W corresponding to the pulse energy of $114 \mu\text{J}$ and the wavelength conversion efficiency (from IR to SHG) of 52%. The average output power of the THG increased monotonically with pump power of the IR wavelength. At a launched pump power of 3.3 W, the sum-frequency-mixing was found to generate an output power of 1.1 W and pulse energy of $74 \mu\text{J}$, corresponding to a slope efficiency of 39% and wavelength conversion efficiency of 33% (from IR to THG). The spatial intensity distribution of the far field of 355 nm output was shown in the inset of Fig. 3.24

Oscilloscope traces of a train of output pulses of the SHG (top) and the THG (bottom) is shown in Fig. 3.25(a). The pulse-to-pulse amplitude fluctuations for SHG and THG were approximately less than 6% and 8% in rms, respectively. Figure 3.25(b) depicts the oscilloscope trace for a single pulse at the maximum output power of THG. The pulse duration was measured to be about 2.1 ns which correspond to the peak

power of 35 kW.

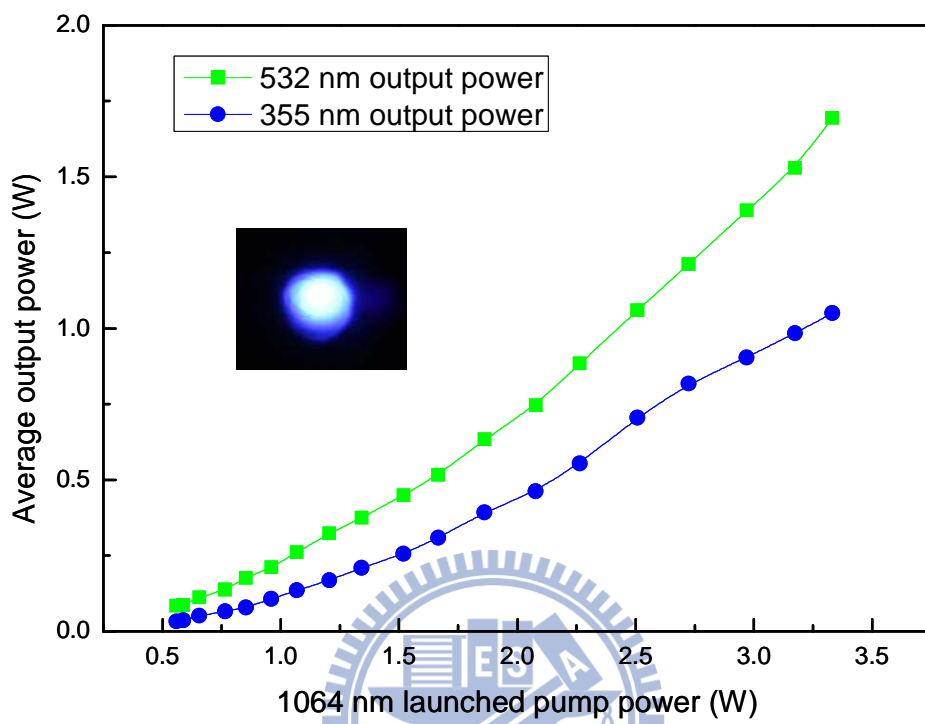


Fig. 3.24 Dependences of the average output power at 532 nm and 355 nm on the incident pump power at 1064 nm. Inset: the spatial intensity distribution of far field of the THG output.

In order to obtain compact, efficient, and shorter pulse duration of the UV light source, single-stage fiber amplifiers were the preferable light sources for extracavity THG rather than fiber lasers. Besides, for higher wavelength conversion efficiency, the selection of the extracavity THG nonlinear crystal is also of great importance. The choice of the THG crystal is the compromise between finding a high nonlinear coefficient and a wide acceptance angle combined with a small walk-off angle [116]. The extracavity THGs by using a type I phase-matched LBO as the THG crystal were demonstrated with single-stage fiber amplifiers [107, 110]. The relatively large walk-off angle of the type I phase-matched LBO for THG (18.3 mrad to type I and 9.3 mrad to type II) [107] will deteriorate the beam overlap between the IR and the green beams that is seriously detrimental to conversion efficiency. Besides, in ref. 110,

Ch3 Pulsed photonic crystal fiber lasers and amplifier

polarization instability caused by using a non-PM fiber as the amplifier also led to the lower wavelength conversion efficiency of only 12%. Furthermore, two type I phase-matched LBO were utilized for SHG and THG with a PM fiber amplifier as the fundamental light source [107]. The conversion efficiency was limited to be 18% because the polarization state between the residual IR beam and the green light in the THG crystal was not re-optimized. Here I realize the efficient extracavity UV light generation by employing the type II LBO as the THG crystal owing to its smaller walk-off angle and relatively large acceptance angle [110] (5.0 mrad cm for type II and 1.7 mrad cm for type I). Combining the efficient THG module and the single-stage PM PCF amplifier, we obtained, to the best of our knowledge, the highest wavelength conversion efficiency of 33% and the short pulse duration of approximately 2 ns in the same time.

(C) Conclusions

In conclusion, I have used a Nd:YVO₄/Cr⁴⁺:YAG PQS laser to seed a single-stage rod-like PCF amplifier to acquire a single polarization, high beam quality, and efficient IR pulsed light source with the pulse energy of 221 μJ and pulse width of 2.2 ns at the PRR of 14.9 kHz. We further utilize the developed PCF amplifier to demonstrate the extracavity SHG and THG. Under an incident pump power of 3.3 W at the IR wavelength, the average output powers of the SHG and the THG were measured to be up to 1.7 W and 1.1 W which amount to the wavelength conversion efficiencies of 52% and 33%, respectively. This is the highest conversion efficiency in the generation of UV light by means of the fiber amplifier pumped THG. It is believed that the high efficiency UV light source suggest further applications such as industrial material processing and scientific researches.

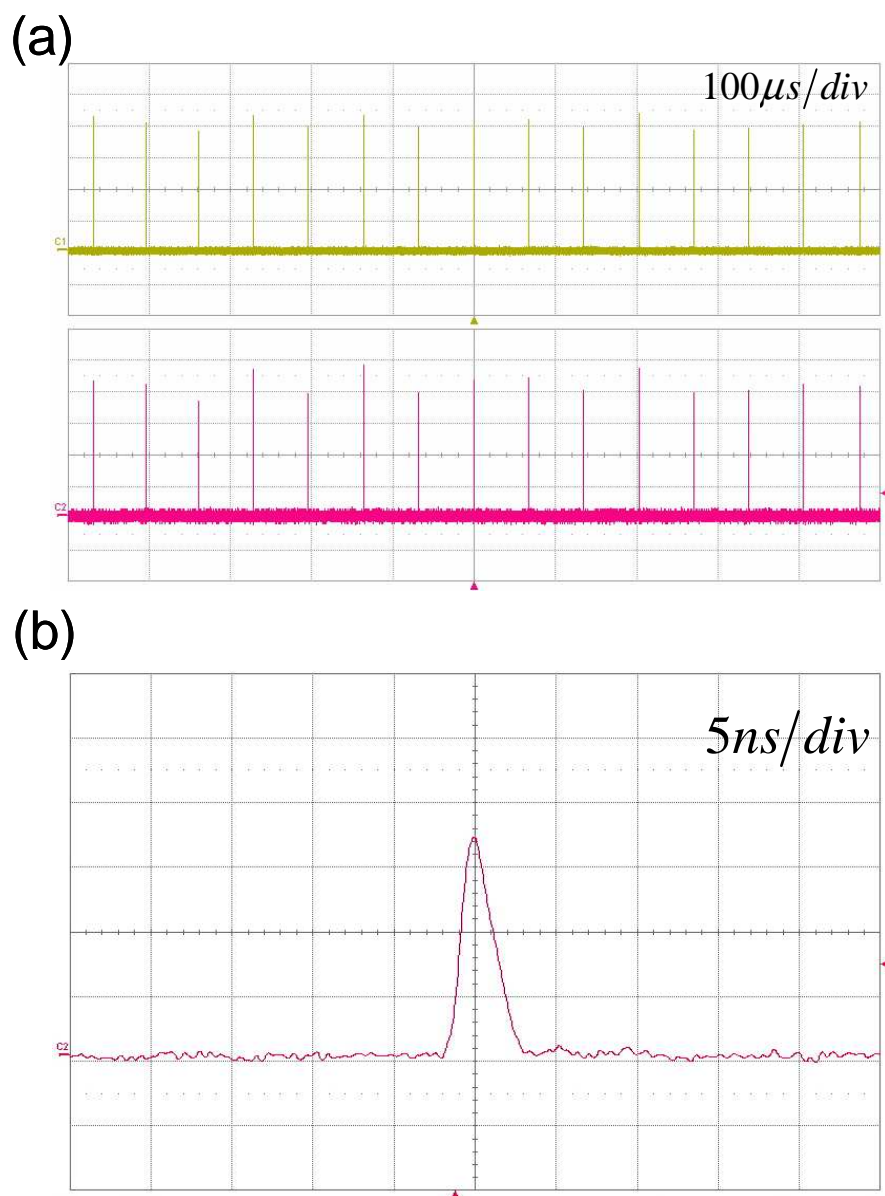


Fig. 3.25 (a) Oscilloscope traces of a train of output pulses of 532 nm (top) and 355 nm (bottom). (b) Oscilloscope trace of a single pulse of the output pulse of the THG.

3.5 Conclusions

In this chapter, I perform efficient, high peak power fiber amplifier and PQS fiber lasers with either Cr^{4+} :YAG crystal or AlGaInAs MQWs as the SA by using ultra-large core photonic crystal fiber of the core diameter of 70 μm . The pulse energy was obviously enhanced due to the enlarged core size and the pulse width was also reduced owing to the shorter fiber length which equals to a shorter cavity length. Table 4.2 summaries the performances obtained with the with the photonic crystal fiber.

With the same Cr^{4+} :YAG crystal of the initial transmission of 28% as in the conventional LMA fiber laser described before, the pulse energy was 1.8 times higher and the pulse width was 2 times smaller which corresponds to 3.5 times higher of pulse peak power compared with the results obtained with the fiber of core diameter of 30 μm . Besides, I also use three types of AlGaInAs QWs that posses 50 groups of three QWs (3×50 QWs), 30 groups of three QWs (3×30 QWs), and 30 groups of two QWs (2×30 QWs) as the saturable absorber. With the same AlGaInAs QWs (3×50 QWs) as in the conventional LMA fiber laser described before, the pulse energy was 2.45 times higher and the pulse width was 6 times smaller which corresponds to 14.7 times higher of pulse peak power compared with the results obtained with the fiber of core diameter of 30 μm .

With the PQS PCF laser, I also demonstrate the intracavity optical parametric oscillator (IOPO) by utilizing the Cr^{4+} :YAG crystal as the saturable absorber and he extracavity optical parametric oscillator (EOPO) by utilizing the AlGaInAs QWs as the saturable absorber. Shorter pulse width and higher peak power can be attained with the IOPO scheme but higher output power and conversion efficiency can be achieved with the EOPO scheme. Besides, thanks to the high refractive-index-temperature coefficient of the PPLN used in the EOPO scheme, the wavelength can be tuned over a broad range.

Furthermore, for generating shorter pulse duration, PCF amplifier was seeded by the PQS Nd:YVO₄/ Cr^{4+} :YAG seed laser mentioned in chapter 2. I demonstrate the different harmonic generations by means of the extracavity wavelength conversion

Ch3 Pulsed photonic crystal fiber lasers and amplifier

pumped by a PCF amplifier. The results manifested that it is efficient and with simplicity to use the single stage PCF amplifier as the fundamental wavelength light source.



Reference

- [1]. J. C. Knight, T. A. Birks, P. S.-J. Russell, and D. M. Atkin, "All-silica single-mode optical fiber with photonic crystal cladding," *Opt. Lett.* **21**, 1547-1549 (1996).
- [2]. T. A. Birks, J. C. Knight, and P. S.-J. Russell, "Endless single-mode photonic crystal fiber," *Opt. Lett.* **22**, 961-963 (1997).
- [3]. J. C. Knight, T. A. Birks, R. F. Cregan, P. S.-J. Russell, and J. P. de Sandro, "Large mode area photonic crystal fiber," *Electron. Lett.* **34**, 1347-1348 (1998).
- [4]. J. Limpert, A. Liem, M. Reich, T. Schreiber, S. Nolte, H. Zellmer, A. Tünnermann, J. Broeng, A. Petersson, and C. Jakobsen "Low-nonlinearity single-transverse-mode ytterbium-doped photonic crystal fiber amplifier," *Opt. Express* **12**, 1313-1319 (2004).
- [5]. J. Limpert, N. Deguil-Robin, I. Manek-Hönninger, F. Salin, F. Röser, A. Liem, T. Schreiber, S. Nolte, H. Zellmer, A. Tünnermann, J. Broeng, A. Petersson, and C. Jakobsen, "High-power rod-type photonic crystal fiber laser," *Opt. Express* **13**, 1055-1058 (2005).
- [6]. J. Limpert, O. Schmidt, J. Rothhardt, F. Röser, T. Schreiber, and A. Tünnermann, "Extended single-mode photonic crystal fiber," *Opt. Express* **14**, 2715-2719 (2006).
- [7]. C. D. Brooks, and F. D. Teodoro, "Multi-megawatt peak power, single-transverse-mode operation of a 100 μm core diameter, Yb-doped rod-like photonic crystal fiber amplifier," *Appl. Phys. Lett.* **89**, 111119-111121 (2006).
- [8]. J. Limpert, N. Deguil-Robin, S. Petit, I. Manek-Hönninger, F. Salin, P. Rigail, C. Hönninger and E. Mottay, "High power Q-switched Yb-doped photonic crystal fiber laser producing sub-10 ns pulses," *Appl. Phys. B* **81**, 19-21 (2005)
- [9]. A. Tünnermann, T. Schreiber, F. Röser, A. Liem, S. Höfer, H. Zellmer, S. Nolte, and J. Limpert, "The renaissance and bright future of fibre lasers," *J. Phys. At. Mol. Opt. Phys.* **38**, S681-S693 (2005).
- [10]. Y. Jeong, J. K. Sahu, M. Laroche, W. A. Clarkson, K. Furusawa, D. J. Richardson, and J. Nilsson, "120-W Qswitched cladding-pumped Yb-doped fibre

Ch3 Pulsed photonic crystal fiber lasers and amplifier

- laser,” in Proc. Conference on Lasers and Electro-Optics Europe, 2003. CLEO/Europe, Munich ICM, Germany, June 22-27, 2003, 626-626 (2003).
- [11]. J. Limpert, S. Höfer, A. Liem, H. Zellmer, A. Tünnermann, S. Knoke, and H. Voelckel, “100-W average-power, high-energy nanosecond fiber amplifier,” *Appl. Phys. B* **75**, 477-479 (2002).
- [12]. Y. Jeong, J. K. Sahu, R. B. Williams, D. J. Richardson, K. Furusawa, and J. Nilsson, “Ytterbium-doped largecore fibre laser with 272 W output power,” *Electron. Lett.* **39**, 977-978 (2003).
- [13]. Y. Jeong, J. K. Sahu, D. N. Payne, and J. Nilsson, “Ytterbium-doped large-core fiber laser with 1.36 kW continuous-wave output power,” *Opt. Express* **12**, 6088-6092 (2004).
- [14]. A. Liem, J. Limpert, H. Zellmer, A. Tünnermann, V. Reichel, K. Mörl, S. Jetschke, S. Unger, H.-R. Müller, J. Kirchhof, T. Sandrock, and A. Harschak, “1.3 kW Yb-doped fiber laser with excellent beam quality,” in Proc. Conference on Lasers and Electro-Optics 2004, San Francisco, USA, May 16-21, 2004, postdeadline paper CPDD2.
- [15]. A. Fotiadi, A. Kurkov, and I. Razdobreev, “All-fiber passively Q-switched ytterbium laser,” *CLEO/Europe- EQEC 2005, Technical Digest, CJ 2-3*, Munich, Germany (2005).
- [16]. Z. J. Chen, A. B. Grudinin, J. Porta, and J. D. Minelly, “Enhanced Q switching in double-clad fiber lasers,” *Opt. Lett.* **23**, 454-456 (1998).
- [17]. O. Schmidt, J. Rothhardt, F. Röser, S. Linke, T. Schreiber, K. Rademaker, J. Limpert, S. Ermeneux, P. Yvernault, F. Salin, and A. Tünnermann, “Millijoule pulse energy Q-switched short-length fiber laser,” *Opt. Lett.* **32**, 1551-1553 (2007).
- [18]. R. Ashinoff, and R. G. Geronemus, “Rapid response of traumatic and medical tattoos to treatment with the Q-switched ruby laser,” *Plast. Reconstr. Surg.* **91**, 841-845 (1993).
- [19]. C. C. Ranaud, H. L. Offerhaus, J. A. Alvarez-Chavez, C. J. Nilsson, W. A. Clarkson, P. W. Turner, D. J. Richardson, and A. B. Grudinin, “Characteristics of Q-switched cladding-pumped ytterbium-doped fiber lasers with different high-energy fiber designs,” *IEEE J. Quantum Electron.* **37**, 199-206 (2001).
- [20]. J. A. Alvarez-Chavez, H. L. Offerhaus, J. Nilsson, P. W. Turner, W. A. Clarkson, and D. J. Richardson, “Highenergy, high-power ytterbium-doped Q-switched fiber

- laser,” *Opt. Lett.* **25**, 37-39 (2000).
- [21]. J. J. Zayhowski, and C. Dill III, “Diode-pumped passively Q-switched picosecond microchip lasers,” *Opt. Lett.* **19**, 1427-1429 (1994).
- [22]. X. Zhang, S. Zhao, Q. Wang, Q. Zhang, L. Sun, and S. Zhang, “Optimization of Cr⁴⁺-doped saturable-absorber Q-switched lasers,” *IEEE J. Quantum Electron.* **33**, 2286-2294 (1997).
- [23]. A. Agnesi, and S. Dell’acqua, “High-peak-power diode-pumped passively Q-switched Nd:YVO₄ laser,” *Appl. Phys. B* **76**, 351-354 (2003).
- [24]. Y. Kalisky, “Cr⁴⁺-doped crystals: their use as lasers and passive Q-switches,” *Prog. Quantum Electron.* **28**(5), 249–303 (2004).
- [25]. A. Sennaroglu, U. Demirbas, S. Ozharar, and F. Yaman, “Accurate determination of saturation parameters for Cr⁴⁺-doped solid-state saturable absorbers,” *J. Opt. Soc. Am. B* **23**, 241-249 (2006).
- [26]. M. Laroche, H. Gilles, S. Girard, N. Passilly, and K. Aït-Ameur, “Nanosecond pulse generation in a passively Qswitched Yb-doped fiber laser by Cr⁴⁺:YAG saturable absorber,” *IEEE Photon. Technol. Lett.* **18**(6), 764-766 (2006).
- [27]. L. Pan, I. Utkin, and R. Fedosejevs, “Passively Q-switched ytterbium-doped double-clad fiber laser with a Cr⁴⁺:YAG saturable absorber,” *IEEE Photon. Technol. Lett.* **19**, 1979-1981 (2007).
- [28]. J. Y. Huang, W. Z. Zhuang, W. C. Huang, K. W. Su, C. Hu, K. F. Huang, and Y. F. Chen, “Comparative studies for Cr⁴⁺:YAG crystal and AlGaInAs semiconductor used as a saturable absorber in Q-switched Yb-doped fiber lasers,” *Opt. Express* **17**, 20800-20805 (2009).
- [29]. Y. X. Fan, F. Y. Lu, S. L. Hu, K. C. Lu, H. J. Wang, X. Y. Dong, J. L. He, and H. T. Wang, “Tunable high-peakpower, high-energy hybrid Q-switched double-clad fiber laser,” *Opt. Lett.* **29**, 724-726 (2004).
- [30]. P. Myslinski, J. Chrostowski, J. Koningstein, and J. Simpson, “Self-mode locking in a Q-switched erbium-doped fiber laser,” *Appl. Opt.* **32**, 286-290 (1993).
- [31]. M. H. Crowell, “Characteristics of mode-coupled lasers,” *IEEE J. Quantum Electron.* **1**, 12-20 (1965).
- [32]. H. Statz, and C. L. Tang, “Phase locking of modes in lasers,” *J. Appl. Phys.* **36**, 3923-3927 (1965).
- [33]. M. A. Duguay, S. L. Shapiro, and P. M. Rentzepis, “Spontaneous appearance of picosecond pulses in ruby and Nd: glass lasers,” *Phys. Rev. Lett.* **19**, 1014-1016

- (1967).
- [34]. O. L. Gaddy, and E. M. Schaefer, "Self locking of modes in the argon ion laser," *Appl. Phys. Lett.* **9**, 281-282 (1966).
- [35]. A. A. Grütter, H. P. Weber, and R. Dändliker, "Imperfectly mode-locked laser emission and its effects on nonlinear optics," *Phys. Rev.* **185**, 629-643 (1969).
- [36]. R. Dändliker, A. A. Grütter, and H. P. Weber, "Statistical amplitude and phase variations in mode-locked lasers," *IEEE J. Quantum Electron.* **6**, 687-693 (1970).
- [37]. H. Statz, "On the condition for self-locking of modes in lasers," *J. Appl. Phys.* **38**, 4648-4655 (1967).
- [38]. H. Statz, and M. Bass, "Locking in multimode solid-state lasers," *J. Appl. Phys.* **40**, 377-383 (1969).
- [39]. P. Glas, and M. Naumann, "Self pulsing versus self locking in a cw pumped neodymium doped double clad fiber laser," *Opt. Commun.* **161**, 345-358 (1999).
- [40]. H. C. Liang, R. C. Chen, Y. J. Huang, K. W. Su, and Y. F. Chen, "Compact efficient multi-GHz Kerr-lens modelocked diode-pumped Nd:YVO₄ laser," *Opt. Express* **16**, 21149-21154 (2008).
- [41]. J. Y. Huang, W. C. Huang, W. Z. Zhuang, K. W. Su, Y. F. Chen, and K. F. Huang, "High-pulse-energy, passively Q-switched Yb-doped fiber laser with AlGaInAs quantum wells as a saturable absorber," *Opt. Lett.* **34**, 2360-2362 (2009).
- [42]. J. Miao, J. Peng, B. Wang, and H. Tan, "Compact KTA-based intracavity optical parametric oscillator driven by a passively Q-switched Nd:GdVO₄ laser," *Appl. Opt.* **47**, 4287-4291 (2008).
- [43]. H. T. Huang, J. L. He, X. L. Dong, C. H. Zuo, B. T. Zhang, G. Qiu, and Z. K. Liu, "High-repetition-rate eye-safe intracavity KTA OPO driven by a diode-end-pumped Q-switched Nd:YVO₄ laser," *Appl. Phys. B* **90**, 43-45 (2008).
- [44]. Z. Liu, Q. Wang, X. Zhang, Z. Liu, J. Chang, H. Wang, S. Fan, W. Sun, G. Jin, X. Tao, S. Zhang, and H. Zhang, "Efficient acousto-optically Q-switched intracavity Nd:YAG/KTiOAsO₄ optical parametric oscillator," *Appl. Phys. B* **92**, 37-41 (2008).
- [45]. E. Gregor, D. E. Nieuwsma, and R. D. Stultz, "20 Hz eyesafe laser rangefinder for air defense," *Proc. SPIE* 1207, 124-134 (1990).
- [46]. L. R. Marshall, A. D. Hays, and J. Kasinski, "Highly efficient optical parametric oscillators," *Proc. SPIE* 1419, 141-152 (1991).
- [47]. J. E. Nettleton, B. W. Schilling, D. N. Barr, and J. S. Lei, "Monoblock laser for a

Ch3 Pulsed photonic crystal fiber lasers and amplifier

- low-cost, eyesafe, microlaser range finder,” *Appl. Opt.* **39**, 2428-2432 (2000).
- [48]. J. Limpert, F. Roser, S. Klingebiel, T. Schreiber, C. Wirth, T. Peschel, R. Eberhardt, and A. Tünnermann, “The rising power of fiber lasers and amplifiers,” *IEEE J. Sel. Top. Quantum Electron.* **13**, 537-545 (2007).
- [49]. S. D. Jackson, and A. Lauto, “Diode-pumped fiber lasers: a new clinical tool?” *Lasers Surg. Med.* **30**, 184-190 (2002).
- [50]. L. Quintino, A. Costa, R. Miranda, D. Yapp, V. Kumar, and C. J. Kong, “Welding with high power fiber lasers – A preliminary study,” *Mater. Des.* **28**, 1231-1237 (2007).
- [51]. J. Y. Huang, H. C. Liang, K. W. Su, and Y. F. Chen, “High power passively Q-switched ytterbium fiber laser with Cr^{4+} :YAG as a saturable absorber,” *Opt. Express* **15**, 473-479 (2007).
- [52]. T. Hakulinen, and O. G. Okhotnikov, “8 ns fiber laser Q switched by the resonant saturable absorber mirror,” *Opt. Lett.* **32**, 2677-2679 (2007).
- [53]. W. Z. Zhuang, W. C. Huang, Y. P. Huang, K. W. Su, and Y. F. Chen, “Passively Q-switched photonic crystal fiber laser and intracavity optical parametric oscillator,” *Opt. Express* **18**, 8969-8975 (2010).
- [54]. K. Alavi, H. Temkin, W. R. Wagner, and A. Y. Cho, “Optically pumped 1.55- μm double heterostructure $\text{Ga}_x\text{Al}_y\text{In}_{1-x-y}\text{As}/\text{Al}_u\text{In}_{1-u}\text{As}$ lasers grown by molecular beam epitaxy,” *Appl. Phys. Lett.* **42**, 254-256 (1983).
- [55]. W. T. Tsang and N. A. Olsson, “New current injection 1.5- μm wavelength $\text{Ga}_x\text{Al}_y\text{In}_{1-x-y}\text{As}/\text{InP}$ double-heterostructure laser grown by molecular beam epitaxy,” *Appl. Phys. Lett.* **42**, 922-924 (1983).
- [56]. D. A. Bender, J. G. Cederberg, and G. A. Hebner, “Parametric results of the AlGaInAs Quantum-Well saturable absorber for use as a passive Q-Switch,” in *Conference on Lasers and Electro-Optics*, (Optical Society of America, San Jose, California, 2010), paper CThL3.
- [57]. J. A. Alvarez-Chavez, H. L. Offerhaus, J. Nilsson, P. W. Turner, W. A. Clarkson, and D. J. Richardson, “High-energy, high-power ytterbium-doped Q-switched fiber laser,” *Opt. Lett.* **25**, 37-39 (2000).
- [58]. A. Piper, A. Malinowski, K. Furusawa, and D. J. Richardson, “High-power, high-brightness, mJ Qswitched ytterbium-doped fibre laser,” *Electron. Lett.* **40**(15), 928–929 (2004).
- [59]. J. Limpert, A. Liem, H. Zellmer, A. Tünnermann, S. Knoke, and H. Voelckel,

Ch3 Pulsed photonic crystal fiber lasers and amplifier

- “High-average-power millijoule fiber amplifier system,” *Lasers and Electro-Optics*, 2002. CLEO’02. Technical Digest, Long Beach, CA, paper CThX3, 591–592 (2002).
- [60]. C. D. Brooks, and F. Di Teodoro, “1-mJ energy, 1-MW peak-power, 10-W average-power, spectrally narrow, diffraction-limited pulses from a photonic-crystal fiber amplifier,” *Opt. Express* **13**(22), 8999–9002 (2005).
- [61]. F. D. Teodoro, M. K. Hemmat, J. Morais, and E. C. Cheung, “High peak power operation of a 100 μ m-core, Yb-doped rod-type photonic crystal fiber amplifier,” *Fiber Lasers VII: Technology, Systems and Applications, Proc. of SPIE vol. 7580*, 758006 (2010).
- [62]. M. Salhi, A. Hideur, T. Chartier, M. Brunel, G. Martel, C. Ozkul, and F. Sanchez, “Evidence of Brillouin scattering in an ytterbium-doped double-clad fiber laser,” *Opt. Lett.* **27**, 1294-1296 (2002).
- [63]. Y. X. Fan, F. Y. Lu, S. L. Hu, K. C. Lu, H. J. Wang, G. Y. Zhang, and X. Y. Dong, “Narrow-linewidth widely tunable hybrid Q-switched double-clad fiber laser,” *Opt. Lett.* **28**, 537-539 (2003).
- [64]. A. A. Fotiadi, P. Mégret, and M. Blondel, “Dynamics of a self-Q-switched fiber laser with a Rayleigh-stimulated Brillouin scattering ring mirror,” *Opt. Lett.* **29**, 1078-1080 (2004).
- [65]. L. Pan, I. Utkin, R. J. Lan, Y. Godwal, and R. Fedosejevs, “High-peak-power subnanosecond passively Q-switched ytterbium-doped fiber laser,” *Opt. Lett.* **35**, 895-897 (2010).
- [66]. Y. F. Chen, S. W. Tsai, and S. C. Wang, “High-power diode-pumped Q-switched and mode-locked Nd:YVO₄ laser with a Cr⁴⁺:YAG saturable absorber,” *Opt. Lett.* **25**, 1442-1444 (2000).
- [67]. Y. F. Chen, and S. W. Tsai, “Simultaneous Q-switching and mode-locking in a diode-pumped Nd:YVO₄-Cr⁴⁺:YAG laser,” *IEEE J. Quantum Electron.* **37**, 580-586 (2001).
- [68]. S. Zhang, E. Wu, H. Pan, and H. Zeng, “Q-switched mode-locking with Cr⁴⁺:YAG in a diode pumped Nd:GdVO₄ laser,” *Appl. Phys. B* **78**, 335-338 (2004).
- [69]. J. Yang, J. Liu, and J. He, “A compact Q-switched and mode-locked diode-pumped Nd:GdVO₄ laser with Cr⁴⁺:YAG,” *Laser Phys.* **15**(8), 1137–1141 (2005).

- [70]. J. A. Fleck, Jr., "Ultrashort-pulse generation by Q-switched lasers," *Phys. Rev. B* **1**, 84-100 (1970).
- [71]. P. G. Kryukov, and V. S. Letokhov, "Fluctuation mechanism of ultrashort pulse generation by laser with saturable absorber," *IEEE J. Quantum Electron.* **8**, 766-782 (1972).
- [72]. S. G. Grubb, in: *Proc. of the Optical Amplifiers and Their Applications Topical Meeting*, Monterey, CA, USA, July 11-13, 42-44 (1996).
- [73]. B. K. Nayar, J. J. Lewandowski, F. J. Wilson, J. A. Chavez, A. B. Grudinin, J. D. Minelly, G. Kennedy, and A. Raven, "High power 1540 nm fibre lasers for surgical applications," in: *Proc. of the IEEE Lasers and Electro-Optics Society Annual Meeting*, Orlando, FL, USA, December 1-4, **2** 397-398 (1998).
- [74]. S. U. Alam, P. W. Turner, A. B. Grudinin, and J. Nilsson, "High energy, high repetition rate, tunable Er–Yb-codoped Q-switched fibre laser," in: *Tech. Digest of the Conference on Lasers and Electro-Optics*, Baltimore, MD, USA, May 6-11, 218-219 (2001).
- [75]. J. E. Nettleton, B. W. Schilling, D. N. Barr, and J. S. Lei, "Monoblock laser for a low-cost, eyesafe, microlaser range finder," *Appl. Opt.* **39**, 2428-2432 (2000).
- [76]. A. Tünnermann, T. Schreiber, F. Röser, A. Liem, S. Höfer, H. Zellmer, S. Nolte, and J. Limpert, "The renaissance and bright future of fibre lasers," *J. Phys. B* **38**, S681-S694 (2005).
- [77]. A. S. Kurkov, Ya. E. Sadovnikova, A. V. Marakulin, and E. M. Sholokhov, "All fiber Er-Tm Q-switched laser," *Laser Phys. Lett.* **7**, 795-797 (2010).
- [78]. M. Němec, W. Zendzian, H. Jelínková, J. K. Jabczynski, J. Šulc, L. Gorajek, and J. Kwiatkowski, "Q-Switched Er:YAG lasers resonantly pumped by erbium fiber laser," *Laser Phys.* **20**, 661-664 (2010).
- [79]. B. Peng, H. Zhang, M. Gong, and P. Yan, "All fiber eye safe pulsed laser with Er-Yb co-doped multi-stage amplifier," *Laser Phys.* **19**, 2019-2022 (2009).
- [80]. G. A. Ball and W. W. Morey, "Continuously tunable single-mode erbium fiber laser," *Opt. Lett.* **17**, 420-422 (1992).
- [81]. H. Zhang, D. Y. Tang, L. M. Zhao, Q. L. Bao, K. P. Loh, B. Lin, and S. C. Tjin, "Compact graphene mode-locked wavelength-tunable erbium-doped fiber lasers: from all anomalous dispersion to all normal dispersion," *Laser Phys. Lett.* **7**, 591-596 (2010).
- [82]. S. K. Liaw, S. Wang, C. S. Shin, Y. L. Yu, N. K. Chen, K. C. Hsu, A. Manshina

- and Y. Tver'yanovich, "Linear cavity fiber laser using subring-cavity incorporated saturable absorber for single-frequency operation," *Laser Phys.* **20**, 1744-1746 (2010).
- [83]. N. K. Chen, Z. Z. Feng, and S. K. Liaw, "All-fiber pulse width tunable actively Q-switched erbium fiber laser using abrupt-tapered Mach-Zehnder block filter," *Laser Phys. Lett.* **7**, 363-366 (2010).
- [84]. Q. H. Mao and J. W. Y. Lit, "Widely tunable L-band erbium-doped fiber laser with fiber Bragg gratings based on optical bistability," *Appl. Phys. Lett.* **82**, 1335-1337 (2003).
- [85]. H. Ahmad, M. Z. Zulkifli, A. A. Latif, and S. W. Harun, "Novel O-band tunable fiber laser using an array waveguide grating," *Laser Phys. Lett.* **7**, 164-167 (2010).
- [86]. D.-F. Liu and C.-H. Wang, "Single linearly polarized, widely tunable Yb³⁺-doped fiber laser with alternative polarization and wavelength," *Laser Phys. Lett.* **7**, 153-157 (2010).
- [87]. A. A. Latif, H. Ahmad, N. A. Awang, M. Z. Zulkifli, C. H. Pua, Z.A. Ghani, and S.W. Harun, "Tunable high power fiber laser using an AWG as the tuning element," *Laser Phys.* **21**, 712-717 (2011).
- [88]. M. R. A. Moghaddam, S. W. Harun, M. R. Tamjis, and H. Ahmad, "Double-clad erbium/ytterbium-doped fiber laser with a fiber Bragg grating," *Laser Phys. Lett.* **6**, 586-589 (2009).
- [89]. M. E. Klein, C. K. Laue, D.-H. Lee, K.-J. Boller, and R. Wallenstein, "Diode-pumped singly resonant continuous-wave optical parametric oscillator with wide continuous tuning of the near-infrared idler wave," *Opt. Lett.* **25**, 490-492 (2000).
- [90]. S. E. Bisson, K. M. Armstrong, T. J. Kulp, and M. Hartings, "Broadly tunable, mode-hop-tuned cw optical parametric oscillator based on periodically poled lithium niobate," *Appl. Opt.* **40**, 6049-6055 (2001).
- [91]. J. Liu, Q. Liu, L. Huang, and M. Gong, "High energy eye-safe and mid-infrared optical parametric oscillator," *Laser Phys. Lett.* **7**, 853-856 (2010).
- [92]. H. Y. Zhu, Y. M. Duan, G. Zhang, C. H. Huang, Y. Wei, W. D. Chen, H. Y. Wang, and G. Qiu, "High-power LD end-pumped intra-cavity Nd:YAlO₃/KTiOAsO₄ optical parametric oscillator emitting at 1562 nm," *Laser Phys. Lett.* **7**, 703-706 (2010).
- [93]. J. W. Liu, C. Q. Gao, L. Wang, L. Zou, and J. Z. Li, "Pulse-series 1.57 μm

- optical parametric oscillator pumped by a Q-switched Nd:YAG Laser with a variable reflectivity mirror,” *Laser Phys.* **20**, 1886-1889 (2010).
- [94]. J. Y. Huang, S. C. Huang, H. L. Chang, K. W. Su, Y. F. Chen, and K.F. Huang, “Passive Q switching of Er-Yb fiber laser with semiconductor saturable absorber,” *Opt. Express* **16**, 3002-3007 (2008).
- [95]. M. M. J. W. van Herpen, S. E. Bisson, and F. J. M. Harren, “Continuous-wave operation of a single-frequency optical parametric oscillator at 4-5 μm based on periodically poled LiNbO₃,” *Opt. Lett.* **28**, 2497-2499 (2003).
- [96]. X.-L. Dong, W.-Y. Yang, B.-G. Sun, J.-F. Yang, B.-T. Zhang, H.-T. Huang, and S.-D. Liu, “Extra-cavity optical parametrical oscillator based on multiple channels periodical poling lithium niobate PPLN,” *Laser Phys.* **20**, 1787-1790 (2010).
- [97]. Z.-Y. Li, H.-T. Huang, J.-L. He, B.-T. Zhang, and J.-L. Xu, “High peak power eye safe intracavity optical parametric oscillator pumped by a diode pumped passively Q-switched Nd:GGG laser,” *Laser Phys.* **20**, 1302-1306 (2010).
- [98] Y. X. Fan, F. Y. Lu, S. L. Hu, K. C. Lu, H. J. Wang, X. Y. Dong, J. L. He, and H. T. Wang, “Tunable high-peak-power, high-energy hybrid Q-switched double-clad fiber laser,” *Opt. Lett.* **29**, 724-726 (2004).
- [99]. M. Laroche, H. Gilles, S. Girard, N. Passilly, and K. Ait-Ameur, “Nanosecond pulse generation in a passively Q-switched Yb-doped fiber laser by Cr⁴⁺:YAG saturable absorber,” *IEEE Photon. Technol. Lett.* **18**, 764-766 (2006).
- [100]. G. J. Edwards and M. Lawrence, “A temperature-dependent dispersion equation for congruently grown lithium niobate,” *Opt. Quantum Electron.* **16**, 373-375 (1984).
- [101]. D. H. Jundt, “Temperature-dependent Sellmeier equation for the index of refraction, n_e , in congruent lithium niobate,” *Opt. Lett.* **22**, 1553-1555 (1997).
- [102]. Y. F. Kong, W. L. Zhang, X. J. Chen, J. J. Xu, and G. Y. Zhang, “OH⁻ absorption spectra of pure lithium niobate crystals,” *J. Phys. Condens. Matter* **11**, 2139-2144 (1999).
- [103]. L. Canioni, M. Bellec, A. Royon, B. Bousquet, and T. Cardinal, “Three-dimensional optical data storage using third-harmonic generation in silver zinc phosphate glass,” *Opt. Lett.* **33**, 360-362 (2008).
- [104]. N. Kramer, M. Niesten, and C. Schönenberger, “Resistless high resolution optical lithography on silicon,” *Appl. Phys. Lett.* **67**, 2989-2991 (1995).
- [105]. R. S. Patel, J. Bovatsek, and A. Tamhankar, “Why pulse duration matters in

- photovoltaics,” *Laser Technik Journal* **7**, 21-24 (2010).
- [106]. A. Tamhankar, and R. S. Patel, “Optimization of UV laser scribing process for light emitting diode sapphire wafers,” *J. Laser Appl.* **23**, 032001 (2011).
- [107]. P. E. Schrader, R. L. Farrow, D. A. V. Kliner, J.-P. Fève and N. Landru, “High-Power fiber amplifier with widely tunable repetition rate, fixed pulse duration, and multiple output wavelengths,” *Opt. Express* **14**, 11528-11538 (2006).
- [108]. J. Saby, B. Cocquelin, A. Meunier, S. Pierrot, P.-J. Devilder, P. Deslandes, and F. Salin, “High average and peak power pulsed fiber lasers at 1030 nm, 515 nm, and 343 nm”, *Proc. SPIE* 7580, (2010).
- [109]. M. Laurila, J. Saby, T. T. Alkeskjold, L. Scolari, B. Cocquelin, F. Salin, J. Broeng, and J. Lægsgaard, “Q-switching and efficient harmonic generation from a single-mode LMA photonic bandgap rod fiber laser,” *Opt. Express* **19**, 10824-10833 (2011).
- [110]. D. A. V. Kliner, F. Di Teodoro, J. P. Koplow, S. W. Moore, and A. V. Smith, “Efficient second, third, fourth, and fifth harmonic generation of a Yb-doped fiber amplifier,” *Opt. Commun.* **210**, 393-398 (2002).
- [111]. C. D. Brooks and F. Di Teodoro, “High peak power operation and harmonic generation of a single-polarization, Yb-doped photonic crystal fiber amplifier,” *Opt. Commun.* **280**, 424-430 (2007).
- [112] W. Z. Zhuang, W. C. Huang, P. Y. Chiang, K. W. Su, K. F. Huang, and Y. F. Chen, “Millijoule-level Yb-doped photonic crystal fiber laser passively Q-switched with AlGaInAs quantum wells,” *Opt. Express* **18**, 27910-27915 (2010).
- [113] H. L. Chang, W. Z. Zhuang, W. C. Huang, J. Y. Huang, K. F. Huang, and Y. F. Chen, “Widely tunable eye-safe laser by a passively Q-switched photonic crystal fiber laser and an external-cavity optical parametric oscillator,” *Laser Phys. Lett.* **8**, 678-683 (2011).
- [114]. Y. J. Huang, Y. P. Huang, P. Y. Chiang, H. C. Liang, K. W. Su, and Y. F. Chen, “High-power passively Q-switched Nd:YVO₄ UV laser at 355 nm,” *Appl. Phys. B* **106**, 893-898 (2012).
- [115]. W. Z. Zhuang, W. C. Huang, C. Y. Cho, Y. P. Huang, J. Y. Huang, and Y. F. Chen, “>100-kW linearly polarized pulse fiber amplifier seeded by a compact efficient passively Q-switched Nd:YVO₄ laser,” *Laser Phys. Lett.* **22**, 1721-1728

Ch3 Pulsed photonic crystal fiber lasers and amplifier

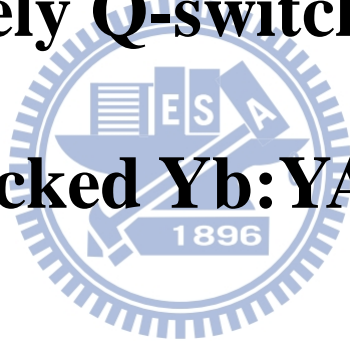
(2012).

- [116]. C. X. Wang, G. Y. Wang, A. V. Hicks, D. R. Dudley, H. Y. Pang, and N. Hodgson, “High power Q-switched TEM₀₀ mode diode-pumped solid state lasers with >30 W output power at 355 nm,” Proc. SPIE 6100, 610019 (2006).
- [117]. P. E. Schrader, R. L. Farrow, D. A. V. Kliner, J.-P. Fève and N. Landru, “High-Power fiber amplifier with widely tunable repetition rate, fixed pulse duration, and multiple output wavelengths,” Opt. Express **14**, 11528-11538 (2006).



Chapter 4

Passively Q-switched and mode-locked Yb:YAG lasers



Motivated by the compactness and simplicity of microchip lasers, many research efforts are directed toward shorter pulses and higher pulse energies either with Q-switched or in mode-locked operations. The diffraction-limited beam quality is ideal for efficiently seedling into large mode area fiber amplifiers. For high peak power Q-switched solid state laser which is advantageous for seed-amplifier applications because no pre-amplification stages are required, it is possible to reduce the Q-switched pulse duration to the sub-nanosecond by shortened cavity length. The promising brightness improvement could be expected by cavity shortening due to high peak power with a single transverse mode. However, in general, solid state lasers have advantages in pulse generation with a few tens of ns pulse widths by Q-switching, and ultrashort pulse generation by mode locking with ps to fs pulse widths as depicted in Fig. 4.1. Thus, it is attractive to generating high energy Q-switched laser pulses with pulse width of a few of ps by microchip lasers. Here, I demonstrate passively Q-switched microchip Yb:YAG laser by using Cr⁴⁺:YAG as the saturable absorber. Besides, high repetition rate mode-locked operations were also demonstrated employing the same gain chip. Self-mode locking pulses were generated with pulse repetition rate up to 240 GHz by etalon effect of the gain chip. Furthermore, using a semiconductor saturable absorber mirror as the output coupler, dual-wavelength operation was attained with modulation frequency of approximately 5 THz by optical beating.

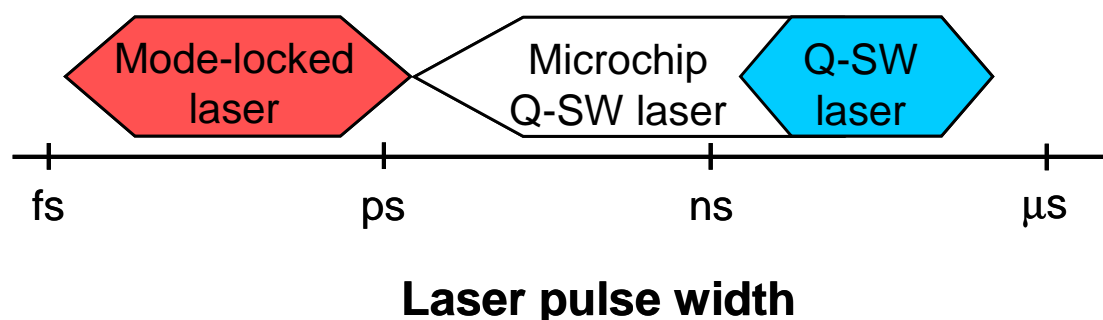


Fig. 4.1 Pulse width region for different pulsed lasers.

4.1 Passively Q-switched with Cr⁴⁺:YAG crystal

High-energy, compact diode-pumped passively Q-switched (PQS) solid state lasers with subnanosecond pulses have a variety of applications such as nonlinear frequency conversion, industrial processing, and remote sensing. Since Cr⁴⁺:YAG crystals possess high damage thresholds and high optical and thermal stabilities, they have been extensively applied as saturable absorbers in PQS laser systems such as Nd³⁺-doped lasers [1-3] and Yb³⁺-doped lasers [4–6]. Comparing with Nd:YAG crystals, Yb:YAG crystals have longer fluorescence lifetimes [7], smaller emission cross sections [8], low quantum defects, and broad absorption bandwidths [8]. Therefore, the Yb:YAG microchips have been employed to construct highpulse-energy light sources with stability, compactness, and reliability [9–11]. The scaling of power and energy in Yb:YAG lasers are strongly impeded by the thermal effect because the quasi-three-level property of the Yb:YAG crystal causes the population on the lower level to significantly increase with rising temperatures. Therefore, efficient thermal management is highly desirable for enhancing the output performance of Yb:YAG PQS lasers. Recently, it has been demonstrated that the synthetic diamond is a promising heat spreader for thermal management in semiconductor disk lasers [12] and Nd-doped vanadate lasers [13–15] due to its excellent optical and mechanical properties together with high thermal conductivity. In addition, cooling along the direction of pumping is practically useful for reducing the thermal lensing and stress in microchip lasers [16, 17]. Even so, the feasibility of cooling Yb:YAG microchip PQS lasers with diamond heat spreaders has never been explored thus far.

In this work, we explore the performance improvement of diode-end-pumped PQS Yb:YAG lasers with diamond windows as surface heat spreaders. Comparing with the results obtained without the diamond heat spreader, the pulse energy obtained with the diamond cooling is found to be enhanced by 1.5 times, where a Cr⁴⁺:YAG absorber with the initial transmission of 84% is used. Furthermore, the standard deviation of the pulse amplitude peakto- peak fluctuation is approximately 3 times lower than that obtained without the diamond heat spreader. Under a pump power of 3.9 W, the passively Q-switched Yb:YAG laser can generate a pulse train of 3.3 kHz

repetition rate with a pulse energy of 287 μJ and with a pulse width of 650 ps. More importantly, the optical-to-optical efficiencies are improved up to 58% and 25% for the continuous-wave (CW) and PQS operations, respectively.

(A) Experimental setup

Figure 4.2 presents the schematic experimental setup. The gain medium was a 1-mm-long, 4 mm in diameter, and 11 at.% doped Yb:YAG crystal. One of the end facet of the crystal was coated with highly reflectivity (HR, $R > 98\%$) at 1030 nm and high-transmission (HT, $T > 95\%$) at 970 nm served as the front mirror, the other facet was with high-transmission (HT, $T > 95\%$) at 1030 nm and highly reflectivity (HR, $R > 95\%$) at 970 nm to increase the absorption efficiency of the pump power. The Cr^{4+} :YAG crystal with initial transmission (T_0) of 84% and 1.4 mm in length was used as the saturable absorber. Both end facets of the Cr^{4+} :YAG crystal were anti-reflection coated (AR, $R < 0.2\%$) at 1030 nm. The output coupler was a flat mirror with partially reflection at 1030 nm ($R = 30\%$). The total cavity length was about 8.4 mm. The uncoated, single crystal synthetic diamond of 4.5 mm square and 0.5 mm thickness was used as the heat spreader and bounded to the front mirror side of the gain medium. The diamond plate was polished to laser quality with flatness of $\lambda/8$ at 632.8 nm and roughness of R_a smaller than 30 nm. The other side of the diamond was in contact with a copper heat sink cooled by a thermal-electric cooler at the temperature of 16°C . The side of the Yb:YAG crystal with the coating of HT at 1030 nm and HR at 970 nm was attached tightly to a copper plate with a hole of 2-mm diameter, where an indium foil was used to be the contact interface. The contact uniformity of the bounded interface between the diamond and the Yb:YAG crystal was further confirmed by means of inspecting the interference fringe resulting from the minute gap between the diamond heat spreader and the gain medium. The birefringence of the single crystal diamond was smaller than 5×10^{-4} . The transmittance of the diamond heat spreader was about 70% at 970 nm owing to the high refractive index contrasts of the air/diamond and diamond/Yb:YAG interfaces (The refractive index of the single crystal diamond is 2.432). The Cr^{4+} :YAG crystal was wrapped within indium foil and mounted in a copper heat sink cooled by water at the temperature of 16°C . The pump source was an 8-W 970-nm fiber-coupled laser diode with a core diameter of 200 μm and a numerical aperture of 0.20. Focusing lens with 25 mm focal length and 87%

coupling efficiency is used to reimaging the pump beam into the laser crystal. The pump diameter is approximately 120 μm . Considering the coupling efficiency of the focusing lens, the transmittance of the diamond, and the effective absorption of the gain medium, the maximum available absorbed pump power is found to be 3.9 W. Note that without using the diamond heat spreader the maximum available absorbed pump power can be up to 5.6 W. The laser spectrum was measured by an optical spectrum analyzer with 0.1 nm resolution (Advantest Q8381A). The pulse temporal behavior was recorded by Agilent digital oscilloscope (infiniium DSO81204B; 40G samples/sec; 12 GHz bandwidth) with a fast InGaAs photodiode of 12.5 GHz bandwidth.

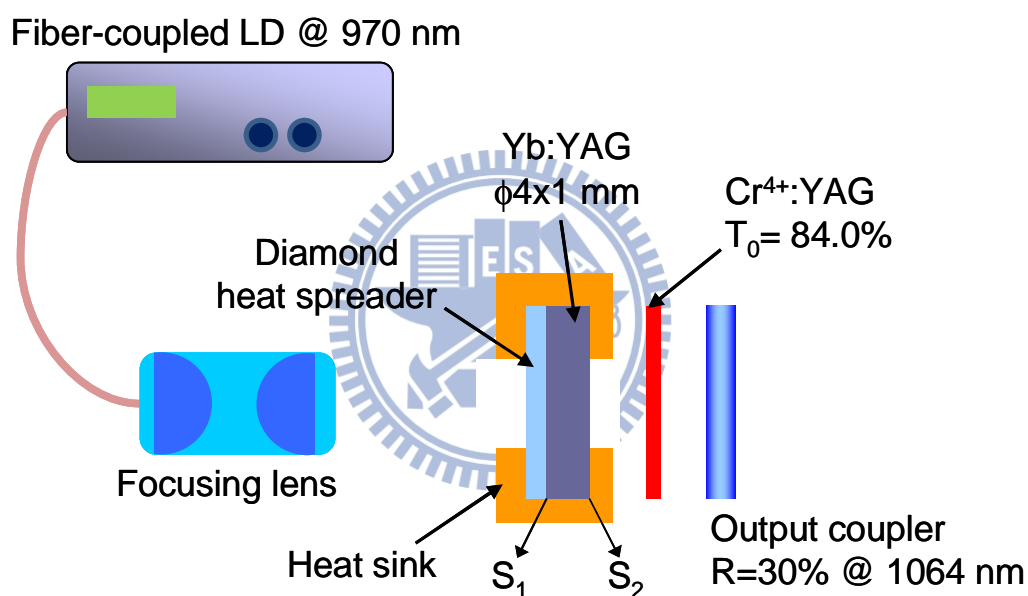


Fig. 4.2 The schematic diagram of the PQS Yb:YAG/Cr⁴⁺:YAG laser experimental setup. (S1: HT at 970 nm, HR at 1030 nm; S2: HT at 1030 nm, HR at 970 nm; HT: high transmission; HR: high reflection).

(B) Experimental results and discussion

We firstly investigate the performance of the Yb:YAG laser with the diamond heat spreader under CW operation without the Cr⁴⁺:YAG crystal in place. Here, we use the output coupler with reflectivity of 80% at 1030 nm to maximize the output power around the wavelength of 1031 nm under CW operation. Figure 4.3 shows the average power with and without the diamond heat spreader with respect to the absorbed pump

power. Without the diamond heat spreader, the output power was 1.3 W under an absorbed pump power of 3.9 W which corresponds to the optical-to-optical efficiency of 33% and the slope efficiency of 50%. The output power started to saturate and the slope efficiency decreased to 17% for an absorbed pump power of 5.6 W. The thermal effects induced power degradation has been widely observed in Yb-doped lasers [18–21] and has been theoretically confirmed [22]. Increasing the pump power, the detrimental effects in the Yb:YAG crystal become more severe including the decrease of the thermal conductivity [22] and the increase of the thermal expansion coefficient [23]. Furthermore, the absorption cross section and the emission cross section of the transitions between the manifolds $^2F_{5/2}$ and $^2F_{7/2}$ in the Yb:YAG crystal are significantly decreased with the increased temperature [24, 25] which lead to the reduction of the laser efficiency [16]. In contrast, the maximum output power was enhanced to 2.25 W under the pump power of 3.9 W when a diamond heat spreader was employed for surface cooling. The optical-to-optical efficiency and the slope efficiency were up to 58% and 86%, respectively.

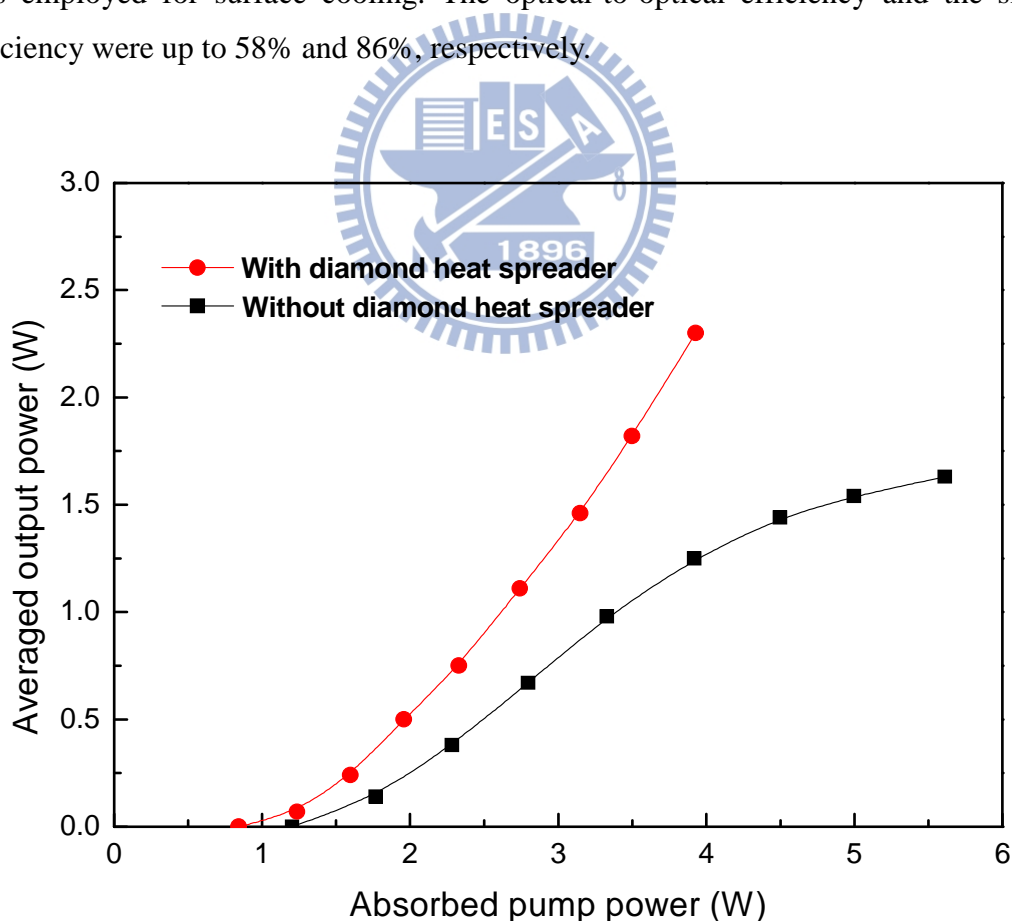


Fig. 4.3 Dependence of the averaged output power on the absorbed pump power under the CW operation.

Under the PQS operation, we change the reflectivity of the output coupler to be 30% at 1030 nm to prevent coating damages of the crystals due to the high intracavity intensity which have been observed in PQS Yb:YAG/Cr⁴⁺:YAG lasers [11]. Figure 4.4(a) depicts the averaged output power versus absorbed pump power under the PQS operation. Without the diamond heat spreader, the maximum output power was found to be limited at 0.47 W under the absorbed pump power of 5.6 W. Like the CW operation, the averaged output power without diamond cooling began to saturate when the absorbed pump power was greater than 4.5 W. On the contrary, the average output power with diamond cooling was 0.96 W at an absorbed pump power of 3.9 W, corresponding to the optical efficiency of 25% and the slope efficiency of 60%. Lower temperature in the Yb:YAG crystal can achieve lower threshold pump power [26] and higher optical efficiency [27] in Yb:YAG lasers. The lower threshold pump power (2.3 W for with diamond heat spreader and 2.8 W for without diamond heat spreader) and higher optical efficiency (25% for with diamond heat spreader and 8.3% for without diamond heat spreader) attained in our results show the effective thermal management of the diamond heat spreader. In comparison with the earlier results such as the self-Q-switched laser that uses composite Yb:YAG/Cr⁴⁺:YAG ceramics [9] and the mechanical contacted Yb:YAG/Cr⁴⁺:YAG microchip lasers that adopt ceramics [10] or crystals [11], the diamond cooling scheme is confirmed to enhance the performance significantly.

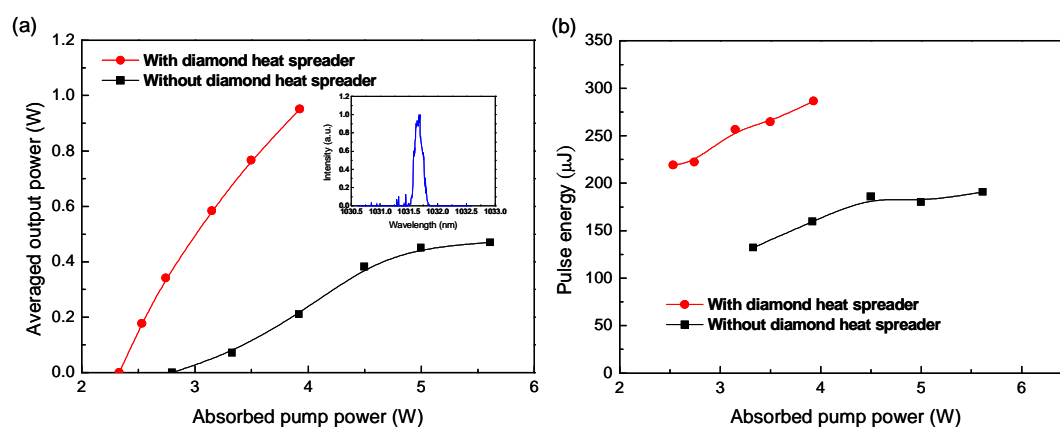


Fig. 4.4 (a) Dependence of the averaged output power on the absorbed pump power under the PQS operation, the inset: typical lasing spectrum. (b) Dependence of the pulse energy on the absorbed pump power.

The lasing spectra for CW and PQS operations with the diamond heat spreader were quite similar with the peaks near 1031.7 nm and bandwidths to be approximately 0.2 nm, as shown in the inset of Fig. 4.4(a).

Figure 4.4(b) shows the pulse energies obtained with and without the diamond heat spreader with respect to the absorbed pump power. It can be seen that the maximum pulse energies obtained without and with diamond cooling are approximately 190 μJ and 287 μJ , respectively. The Yb:YAG crystal, as a quasi-three-level laser gain medium, certainly suffers from the increase of the fractional thermal population on the lower laser level and the decrease of the fractional population on the upper laser level which decrease the maximum stored energy in the Yb:YAG crystal [28] for increasing the pump power. Furthermore, the strong thermal lensing in the end-pumped Yb:YAG microchip laser which results from the thermal gradients within the gain medium [17] usually leads to a smaller cavity mode size that will reduce the output pulse energy [29]. Millar et al. [15] and our previous results [30] in semiconductor disk lasers which use diamond heat spreader for thermal management of the gain medium have evidence its effectualness. Smaller red-shift in wavelength when the diamond heat spreader was in place [15, 30] confirms that the gain medium heating to be considerably improved by using the diamond heat spreader. By using the same diamond heat spreader and the same bounding method of the diamond/gain medium composite as in this experiment, our previous result [30] shows that the gain medium temperature rise per unit pump power ($\Delta T/\Delta P$) are 20.5 K/W and 3.3 K/W for without and with the diamond heat spreader. The temperature rise in the diamond-gain medium composite is 6.2 times lower than in the gain medium without a diamond heat spreader, emphasizing the efficiency of the diamond heat spreader for thermal management. Besides, Millar et al. [15] theoretically simulates that using the diamond heat spreader can effectively reduce the maximum temperature rise together with temperature gradients and decrease the thermal stress and distortion in Yb:YAG lasers. Our experimental results confirm that diamond cooling is truly an efficient thermal management for the Yb:YAG microchip laser to enhance the output performance. To the best of our knowledge, this is the highest pulse energy obtained with Yb:YAG/Cr⁴⁺:YAG microchip laser. The overall pulse energy scaling was 1.9 times as high as the one in Ref [9], 5.7 times as that in Ref [10], and 22 times as that in Ref [11]. The diamond heat spreader not only reduces the maximum temperature rise in the gain medium to enhance the laser efficiency but

also decreases the thermal-induced bending and bowing of the gain medium to improve the beam distortion [15, 16]. Furthermore, bounding the diamond heat spreader to the pumped side of the gain medium makes the temperature distribution more uniform [16] that reduces the thermal lens in the Yb:YAG crystal and prevents the cavity mode size from shrinking as the result of the thermal lens effect [31, 32].

Figures 4.5(a) and 4.5(b) show the oscilloscope traces obtained with and without diamond cooling, respectively, for the single pulse of the PQS Yb:YAG/Cr⁴⁺:YAG laser at the maximum absorbed pump powers. The pulse widths can be seen to be 650 ps and 764 ps for the operations with and without diamond cooling, respectively. With the pulse energy shown in Fig. 4.3(b), the peak powers obtained with and without diamond cooling can be calculated to be 442 kW and 262 kW, respectively. In other words, diamond cooling enhances the peak power by a factor of 1.7 times.

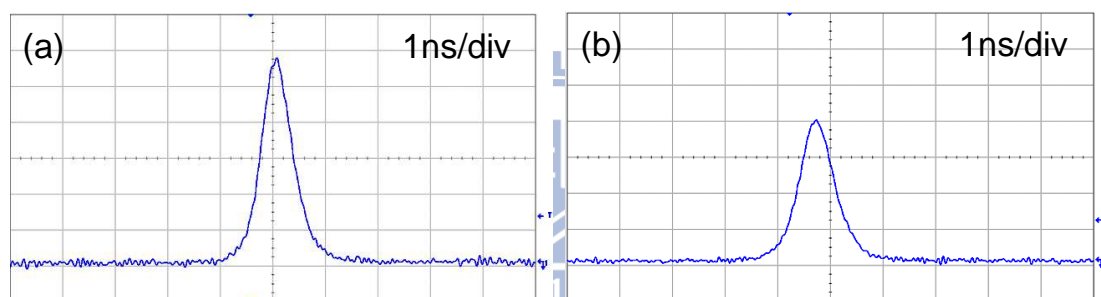


Fig. 4.5 Oscilloscope traces of a single pulse of the output pulse of (a) with the diamond heat spreader, (b) without the diamond heat spreader.

Zayhowski et al. demonstrated PQS microchip lasers constructed of diffusion-bounded Nd:YAG/Cr⁴⁺:YAG crystals [33–35]. By optically bounding a 4-mm-long Nd:YAG crystal doped with 1.1 at.% Nd³⁺ ions and a 2.25-mm-thick Cr⁴⁺:YAG, laser pulses with pulse energy of 250 μJ and pulse width of 380 ps at the pulse repetition rate of 1 kHz were obtained under 15 W of pump power, the corresponding peak power of 565 kW was attained. Compared to our result of Yb:YAG/Cr⁴⁺:YAG laser, although the pulse width achieved by Nd:YAG/Cr⁴⁺:YAG laser was shorter than ours owing to the shorter laser resonator, the optical-to-optical efficiency was less than 2% which was much inferior to ours of 25%. Besides, the Nd:YAG/Cr⁴⁺:YAG laser can only be pulse pumped which limited the pulse repetition rate to be merely up to 1 kHz as the result of the thermal effects. At higher repetition rates, the pulse energy of the Nd:YAG/Cr⁴⁺:YAG laser decreased due

to the cavity mode shrinking induced by the thermal lens effect. The output pulses start to bifurcate with varied pulse amplitudes in different longitudinal and polarization modes when the laser was CW pumped [33]. Our results provide the solution for improved thermal management by using a diamond heat spreader in the Yb:YAG/Cr⁴⁺:YAG laser, nevertheless, this method also can be expected to be useful in the Nd:YAG/Cr⁴⁺:YAG system. Figures 4.6(a) and 4.6(b) depict the typical oscilloscope traces measured with and without the diamond heat spreader, respectively, for the Q-switched pulse trains at the maximum absorbed pump powers. The standard deviations of the pulse amplitude peak-to-peak fluctuations are analyzed to be approximately 3% and 9% for the operations with and without the diamond heat spreader, respectively. The pulse amplitude fluctuation with the heat spreader is also superior to the earlier results such as 6% in Ref [9], and 8% in Ref [10], demonstrating an effective improvement in the PQS stability.

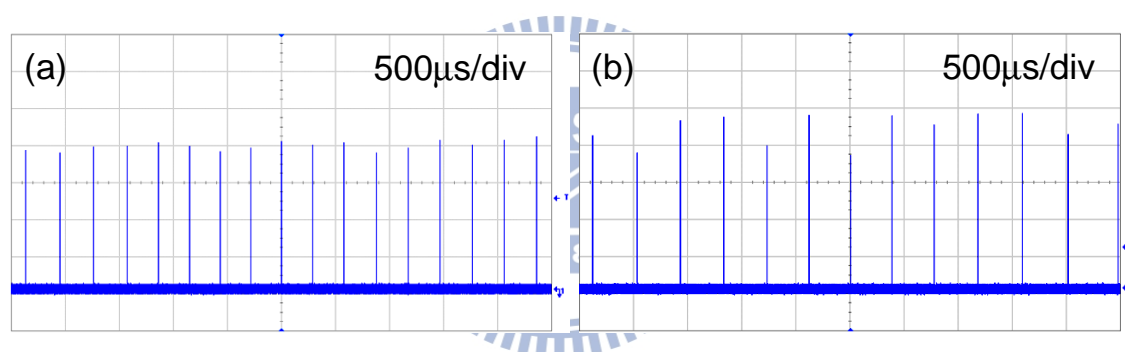


Fig. 4.6 Oscilloscope traces of a train of output pulses of (a) with the diamond heat spreader, (b) without the diamond heat spreader.

(C) Conclusions

I have experimentally confirmed that employing diamond windows as surface heat spreaders can remarkably improve the performance of diode-end-pumped PQS Yb:YAG lasers. The pulse energy obtained with the diamond cooling was found to be 1.5 times higher than that obtained without the diamond heat spreader, where a Cr⁴⁺:YAG absorber with the initial transmission of 84% was employed in experiment. Under a pump power of 3.9 W, a pulse train of 3.3 kHz repetition rate could be efficiently generated from the passively Qswitched Yb:YAG laser with a pulse energy of 287 μ J and with a pulse width of 650 ps. In addition, the optical-to-optical efficiencies were found to be improved up to 58% and 25% for the CW and PQS

Ch4 Passively Q-switched and mode-locked Yb:YAG lasers

operations, respectively. The standard deviations of the pulse amplitude peak-to-peak fluctuations were measured to be approximately 3% and 9% for the operations with and without the diamond heat spreader, respectively. This result indicates that the amplitude fluctuation obtained with diamond cooling was approximately 3 times lower than that obtained without diamond cooling.



4.2 Self-mode-locked operation

Pulsed lasers with repetition rates higher than 10 GHz attract noticeable interest for applications such as in wireless communication [36], telecommunication [37], quantum communication [38], high signal-to-noise ratio measurements [39], photonic switching [40], and large-mode-spacing supercontinuum generation [41]. The methods for achieving such high-repetition-rate light sources include harmonically mode-locked fiber lasers [42, 43], quantum-well Fabry–Perot lasers [44], quantum-dash-based Fabry–Perot mode-locked lasers [145], passively harmonically mode-locked vertical-external-cavity surface-emitting lasers [46, 47], and passively mode-locked solid-state lasers [48, 49]. Among solid-state gain media, diode-pumped ytterbium (Yb) doped lasers have been identified as excellent systems for compact efficient femtosecond light sources because Yb-doped materials have small quantum defects and high quantum efficiencies. Recently, Kerr-lens mode-locking experiments have been demonstrated for the Yb-doped gain media including Yb:KY(WO₄)₂ [50], Yb:YVO₄ [51], Yb:Y₂O₃ [52], and Yb:YAG [53] crystals. However, so far the pulse repetition rates never exceed 1 GHz in the Kerr-lens mode-locked Yb-doped lasers. More recently, self-mode-locked operation with a linear cavity has also been observed in numerous end-pumped solid-state and semiconductor lasers [54-57]. The physical mechanism is speculated to be associated with the combined effects of the Kerr-lensing and thermal lensing [52-57]. The feasibility of compact linear cavities paves the way for the development of mode-locked lasers with ultra-high repetition rates.

In this part, I demonstrate a high-power subpicosecond harmonically mode-locked laser with sub-terahertz pulse repetitions by means of a specially coated Yb:YAG microchip in a linear Fabry–Perot cavity. The front surface of the gain medium is coated to form a cavity mirror and is bonded with a diamond heat spreader to significantly enhance the output performance. The rear surface of the Yb:YAG plate is coated not only to lead to a second pass of the pump light but also to act as an etalon for achieving harmonic mode locking. I also confirm that the diamond heat spreader can enhance the output performance of the Yb:YAG microchip laser. Experimental

results reveal that when the optical length of the laser cavity is close to a commensurate ratio of the optical length of the Yb:YAG plate, the laser output displays a single-pulse harmonic mode locking. The pulse repetition rate is found to be a multiple of the free spectral range caused by the etalon effect of the Yb:YAG plate, ranging from 80 to 240 GHz. Under the absorbed pump power of 8.3 W, an average output power of 4.6 W is achieved with a pulse duration of 630 fs and repetition rate of 240 GHz, corresponding to an optical efficiency of 55.4%.

(A) Experimental setup

Figure 4.7 shows the schematic diagram for the experimental setup of harmonically self-mode-locked Yb:YAG lasers formed by a Fabry–Perot flat–flat cavity. The gain medium is an 11 at.% Yb:YAG crystal with a length of 1.03 mm and a diameter of 4.0 mm. The Yb:YAG crystal is cut along the [111] direction. The front surface of the Yb:YAG plate is coated to form a cavity mirror with high transmission ($T > 95\%$) at the wavelength 970 nm of pump light and with high reflection ($R > 99.8\%$) for the lasing wavelength of 1030–1060 nm. The rear surface of the Yb:YAG crystal is coated for high reflection ($R > 95\%$) at 970 nm to lead to a second pass of the pump light and for high transmission ($T \approx 95\%$) for the lasing wavelength. The double-pass absorption of the gain medium is measured to be approximately 83%. Note that the partial reflection ($R \approx 5\%$) on the rear surface for the lasing wavelength is employed to act as an etalon for achieving harmonic mode locking. A 4.5 mm square, 0.5 mm thick piece of uncoated single crystal diamond heat spreader was bonded to the front surface of the gain medium to improve the heat removal [12, 58–59]. The transmittance of the diamond heat spreader is approximately 70% at 970 nm. The front surface of the diamond is in contact with a copper heat sink which is cooled by a thermal-electric cooler (TEC), where the temperature was maintained at 15°C. The rear surface of the gain medium is attached tightly to a copper plate with a hole of 2 mm diameter, where an indium foil is employed to be the contact interface. The contact uniformity is further confirmed by inspecting the interference fringe coming from the minute gap between the gain chip and the diamond heat spreader. A flat wedged output coupler with 7% transmission at 1040 nm is used in the experiment. The pump source is a 16W 970 nm fiber-coupled laser diode with a core diameter of 200 μm and numerical aperture of 0.20. A focusing lens with 25 mm focal length and

87% coupling efficiency is used to reimagine the pump beam into the laser crystal. The average pump diameter is approximately 130 μm . Considering the coupling efficiency of the focusing lens, the transmittance of the diamond, and the effective absorption of the gain medium, the maximum available absorbed pump power is found to be 8.3 W. Note that without using the diamond heat spreader the maximum available absorbed pump power can be up to 11 W.

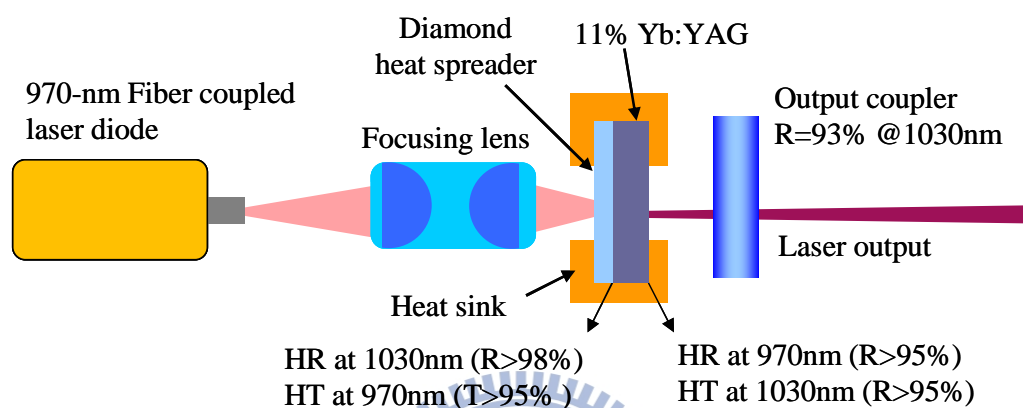


Fig. 4.7 Schematic diagram for the experimental setup of harmonically self-mode-locked Yb:YAG lasers formed by a Fabry-Perot flat-flat cavity.

First of all, we investigate the stable region of the optical cavity length L_{cav} at the maximum absorbed pump power of 8.3 W. The output power is found to be nearly the same for $L_{\text{cav}} < 9.0$ mm. On the other hand, the output power obviously starts to decrease with increasing the cavity length for $L_{\text{cav}} > 10.0$ mm because of the thermal lensing effect. Figure 4.8 shows the output power versus absorbed pump power for the laser schemes without and with using the diamond heat spreader at a cavity length of 5.0 mm. It can be seen that the diamond heat spreader significantly improves the slope efficiency to enhance the maximum output power up to 4.6W. Since the diamond effectively reduces the thermal effect, the overall beam quality M^2 is found to be better than 1.3 for all the pump powers.

I exploit the schemes of first- and second-order autocorrelations to analyze the temporal behavior of the laser output. The first-order autocorrelation trace is performed with a Michelson interferometer (Advantest, Q8347) that is also capable of performing optical spectral analysis by Fourier transforming the first-order field autocorrelation. The second-order autocorrelation trace is performed with a commercial autocorrelator (APE pulse check, Angewandte Physik & Elektronik

GmbH). For most cavity lengths between 4.0 and 9.0 mm, we experimentally find that the laser output displays a state of multiple-pulse mode locking with a repetition rate that is a multiple of ~ 80 GHz. The frequency of 80 GHz can be confirmed to come from the free spectral range of the etalon effect caused by the Yb:YAG crystal with an optical length of $L_{\text{cry}} \approx 1.87$ mm. Figures 4.9(a) and (b) depict the experimental traces of first- and second-order autocorrelations for the operation of a multiple-pulse mode locking obtained at a cavity length of 6.08 mm. It can be seen that the pulse separation and the temporal structure are almost the same as for the results obtained with the first- and second-order autocorrelation traces. The great resemblance between the first- and second-order autocorrelation traces implies that the phase of the optical spectrum is nearly constant [60].

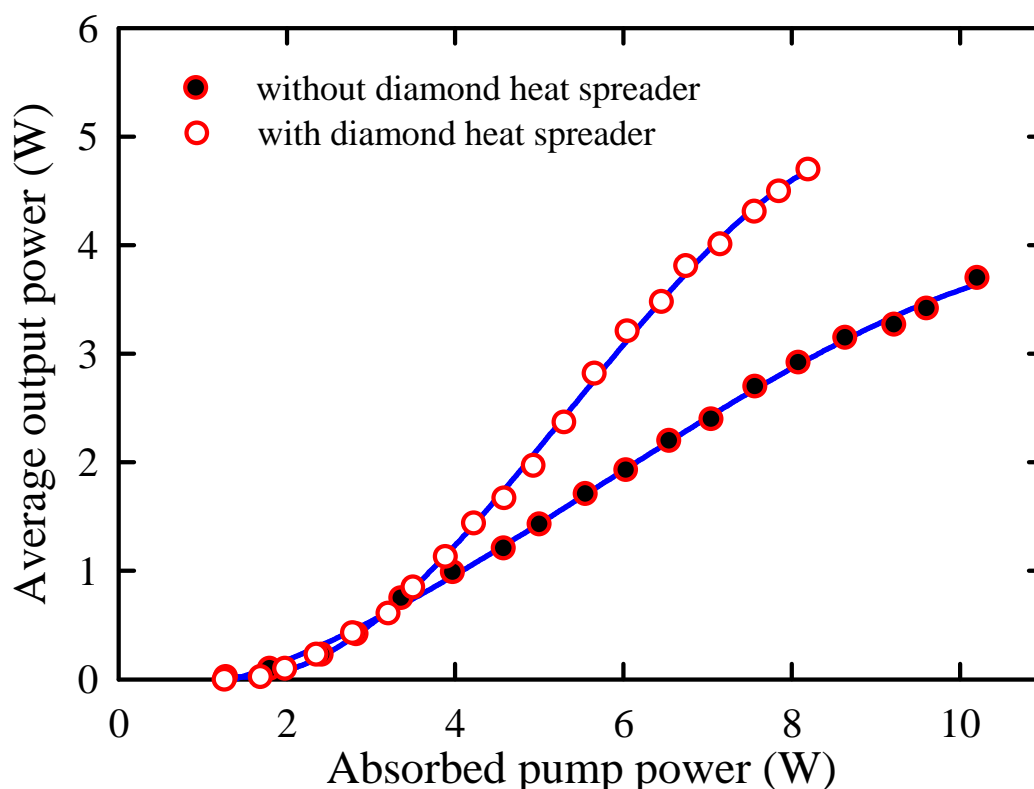


Fig. 4.8 Output power versus absorbed pump power for the laser schemes without and with using the diamond heat spreader at a cavity length of $L_{\text{cav}} = 5.0$ mm. Note that the output characteristics are almost the same for $L_{\text{cav}} < 9.0$ mm.

(B) Experimental results

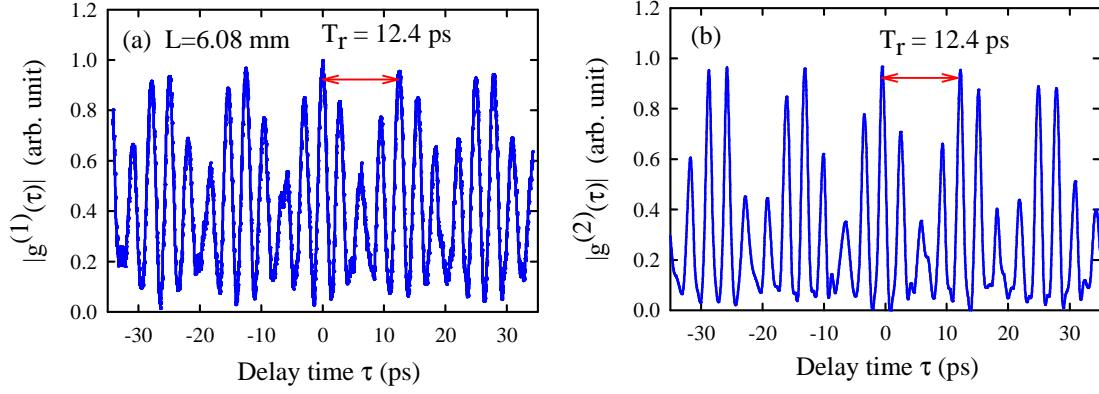


Fig. 4.9 Experimental traces of (a) first- and (b) second-order autocorrelations for the operation of a multiple-pulse mode locking obtained at a cavity length of 6.08 mm.

By scanning all the optical cavity lengths, we experimentally find that when the optical cavity length L_{cav} is adjusted to be close to a commensurate ratio of the crystal length L_{cry} , the single-pulse harmonically mode-locked operation can be achieved. Figures 4.10(a)-(c) show the experimental results of the second-order autocorrelation at the maximum output power of 4.6 W for three cases of single-pulse harmonic mode locking observed at the cavity lengths of 5.47, 6.54, and 6.91 mm, respectively. The pulse repetition rates can be seen to be approximately 80, 160, and 240 GHz for the operations shown in figure 4.10(a)-(c). The free spectral ranges of the laser cavities are 27.7, 23.1, and 21.9 GHz for the cavity lengths of 5.47, 6.54, and 6.91 mm. With these free spectral ranges, we can deduce that the operations of harmonic mode locking in figures 4.10(a)-(c) are third, seventh, and 11th orders, respectively. The ratios $L_{\text{cry}}/L_{\text{cav}}$ for the cases shown in figures 4.10(a)-(c) are indeed quite close to the fractional numbers $1/3$, $2/7$, and $3/11$, respectively. Figures 4.10(a')-(c') depict the full width at half maximum (FWHM) widths of the central peaks of the second-order autocorrelation traces shown in figures 4.10(a)-(c), respectively. Assuming the temporal intensity to be a sech^2 profile, the pulse durations can be found to be 2.17, 0.57, and 0.63 ps for the cases shown in figure 4.10(a')-(c'). To further validate the quality of harmonic mode locking, we also employ the digital oscilloscope for the real-time trace and RF power spectrum analyzer with the bandwidth limit of the instrument up to 10 GHz. We also do not observe any sign of Q-switched modelocking in either autocorrelation or the RF spectrum.

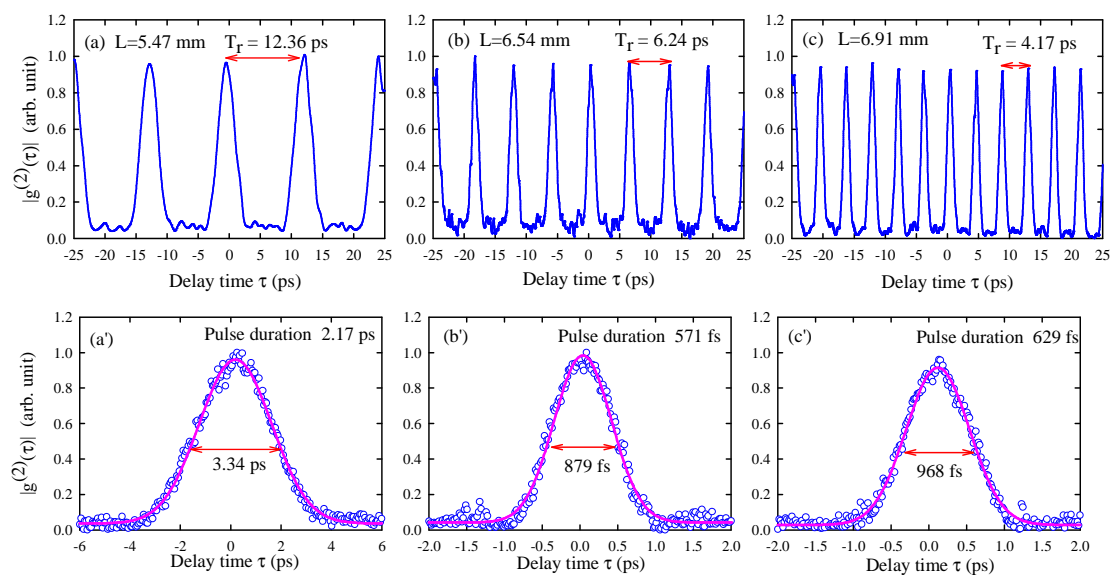


Fig. 4.10 (a)-(c) Experimental results of the second-order autocorrelation at the maximum output power of 4.6 W for three cases of single-pulse harmonic mode locking observed at the cavity lengths of 5.47, 6.54, and 6.91 mm, respectively. (a')-(c') FWHM widths of the central peaks of the second-order autocorrelation shown in (a)–(c), respectively.

Figures 4.11(a)-(c) show the measured results of the first-order autocorrelation corresponding to the cases shown in figures 4.10(a)-(c). Similar to the result shown in figure 4.9, the pulse separation and the temporal structure obtained with the first-order autocorrelation traces are nearly the same as the results obtained with the second-order scheme. Figures 4.11(a')-(c') depict the optical spectra derived from the experimental first-order autocorrelation traces shown in figures 4.11(a)-(c), respectively. It can be seen that the numbers of principal lasing modes are approximately four-five. The values of the mode spacing for all cases are consistent with the pulse repetition rates shown in figures 4.10(a)-(c).

(C) Conclusion

In conclusion, we have demonstrated the experimental observation of high-power self-mode-locked operation in a diode-pumped Yb:YAG microchip laser with a pulse repetition rate of up to 240 GHz. The front surface of the gain medium is coated to form a cavity mirror and its rear surface is coated to lead to a second pass of the pump light and to act as an etalon for achieving harmonic mode locking. A diamond heat

spreader is employed to reduce the thermal effects for power scale-up. It is experimentally found that the single-pulse harmonically mode-locked operation can be acquired by adjusting the optical lengths of the laser cavity to be close to a commensurate ratio of the optical length of the Yb:YAG plate. At an absorbed pump power of 8.3 W, an average output power of 4.6 W is achieved with a pulse duration of 630 fs and a repetition rate of 240 GHz.

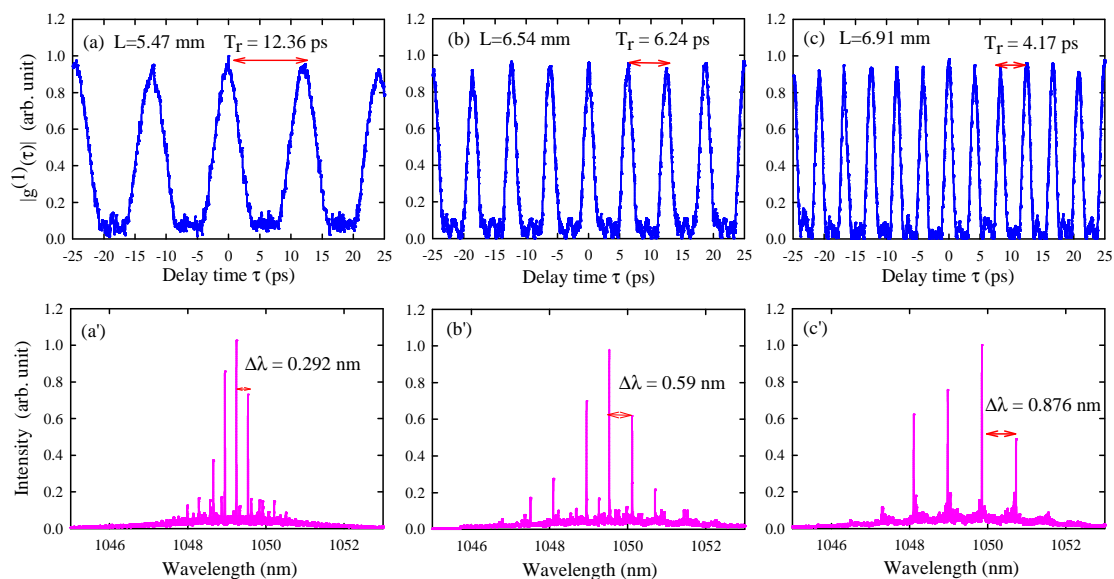


Fig. 4.11 (a)-(c) Experimental results of the first-order autocorrelation traces corresponding to the results shown in figures 4(a)–(c), respectively. (a')-(c') Optical spectra corresponding to the first-order autocorrelation traces shown in (a)–(c), respectively.

4.3 Dual-wavelength mode-locked operation

Ultrashort pulse lasers with terahertz (THz) beat frequency have become more and more important to wide applications such as medical imaging [61], plasma physics [62], quantum communication [63], optical sampling [64], and astrophysics [65]. Dual-wavelength synchronously mode-locked lasers [66-68] have been extensively used to generate the ultrashort optical pulse train with THz beat frequency. The demonstrations for dual-wavelength synchronous mode locking include Ti:sapphire lasers [68-75], semiconductor lasers [66], and rare-earth doped solid state lasers such as Nd-doped disordered crystal lasers [67, 76-79] and Yb:LYSO laser [80].

Among rare-earth doped crystals, the Yb:YAG crystal has been identified to be a promising material for generating compact efficient ultrashort laser pulses [81-86] owing mainly to the small quantum defect, broad absorption and fluorescence spectra, and high quantum efficiency. A dual-wavelength mode-locked Yb:YAG ceramic laser at 1033.6 nm and 1047.6 nm was recently demonstrated in single cavity [85]. However, since the optical paths of the dual-wavelength modes were spatially separate in the laser cavity, there was no observation of ultrashort pulse train with THz beat frequency. Besides, the low optical-to-optical conversion efficiency leads to the average output power to be only 8 mW. Therefore, it is highly desirable and practically useful to develop a high-power dual-wavelength synchronously mode-locked Yb:YAG laser for generating ultrashort pulses with THz beat frequency.

The spontaneous emission spectrum of the Yb:YAG crystal reveals that there are two main peaks under the optical excitation at 940 nm [87]: the primary and secondary peaks are located around 1032 nm and 1049 nm, respectively. One of the key issues for achieving dual-wavelength operation in a Yb:YAG laser is to precisely control the gain-to-losses ratios at 1032 nm and 1049 nm [88-89]. On the other hand, the synchronization of dual-wavelength mode-locked beams is indispensable for generating an ultrashort pulse train with THz beat frequency. It has been shown that the cross saturation of the saturable absorber is beneficial to the synchronization of dual-wavelength mode-locked beams [67, 76]. In this work, we design a semiconductor saturable absorber mirror (SESAM) not only to assist the synchronous

mode locking but also to balance the output coupling for achieving dual-wavelength operation at 1032 nm and 1049 nm. With the fabricated SESAM, we successfully develop a high-power dual-wavelength harmonically mode-locked Yb:YAG laser to generate a pulse train with a pulse duration of 1.54 ps at a repetition rate of 80.3 GHz. A diamond heat spreader is employed to enhance the heat removal efficiency of the Yb:YAG medium for scaling up the output power [83, 86]. The maximum average output power can be up to 1.1 W under the absorbed pump power of 5.18 W, corresponding to the optical-to-optical conversion efficiency of 21.2% and slope efficiency of 29.4%. The autocorrelation traces display a profound modulation with the period corresponding to the beat frequency of 4.92 THz. Since the overall modulation depth is greater than 80%, the effective pulse duration within the mode-locked pulse is as short as 83 fs.

(A) Experimental setup

Figure 4.12 presents the schematic of the experimental setup. The gain medium was an 11 at.% doped Yb:YAG crystal cut along the [111] direction with 1.03 mm in length and 4 mm in diameter. One of the end facet of the crystal was coated for high reflection (HR, $R > 99.8\%$) from 1030 nm to 1100 nm and high transmission (HT, $T > 95\%$) at 940 nm served as the front mirror. The rear facet was coated for high reflection (HR, $R > 99\%$) at 940 nm to increase the absorption efficiency of the pump power and with high-transmission (HT, $T \approx 95\%$) from 1030 nm to 1100 nm. It has been confirmed [83] that the partial reflection ($R \approx 5\%$) on the rear facet for the lasing spectral range can introduce a significant etalon effect to achieve the harmonic mode locking. The uncoated, single crystal synthetic diamond of 4.5 mm square and 0.5 mm thickness was used as a heat spreader and capillary bounded to the front mirror side of the gain medium as described in Ref. [83, 86]. The transmittance of the diamond heat spreader was about 70% at 940 nm. The front facet of the diamond was in contact with a copper heat sink which is cooled by a thermal-electric cooler (TEC) and maintained at a temperature of 14°C. The rear facet of the gain medium was tightly attached to a copper plate with a hole of 2 mm in diameter, where an indium foil was used to improve the thermal contact. The pumping source was a 940-nm fiber-coupled laser diode with a core diameter of 400 μm and a numerical aperture of 0.2. The focusing lens with 25 mm focal length and 90% coupling efficiency was used to

re-image the pump beam into the laser crystal. The pump spot radius was approximately 220 μm .

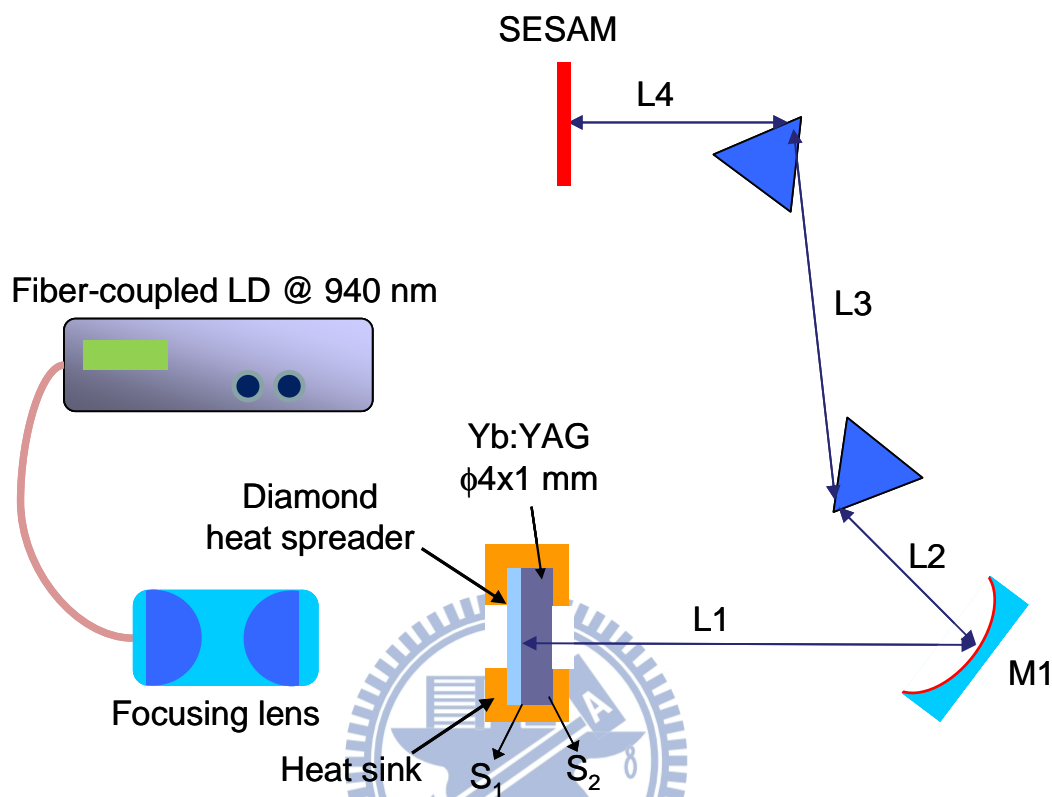


Fig. 4.12 The schematic diagram of the mode-locked Yb:YAG laser experimental setup. (S_1 : HT at 940 nm, HR at 1030~1100 nm; S_2 : HT at 1030~1100 nm, HR at 940 nm; HT: high transmission; HR: high reflection).

A V-shaped cavity was used in the experiment where L1, L2, and L4 were 275 mm, 244 mm, and 65 mm, respectively. M1 was a concave mirror with a radius of curvature (ROC) of 550 mm and coated for high reflection (HR, $R > 99\%$) from 1030 nm to 1100 nm. A pair of SF10 prisms with a tip-to-tip distance (L3) of 480 mm was employed to compensate the cavity dispersion. A SESAM was designed to assist the synchronous mode locking and to balance the output coupling for achieving dual-wavelength operation. The modulation depth of the SESAM was found to be approximately 1.2% at 1040 nm. The SESAM device was monolithically grown on an undoped 350 μm thick GaAs substrate by metalorganic chemical vapor deposition (MOCVD) to comprise single strained $\text{In}_{0.27}\text{Ga}_{0.73}\text{As}/\text{GaAs}$ quantum well (QW) grown on the Bragg mirror. The QW has a thickness of 8 nm. The Bragg mirror consists of ten-pair AlAs/GaAs quarter-wavelength layers. Figure 4.13 shows the

transmittance spectrum for the SESAM. It can be seen that the transmittances are approximately 5.8% and 3.8% at 1032 nm and 1049 nm. The back side of the GaAs substrate was coated for antireflection at 1040 nm ($R < 1\%$).

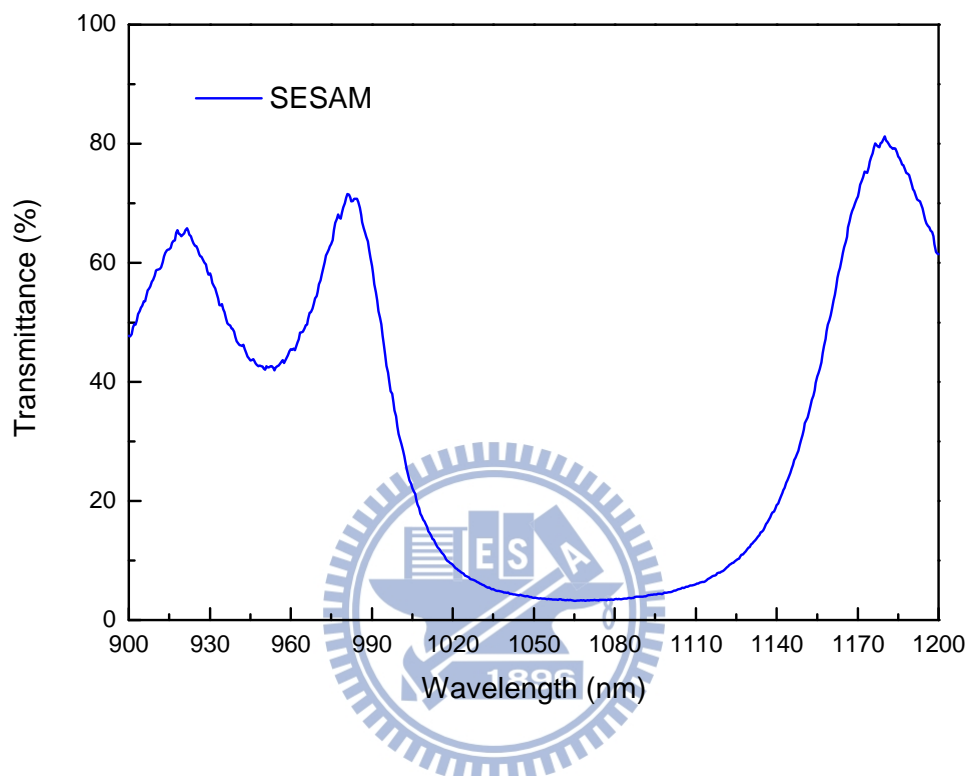


Fig. 4.13 Transmittance spectra of the SESAM.

(B) Experimental results and discussion

Figure 4.14 depicts the average output power versus the absorbed pump power in the dual-wavelength harmonically mode-locked operation. The maximum average output power is approximately 1.1 W under the maximum absorbed pump power of 5.18 W, corresponding to the optical-to-optical conversion efficiency of 21.2% and slope efficiency of 29.4%. The optical-to-optical conversion efficiency is considerably higher than the earlier results of dual-wavelength mode-locked lasers which range from 0.03% to 10% by utilizing rare-earth doped crystals such as Nd-doped disordered crystals [67, 76-79], Yb: LYSO crystal [80], and Yb:YAG ceramics [85]. With the thermal management of a diamond heat spreader, not only the output efficiency is remarkably increased but also the beam distortion is significantly

improved [15].

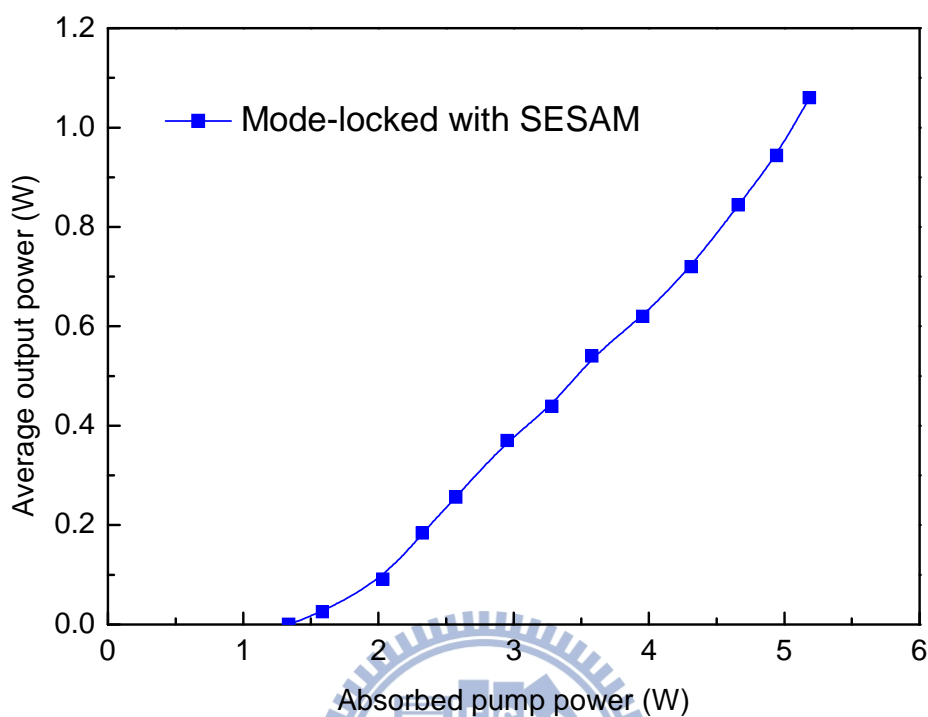


Fig. 4.14 Dependence of the average output power on the absorbed pump power in the dual-wavelength harmonically mode-locked operation.

The optical spectrum of laser output was measured with a Fourier-Michelson optical interferometer (Advantest, Q8347) with a resolution of 0.003 nm. Figure 4.15 depicts the experimental result for the lasing spectrum at the maximum absorbed pump power of 5.18 W. It can be seen that there are dual lasing bands with central wavelengths at 1031.67 nm and 1049.42 nm. As a result, the difference between the central frequencies is 4.92 THz. The values for the full width at half maximum (FWHM) of the spectral bands at 1031.67 nm and 1049.42 nm are 1.08 nm and 0.89 nm, respectively. The spectral intensity ratio of the two bands was numerically calculated to be 1:0.8. The values of the mode spacing within each spectral band are found to be approximately 80.3 GHz. This mode spacing precisely corresponds to the free spectral range of the etalon effect caused by the Yb:YAG crystal with an optical length of about 1.87 mm. It has been demonstrated [83] that the partial reflection on the surface of the gain medium could introduce a significant mode selection for

effectively generating high-order harmonic mode locking.

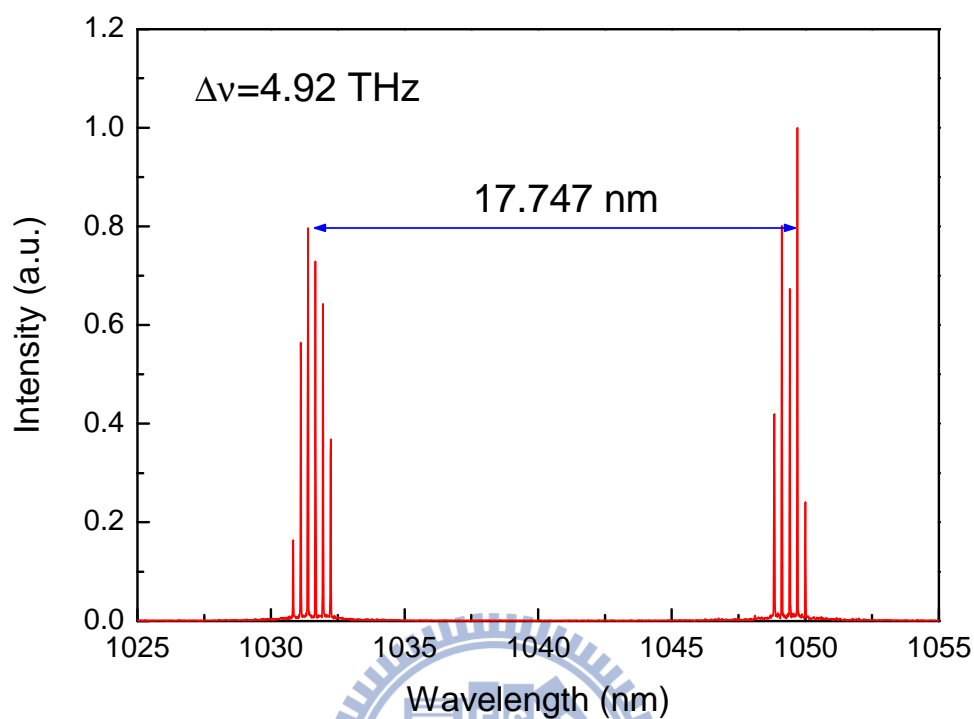


Fig. 4.15 Optical lasing spectrum obtained at the maximum absorbed pump power of 5.18 W.

The temporal behavior of the laser output was analyzed by exploiting the schemes of first- and second-order autocorrelations. The first-order autocorrelation trace was measured with a Michelson interferometer. The second-order autocorrelation trace was performed with a commercial autocorrelator (APE GmbH, PulseCheck). First of all, we measured the autocorrelation traces in a delay-time span of 50 ps to display the pulse repetition rate of the experimental mode-locked pulse train. Under this time span, the resolutions of the first- and second-order autocorrelations are 67 fs and 200 fs, respectively. Figures 4.16(a) and 4.16(b) show the measured results at the maximum absorbed pump power. It can be seen that the laser output exhibits a state of tenth-order harmonic mode locking (relative to the fundamental mode locking pulse repetition rate of 80.3 MHz) with the pulse repetition rate of 80.3 GHz. The tenth-order harmonic mode locking originates from the etalon effect that is caused by the partial reflection on the surface of the gain medium. The

traces of the first- and second-order autocorrelation traces reveal the same pulse period. The sameness indicates that the phase of the optical spectrum is nearly constant [60, 83]. Note that the sampling resolutions shown in Figs. 4.15(a) and 4.15(b) are not high enough to display the temporal behavior of the THz beat frequency.

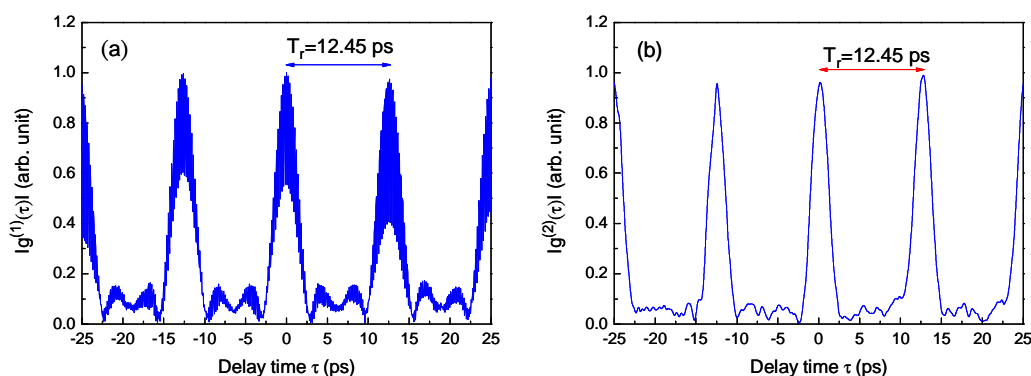


Fig. 4.16 Experimental traces of the temporal behavior of (a) first- and (b) second-order autocorrelations in a delay-time span of 50 ps. Resolution: 67 fs and 200 fs for the first- and second-order autocorrelations, respectively.

To identify the modulation of the beat frequency, we measured the autocorrelation traces with higher resolutions in a delay-time span of 8 ps. Under this time span, the resolutions of the first- and second-order autocorrelations are 8 fs and 20 fs, respectively. Figures 4.17(a) and 4.17(b) show the measured results at the maximum absorbed pump power. It can be seen that both the first- and second-order autocorrelations display interference patterns with modulation depths higher than 80% in the mode-locked pulse. Assuming the temporal intensity of the second-order autocorrelation trace to be a sech^2 profile, the duration of the mode-locked pulse can be deduced to be 1.54 ps, as shown in Fig. 4.17(b). The periodic modulation within the autocorrelation traces clearly corresponds to the 4.92-THz beat frequency of the dual-wavelength laser. The deep modulations in autocorrelation traces indicate that the dual-wavelength mode-locked pulses are synchronous to a certain extent. Figure 4.18 shows the second-order autocorrelation trace in a delay-time span of 180 fs to evaluate the pulse duration arising from the beating. In terms of a cosine-like shape, the effective pulse duration of the beating exactly corresponds to the FWHM of the

measured autocorrelation trace. As a consequence, the effective pulse duration of the dual-wavelength mode-locked laser is approximately 83 fs.

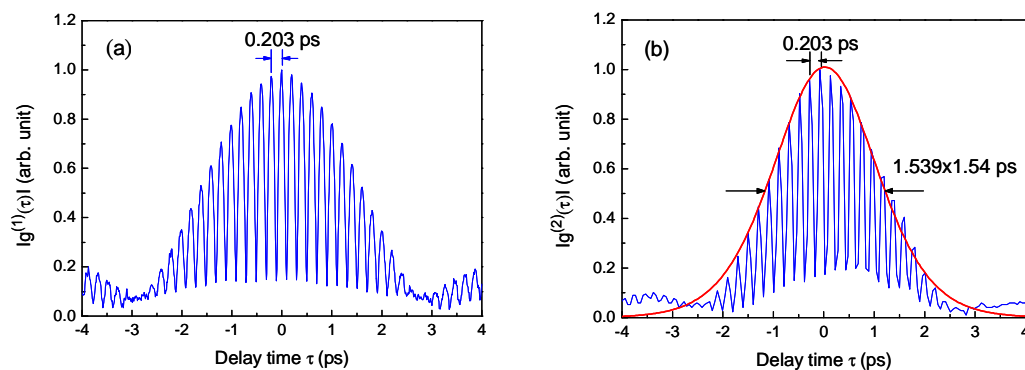


Fig. 4.17 Experimental traces of the temporal behavior of (a) first- and (b) second-order autocorrelations in a delay-time span of 8 ps. Resolution: 8 fs and 20 fs for the first- and second-order autocorrelations, respectively.

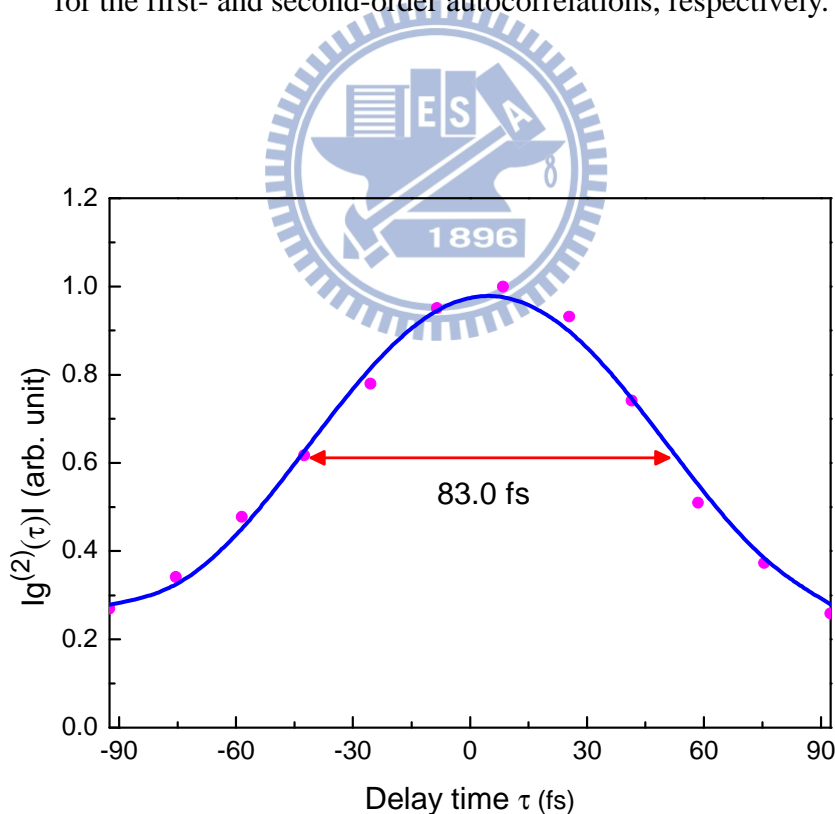


Fig. 4.18 Experimental trace of the temporal behavior of second-order autocorrelation of the single beat pulse.

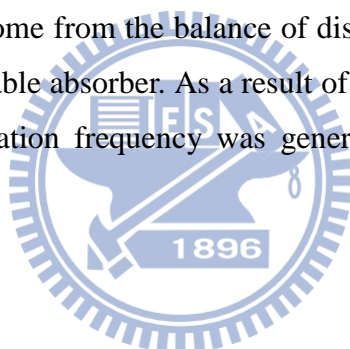
(C) Conclusions

I have experimentally demonstrated a high-power harmonically mode-locked Yb:YAG laser with a pulse duration of 1.54 ps at a repetition rate of 80.3 GHz. The power scale-up was improved by employing a diamond heat spreader to enhance the heat removal efficiency of the Yb:YAG crystal. At the absorbed pump power of 5.18 W, the maximum average output power was up to 1.1 W, corresponding to the optical-to-optical conversion efficiency of 21.2% and slope efficiency of 29.4%. An appropriate SESAM has been developed to balance the output coupling and to achieve the dual-wavelength synchronous mode-locked operation at 1032 nm and 1049 nm. The autocorrelation traces revealed that the modulation depth of the mode-locked pulse in the beat frequency of 4.92 THz could be generally higher than 80% and the effective pulse duration was as short as 83 fs.



4.4 Conclusions

In this chapter, I demonstrate efficient, high peak power PQS Yb:YAG microchip laser by using Cr⁴⁺:YAG crystal as the saturable absorber. Energy and output power scaling together with pulse stability improvement were achieved via employing a diamond window as the heat spreader. Besides, high repetition rate, self-mode-locked operation was also attained using the same gain chip and heat spreader. Various order of harmonic mode locking was obtained by means of tuning the cavity length to match a commensurate ratio of the gain chip length. Furthermore, by replacing a semiconductor saturable absorber mirror as the output coupler, dual-wavelength mode-locked Yb:YAG laser was demonstrated. Synchronous, dual-wavelength mode locking was speculated to come from the balance of dispersion compensation and the cross-saturation of the saturable absorber. As a result of the optical beating of the dual spectral bands, THz modulation frequency was generated with an ultrashort pulse duration.



Reference

- [1]. R. Bhandari and T. Taira, “> 6 MW peak power at 532 nm from passively Q-switched Nd:YAG/Cr⁴⁺:YAG microchip laser,” *Opt. Express* **19**, 19135-19141 (2011).
- [2]. Z. Zhuo, S. G. Li, T. Li, C. X. Shan, J. M. Jiang, B. Zhao, J. Li, and J. Z. Chen, “Diode-end-pumped passively Q-switched Nd:Y_{0.8}Lu_{0.2}VO₄ laser with Cr⁴⁺:YAG crystal,” *Opt. Commun.* **283**, 1886-1888 (2010).
- [3]. B. Y. Zhang, J. L. Xu, G. J. Wang, J. L. He, W. J. Wang, Q. L. Zhang, D. L. Sun, J. Q. Luo, and S. T. Yin, “Continuous-wave and passively Q-switched laser performance of a disordered Nd:GYSGG crystal,” *Opt. Commun.* **284**, 5734-5737 (2011).
- [4]. W. Z. Zhuang, W. C. Huang, Y. P. Huang, K. W. Su, and Y. F. Chen, “Passively Q-switched photonic crystal fiber laser and intracavity optical parametric oscillator,” *Opt. Express* **18**, 8969-8975 (2010).
- [5]. J. Liu, U. Griebner, V. Petrov, H. Zhang, J. Zhang, and J. Wang, “Efficient continuous-wave and Q-switched operation of a diode-pumped Yb:KLu(WO₄)₂ laser with self-Raman conversion,” *Opt. Lett.* **30**, 2427-2429 (2005).
- [6]. J. Dong, K. Ueda, and A. A. Kaminskii, “Efficient passively Q-switched Yb:LuAG microchip laser,” *Opt. Lett.* **32**, 3266-3268 (2007).
- [7]. D. S. Sumida and T. Y. Fan, “Effect of radiation trapping on fluorescence lifetime and emission cross section measurements in solid-state laser media,” *Opt. Lett.* **19**, 1343-1345 (1994).
- [8]. H. W. Bruesselbach, D. S. Sumida, R. A. Reeder, and R. W. Byren, “Low-heat high-power scaling using InGaAs-diode-pumped Yb:YAG lasers,” *IEEE J. Sel. Top. Quantum Electron.* **3**, 105-116 (1997).
- [9]. J. Dong, K. Ueda, A. Shirakawa, H. Yagi, T. Yanagitani, and A. A. Kaminskii, “Composite Yb:YAG/Cr⁴⁺:YAG ceramics picosecond microchip lasers,” *Opt. Express* **15**, 14516-14523 (2007).
- [10]. J. Dong, A. Shirakawa, K. Ueda, H. Yagi, T. Yanagitani, and A. A. Kaminskii, “Near-diffraction-limited passively Q-switched Yb:Y₃Al₅O₁₂ ceramic lasers with

- peak power >150kW,” *Appl. Phys. Lett.* **90**, 131105 (2007).
- [11]. J. Dong, A. Shirakawa, and K. Ueda, “Sub-nanosecond passively Q-switched Yb:YAG/Cr⁴⁺:YAG sandwiched microchip laser,” *Appl. Phys. B* **85**, 513-518 (2006).
- [12]. J. M. Hopkins, S. A. Smith, C. W. Jeon, H. D. Sun, D. Burns, S. Calvez, M. D. Dawson, T. Jouhti, and M. Pessa, “0.6 W CW GaInNAs vertical external-cavity surface emitting laser operating at 1.32 μm ,” *Electron. Lett.* **40**, 30-31 (2004).
- [13]. Y. Tzuk, A. Tal, S. Goldring, Y. Glick, E. Lebiush, G. Kaufman, and R. Lavi, “Diamond cooling of high-power diode-pumped solid-state lasers,” *IEEE J. Quantum Electron.* **40**, 262-269 (2004).
- [14]. P. Millar, A. J. Kemp, and D. Burns, “Power scaling of Nd:YVO₄ and Nd:GdVO₄ disk lasers using synthetic diamond as a heat spreader,” *Opt. Lett.* **34**, 782-784 (2009).
- [15] P. Millar, R. B. Birch, A. J. Kemp, and D. Burns, “Synthetic diamond for intracavity thermal management in compact solid-state lasers,” *IEEE J. Quantum Electron.* **44**, 709-717 (2008).
- [16]. W. Koechner, *Solid State Laser Engineering* (Springer, 2006).
- [17]. Y. Kalisky, C. Labbe, K. Waichman, L. Kravchik, U. Rachum, P. Deng, J. Xu, J. Dong, and W. Chen, “Passively Q-switched diode-pumped Yb:YAG laser using Cr⁴⁺-doped garnets,” *Opt. Mater.* **19**, 403-413 (2002).
- [18]. Q. Hao, W. Li, H. Pan, X. Zhang, B. Jiang, Y. Pan, and H. Zeng, “Laser-diode pumped 40-W Yb:YAG ceramic laser,” *Opt. Express* **17**, 17734-17738 (2009).
- [19]. J. Dong, J. Ma, Y. Cheng, Y. Y. Ren, K. Ueda, and A. A. Kaminskii, “Comparative study on enhancement of self-Q-switched Cr,Yb:YAG lasers by bonding Yb:YAG ceramic and crystal,” *Laser Phys. Lett.* **8**, 845-852 (2011).
- [20]. J. Dong, J. Li, S. Huang, A. Shirakawa, and K. Ueda, “Multi-longitudinal-mode oscillation of self-Q-switched Cr,Yb:YAG laser with a plano-concave resonator,” *Opt. Commun.* **256**, 158-165 (2005).
- [21]. J. Dong, A. Shirakawa, K. I. Ueda, and A. A. Kaminskii, “Effect of ytterbium concentration on cw Yb:YAG microchip laser performance at ambient temperature - Part I: Experiments,” *Appl. Phys. B* **89**, 359-365 (2007).
- [22]. J. Dong, A. Shirakawa, K. I. Ueda, and A. A. Kaminskii, “Effect of ytterbium concentration on cw Yb:YAG microchip laser performance at ambient temperature - Part II: Theoretical modeling,” *Appl. Phys. B* **89**, 367-376 (2007).

- [23]. D. C. Brown, "Ultrahigh-average-power diode-pumped Nd:YAG and Yb:YAG lasers," *IEEE J. Quantum Electron.* **33**, 861-873 (1997).
- [24]. Q. Liu, X. Fu, M. Gong, and L. Huang, "Effects of the temperature dependence of the absorption coefficients in edge-pumped Yb:YAG slab lasers," *J. Opt. Soc. Am. B* **24**, 2081-2089 (2007).
- [25]. J. Dong, M. Bass, Y. Mao, P. Deng, and F. Gan, "Dependence of the Yb³⁺ emission cross section and lifetime on temperature and concentration in yttrium aluminum garnet," *J. Opt. Soc. Am. B* **20**, 1975-1979 (2003).
- [26]. T. Kasamatsu, H. Sekita, and Y. Kuwano, "Temperature dependence and optimization of 970-nm diode-pumped Yb:YAG and Yb:LuAG lasers," *Appl. Opt.* **38**, 5149-5153 (1999).
- [27]. J. Dong and K. Ueda, "Temperature-tuning Yb:YAG microchip lasers," *Laser Phys. Lett.* **2**, 429-436 (2005).
- [28]. M. Ostermeyer and A. Straesser, "Theoretical investigation of feasibility of Yb:YAG as laser material for nanosecond pulse emission with large energies in the Joule range," *Opt. Commun.* **274**, 422-428 (2007).
- [29]. C. Li, Q. Liu, M. Gong, G. Chen, and P. Yan, "Q-switched operation of end-pumped Yb:YAG lasers with nonuniform temperature distribution," *Opt. Commun.* **231**, 331-341 (2004).
- [30]. Y. F. Chen, K. W. Su, W. L. Chen, K. F. Huang, and Y. F. Chen, "High-peak-power optically pumped AlGaInAs eye-safe laser at 500-kHz repetition rate with an intracavity diamond heat spreader," *Appl. Phys. B* ((to be published), doi:10.1007/s00340-012-4954-4.
- [31]. Y. F. Chen, "High-power diode-pumped Q-switched intracavity frequency-doubled Nd:YVO₄ laser with a sandwich-type resonator," *Opt. Lett.* **24**, 1032-1034 (1999).
- [32]. W. A. Clarkson and D. C. Hanna, "Efficient Nd:YAG laser end pumped by a 20-W diode-laser bar," *Opt. Lett.* **21**, 869-871 (1996).
- [33]. J. J. Zayhowski, C. Dill III, C. Cook, and J. L. Daneu, "Mid-and high-power passively Q-switched microchip lasers," in *Proceeding of Advanced Solid-State Lasers*, M. M. Fejer, H. Injeyan, and U. Keller, eds., Vol. 26 of OSA Trends in Optics and Photonic Series (Optical Society of America, Washington, D. C., 1999), pp. 178-186.
- [34]. J. J. Zayhowski, "Microchip lasers," *Opt. Mater.* **11**, 255-267 (1999).

- [35]. J. J. Zayhowski, "Passively Q-switched Nd:YAG microchip lasers and applications," *J. Alloy. Comp.* **303**, 393-400 (2000).
- [36]. J. Federici and L. Moeller, "Review of terahertz and subterahertz wireless communications," *J. Appl. Phys.* **107**, 111101 (2010).
- [37]. T. Tomaru and H. Petek, "Femtosecond Cr⁴⁺:YAG laser with an L-fold cavity operating at a 1.2-GHz repetition rate," *Opt. Lett.* **25**, 584-586 (2000).
- [38]. Ch. Silberhorn, P.K. Lam, O. Weiß, F. König, N. Korolkova, and G. Leuchs, "Generation of continuous variable Einstein-Podolsky-Rosen entanglement via the Kerr nonlinearity in an optical fiber," *Phys. Rev. Lett.* **86**, 4267-4270 (2001).
- [39]. A. Bartels, T. Dekorsy, H. Kurz, "Femtosecond Ti:sapphire ring laser with a 2-GHz repetition rate and its application in time-resolved spectroscopy," *Opt. Lett.* **24**, 996-998 (1999).
- [40]. D. A. B. Miller, "Optics for low-energy communication inside digital processors: quantum detectors, sources, and modulators as efficient impedance converters," *Opt. Lett.* **14**, 146-148 (1989).
- [41]. A. Bartels, D. Heinecke, and S. A. Diddams, "10-GHz self-referenced optical frequency comb," *Science* **326**, 681 (2009).
- [42]. E. Yoshida and M. Nakazawa, "80~200 GHz erbium doped fibre laser using a rational harmonic mode-locking technique," *Electron. Lett.* **32**, 1370-1372 (1996).
- [43]. J. Schröder, S. Coen, F. Vanholsbeek, and T. Sylvestre, "Passively mode-locked Raman fiber laser with 100 GHz repetition rate," *Opt. Lett.* **31**, 3489-3491 (2006).
- [44]. K. Sato, "Optical pulse generation using fabry-Pe´rot lasers under continuous-wave operation," *IEEE J. Sel. Top. Quantum Electron.* **9**, 1288-1293 (2003).
- [45]. C. Gosset, K. Merghem, A. Martinez, G. Moreau, G. Patriarche, G. Aubin, A. Ramdane, J. Landreau, and F. Lelarge, "Subpicosecond pulse generation at 134 GHz using a quantum-dash-based Fabry-Perot laser emitting at 1.56 μm ," *Appl. Phys. Lett.* **88**, 241105-241105-3 (2006).
- [46]. A. H. Quarterman, K. G. Wilcox, V. Apostolopoulos, Z. Mihoubi, S. P. Elsmere, I. Farrer, D. A. Ritchie, and A. C. Tropper, "A passively mode-locked external-cavity semiconductor laser emitting 60-fs pulses," *Nature Photonics* **3**, 729 - 731 (2009).
- [47]. P. Klopp, U. Griebner, M. Zorn, and M. Weyers, "Pulse repetition rate up to 92 GHz or pulse duration shorter than 110 fs from a mode-locked semiconductor disk

- laser,” *Appl. Phys. Lett.* **98**, 071103-071103-3 (2011).
- [48]. A. E. H. Oehler, T. Südmeyer, K. J. Weingarten, and U. Keller, “100 GHz passively mode-locked Er:Yb:glass laser at 1.5 μm with 1.6-ps pulses,” *Opt. Express* **16**, 21930-21935 (2008).
- [49]. Y. F. Chen, H. C. Liang, J. C. Tung, K. W. Su, Y. Y. Zhang, H. J. Zhang, H. H. Yu, and J. Y. Wang, “Spontaneous subpicosecond pulse formation with pulse repetition rate of 80 GHz in a diode-pumped Nd:SrGdGa₃O₇ disordered crystal laser,” *Opt. Lett.* **37**, 461-463 (2012).
- [50]. H. Liu, J. Nees, and G. Mourou, “Diode-pumped Kerr-lens mode-locked Yb:KY(WO₄)₂ laser,” *Opt. Lett.* **26**, 1723-1725 (2001).
- [51]. A. A. Lagatsky, A. R. Sarmani, C. T. A. Brown, W. Sibbett, V. E. Kisel, A. G. Selivanov, I. A. Denisov, A. E. Troshin, K. V. Yumashev, N. V. Kuleshov, V. N. Matrosov, T. A. Matrosova, and M. I. Kupchenko, “Yb³⁺-doped YVO₄ crystal for efficient Kerr-lens mode locking in solid-state lasers,” *Opt. Lett.* **30**, 3234-3236 (2005).
- [52]. G. Q. Xie, D. Y. Tang, L. M. Zhao, L. J. Qian, and K. Ueda, “High-power self-mode-locked Yb:Y₂O₃ ceramic laser,” *Opt. Lett.* **32**, 2741-2743 (2007).
- [53]. S. Uemura and K. Torizuka, “Kerr-lens mode-locked diode-pumped Yb:YAG laser with the transverse mode passively stabilized,” *Appl. Phys. Express* **1**, 012007 (2008).
- [54]. H. C. Liang, R. C. C. Chen, Y. J. Huang, K. W. Su, and Y. F. Chen, “Compact efficient multi-GHz Kerr-lens mode-locked diode-pumped Nd:YVO₄ laser,” *Opt. Express* **16**, 21149-21154 (2008).
- [55]. H. C. Liang, Y. J. Huang, W. C. Huang, K. W. Su, and Y. F. Chen, “High-power, diode-end-pumped, multigigahertz self-mode-locked Nd:YVO₄ laser at 1342 nm,” *Opt. Lett.* **35**, 4-6(2010).
- [56]. R. Paiella, F. Capasso, C. Gmachl, D. L. Sivco, J. N. Baillargeon, A. L. Hutchinson, A. Y. Cho, and H. C. Liu, “Self-mode-locking of quantum cascade lasers with giant ultrafast optical nonlinearities,” *Science* **290**, 1739-1742 (2000).
- [57]. Y. F. Chen, Y. C. Lee, H. C. Liang, K. Y. Lin, K. W. Su, and K. F. Huang, “Femtosecond high-power spontaneous mode-locked operation in vertical-external cavity surface-emitting laser with gigahertz oscillation,” *Opt. Lett.* **36**, 4581-4583 (2011).
- [58]. H. Lindberg, M. Strassner, E. Gerster, and A. Larsson, “0.8 W optically pumped

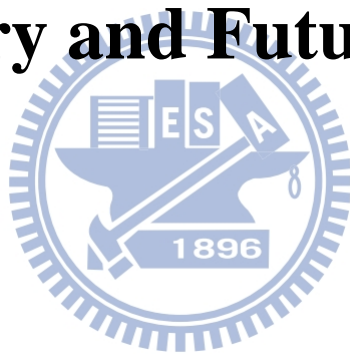
- vertical external cavity surface emitting laser operating CW at 1550 nm,” *Electron. Lett.* **40**, 601-602 (2004).
- [59]. V. M. Korpijärvi, T. Leinonen, J. Puustinen, A. Härkönen, and M. D. Guina, “11 W single gain-chip dilute nitride disk laser emitting around 1180 nm,” *Opt. Express* **18**, 25633-25641, 641 (2010).
- [60]. Andrew M. Weiner, *Ultrafast Optics* (John Wiley & Sons Inc., Hoboken, NJ, 2009).
- [61]. T. J. Wang, C. Marceau, S. Yuan, Y. Chen, Q. Wang, F. Théberge, M. Châteauneuf, J. Dubois, and S.L. Chin, “External focusing effect on terahertz emission from a two-color femtosecond laser-induced filament in air,” *Laser Phys. Lett.* **8**, 57-61 (2011).
- [62]. T. J. Wang, S. Yuan, Z. D. Sun, C. Marceau, Y. Chen, F. Théberge, M. Châteauneuf, J. Dubois, and S.L. Chin, “Molecular alignment control of terahertz emission from a two-color filament in air,” *Laser Phys. Lett.* **8**, 295-300 (2011).
- [63]. B. E. Cole, J. B. Williams, B. T. King, M. S. Sherwin, and C. R. Stanley, “Coherent manipulation of semiconductor quantum bits with terahertz radiation,” *Nature* **410**, 60-63 (2001).
- [64]. C. Fortier, B. Kibler, J. Fatome, C. Finot, S. Pitois, and G. Millot, “All-fibered high-quality low duty-cycle 160-GHz femtosecond pulse source,” *Laser Phys. Lett.* **5**, 817-820 (2008).
- [65]. P. H. Siegel, “THz Instruments for Space,” *IEEE Trans. Antenn. Propag.* **55**, 2957-2965 (2007).
- [66]. M. D. Pelusi, H. F. Liu, D. Novak, and Y. Ogawa, “THz optical beat frequency generation from a single mode locked semiconductor laser,” *Appl. Phys. Lett.* **71**, 449-451 (1997).
- [67]. G. Q. Xie, D. Y. Tang, H. Luo, H. J. Zhang, H. H. Yu, J. Y. Wang, X. T. Tao, M. H. Jiang, and L. J. Qian, “Dual-wavelength synchronously mode-locked Nd:CNGG laser,” *Opt. Lett.* **33**, 1872-1874 (2008).
- [68]. C. J. Zhu, J. F. He, and S. C. Wang, “Generation of synchronized femtosecond and picosecond pulses in a dual-wavelength femtosecond Ti:sapphire laser,” *Opt. Lett.* **30**, 561-563 (2005).
- [69]. W. H. Knox and F. A. Beisser, “Two-wavelength synchronous generation of femtosecond pulses with <100-fs jitter,” *Opt. Lett.* **17**, 1012-1014 (1992).
- [70]. Z. Zhang and T. Yagi, “Dual-wavelength synchronous operation of a

- mode-locked Ti:sapphire laser based on self-spectrum splitting,” *Opt. Lett.* **18**, 2126-2128 (1993).
- [71]. M. R. X. de Barros and P. C. Becker, “Two-color synchronously mode-locked femtosecond Ti:sapphire laser,” *Opt. Lett.* **18**, 631-633 (1993).
- [72]. A. Leitenstorfer, C. Fürst, and A. Laubereau, “Widely tunable two-color mode-locked Ti:sapphire laser with pulse jitter of less than 2 fs,” *Opt. Lett.* **20**, 916-918 (1995).
- [73]. Z. Wei, Y. Kobayashi, Z. Zhang, and K. Torizuka, “Generation of two-color femtosecond pulses by self-synchronizing Ti:sapphire and Cr:forsterite lasers,” *Opt. Lett.* **26**, 1806-1808 (2001).
- [74]. Z. Wei, Y. Kaboyashi, and K. Torizuka, “Passive synchronization between femtosecond Ti:sapphire and Cr:forsterite lasers,” *Appl. Phys. B* **74**, 171-176 (2002).
- [75]. C. Zhu, Y. Wang, J. He, S. Wang, and X. Hou, “Generation and evaluation of synchronous femtosecond and picosecond pulses in a dual-wavelength Ti:sapphire laser,” *J. Opt. Soc. Am. B* **22**, 1221-1227 (2005).
- [76]. G. Q. Xie, D. Y. Tang, W. D. Tan, H. Luo, S. Y. Guo, H. H. Yu, and H. J. Zhang, “Diode-pumped passively mode-locked Nd:CTGG disordered crystal laser,” *Appl. Phys. B* **95**, 691-695 (2009).
- [77]. A. Agnesi, F. Pirzio, G. Reali, A. Arcangeli, M. Tonelli, Z. Jia, and X. Tao, “Multi-wavelength diode-pumped Nd:LGGG picosecond laser,” *Appl. Phys. B* **99**, 135-140 (2010).
- [78]. Z. H. Cong, D. Y. Tang, W. D. Tan, J. Zhang, C. W. Xu, D. W. Luo, X. D. Xu, D. Z. Li, J. Xu, X. Y. Zhang, and Q. P. Wang, “Dual-wavelength passively mode-locked Nd:LuYSiO₅ laser with SESAM,” *Opt. Express* **19**, 3984-3989 (2011).
- [79]. J. L. Xu, S. Y. Guo, J. L. He, B. Y. Zhang, Y. Yang, H. Yang, and S. D. Liu, “Dual-wavelength asynchronous and synchronous mode-locking operation by a Nd:CLTGG disordered crystal,” *Appl. Phys. B* **107**, 53-58 (2012).
- [80]. Q. Yang, Y. G. Wang, D. H. Liu, J. Liu, L. H. Zheng, L. B. Su, and J. Xu, “Dual-wavelength mode-locked Yb:LuYSiO₅ laser with a double-walled carbon nanotube saturable absorber,” *Laser Phys. Lett.* **9**, 135-140 (2012).
- [81]. S. Uemura and K. Torizuka, “Center-wavelength-shifted passively mode-locked diode-pumped ytterbium(Yb):yttrium aluminum garnet(YAG) laser,” *Jpn. J. Appl.*

- Phys. **44**, L361-L363 (2005).
- [82]. A. Agnesi, A. Greborio, F. Pirzio, and G. Reali, "Efficient femtosecond Yb:YAG laser pumped by a single-mode laser diode," *Opt. Commun.* **284**, 4049-4051 (2011).
- [83]. Y. F. Chen, W. Z. Zhuang, H. C. Liang, G. W. Huang, and K. W. Su, "High-power subpicosecond harmonically mode-locked Yb:YAG laser with pulse repetition rate up to 240 GHz," *Laser Phys. Lett.* **10**, 1-4 (2012).
- [84]. J. Y. Zhou, J. Ma, J. Dong, Y. Cheng, K. Ueda, and A. A. Kaminskii, "Efficient, nanosecond self-Q-switched Cr,Yb:YAG lasers by bonding Yb:YAG crystal", *Laser Phys. Lett.* **8**, 591-597 (2011).
- [85]. H. Yoshioka, S. Nakamura, T. Ogawa, and S. Wada, "Dual-wavelength mode-locked Yb:YAG ceramic laser in single cavity," *Opt. Express* **18**, 1479-1486 (2010).
- [86]. W. Z. Zhuang, Yi-Fan Chen, K. W. Su, K. F. Huang, and Y. F. Chen, "Performance enhancement of sub-nanosecond diode-pumped passively Q-switched Yb:YAG microchip laser with diamond surface cooling," *Opt. Express* **20**, 22602-22608 (2012).
- [87]. X. Wang, X. Xu, Z. Zhao, B. Jiang, J. Xu, G. Zhao, P. Deng, G. Bourdet, and J.-C. Chanteloup, "Comparison of fluorescence spectra of Yb:Y₃Al₅O₁₂ and Yb:YAlO₃ single crystals," *Opt. Mater.* **29**, 1662-1666 (2007).
- [88]. J. Dong, A. Shirakawa, K. I. Ueda, and A. A. Kaminskii, "Effect of ytterbium concentration on cw Yb:YAG microchip laser performance at ambient temperature - Part I: Experiments," *Appl. Phys. B* **89**, 359-365 (2007).
- [89]. J. Dong, A. Shirakawa, K. I. Ueda, and A. A. Kaminskii, "Effect of ytterbium concentration on cw Yb:YAG microchip laser performance at ambient temperature - Part II: Theoretical modeling," *Appl. Phys. B* **89**, 367-376 (2007).
- [90]. P. Millar, R. B. Birch, A. J. Kemp, and D. Burns, "Synthetic diamond for intracavity thermal management in compact solid-state lasers," *IEEE J. Quantum Electron.* **44**(8), 709-717 (2008).

Chapter 5

Summary and Future works



5.1 Summary

(A) Q-switched lasers and amplifiers with conventional large mode area fiber

Type	Mechanism	Energy	Repetition rate	Pulse width	Peak power
Laser	PQS with Cr ⁴⁺ :YAG	0.35 mJ	38 kHz	70 ns	5 kW
Laser	PQS with AlGaInAs	0.45 mJ	30 kHz	60 ns	7.5 kW
Laser	HQS with A.O. and AlGaInAs	0.56 mJ	23 kHz	50 ns	11.2 kW
Amplifier	Seeded with PQS Nd:YVO ₄ /Cr ⁴⁺ :YAG lasers	0.178 mJ	50 kHz	4.8 ns	37.1 kW
Amplifier	Seeded with PQS Nd:YVO ₄ /Cr ⁴⁺ :YAG lasers	0.192 mJ	25 kHz	1.6 ns	120 kW

Table 5.1: Summary of the performance obtained with the conventional LMA fiber.

In this section I demonstrate efficient, high peak power fiber amplifier and PQS fiber lasers with either Cr⁴⁺:YAG crystal or AlGaInAs MQWs as the SA. For timing jitter reduction, I also utilize the “hybrid Q-switch” technique by combining AQS and PQS into a single laser resonator. The pulse energy can be further enhanced and the pulse duration was also reduced. For applications that need short durations, I also demonstrate fiber amplifiers that seeded by Nd:YVO₄/Cr⁴⁺:YAG PQS lasers with different pulse repetition rate. However, the pulse peak power was limited by the fiber end facet damage that suggests the enlargement of the fiber core size. Nevertheless, the pulse energies were still superior to those of others due to the use of a LMA fiber with core diameter of 30 μm and SAs with large modulation depth and low non-saturable loss. Table 4.1 summaries the performances obtained with the conventional LMA fiber.

(B) Q-switched lasers and amplifiers with photonic crystal fiber

Type	Mechanism	Energy	Repetition rate	Pulse width	Peak power
Laser	PQS with Cr ⁴⁺ :YAG	0.63 mJ	5.6 kHz	36 ns	17.5 kW
Laser	PQS with 3x50 AlGaInAs QWs	1.1 mJ	6.5 kHz	10 ns	110 kW
Laser	PQS with 3x30 AlGaInAs QWs	0.49 mJ	16 kHz	38 ns	12.8 kW
Laser	PQS with 2x30 AlGaInAs QWs	0.35 mJ	23 kHz	47.3 ns	7.4 kW
Amplifier	Seeded with PQS Nd:YVO ₄ /Cr ⁴⁺ :YAG lasers	0.221 mJ	14.9 kHz	2.2 ns	100 kW

Table 5.2: Summary of the performance obtained with the photonic crystal fiber.

In this part, I perform efficient, high peak power fiber amplifier and PQS fiber lasers with either Cr⁴⁺:YAG crystal or AlGaInAs MQWs as the SA by using ultra-large core photonic crystal fiber of the core diameter of 70 μm . The pulse energy was obviously enhanced due to the enlarged core size and the pulse width was also reduced owing to the shorter fiber length which equals to a shorter cavity length. Table 4.2 summaries the performances obtained with the with the photonic crystal fiber.

With the same Cr⁴⁺:YAG crystal of the initial transmission of 28% as in the conventional LMA fiber laser described before, the pulse energy was 1.8 times higher and the pulse width was 2 times smaller which corresponds to 3.5 times higher of pulse peak power compared with the results obtained with the fiber of core diameter of 30 μm . Besides, I also use three types of AlGaInAs QWs that posses 50 groups of three QWs (3×50 QWs), 30 groups of three QWs (3×30 QWs), and 30 groups of two QWs (2×30 QWs) as the saturable absorber. With the same AlGaInAs QWs (3×50 QWs) as in the conventional LMA fiber laser described before, the pulse energy was 2.45 times higher and the pulse width was 6 times smaller which corresponds to

14.7 times higher of pulse peak power compared with the results obtained with the fiber of core diameter of 30 μm .

With the PQS PCF laser, I also demonstrate the intracavity optical parametric oscillator (IOPO) by utilizing the Cr^{4+} :YAG crystal as the saturable absorber and the extracavity optical parametric oscillator (EOPO) by utilizing the AlGaInAs QWs as the saturable absorber. Shorter pulse width and higher peak power can be attained with the IOPO scheme but higher output power and conversion efficiency can be achieved with the EOPO scheme. Besides, thanks to the high refractive-index-temperature coefficient of the PPLN used in the EOPO scheme, the wavelength can be tuned over a broad range. Table 4.3 summarizes the performances obtained with the IOPO and the EOPO.

Scheme	Average power	Conversion efficiency	Wavelength	Energy	Repetition rate	Peak power
IOPO with KTP	0.47 W	22.3%	1515 nm	0.14 mJ	3.3 kHz	140 kW
EOPO with PPLN	0.9 W	35%	1513nm ~1593nm	0.14 mJ	6.5 kHz	19 kW

Table 5.3: Performance summary of the OPO obtained with the photonic crystal fiber.

Furthermore, I demonstrate the different harmonic generations by means of the extracavity wavelength conversion pumped by a PCF amplifier. The results manifested that it is efficient and with simplicity to use the single stage PCF amplifier as the fundamental wavelength light source.

(C) Passively Q-switched and mode-locked Yb:YAG lasers

In this part, I demonstrate efficient, high peak power PQS Yb:YAG microchip laser by using Cr^{4+} :YAG crystal as the saturable absorber. Energy and output power scaling together with pulse stability improvement were achieved via employing a diamond window as the heat spreader. Besides, high repetition rate, self-mode-locked operation was also attained using the same gain chip and heat spreader. Various order of

Chapter 5 Summary and Future works

harmonic mode locking was obtained by means of tuning the cavity length to match a commensurate ratio of the gain chip length. Furthermore, by replacing a semiconductor saturable absorber mirror as the output coupler, dual-wavelength mode-locked Yb:YAG laser was demonstrated. Synchronous, dual-wavelength mode locking was speculated to come from the balance of dispersion compensation and the cross-saturation of the saturable absorber. As a result of the optical beating of the dual spectral bands, THz modulation frequency was generated with an ultrashort pulse duration.



5.2 Future works

It is well known that shorter mode-locked pulse duration is available by using gain materials with larger gain bandwidth. The initial choice of Yb:YAG was due to its relaxed demands of the pump diodes, high gain cross section compared to other Yb-doped laser materials, and mass production. The limited gain bandwidth of Yb:YAG crystal does not support pulse durations shorter than 700 fs in efficient, high power operation under fundamental pulse repetition rate [1]. The Yb-doped double tungstates such as Yb:KYW and Yb:KGW are promising candidates for efficient, high power ultrashort pulse generation. Besides, the emission cross section ($2.8 \times 10^{-20} \text{cm}^2$) was larger than Yb:YAG ($1.89 \times 10^{-20} \text{cm}^2$) which promises efficient, high power operation. Passively mode-locked diode-pumped laser oscillators based on Yb:KGW were established as versatile and reliable light sources of sub-200 fs pulses [2-3], and ideal candidates for Yb-doped fiber amplifiers. The broad emission bandwidth of Yb:KGW allows the generation of ultrashort pulses in the 1020-1070 spectral region. By seeding this light source into the PCF, power scaling that was hindered by thermal effect in bulk-crystal lasers can be expected.

Reference

- [1]. R. Paschotta, J. Aus der Au, G. J. Spühler, S. Erhard, A. Giesen, and U. Keller, “Passive mode locking of thin disk lasers: effects of spatial hole burning,” *Appl. Phys. B* **72**, 267-278 (2001).
- [2]. G. Paunescu, J. Hein, and R. Sauerbrey, “100-fs diode-pumped Yb:KGW mode-locked laser,” *Appl. Phys. B* **79**, 555-558 (2004).
- [3]. F. Brunner, G. J. Spühler, J. Aus der Au, L. Krainer, F. Morier-Genoud, R. Paschotta, N. Lichtenstein, S. Weiss, C. Harder, A. A. Lagatsky, A. Abdolvand, N. V. Kuleshov, and U. Keller, “Diode-pumped femtosecond Yb:KGd(WO₄)₂ laser with 1.1-W average power,” *Opt. Lett.* **25**, 1119-1121 (2000).



Curriculum Vitae

Personal Data

Name: Wei-Zhe Zhuang

Sex: Male

Birthday: Sep. 27, 1985

Nationality: Taiwan

E-mail: edward10517@yahoo.com.tw

edward.ep97g@nctu.edu.tw

Mobile Phone: 886-918-843279

Education

2001-2004 National Taichung First Senior High School, Taichung, Taiwan.

2003-2007 B.S. in Department of Electrophysics, National Chiao Tung University, Hsinchu, Taiwan.

2007-2012 Ph.D. in Department of Electrophysics, National Chiao Tung University, Hsinchu, Taiwan.

Research Interest

Fiber lasers

Yb-doped pulsed lasers

Publication List

(A) Journal papers:

1. J. Y. Huang, W. C. Huang, W. Z. Zhuang, K. W. Su, Y. F. Chen, and K. F. Huang, “High-pulse-energy, passively Q-switched Yb-doped fiber laser with AlGaInAs quantum wells as a saturable absorber,” *Opt. Lett.* **34**(15), 2360-2362 (2009).
2. J. Y. Huang, W. Z. Zhuang, W. C. Huang, K. W. Su, C. Hu, K. F. Huang, and Y. F. Chen, “Comparative studies for Cr⁴⁺:YAG crystal and AlGaInAs semiconductor used as a saturable absorber in Q-switched Yb-doped fiber lasers,” *Opt. Express* **17**(23), 20800-20805 (2009).
3. W. Z. Zhuang, W. C. Huang, Y. P. Huang, K. W. Su, and Y. F. Chen, “Passively Q-switched photonic crystal fiber laser and intracavity optical parametric oscillator,” *Opt. Express* **18**(9), 8969-8975 (2010).
4. W. Z. Zhuang, W. C. Huang, P. Y. Chiang, K. W. Su, K. F. Huang, and Y. F. Chen, “Millijoule-level Yb-doped photonic crystal fiber laser passively Q-switched with AlGaInAs quantum wells,” *Opt. Express* **18**(26), 27910-27915 (2010).
5. J. Y. Huang, W. Z. Zhuang, W. C. Huang, K. W. Su, K. F. Huang, and Y. F. Chen, “Hybrid Q-switched Yb-doped fiber laser,” *Opt. Express* **19**(10), 9364-9370 (2011).
6. H. L. Chang, W. Z. Zhuang, W. C. Huang, J. Y. Huang, K. F. Huang, and Y. F. Chen, “Widely tunable eye-safe laser by a passively Q-switched photonic crystal fiber laser and an external-cavity optical parametric oscillator,” *Laser Phys. Lett.* **8**(9), 678-683 (2011).
7. W. Z. Zhuang, W. C. Huang, C. Y. Cho, Y. P. Huang, J. Y. Huang, and Y. F. Chen, “>100-kW linearly polarized pulse fiber amplifier seeded by a compact

efficient passively Q-switched Nd:YVO₄ laser,” *Laser Phys.* **22**(11), 1721-1728 (2012).

8. J. Y. Huang, W. Z. Zhuang, Y. P. Huang, Y. J. Huang, K. W. Su, and Y. F. Chen, “Improvement of stability and efficiency in diode-pumped passively Q-switched intracavity optical parametric oscillator with a monolithic cavity,” *Laser Phys. Lett.* **9**(7), 485-490 (2012).
9. Y. F. Chen, Y. C. Lin, W. Z. Zhuang, H. L. Liang, K. W. Su, and K. F. Huang, “Generation of large orbital angular momentum from superposed Bessel beams corresponding to resonant geometric modes,” *Phys. Rev. A* **85**(4), 043833 (2012).
10. W. Z. Zhuang, Yi-Fan Chen, K. W. Su, and Y. F. Chen, “Performance enhancement of sub-nanosecond diode-pumped passively Q-switched Yb:YAG microchip laser with diamond surface cooling,” *Opt. Express* **20**(20), 22602-22608 (2012).
11. Y. F. Chen, W. Z. Zhuang, H. C. Liang, G. W. Huang, and K. W. Su, “High-power subpicosecond harmonically mode-locked Yb:YAG laser with pulse repetition rate up to 240 GHz,” *Laser Phys. Lett.* **10**(1), 015803 (2013).

(B) Conference papers:

1. K. W. Su, W. Z. Zhuang, W. C. Huang, Y. F. Chen, and C. Hu, “The study of UV light generation based on conventional pulsed fiber lasers and Q-switched photonic crystal fiber lasers,” in *Photonics Global Conference 2010*, (Singapore, 14-16 Dec. 2010).
2. 莊威哲, 黃依萍, 蘇冠暉, 陳永富, 黃凱風, “被動與主動式Q開關鐳摻雜光子晶體光纖雷射之比較性研究,” 國防科技學術合作計畫成果發表會論文集, (龍潭 桃園, 98年11月26日).
3. 莊威哲, 蘇冠暉, 陳永富, 黃凱風, “光子晶體光纖之被動式Q開關與放大器之比較性研究,” 國防科技學術合作計畫成果發表會論文集, (龍潭 桃園,

99年11月18日).

